UNIVERSITÀ DI PARMA

UNIVERSITA' DEGLI STUDI DI PARMA

DOTTORATO DI RICERCA IN
"Scienze Chimiche"

CICLO XXXII

Enzyme-labelled amperometric genosensors and immunosensors based on advanced nanomaterials

Coordinatore:
Chiar.mo Prof. Roberto Corradini

Tutore:
Chiar.mo Prof. Marco Giannetto

Dottorando: Simone Fortunati

Anni 2016/2019

To Mom and Dad

Summary

1. Chemical Sensors

1.1. Introduction

Although a comprehensive and universally accepted definition of chemical sensors has not yet been recognised by the scientific community, one of the most fitting definition has been given by the IUPAC in 1991: "a chemical sensor is a device that transforms chemical information, ranging from the concentration of a specific sample component to total composition analysis, into an analytically useful signal" [1].

In general, these devices are comprised of a receptor, a transducer, electronics and circuiting for signal manipulation and a device for output visualization (e.g. personal computer, smartphone, etc.). However, the first two components represent the core elements of the sensor, as they are responsible for the device's analytical performance. In particular, the recognition event with the target analyte occurs on the receptor surface and is then translated into an electrical signal thanks to the activity of the transducer. The importance of the latter is proved by the fact that a common sensors' classification is based on the signal transduction mechanism [2]. This classification generates the following classes:

- Electrochemical sensors, such as voltammetric and potentiometric sensors.
- Electronic sensors, among which are Metal Oxide-based and organic semiconductor- based sensors.
- Optical sensors, where the signal is obtained following absorbance, reflectance, luminescence, fluorescence, refractive index, etc.
- Mass Sensitive sensors, such as piezoelectric sensors.

A classification of its own has been given for biosensors, which are defined as sensors on which the recognition of the target analyte involves a biochemical or biological mechanism.

An ideal chemical sensor, besides being able to transform a chemical quantity into a detectable electrical signal, should be small, cheap, have some degree of selectivity for a target molecule and be capable of maintaining its activity over a long period of time.

More in depth, the analytical performance of a sensing device is defined based on the following parameters:

- Sensitivity, characterized as the signal's variation generated as a consequence of the change in analyte concentration
- Limit of detection (LOD), which is the lowest analyte concentration value that yields a sensor response. The limit of quantification (LOQ) is the lowest analyte concentration that can be quantitatively detected with an established degree of accuracy and precision.
- Dynamic range, defined as the concentration interval where there is a dynamic response of the sensor. Usually it is found between the LOD and the upper limiting concentration at which the saturation of the signal is achieved.
- Selectivity expresses the capability of the sensor to respond selectively to a class of compounds or specifically to a single analyte.
- Linearity range is the analyte concentration interval where the sensor's response is linearly correlated to the variation of analyte concentration.
- Resolution is described as the lowest concentration difference that can be distinguished upon continuous variation of the solution's composition. It is mainly used for sensor working in continuous flow.
- Response time defines the time necessary for the sensor to reach a specific output value.
- Hysteresis is defined as the difference in output when a value is approached with an increasing and decreasing analyte concentration range respectively.
- Stability characterize the ability of the sensor to maintain its activity over a certain period of time.
- Life cycle is the amount of time over which the sensor will operate.

Taking into account the desirable properties of chemical sensors as analytical devices, it is easy to understand why, during the last decades, many efforts have been dedicated to the development of innovative chemical sensors for a remarkably wide range of applications [3-5].

1.2. Amperometric sensors

Electrochemical sensors are capable of directly transform the recognition event occurring on the receptor surface into an electrical signal thanks to an electrochemical transduction mechanism. As for other class of sensors, electrochemical sensors can employ two type of transducers.

The *energy conversion* transducer is employed when no voltage is applied to the circuit but rather the sensor itself produces electrical energy. This is the case of potentiometric sensors, where the sensor generates a voltage which is correlated to the amount of analyte binding to the receptor surface. Usually there is a logarithmic correlation between the analyte concentration and the electrical response generated.
With the *limiting-current* transducer, on the other hand, a voltage is applied to the electrochemical cell and a state is reached where the current flowing through the circuit linearly depends on the concentration of the electroactive species reacting. This kind of transduction is commonly used in voltammetric sensors, where the operator applies a potential that induces the electrochemical reaction of the analyte, thus allowing for both a qualitative and quantitative assessment.
Voltammetric sensors are based on a three-electrode cell, allowing to apply and control the voltage, which is usually varied within a defined potential range, in a specific branch of the circuit, while, in the other branch of the circuit, the developed current is registered. The three-electrode cells are composed of:

- Working electrode (WE): on its surface the redox reaction of the analyte occurs. Depending on the nature of the analyte, it can either act as cathode (for analyte reduction) or anode (for analyte oxidation). It is usually composed of noble metals such as gold, silver or platinum but also carbon-based materials.
- Counter electrode (CE): its presence allows to register the current flowing through the circuit. It is usually made of inert materials similar to those used for WE.
- Reference electrode (RE): since its presence is required to evaluate the voltage applied to the cell, it is crucial that this electrode is stable and at a known potential. Usually Ag/AgCl or Saturated Calomel Electrode are used.

The current developed after the reaction of the electroactive species on the working electrode is registered in the branch of the circuit between working and counter electrode, where the amperometer is placed, while the voltmeter is placed between working and reference electrode (**Figure 1.1**).

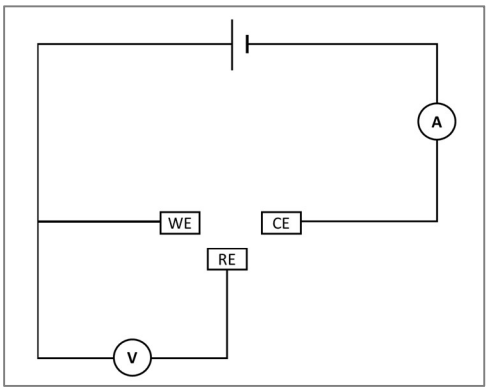

Figure 1.1. Schematic representation of a three-electrode cell.

During a voltammetric analysis two crucial phenomena control the analyte reaction: the mass transport of the analyte from the solution bulk to the electrode and the electron transfer between the species and the electrode. The mass transport can occur under three different regimes: convection, migration and diffusion.

The first is imposed by the operator by stirring the solution. The second is given by the ionic nature of the electroactive species which migrate to the electrode as a consequence of the electric field produced by the application of the voltage to the cell. However, this regime cannot be correlated to the analyte concentration and must therefore be avoided. This is achieved by adding in solution an excess of supporting electrolyte that moves to the electrode in the migration regime, avoiding the movement of the analyte under the same regime. Finally, the diffusion is the desirable regime by which analyte should move to the electrode in order to obtain information on the analyte concentration. A concentration gradient of the unreacted species is generated upon reaction of the electroactive species at the electrode/solution interface, which induces the movement of the analyte towards the surface, and this flow can be correlated to the analyte concentration through Fick's law. As for the electron transfer phenomena, it can be rationalized by taking into account the Butler-Volmer equation, which describes the current passing through an electrode as a function of the potential applied. In particular, two formulations of the equation (**Equation 1.1** and **Equation 1.2**) are reported below:

Equation 1.1 $$i(t) = nF\{k_{c,f}C_O(0,t)\exp\left[-\beta nF\left((\Delta\Phi)_{eq}+\eta\right)/RT\right] - k_{c,b}C_R(0,t)\exp\left[(1-\beta)nF\left((\Delta\Phi)_{eq}+\eta\right)/RT\right]\}$$

Where:

- $k_{c,f}$, $k_{c,b}$= chemical rate constants of the forward (f) or backward (b) reactions
- $C_O(0,t)$, $C_R(0,t)$= concentration of oxidized (O) or reduced (R) species at distance *0* from the electrode and time *t.*
- β = symmetry factor
- $(\Delta\Phi)_{eq}$= equilibrium potential
- η = overpotential

Equation 1.2 $i(t) = nFk_{s,h}\{C_O(0,t)\exp[-\beta nF(E-E^{0\prime})/RT] - -C_R(0,t)\exp[(1-\beta)nF(E-E^{0\prime})/RT]\}$

Equation 1.3 $k_{s,h} = k_{c,f}\exp\left[-\beta nF(\Delta\Phi^{0\prime})/RT\right] = k_{c,b}\exp\left[(1--\beta)nF(\Delta\Phi^{0\prime})/RT\right]$

Where:

- $k_{s,h}$ = heterogeneous standard rate constant for the charge transfer, explicited in **Equation 1.3**
- $E^{0\prime}$ = Standard reduction potential
- $\Delta\Phi^{0\prime}$= potential of the Oxidized/Reduced couple

The Butler-Volmer equation describes how the current increases exponentially with the increase of the applied voltage. Furthermore, the increase in current also depends on β, which is a factor that describes the symmetry of the current vs. overpotential plot (**Figure 1.2**) and it is a direct measure of the reversibility of the reaction.

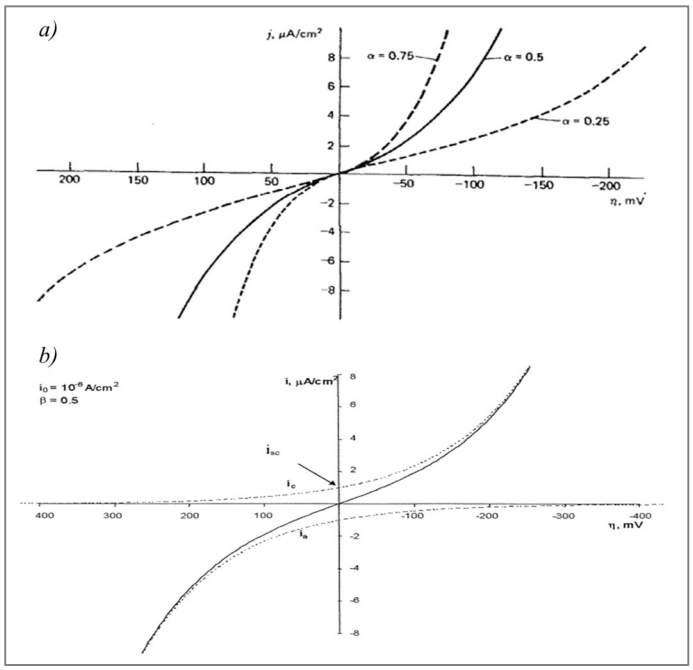

Figure 1.2. Current vs overpotential plots highlighting a) the effect of the reversibility of the electrochemical reaction on the curve and b) the contribution of the anodic and cathodic current to the final shape of the curve.

Different voltammetric techniques can be used employing the above-descripted three-electrode cell in order to evaluate the current developed by the system as a function of the applied voltage.

The most simple and straightforward is the Linear Sweep Voltammetry, where a linear ramp of potential is applied (**Figure 1.3a**) and the generated response current is registered. The peaks obtained with this technique show a unique shape (**Figure 1.3b**) where we have a first ascending part, where the current increases due to the increase in voltage applied and the electron transfer is the predominant factor, then the current peaks when the electron transfer reaches its maximum speed and the mass transfer begins to factor, resulting in the descending part of the peak until, finally, a constant flux of analyte reaches the electrode giving a stable current over time.

More information about the system can be obtained using the Cyclic Voltammetry (CV) technique, where the voltage is first linearly increased and then linearly decreased for repeated cycles (**Figure 1.3c**). The typical shape of the voltammogram (**Figure 1.3d**) shows a forward (oxidation) and backward (reduction) peaks, whose position and intensity gives an important information about the reversibility degree of the analyte under examination. In fact, for an

ideally reversible reaction, the distance in terms of voltage between the anodic and cathodic peak should be 57 mV/z, where z is the number of electrons involved in the electrochemical reaction of the analyte, and the intensity of the two peaks should be equal.

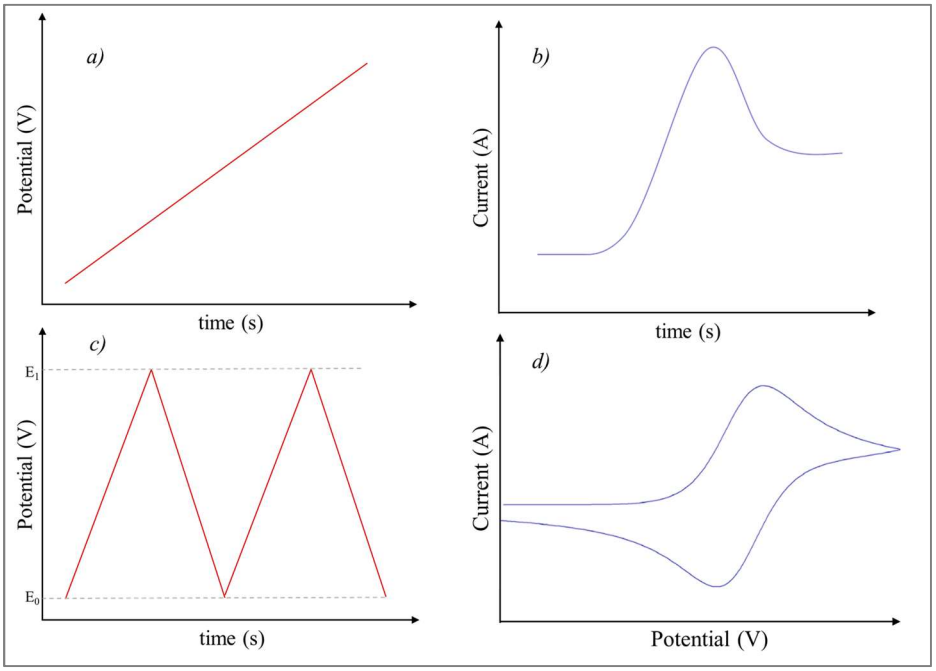

Figure 1.3.Representation of voltage applied over time for a) LSV and c) CV experiments and voltammograms generated through b) LSV and d) CV

However, for these techniques a critical limitation is given by the presence of a current which is not correlated to the analyte activity, i.e. the capacitive current. The latter is a direct consequence of the presence of supporting electrolyte, which, due to its charged nature, tends to concentrate on the electrode surface forming a charged double layer that acts as a capacitor. However, the capacitive current is subject to an exponential decrease with time, while the Faradaic current (i.e. the current given by the electrochemical species activity) follows a square root decrease with time. This principle is exploited in pulsed methods in order to clean the signal from the capacitive current. In particular, for the Differential Pulse Voltammetry (DPV), a series of pulses are superimposed to a step-increasing voltage ramp (**Figure 1.4a**) and the current is sampled shortly before the application and before the end of each pulse. In the final voltammogram the difference between the two measured currents is plotted against the applied voltage. This way, during the pulse the capacitive current tends to a minimum, and through the difference between the current it is

possible to "clean" the signal from this current (**Figure 1.4b**). However, it is of critical importance to optimize the parameter involved in the application of the pulses that are reported below:

- Step potential (SP), which is the difference between the potential before and after the pulse.
- Pulse amplitude (PA), which is the difference between the potential before and during the pulse.
- Interval time (IT), which is the time spanning from one pulse to the next.
- Pulse time (PT), which is the length of time over which the pulse is applied. This is probably the most critical parameter, since a too short PT would not reduce sufficiently the capacitive current, while a too long PT would decrease not only the capacitive but also the Faradaic current.

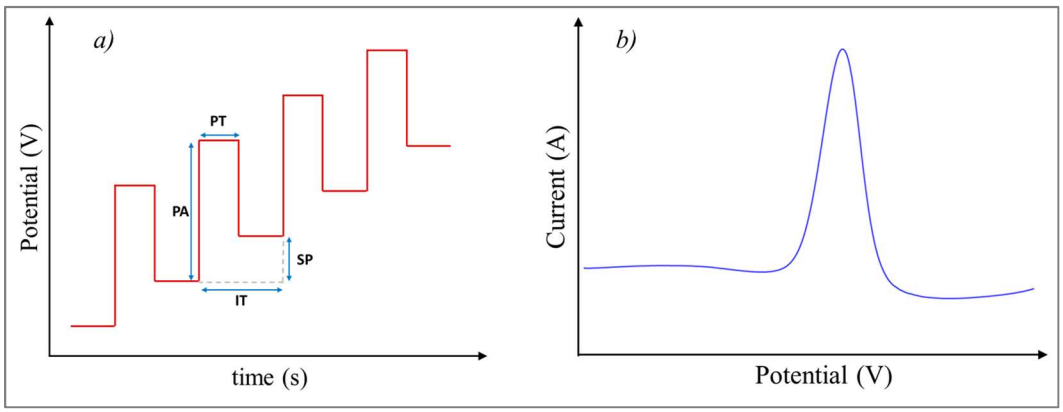

Figure 1.4. Representation of a) DPV potential ramp and b) example of DPV output voltammogram

The use of differential techniques such as DPV results in a significant improvement of the method in terms of sensitivity and limit of detection.

1.3. Screen printed electrodes (SPEs)

As previously discussed, a three-electrodes cell is required in order to conduct voltammetric analyses and it is commonly assembled using rods or disks of conducting materials for the electrodes. However, a cell based on rods/disks as electrodes usually requires a high volume of solutions for the functionalization and read-out steps which can be a major issue when working with biological material such as enzymes, oligonucleotides (both natural and synthetic), etc., given their high cost. However, a three-electrodes cell can also be obtained through serigraphic techniques. In fact, by using electrode materials (e.g.

graphite, silver, gold) as inks, it is possible to print a three-electrode cell on a support, such as ceramic, plastic or paper, thus obtaining a so-called Screen-Printed Electrode (SPE). Since this kind of electrodes can be mass-produced, they are commercially available at contained costs (typically 2-4 € per piece) [6] which is compatible with their disposable nature. Given the reduced dimension of the electrode surface (the WE has a diameter of 4 mm), SPEs require a much lower amount of solution per functionalization step, making them more fit for assays involving expensive biomolecules. Furthermore, a wide range of modified SPEs are commercially available already modified with different kinds of working electrodes substrates, including gold, glassy carbon, graphene, graphene oxide, reduced graphene oxide, carbon coated with streptavidin and with nanomaterials such as carbon nanotubes, carbon nanofibers, gold nanoparticles and quantum dots. (**Figure 1.5**).

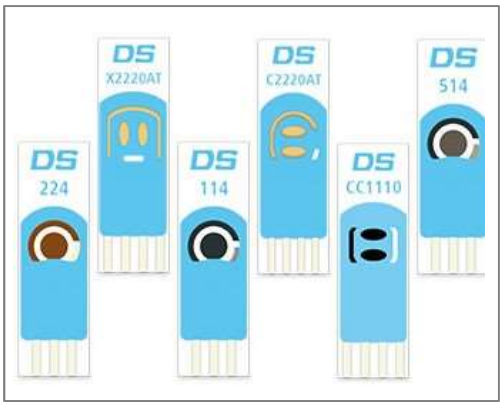

Figure 1.5. Examples of commercially available SPEs.

These variety in substrate composition translates into an increased number of techniques available for the immobilization of biomolecules, which can range from covalent immobilization on carboxylic functions of carbon nanotubes or on carboxylic functions electrochemically generated on carbon substrate [7], to direct adsorption of protein on gold employing the cysteine residues, or by creation of a self-assembled monolayer (SAM).
Thanks to the above cited features, SPEs represent a valuable analytical tool on which bio-assays can be studied and developed.

1.4. Biosensors

As stated previously, biosensors are defined as a separate class of sensors that employs a biochemical or biological mechanism for the recognition event. The

main advantage given by these systems is the very high specificity in analyte binding, as a consequence of the biological interactions involved, e.g. antigen-antibody, oligonucleotide hybridization, enzymatic reactions, etc. However, the downside of using such devices is represented by a usually high cost due to the biological materials involved in sensor development and an often low stability, either in working conditions or in long-term stocking.
The biological element of recognition is usually placed in close proximity of the transducer, however, in order to directly detect a biological analyte, this has to be electroactive with a moderate oxidation/reduction potential. Since these criteria are seldom met, biosensors often employ redox mediators for signal generations. Such species are proportional to the analyte concentration and they should have an easily achievable redox potential, highly reversible electrochemical properties, both oxidized and reduced form should be stable and no side reaction should occur.
An example of biosensor platform is represented by immunosensors, where the antigen-antibody specific interactions is used as recognition element for the determination of either antibody or antigen concentration. Another example is given by genosensors, where, in order to determine the concentration of a specific DNA/RNA sequence, its hybridization with an oligonucleotide capture probe sequence is employed.
Biosensors are widely used in a range of different fields, spanning from healthcare applications [8,9] to environmental monitoring [10-12] etc.

1.5. Nanomaterials application in chemical sensors

Nanomaterial is a broad concept indicating objects that have at least one of their dimensions in the nanometric scale. As a consequence, depending on how many dimensions fall within this size we can define nanoparticle, nanowires and nanosheets. The reduced dimensions have a profound impact on the properties which differ from the bulk material, e.g. effect on the distribution of the electronic levels in semiconductors. Upon implementation of these structures in chemical sensors [13-15] benefits can be obtained which derive mainly from an enhanced active surface area, as a consequence of the nanomaterials increased surface to volume ratio. Furthermore, nanomaterials offer advantages in biosensor fabrication given by the compatibility between the material and the biomolecules dimensions. As a consequence, a classic configuration for implementation of nanomaterial in biosensors consists on

conjugation of a biological unit (e.g. oligonucleotides, antibodies, proteins, etc.) with a nanomaterial, which can be useful for different purposes, e.g. signal enhancement, labelling, etc. Below are reported some of the most employed nanomaterials in biosensors fabrication.

1.5.1. Gold nanoparticles

Gold nanoparticles are exploited mainly for their desirable electronic properties and inert nature [16]. They can be obtained by reduction of $AuCl_4^-$ with sodium borohydride ($NaBH_4$). The obtained particles tend to aggregate in solution, therefore an agent that prevents this occurrence must be present in the reaction medium. For this purpose, citric acid can be used as both a reducing and protecting agent against particles coagulation. However, by using a thiol molecule, it is possible to also incorporate new functionalities in the nanoparticles through reaction with a heterobifunctional molecule that bears a functional group such as carboxyl or amine, which can be exploited for conjugation with biomolecules.

On this topic, different strategies have been devised [17]. The most common approach for conjugation relies on the high affinity between sulphur and gold (**Figure 1.6B**). In fact, proteins bearing thiol residues such as cysteine can be directly chemisorbed on the nanoparticles surface [18]. If no cysteine residues are available on the target protein but amine residues are present, the Traut's reagent (2-iminothiolane) has been used in order to induce the presence of sulphur on the protein prior to interaction with the gold nanoparticle (**Figure 1.6C**). Finally, streptavidin or avidin can be conjugated with gold nanoparticles in order to immobilize protein or oligonucleotides modified with a biotin (**Figure 1.6D**).

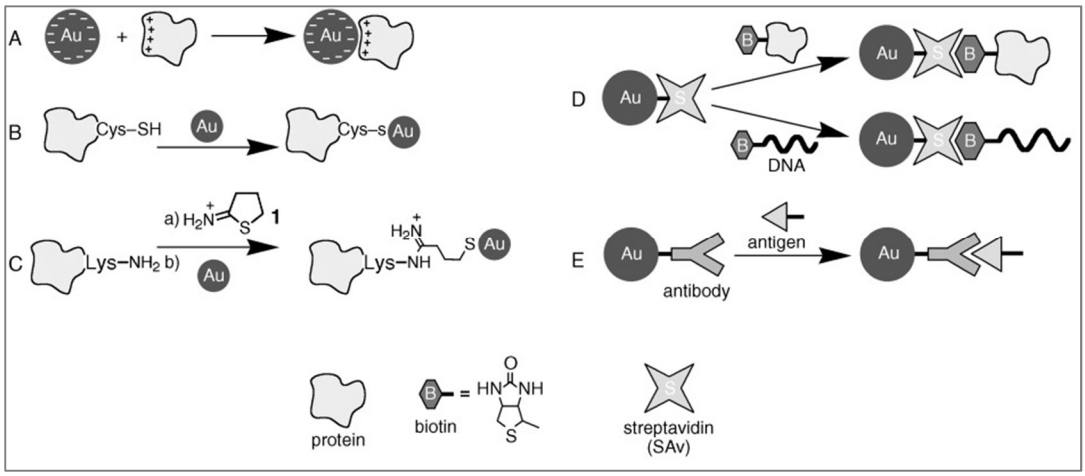

Figure 1.6. Strategies for conjugation of Au-NPs with biomolecules. Reprinted with permission from E. Katz, et al. © 2004 WILEY-VCH Verlag.

The implementation of gold nanoparticles to electrochemical sensors surface yields an enhancement in signal intensity given by the increase in both electrical conductivity and active surface area onto which receptors can be immobilized. Gold nanoparticles properties can be exploited also for optical transduction. In fact, metal nanoparticles are capable of interacting with incident light by adsorbing part of the radiation and scatter light. This is the result of the nanoparticles electrons behaviour, which is to collectively oscillate under an incident electromagnetic field, generating a so-called plasmon resonance [19].
In optical sensors, gold nanoparticles can be exploited to monitor changes in the shift of the plasmon frequency as a consequence of interaction with the analyte. Gold nanoparticles can also act as quencher for fluorescence in molecular beacon approach [20]. Finally, gold nanoparticles can be exploited in mass-sensitive sensors as labels [21-23], where the conjugation between the target analyte and a metal nanoparticle would result in a great enhancement of the mass change upon recognition and immobilization of the analyte on the sensitive surface.

1.5.2. Dendrimers

These molecular nanomaterials are obtained by consecutive covalent bonding reactions starting from a core molecule and resulting in a characteristic branched spherical structure, typically less than 10 nm wide [24]. Starting from the core, on each reaction step a new bifunctional molecule is introduced with new functionalities that will react in the following step, becoming a so-called

branching point. The number of branching points that can be found moving from the centre to the terminal functionalities of the structure defines the generation of the dendrimer. The final polymeric molecule is composed of a core, an inner shell and an outer shell bearing the functionalities exposed for conjugation purposes (**Figure 1.7**). The main application of dendrimers to chemical sensors are related to their ability to greatly enhance the number of active functionalities upon immobilization on the sensor surface. This way, an increased number of receptors can be bound to the dendrimer and interact with the target analyte, resulting in an enhancement of the output signal [25,26].

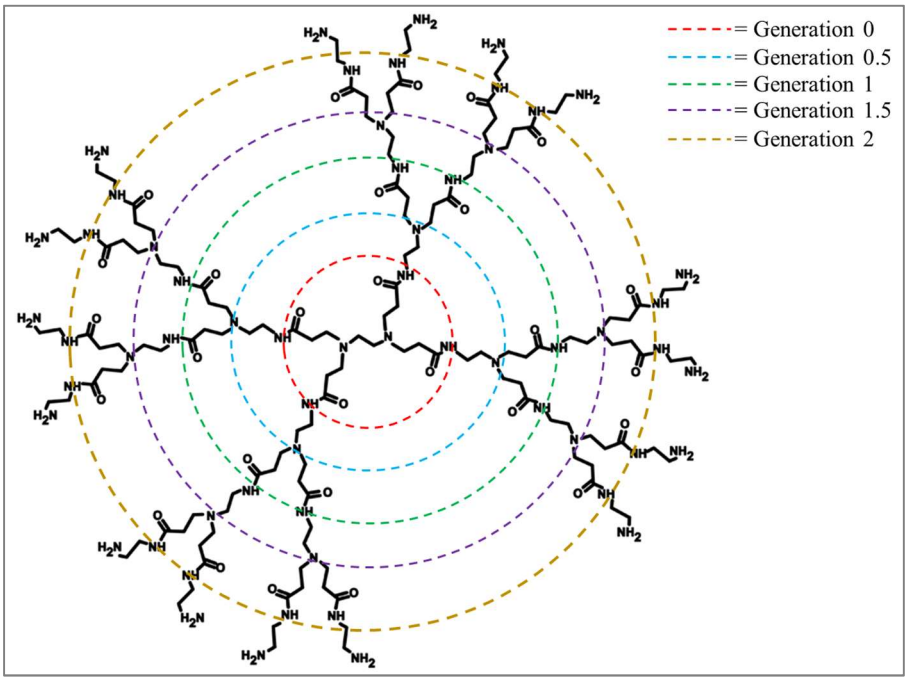

Figure 1.7. Structure of a generation 2 PAMAM dendrimer.

1.5.3. Quantum Dots

Among semiconductor materials exploited for chemical sensor fabrication, nanosized crystals of elements of the II and VI group such as cadmium selenide (CdSe) and cadmium telluride (CdTe), are among the most promising. That is because these semiconducting compounds, also known as Quantum Dots (QDs) [27-29], display discrete energy levels for both bonding and antibonding levels, as a consequence of their reduced size. In particular, the bandgap separating these levels is dependent on the dimensions of the nanoparticle, therefore QDs

can absorb the incident light at a specific wavelength and subsequently relax to fundamental state by emission at a wavelength that depends on the particles size. As a consequence of the possibility to tune the optical properties as a function of the particles size, the most relevant applications of QDs are found in the optics field [30].
The classical synthetic pathways yield QDs with hydrophobic surface [31]. Therefore, for functionalization of these nanosized structure, bifunctional molecules containing thiols are used which introduce new functionalities useful for immobilization of biomolecules.
The main application of QDs in sensing techniques consists in their employment as fluorescence label. In fact, they represent an improvement over traditional fluorophores since they possess a high quantum yield (between 20% and 70%), high stability under extended excitation and their efficiency is not related to pH. Furthermore, since they display a broad absorption and narrow emission band, several different QDs can be excited with a single beam and emit at different wavelength, which is crucial when using diversely labelled analytes and cannot be easily achieved with traditional fluorophores. For these reason QDs are widely employed through conjugation with biomolecules of interest such as oligonucleotides, antibodies and proteins [32-33].

1.5.4. Magnetic micro- and nano-particle

Beads in the micro- (2 – 400 μm) and nano-scale (10 – 100 nm) can be obtained from materials such as Fe_2O_3, Fe_3O_4 etc. The resulting compounds show a paramagnetic behaviour, where the application of a magnetic field results in a magnetization of the material, however, when the magnetic field is removed, no residual magnetization is maintained. In particular, nanosized magnetic particle possess a superparamagnetic behaviour, where particles behave as paramagnetic materials above a certain temperature (blocking temperature), however below this temperature their behaviour becomes ferromagnetic, retaining a residual magnetization even after the removal of the magnetic field. They can be obtained through liquid-phase reaction in presence of an agent that prevents self-aggregation, yielding particles with hydrophobic coatings [34]. However, such coating is incompatible with biological interactions, therefore different methodologies have been conceived in order to obtain a hydrophilic surface containing functionalities useful for biomolecules conjugation. For example, an amphiphilic surfactant can be added to the

solution so that its hydrophobic region interacts with the particle surface while the hydrophilic surface is exposed to the solvent. Another strategy consists in replacing the hydrophobic coating by using small bifunctional molecules such as cysteamine.

Magnetic particles are mainly employed in biosensor design in relation with the advantages offered by magnetic separation [35]. In fact, biomolecules covalently bound to magnetic beads can be easily and quickly separated from the reaction solution by application of a magnetic field. This results in more efficient separation and washing step. Furthermore, the interaction between the receptor and the analyte when the former is anchored to the sensing surface is restricted by diffusion of the target from the bulk solution to the receptor. However, when the receptor is immobilized on a magnetic particle the diffusion phenomena is less critical since the beads are dispersed in solution. As a result, the transduction element surface can be left free of functionalization.

1.5.5. Carbon Nanotubes

In recent years, different carbon-based materials proved particularly apt for sensor fabrication thanks to their desirable physical and chemical properties [35-36]. Such materials consist of carbon in its graphite allotropic form, with a structure composed of carbon atoms in their sp^2 hybridization state interconnected through π-type bonds. Among these materials, Carbon NanoTubes (CNTs) have been extensively studied and applied in chemical sensing [13, 37-41]. Their structure can be visualized as sheets of graphene (a monoatomic graphite layer) rolled up to form hollow tubes. In the case of Single-walled CNTs (SWCNTs) a single cylindrical unit is obtained, while Multi-Walled CNTs (MWCNTs) present a given number of concentric cylindrical unit. The final materials have a diameter size ranging from 0,4 to 2 nm and a length which varies between 50 nm to approximately 1 cm (**Figure 1.8**).

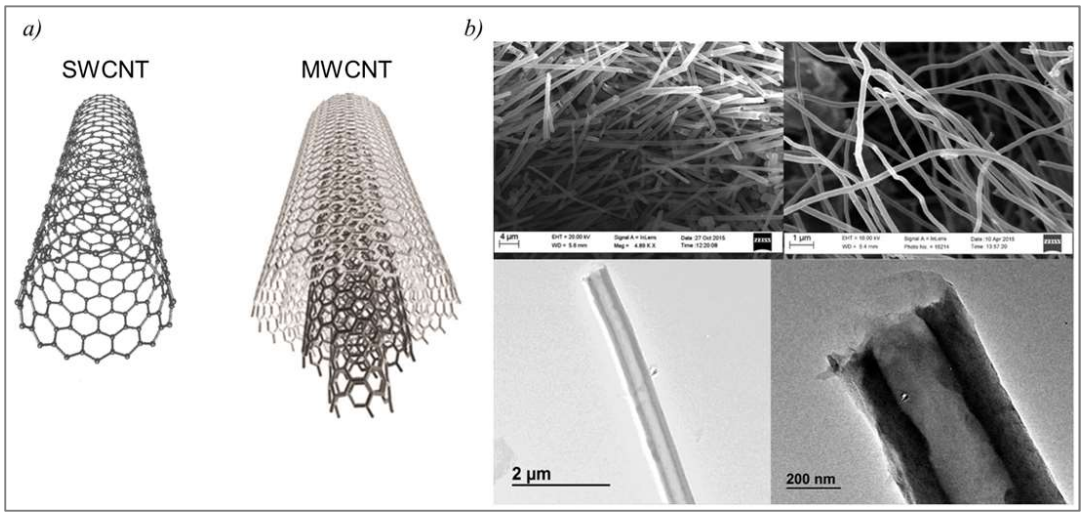

Figure 1.8. a) Schematic representation of Single-Walled Carbon Nanotubes and Multi-Walled Carbon Nanotubes and b) SEM and TEM images of SWCNT reported by J. Ren et al. in [42].

The most efficient method for CNT synthesis consists in Chemical vapour deposition (CVD) technique, where a mixture of carbon gases (acetylene, ethylene, ethanol or methane) and carrier gas (nitrogen, argon or hydrogen) is fluxed at hundreds of Celsius degrees over a metal catalyst (typically nickel, cobalt or iron) onto which CNTs grow and are subsequently cleaved from through acid treatment.

SWCNTs can either display a metallic or a semiconducting behaviour, depending on geometrical parameters of the structure, while MWCNTs can only be metallic substrate. Unfortunately control over CNTs final structure during synthesis remains a challenge, therefore purification methods must be applied to isolate the desired form.

The obtained CNTs show a closed structure where the tube terminals are capped and must be opened by acid treatment for further applications. In fact, through tube opening, oxygen groups such as carboxylic, hydroxyl and quinones are obtained at the rims of the cylinder, which provide useful anchoring point for biomolecules or for immobilization of the CNTs [43,44]. Besides covalent immobilization exploiting the terminal oxygen functionalities, CNTs functionalization can be carried out also through non-covalent attachment and encapsulation [45]. The former exploits the π-π stacking phenomenon between the tube's walls and an aromatic molecule such as pyrene [46,47]. In particular by functionalization of a bio-compound with pyrene moieties, non-covalent attachment to CNTs surface can be obtained. Oligonucleotides can establish the same kind of interaction through π-π

stacking with nucleobases, which can lead to the wrapping of the oligonucleotide around the CNT. As for encapsulation, taking into account the nano-size of CNTs cavity, it is also possible for species of compatible size to be inserted in the hollow cylinder. In the case of inorganic compounds such as metals and metallocenes the encapsulation can be monitored by changes in the CNT electronic properties.

One of the main applications of CNTs is given by their implementation as electrode material, resulting in both an increased electrode surface area, useful for receptor immobilization purposes, and an enhancement in the electron transfer phenomena [48], thanks to their electrical conductivity and overall electronic properties. Semiconducting type SWCNTs have been also implemented to develop field-effect transistor-based biosensors.

Beside electrical application, it is also worth mentioning that CNTs can be employed in optical sensing [49]. In fact, semiconducting SWCNTs possess the valence and conduction bands separated by a well-defined bandgap, therefore an electron can be excited through absorption of incident light from the valence to the conducting band and subsequently relax back to the fundamental state by emission of light. The energy difference between the two states in semiconducting CNTs requires a wavelength for electron excitation which is in the near-infrared region, where no interferences are present from fluorescence of biological components. However, the quantum yield for CNTs fluorescence is very modest. Alternatively, CNTs can be exploited to monitor the Raman scattering, which occurs for both semiconducting and metallic CNTs. The advantages of using this optical mode are given by the high signal over noise ratio displayed by CNTs Raman signal which allows to obtain low detection limits.

1.6. References

[1] Pure and Applied Chemistry, Chemical sensors definitions and classification 63(9), 1991, 1247-1250.

[2] Gründler, P. (2007) Chemical sensors: an introduction for scientists and engineers. Springer Science & Business Media.

[3] Shao, Y., Wang, J., Wu, H., Liu, J., Aksay, I. A., & Lin, Y. (2010). Graphene based electrochemical sensors and biosensors: a review. *Electroanalysis: An International Journal Devoted to Fundamental and Practical Aspects of Electroanalysis*, 22(10), 1027-1036.

[4] Fan, X., White, I. M., Shopova, S. I., Zhu, H., Suter, J. D., & Sun, Y. (2008). Sensitive optical biosensors for unlabeled targets: A review. *Analytica Chimica Acta*, 620(1-2), 8-26.

[5] Janshoff, A., Galla, H. J., & Steinem, C. (2000). Piezoelectric mass-sensing devices as biosensors—an alternative to optical biosensors? *Angewandte Chemie International Edition*, 39(22), 4004-4032.

[6] Ricci, F., Adornetto, G., & Palleschi, G. (2012). A review of experimental aspects of electrochemical immunosensors. *Electrochimica Acta*, 84, 74-83.

[7] Zanardi, C., Ferrari, E., Pigani, L., Arduini, F., & Seeber, R. (2015). Development of an electrochemical sensor for NADH determination based on a caffeic acid redox mediator supported on carbon black. *Chemosensors*, 3(2), 118-128

[8] Kim, J., Campbell, A. S., de Ávila, B. E. F., & Wang, J. (2019). Wearable biosensors for healthcare monitoring. *Nature biotechnology*, 37(4), 389-406.

[9] Kumar, S., Ahlawat, W., Kumar, R., & Dilbaghi, N. (2015). Graphene, carbon nanotubes, zinc oxide and gold as elite nanomaterials for fabrication of biosensors for healthcare. *Biosensors and Bioelectronics*, 70, 498-503.

[10] Palchetti, I., & Mascini, M. (2008). Nucleic acid biosensors for environmental pollution monitoring. *Analyst*, 133(7), 846-854.

[11] Bidmanova, S., Kotlanova, M., Rataj, T., Damborsky, J., Trtilek, M., & Prokop, Z. (2016). Fluorescence-based biosensor for monitoring of environmental

pollutants: from concept to field application. *Biosensors and Bioelectronics*, 84, 97-105.

[12] Bahadır, E. B., & Sezgintürk, M. K. (2015). Applications of commercial biosensors in clinical, food, environmental, and biothreat/biowarfare analyses. *Analytical biochemistry*, 478, 107-120

[13] Maduraiveeran, G., Sasidharan, M., & Ganesan, V. (2018). Electrochemical sensor and biosensor platforms based on advanced nanomaterials for biological and biomedical applications. *Biosensors and Bioelectronics*, 103, 113-129.

[14] Maduraiveeran, G., & Jin, W. (2017). Nanomaterials based electrochemical sensor and biosensor platforms for environmental applications*. Trends in Environmental Analytical Chemistry*, 13, 10-23.

[15] Kurbanoglu, S., Ozkan, S. A., & Merkoci, A. (2017). Nanomaterials-based enzyme electrochemical biosensors operating through inhibition for biosensing applications. *Biosensors and bioelectronics*, 89, 886-898.

[16] Daniel, M. C., & Astruc, D. (2004). Gold nanoparticles: assembly, supramolecular chemistry, quantum-size-related properties, and applications toward biology, catalysis, and nanotechnology. *Chemical reviews*, 104(1), 293-346.

[17] Katz, E., & Willner, I. (2004). Integrated nanoparticle–biomolecule hybrid systems: synthesis, properties, and applications. *Angewandte Chemie International Edition*, 43(45), 6042-6108.

[18] Lee, J. M., Park, H. K., Jung, Y., Kim, J. K., Jung, S. O., & Chung, B. H. (2007). Direct immobilization of protein G variants with various numbers of cysteine residues on a gold surface. *Analytical chemistry*, 79(7), 2680-2687

[19] Sau, T. K., Rogach, A. L., Jäckel, F., Klar, T. A., & Feldmann, J. (2010). Properties and applications of colloidal nonspherical noble metal nanoparticles. *Advanced Materials*, 22(16), 1805-1825.

[20] Dou, X., Chu, X., Kong, W., Luo, J., & Yang, M. (2015). A gold-based nanobeacon probe for fluorescence sensing of organophosphorus pesticides. *Analytica chimica acta*, 891, 291-297.

[21] Manfredi, A., Mattarozzi, M., Giannetto, M., & Careri, M. (2014). Piezoelectric immunosensor based on antibody recognition of immobilized open-tissue transglutaminase: An innovative perspective on diagnostic devices for celiac disease. *Sensors and Actuators B: Chemical*, 201, 300-307.

[22] Patolsky, F., Ranjit, K. T., Lichtenstein, A., & Willner, I. (2000). Dendritic amplification of DNA analysis by oligonucleotide-functionalized Au-nanoparticles. *Chemical Communications*, (12), 1025–1026.

[23] Nie, L. B., Yang, Y., Li, S., & He, N. Y. (2007). Enhanced DNA detection based on the amplification of gold nanoparticles using quartz crystal microbalance. *Nanotechnology*, 18(30), 305501.

[24] Lee, C. C., MacKay, J. A., Fréchet, J. M., & Szoka, F. C. (2005). Designing dendrimers for biological applications. *Nature biotechnology*, 23(12), 1517.

[25] Giannetto, M., Mori, L., Mori, G., Careri, M., & Mangia, A. (2011). New amperometric immunosensor with response enhanced by PAMAM-dendrimers linked via self assembled monolayers for determination of alpha-fetoprotein in human serum. Sensors and Actuators B: Chemical, 159(1), 185-192.

[26] Giannetto, M., Umiltà, E., & Careri, M. (2014). New competitive dendrimer-based and highly selective immunosensor for determination of atrazine in environmental, feed and food samples: The importance of antibody selectivity for discrimination among related triazinic metabolites. *Analytica chimica acta*, 806, 197-203.

[27] Alivisatos, A. P. (1996). Semiconductor Clusters, Nanocrystals, and Quantum Dots. *Science*, 271(5251), 933–937.

[28] Baker, S. N., & Baker, G. A. (2010). Luminescent carbon nanodots: emergent nanolights. *Angewandte Chemie International Edition*, 49(38), 6726-6744.

[29] Burda, C., Chen, X., Narayanan, R., & El-Sayed, M. A. (2005). Chemistry and properties of nanocrystals of different shapes. *Chemical reviews*, 105(4), 1025-1102.

[30] Murphy, C.J. (2002) Optical sensing with quantum dots. *Analytical Chemistry*, 74, 520A–526A.

[31] Trindade, T., O'Brien, P., & Pickett, N. L. (2001). Nanocrystalline semiconductors: synthesis, properties, and perspectives. *Chemistry of Materials*, 13(11), 3843-3858.

[32] Michalet, X., Pinaud, F. F., Bentolila, L. A., Tsay, J. M., Doose, S. J. J. L., Li, J. J., Sundaresan, G., Wu, A. M., Gambhir, S. S. & Weiss, S. (2005). Quantum dots for live cells, in vivo imaging, and diagnostics. *Science*, 307(5709), 538-544.

[33] Jamieson, T., Bakhshi, R., Petrova, D., Pocock, R., Imani, M., & Seifalian, A. M. (2007). Biological applications of quantum dots. *Biomaterials*, 28(31), 4717-4732.

[34] Frey, N. A., Peng, S., Cheng, K., & Sun, S. (2009). Magnetic nanoparticles: synthesis, functionalization, and applications in bioimaging and magnetic energy storage. *Chemical Society Reviews*, 38(9), 2532-2542.

[35] Stankovich, S., Dikin, D. A., Dommett, G. H., Kohlhaas, K. M., Zimney, E. J., Stach, E. A., Piner, R. D., Nguyen, S. T. & Ruoff, R. S. (2006). Graphene-based composite materials. *Nature*, 442(7100), 282.

[36] Hsing, I. M., Xu, Y., & Zhao, W. (2007). Micro-and nano-magnetic particles for applications in biosensing. *Electroanalysis: An International Journal Devoted to Fundamental and Practical Aspects of Electroanalysis*, 19(7-8), 755-768.

[37] Baughman, R. H., Zakhidov, A. A., & De Heer, W. A. (2002). Carbon nanotubes--the route toward applications. *Science*, 297(5582), 787-792.

[38] Yang, N., Chen, X., Ren, T., Zhang, P., & Yang, D. (2015). Carbon nanotube based biosensors. *Sensors and Actuators B: Chemical*, 207, 690-715.

[39] Łukaszewicz, J. P. (2006). Carbon materials for chemical sensors: a review. *Sensor Letters*, 4(2), 53-98.t

[40] Rivas, G. A., Rodriguez, M. C., Rubianes, M. D., Gutierrez, F. A., Eguilaz, M., Dalmasso, P. R., Primo, E. N., Tettamanti, C., Ramirez, M. L., Montemerlo, A., Parrado, C., & Gallay, P. (2017). Carbon nanotubes-based electrochemical (bio) sensors for biomarkers. *Applied Materials Today*, 9, 566-588.

[41] Giannetto, M., Bianchi, M. V., Mattarozzi, M., & Careri, M. (2017). Competitive amperometric immunosensor for determination of p53

protein in urine with carbon nanotubes/gold nanoparticles screen-printed electrodes: A potential rapid and noninvasive screening tool for early diagnosis of urinary tract carcinoma. *Analytica chimica acta*, 991, 133-141.

[42] Ren, J., & Licht, S. (2016). Tracking airborne CO 2 mitigation and low cost transformation into valuable carbon nanotubes. *Scientific reports*, 6, 27760.

[43] Balasubramanian, K., & Burghard, M. (2006). Biosensors based on carbon nanotubes. *Analytical and Bioanalytical Chemistry*, 385(3), 452–468

[44] Li, J., Ng, H. T., Cassell, A., Fan, W., Chen, H., Ye, Q., Koehne, J., Han, J., & Meyyappan, M. (2003). Carbon nanotube nanoelectrode array for ultrasensitive DNA detection. *Nano letters*, 3(5), 597-602.

[45] Zhou, Y., Fang, Y., & Ramasamy, R. P. (2019). Non-covalent functionalization of carbon nanotubes for electrochemical biosensor development. *Sensors*, 19(2), 392.

[46] García-Aljaro, C., Cella, L. N., Shirale, D. J., Park, M., Muñoz, F. J., Yates, M. V., & Mulchandani, A. (2010). Carbon nanotubes-based chemiresistive biosensors for detection of microorganisms. *Biosensors and Bioelectronics*, 26(4), 1437–1441

[47] Taft, B. J., Lazareck, A. D., Withey, G. D., Yin, A., Xu, J. M., & Kelley, S. O. (2004). Site-Specific Assembly of DNA and Appended Cargo on Arrayed Carbon Nanotubes. *Journal of the American Chemical Society*, 126(40), 12750–12751.

[48] Musameh, M., Wang, J., Merkoci, A., & Lin, Y. (2002). Low-potential stable NADH detection at carbon-nanotube-modified glassy carbon electrodes. *Electrochemistry Communications*, 4(10), 743-746.

[49] Kruss, S., Hilmer, A. J., Zhang, J., Reuel, N. F., Mu, B., & Strano, M. S. (2013). Carbon nanotubes as optical biomedical sensors. *Advanced drug delivery reviews*, 65(15), 1933-1950

2. Genosensors

2.1. Genosensor working principles

Deoxyribonucleic acid (DNA) is a biological molecule composed of repeating units called nucleotides. Such monomers are in turn composed of a deoxyribose unit possessing a phosphate group at the 5' position and a nucleobase in the 1' position. The Ribonucleic Acid (RNA) is an analogous molecule that, however, presents a ribose instead of the deoxyribose unit (**Figure 2.1**). There are 4 fundamental nucleobases that can be found in DNA, namely Adenine (A), Guanine (G), Cytosine (C) and Thymine (T), while in RNA the latter is replaced by Uracil (U) (**Figure 2.1**). The nucleotide units are joined through a phosphate bond, where a phosphoric group on the 5' position, binds the hydroxyl function on the 3' position of the adjacent nucleotide. Through this mechanism a DNA strand composed of several nucleotide is formed, with a different nucleobase on each unit, thus determining the oligonucleotide sequence.

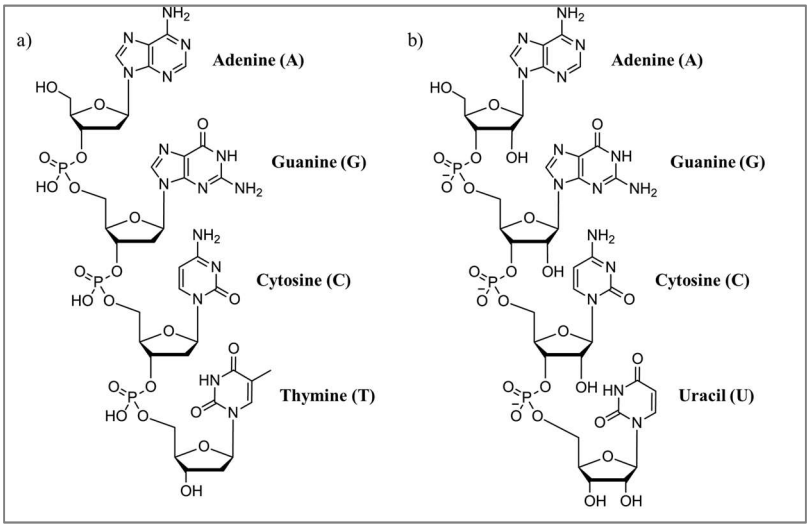

Figure 2.1. Backbone structures of a) DNA and b) RNA molecules

Nucleobases are capable of establishing specific hydrogen bond, called "Watson-Crick" interactions, between pairs, in particular, C can pair with G and A can pair with T (or U in the case of RNA). Thanks to these interactions, and an additional gain given by the stabilizing stacking interactions between paired nucleobases, two oligonucleotide strands can interact and be joined in the so-called hybridization event to form the well-known double helix structure.

DNA performs a fundamental role in nearly every cell of a living organism, that is the storage and transmission of the genetic information. In fact, the expression of a protein in a cell requires the transcription of the DNA sequence coding for that specific protein in a messenger RNA (mRNa) strand. The latter is subsequently translated inside the ribosome into transfer RNA (tRNA) molecules bearing specific amino acids that are coupled to form the final protein.

Given its ubiquitous presence in biological organisms, the detection of a selected DNA sequence with a high degree of specificity granted by the hybridization event, is a powerful tool for analytical purposes. In fact, it can be exploited for the detection of Single Nucleotide Polymorphism (SNP), often involved in the development of diseases, or sequences introduced for genetic mutation purposes. For this reason, genosensing systems are conceived to both determine the presence of a specific oligonucleotide sequence and measure its concentration. In order to do so, they rely on the hybridization event occurring between a target analyte and a probe immobilized on the sensor, which, based on its sequence, is capable to discriminate between target oligonucleotide and other non-complementary strands. Once the hybridization has occurred, a difference in the measured signal is required and must be proportional to the concentration of the hybridized species.

2.2. Oligonucleotide mimics

Over the years a need for innovative molecules capable of hybridizing oligonucleotides has arisen, not only for diagnostic but also therapeutic purposes. An example is given by antisense therapy [50], where genetic disorders are treated by inactivation of the mRNA through hybridization with a compatible probe. However, ordinary DNA or RNA-based probes perform poorly for mRNA inhibition, since they are susceptible to nuclease degradation, for this purpose oligonucleotide mimics have been developed [51,52] (**Figure 2.2**). These can efficiently hybridize the mRNA target, but are resistant to nuclease degradation and, in some cases, are capable of recruiting the enzyme RNAse-H to degrade the mRNA to which they are hybridized.

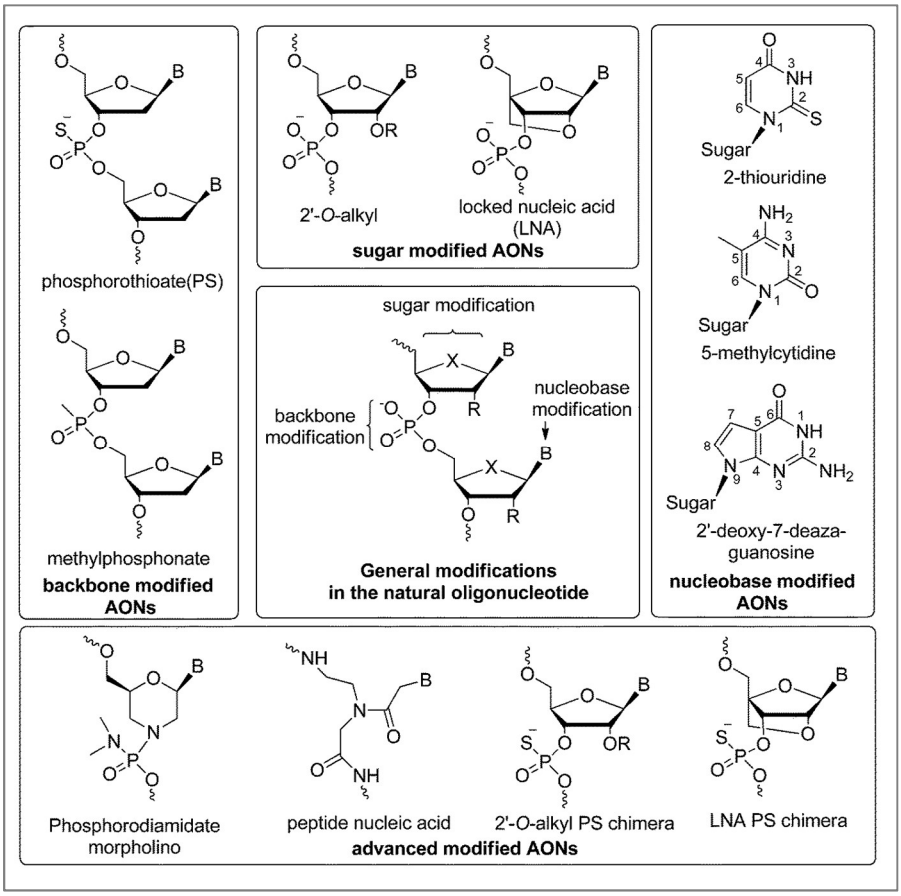

Figure 2.2. Ensemble of different generation of oligonucleotide mimics (Antisense Oligonucleotides; AONs). Reprinted with permission from V.K. Sharma et al. [53] © 2014 Royal Society of Chemistry

Early attempt to modification led to the first generation of modified oligonucleotides, where an oxygen of the phosphate group has been replaced with a sulphur (phosphorothioate) or a methyl. Several phosphorothioates-based drugs are currently in use for medical treatment through antisense therapy, e.g. Fomivirsen, Mipomersen, Eteplirsen. Even though first-generation oligonucleotide mimics show an enhanced resistance to nuclease, ability to recruit RNAse H and good pharmacokinetics, on the downside they have low selectivity and, when used in high dosage, cytotoxicity issues arise. To improve these aspects, further generations of antisense oligonucleotides (ASOs) have been explored.

Second generation introduced modification on the ribose unit of the RNA backbone, namely the substitution of the hydroxyl group on the 2' C with an O-methyl or O-methoxyethyl group [54]. This modification decreased the occurrence of cytotoxic events, however the ability to induce RNA degradation

through RNAse H activity, which is believed to be the main working principle behind efficient antisense therapy, cannot be achieved with this generation of ASOs [55]. This aspect can be overcome by using the so-called chimeric oligonucleotides [56], where the external regions of the probe are composed of 2'-O-methyl-modified ribonucleotides while the central region consists of phosphorothioates capable of inducing RNAse H activity. These mixed-backbone oligonucleotides allow to maintain the advantages of the first-generation while reducing the side effects by incorporation of the second-generation modifications in the terminal regions of the strand.
To further improve the stability, affinity and efficiency, a large number of third-generation ASOs has been developed, among which Locked-Nucleic Acids (LNAs) [57], Phosphoroamidate Morpholino Oligonucleotides (PMOs) [58] and Peptide Nucleic Acids (PNAs) are some of the most promising [59].
LNA structure presents a methylene bridge connecting the oxygen on the 2' position with the 4' C. This modification leads to a great enhancement in the hybridization efficiency of the probe, as proved by the increase in melting temperature (T_m) of the LNA/DNA hybrid [60,61].While the LNAs maintain the resistance to nuclease, they are not capable to induce RNAse H degradation of the mRNA target, it is however suitable to be integrated in a chimeric oligonucleotide assembly with DNA/RNA and can therefore be used for antisense therapy [62].
PMOs modification consists in a replacement of the ribose ring with a morpholine ring and each unit is connected by phosphoroamidate bonds instead of phosphodiester bond, rendering the molecule neutral. Like many other ASOs, it is not capable of recruiting RNAse H, however it is capable of blocking the translational event by steric hindrance effect, that prevents ribosomal assembly.

2.2.1. Peptide Nucleic Acids

In 1991, Nielsen et al. reported a study conducted on a novel class of molecules capable of hybridizing DNA strands called Peptide Nucleic Acids [63,64]. PNAs have a structure that only loosely resembles the DNA, in fact the sugar and phosphate backbone is replaced altogether by amino acids which are concatenated together through amide bonds to form the PNA strand backbone. More in depth, 2-aminoethylglycine units are modified in order to bear a nucleobase, then through solid phase synthesis small peptides are obtained,

where on each amino acid a nucleobase is present (**Figure 2.3a**). The peculiarity of PNA is that the nucleobases in a strand possess the correct distance in order to be able to hybridize natural oligonucleotides. Furthermore, since PNA backbone bears no negatively charged group, it doesn't suffer from electrostatic repulsion upon hybridization with another oligonucleotide strand, resulting in an enhanced stability of the duplex, as proved by the higher melting temperatures obtainable. This translates into an increased hybridization efficiency and a superior capability of discrimination against nucleobase mutation in the target strand. It is also worth mentioning that PNAs can give both Watson-Crick interactions, used to form a duplex structure with DNA or RNA (**Figure 2.3b**), and Hoogsteen interactions (**Figure 2.3c**), that occur between a PNA strand and the functional groups of nucleobases that are left free after duplex formation, thus resulting in a triplex PNA-DNA-PNA structure [65]. PNA can hybridize oligonucleotides both in a parallel (peptide C-Term facing the 3'- oligonucleotide end) and anti-parallel (peptide N-Term facing the 3'-oligonucleotide end) manner, however the latter is preferred (**Figure 2.3b**), leading to a higher duplex stability. PNAs show a high chemical and biological stability, being resistant to nuclease, but they are not suitable for RNAse H activity, in fact its antisense activity relies on the steric hindrance of the PNA-RNA duplex which prevents the translational event [66,67].

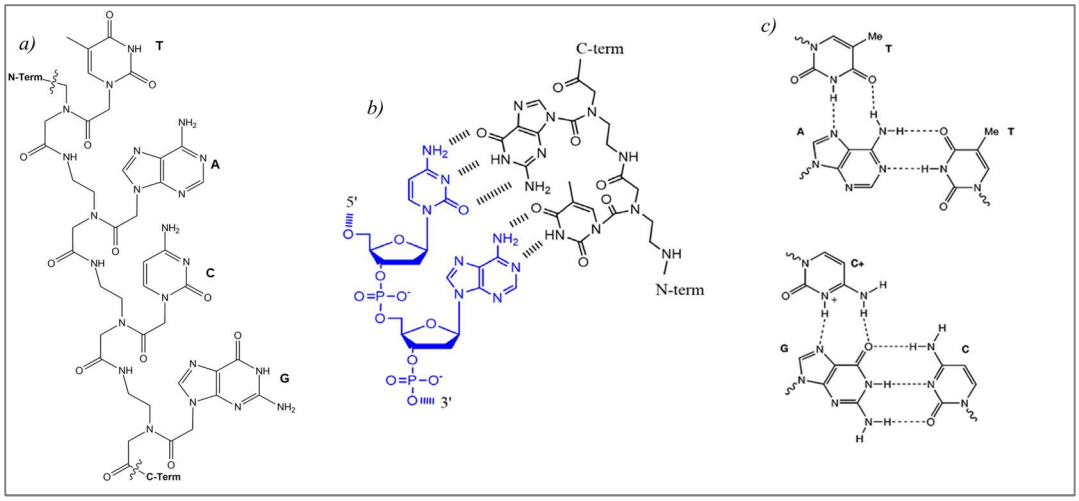

Figure 2.3. Representation of a) PNA backbone structure, b) hybridization of a PNA (black) and DNA (blue) strand through Watson-Crick interactions in an antiparallel duplex and c) nucleobases involved in both Watson-Crick and Hoogsteen interaction, reprinted with permission from M.J. Hannon [68] © 2007 Royal Society of Chemistry.

Another feature that distinguish PNAs as powerful tools both in diagnostic and therapeutic fields, is the synthetic pathway through which they are obtained (i.e. solid-phase synthesis) [69], which allows for direct introduction of new functionalities. For PNA solid phase synthesis, a resin modified with a spacer bearing a terminal amino or hydroxyl function is commonly employed. The spacer binds the carboxyl function of the first amino acid, leading to, respectively, an amide or ester bond. The resin must possess specific requirements:

- Contain reactive sites on which the peptide chain can be bound and grown
- Show high stability in the reaction working conditions
- Allow a fast and free interaction between reagents and the growing peptide chain
- Be easily separable from the liquid phase in every step of the reaction
- Be highly functionalized in order to achieve high yield

One of the main advantages given by this type of synthesis is the fact that, on each step, the separation of reagents from products can be achieved by simple wash and filtration of the resin. This allows to reach high yields in short times and with a good level of purity. PNA monomers require the protection of the terminal amine group and of other amine group that might be present on the molecule with orthogonal groups in order to avoid side reactions. The main protection strategies used for PNA are the Boc (tert-butyloxycarbonyl) and Fmoc (Fluorenylmethyloxycarbonyl) strategy. The choice of either one is based on what kind of functionalities the molecules conjugated to PNA possess, e.g. if acid-sensitive groups are present, Boc strategy cannot be followed because it requires the use of acid for deprotection steps. The amine groups of the heterocycles of A, T, C, G and U must be protected in a semipermanent way, i.e. using groups that are stable during each phase of the synthesis. Some examples of these orthogonal groups are Carbobenzyl (Cbz) for Boc strategy and Boc or Benzhydryloxycarbonyl (Bhoc) for Fmoc strategy (**Figure 2.4**).

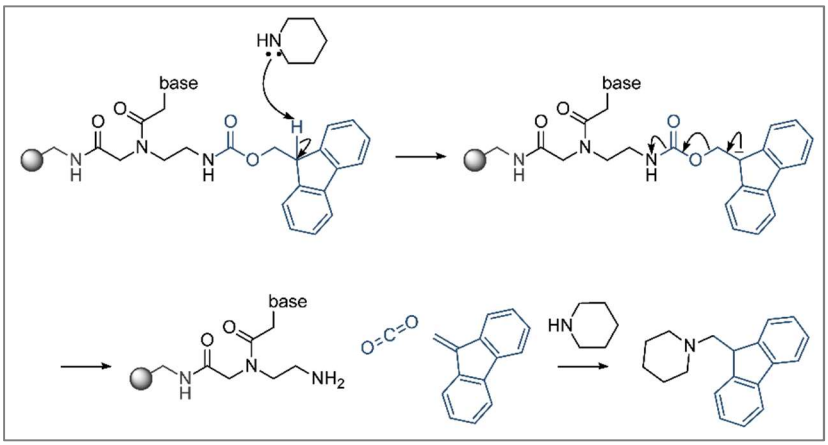

Figure 2.4. Deprotection mechanism of the Fmoc protecting group (light blue) with piperidine

The solid-phase synthesis consists of a number of reiterated steps that are carried out for every amino acid that is bound to the final peptide chain (**Figure 2.6**). The cycle starts with the deprotection of the terminal nitrogen of the last amino acid bound to the resin or the growing peptide chain. Then a new protected monomer undergoes coupling with the previously deprotected amino acid. To carry out this condensation, activating reagents are required, e.g. an uronium salt such as HBTU (2-(1H-benzotriazol-1-yl)-1,1,3,3-tetramethyluronium hexafluorophosphate) (**Figure 2.5**).

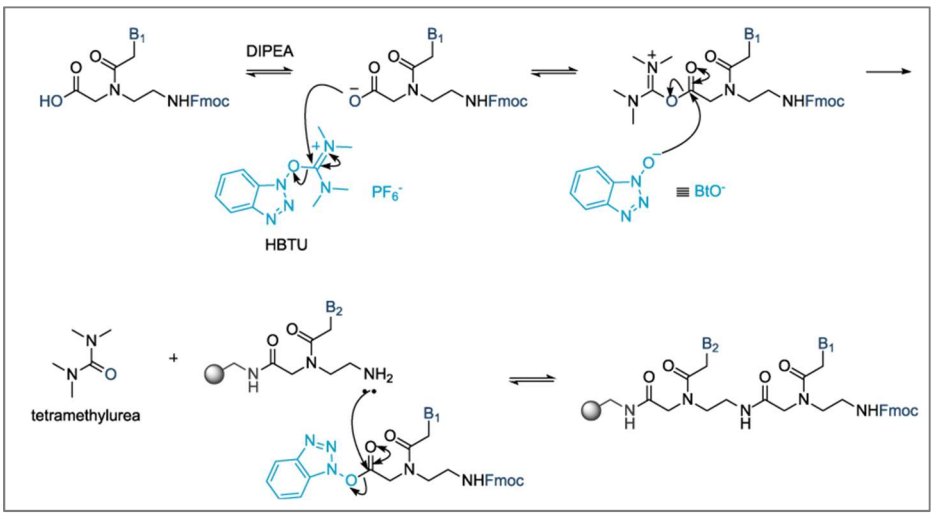

Figure 2.5. Mechanism of the coupling reaction assisted by the activation of the carboxylic function by HBTU (light blue).

After the coupling step, the final step consists of an acylation of the residual activated carboxyl functions with acetic anhydride solution, in order to block those chains in which the coupling reaction hasn't been successful. In fact, the

acetylation, or capping, is very important because it avoids the growth of chains with errors in the nucleobase sequence due to a failed coupling step. Once these chains are blocked, they are no longer capable of being activated and undergo coupling and during the purification step they can be removed. These steps are reiterated until the final sequence is obtained, then the PNA is cleaved from the resin using conditions that simultaneously deprotect the semi-permanent protecting groups (e.g. Trifluoroacetic acid, TFA).

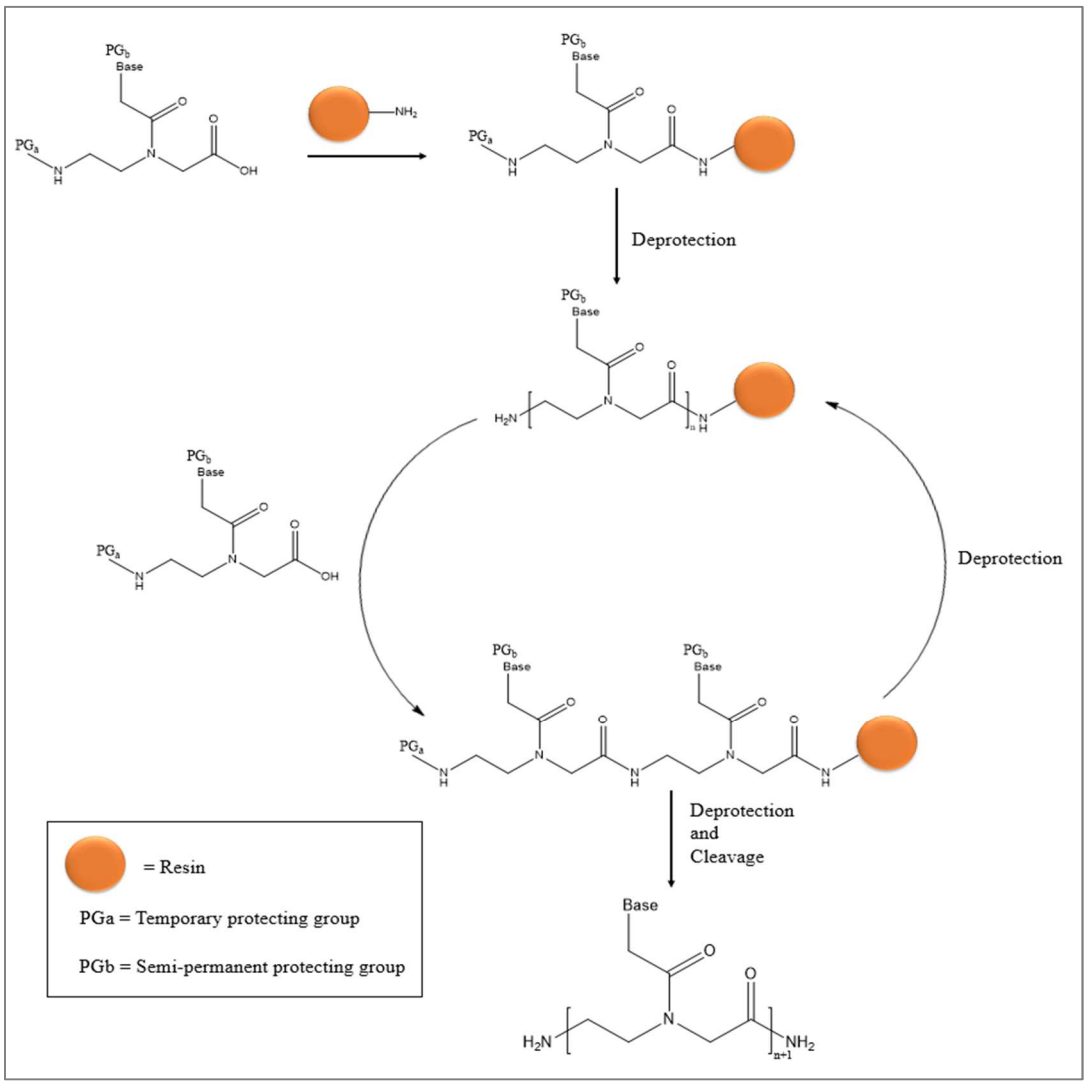

Figure 2.6. General scheme for solid-phase synthesis of PNA

It is fairly easy to insert modification in the PNA strand simply by using modified monomers during the synthesis. As a consequence, it is possible to

obtain PNA modified with functional groups that enhance their application in many fields [70]. For example, reactive groups for surface immobilization can be introduced (e.g. thiol, amine and biotin), electroactive species (e.g. ferrocene and methylene blue), amino acids with modified nucleobases can be used, etc.

2.3. Genosensing technologies

During the last decades genosensors have been developed exploiting a wide range of transduction mechanism. Reported below are some of the techniques and methods used as of this day to detect and quantify specific oligonucleotides sequence.

2.3.1. Colorimetric assays

Colorimetry is a technique that allows for determination of a species concentration by measurement of the absorption at a selected wavelength in the visible range (390 - 700 nm). Several analytes, among which nucleotides, do not absorb in the visible spectrum, therefore a species that changes its absorption properties after interaction with analytes is required.
Metal nanoparticles are often used for this purpose, among which gold nanoparticles (AuNPs) have been extensively exploited. In fact, AuNPs show a shift from red to blue in the absorption as a consequence of their aggregation in solution [71]. This property can be exploited to devise new biosensing assays. For example, it has been shown that double stranded DNA (dsDNA) does not adsorb to AuNPs while single stranded DNA (ssDNA) is capable of interacting with the gold surface. The reason for this behaviour is given by electrostatic interactions, in fact, AuNPs in solution are usually stabilized by the presence of negatively charged species such as citrate that adsorbs on the nanoparticles surface. Given that dsDNA only exposes the negatively charged phosphates, the electrostatic repulsion with the citrate ions prevents its adsorption on the AuNPs, while ssDNA has free nucleobases that can interact strongly with gold, overcoming the electrostatic repulsion of phosphate groups. As a consequence of ssDNA adsorption, the aggregation of AuNPs in solution is hindered [72]. Therefore, colloidal AuNPs can be added to a solution containing two ssDNAs; if these are not complementary, then they can adsorb on the gold surface preventing nanoparticles aggregation and the solution will maintain a red colour, conversely, if the two ssDNAs are complementary, dsDNA is formed which cannot adsorb on AuNPs resulting in nanoparticle aggregation shifting

the solution colour to blue. A critical parameter for this kind of assays is represented by salt concentration, which can screen the electrostatic repulsion and lead to the formation of AuNPs aggregates.
An improvement for colorimetric techniques has been achieved by modification of AuNPs with carbohydrates, which allowed to overcome limitations such as the need of a low salt concentration which is not compatible with biological fluids and sustainability of nanoparticles synthesis [73].
In 2018 Baetsen-Young et al. reported a colorimetric method for detection of pathogen DNA using dextrin modified AuNPs [74]. The assay employs a ssDNA probe, which is capable of hybridizing the genomic DNA after the latter has been partially denatured. After hybridization, a portion of the genomic DNA will be left as ssDNA since it has been replaced by the probe and such genomic ssDNA is capable of stabilizing AuNPs preventing their aggregation (**Figure 2.7**). The proposed method is capable of working at relatively high salt concentration and leads to a limit of detection of 2.94 fM of unamplified genomic DNA.

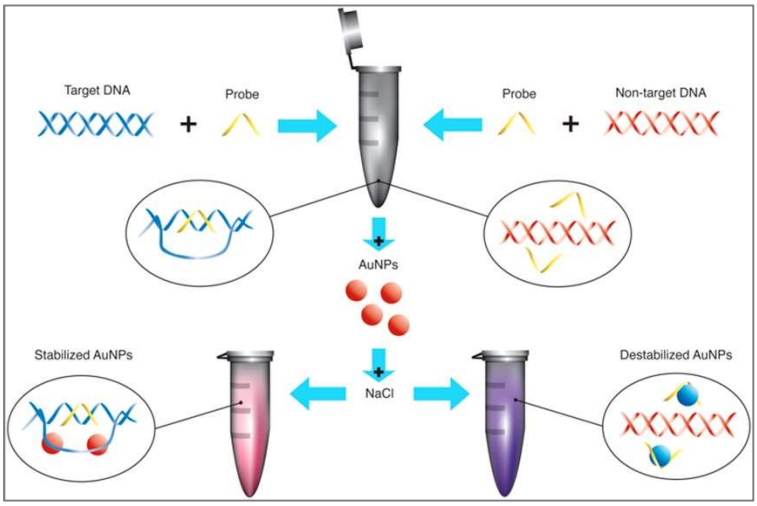

Figure 2.7. Colorimetric assay mechanism proposed in [74]. Reprinted with permission from Baetsen-Young et al. © 2018 Elsevier.

2.3.2. *Fluorescence*

Fluorescence is a property of specific molecules which, upon excitation by light absorption, relax to the fundamental state by emission of an electromagnetic wave. This property has been extensively exploited in biosensing over the years and frequently applied to genosensing. The advantages in using fluorescence for sensor fabrication are connected primarily to the high specificity of the

phenomenon, which can only occur when a proper molecule (i.e. the fluorophore) is excited, thus reducing the probability of false positive or interferents in solution.
The most direct application of fluorescence to DNA detection is to label the analyte with a fluorophore, this way, after hybridization with a capture probe bound to the sensor surface, fluorescence emission will be measured. The labelling of DNA can be carried out with modest yields [75,76] or using a labelled primer during PCR amplification of the target DNA (see paragraph 2.3.7).
Some fluorescent molecules (**Figure 2.8**) are capable of inserting between two layers of paired nucleobases in dsDNA through a mechanism called intercalation [77]. Despite the lack of recognition of the hybridized oligonucleotides in which intercalators insert, they are capable of revealing the occurrence of the hybridization event. One of the first molecule employed for these assays is ethidium bromide [78], however novel complexes have been explored in order to improve the sensitivity of the method. For example, Wu et al. reported in 2007 the development of a fluorescent Zn complex with intercalating properties, used to reach a limit of detection of 19,3 nM [79].

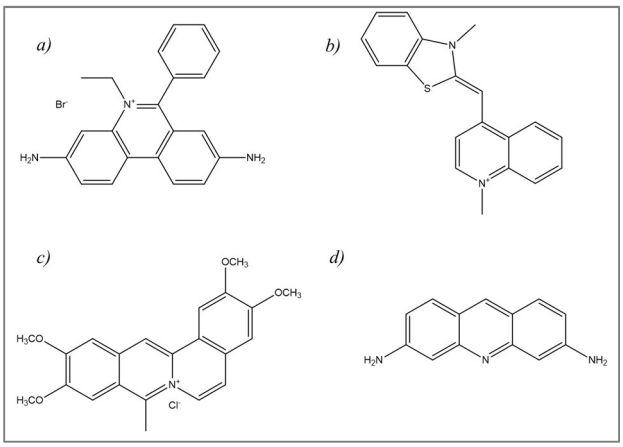

Figure 2.8. Structures of fluorescent intercalators. a) Ethidium bromide, b) thiazole orange, c) coralyne and d) proflavine.

Other methods do not require the derivatization of the analyte. In fact, it is possible to use a secondary probe, bearing the fluorophore, complementary to the target DNA in a portion of the sequence different to the one recognized by the capture probe. After the hybridization between target oligonucleotide and capture probe has occurred, a second hybridization with the fluorophore-labelled probe is carried out, thus forming a sandwich complex [80].

One of the most common formats for implementation of fluorescence detection in genosensing systems involves the exploitation of a molecular beacon [81]. Usually in this configuration, a fluorophore is inserted at the 5'-end while a quencher is inserted at the 3'-end. The role of a quencher is to provide an alternative way for the relaxation of the fluorophore through FRET (Forster Resonance Energy Transfer) phenomenon, thus preventing the emission of the fluorophore. In order to observe energy transfer between fluorophore and quencher under FRET regime, the two species must be in very close proximity (i.e. 3-9 nm) which is the case when the hairpin loop is closed. In fact, a hairpin loop is a ss-DNA molecule, usually bound to the sensor surface, which has two region of its sequence which are complementary and spontaneously undergo hybridization, resulting in a close configuration where the two ends of the DNA are spatially close. When the stem loop is closed, the fluorophore and quencher are close enough to be in the FRET regime, while, when the complementary target analyte is present, the hybridization of the latter with the hairpin central sequence causes the stem loop to unfold and drives the fluorophore away from the quencher, allowing the fluorescence emission to be detected (**Figure 2.9a**).

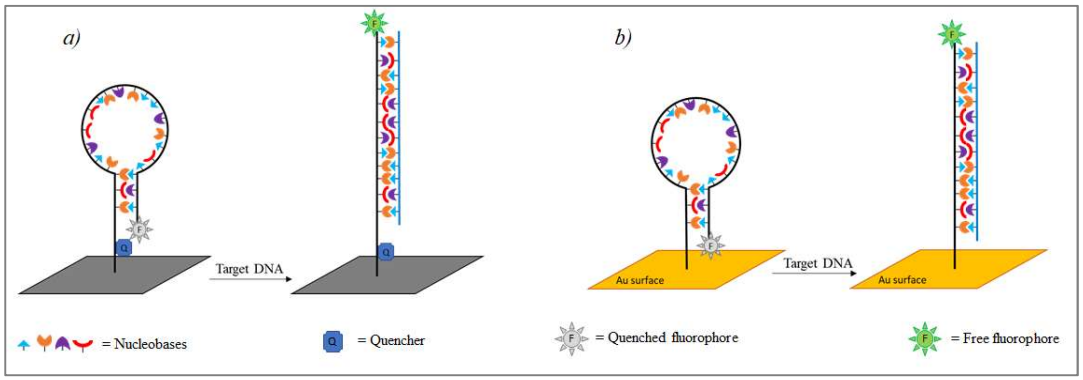

Figure 2.9. Schematic working mechanism of fluorescent molecular beacon. a) the closed structure keeps the fluorescent molecule and the quencher in close proximity, while hybridization with the target opens the structure allowing the fluorophore activity. b) when the molecular beacon is immobilized on a gold substrate, the latter acts as a quencher for the molecule fluorescence.

A molecular beacon that requires no quencher has been reported by Huang et al. in 2010 [82], since the immobilization of the hairpin was conducted on a gold surface that acts on its own as a quencher for fluorescence emission. Therefore, also in this case when the stem loop is closed no signal is detected since the fluorophore is in close proximity of the gold surface (**Figure 2.9b**). The application of this method resulted in a simplification of the sensor design and resulted in a limit of detection of 0.3 nM concentration of target DNA.

2.3.3. SPR

Surface Plasmon Resonance is an optical technique extensively employed in sensing and biosensing. The working principle exploits the property of noble metals, among which gold is the most used for SPR measurements, to generate surface plasmons, i.e. electrons in an oscillating state, after being irradiated by a light source [83]. A widely used configuration for the instrument is the Kretschmann configuration (**Figure 2.10**) where a laser irradiates, through a prism, a thin gold layer. When the angle of the incident light reaches the total internal reflection, surface plasmon resonance is observed and the plasmons generated in the metal are capable of absorbing a portion of the energy from the laser, thus decreasing the intensity of reflected light. A minimum in reflection is achieved at a specific angle called "surface plasmon resonance angle". While the electrons oscillate in the gold layer, they generate an evanescent wave that propagates outside the metal and probes the surrounding region. Being the position of the minimum critically dependent on the refractive index of the medium, when the evanescent wave propagates through a surface that has undergone some degree of functionalization, the position of the minimum shifts compared to the untreated surface. So, by fixing the incident angle of the light, it is possible to monitor the variation of the signal over time given by modification of the surface. Such modification can be the consequence of the binding of a protein, the antigen-antibody interaction or hybridization of two oligonucleotide strands. The evanescent wave can penetrate and probe the surface for a depth in the range of several hundreds of nanometres [84].

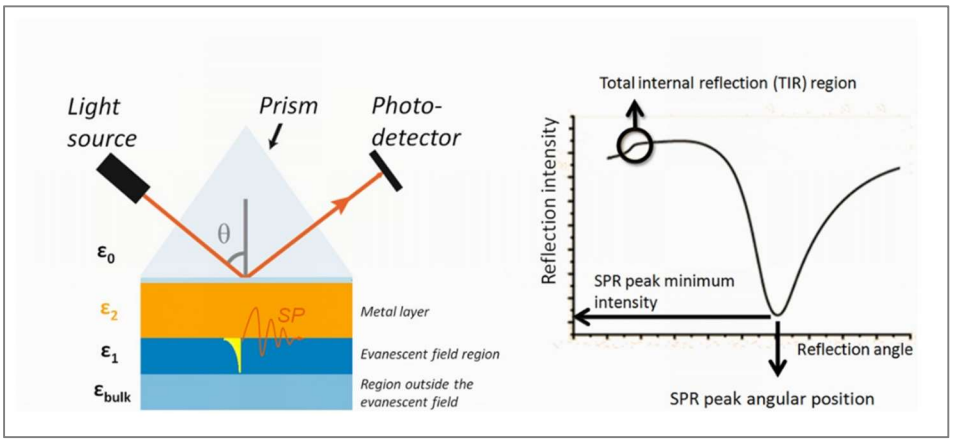

Figure 2.10. Kretschmann configuration of the SPR technique (left) and variation of the reflection intensity as a function of the angle of incidence (right). Reprinted with permission from Vitala et al. [84] © (2013) PloS one

SPR represents a powerful technique given that it does not require any type of labelling to generate the analytical signal and can perform time resolved measurements yielding information on systems kinetics [85]. Furthermore, the evanescent wave generated during an SPR experiment can be exploited in order to excite a fluorophore and carry out a simultaneous fluorescence measurement in the so-called surface plasmon field-enhanced fluorescence spectroscopy [86].

Genosensing systems that employ SPR technology for transduction are based on the hybridization of target DNA to an oligonucleotide immobilized on the sensor surface through different techniques. For instance, in 2004 Wang et al. employed a thiol-functionalized oligonucleotide capture probe, which self-assembles on the surface thanks to the formation of spontaneous gold-thiol interactions [87]. The authors reported an improvement of such immobilization method as compared to biotin-streptavidin interactions for immobilization of a biotinylated oligonucleotide [88] and a limit of detection of the method of 2,5 nM. In 2008, Xu et al. employed the surface plasmon field-enhanced fluorescence spectroscopy in order to evaluate the effect that probe density has on hybridization efficiency on surfaces with different geometry [89]. Flat gold surface has been compared to gold particle layer (**Figure 2.11**). To obtain different surface coverages of biotinylated capture probe the surface was functionalized in order to have increasing streptavidin densities. The target DNA was labelled with a fluorescent tagged to increase the system sensitivity. Furthermore, a neutrally charged DNA-mimic, i.e. Peptide Nucleic Acid, was also

employed as capture probe and compared with the DNA capture probe in order to better understand the effect of electrostatic repulsion.

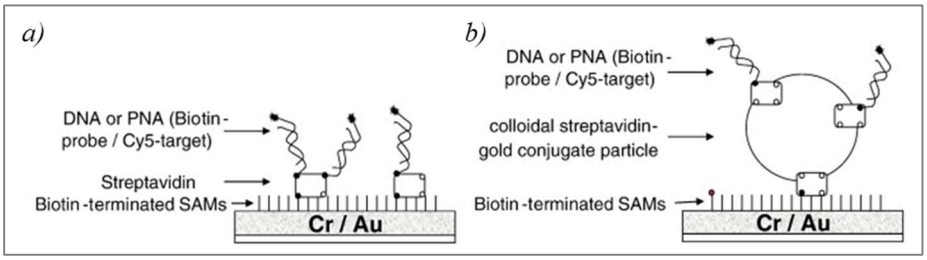

Figure 2.11. Different surface functionalization obtained using a) streptavidin and b) streptavidin-gold nanoparticle conjugate on biotin-functionalized sensor surface to evaluate the effect of surface geometry on hybridization efficiency. Reprinted with permission from Xu et al. [89] © 2008 Elsevier

It was found that electrostatic interactions critically affect the hybridization efficiency due to the repulsion between neighbouring double strands as well as between strands that from the bulk solution approach the surface negatively charged by DNA already hybridized. Furthermore, the use of PNA can improve the hybridization efficiency given its neutral nature, even though a negative hindrance effect is still present.

2.3.4. FET

A Field-Effect Transistor (FET) (**Figure 2.12**) is a device capable of controlling the current flow between two electrodes, namely the source and drain. In fact, the current is regulated by an electrical field generated by the application of a potential difference between the gate and source electrode. However, perturbations of the electrical field, such as interactions with charged species, influence the current intensity that flows between the source and drain electrodes, which are connected by a semiconductive material. Therefore, in a FET biosensor [90-92] the interaction with charged biological species such as protein and oligonucleotides in close proximity of the semiconductive material or on the gate terminal generates a difference in the signal output as a consequence of the perturbation of the electrical field. Being DNA a polyanionic molecule, its immobilization and hybridization in the surface area generates a shift in signal useful for the development of FET-based genosensors [93].

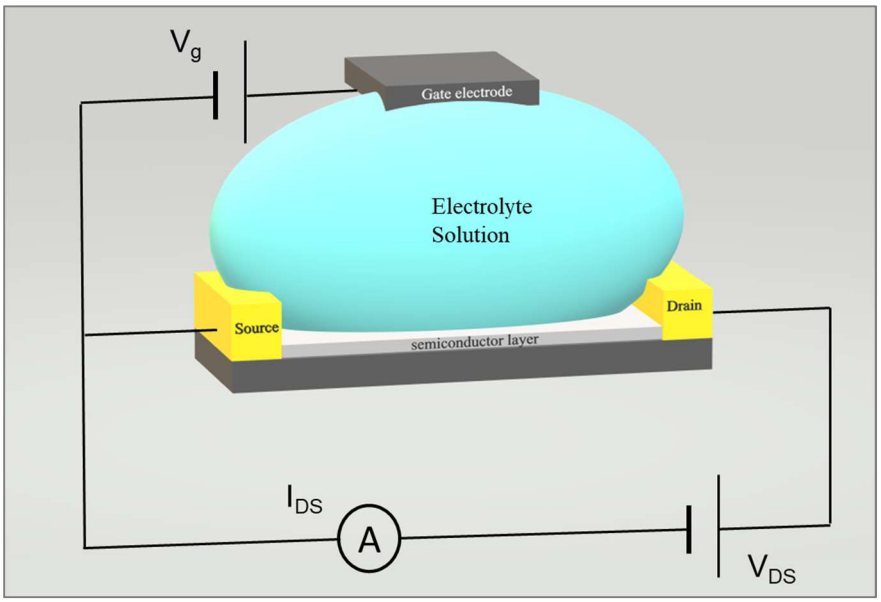

Figure 2.12. Schematic example of an electrolyte-gated Field Effect Transistor.

A recent trend marked a growing implementation of carbon-based materials as semiconducting substrates for FET, exploiting in particular Carbon Nanotubes [94] and graphene [95]. The choice of graphene as semiconducting materials is based on its outstanding electronic properties [96] and enhanced active surface. Furthermore, taking into account that graphene is a monolayer of carbon atoms, each atom interacts with the analyte, allowing to reach a better sensitivity.

In 2014 Cai et al. published a work reporting the development of a genosensing system based on a reduced Graphene Oxide (rGO)-FET, where the rGO was deposited on the FET and employed both as semiconductive material and immobilization substrate for the capture probe [97]. For the latter, a PNA-based probe was chosen, and its immobilization was carried through the use of a heterobifunctional linker bearing a pyrene at one end, that interacts through π-π stacking with the rGO, and an ester at the other end that covalently binds the capture probe that will subsequently hybridize the target DNA (**Figure 2.13**). This technique led to a detection limit of 100 fM, with a good differentiation between full-match target DNA and single-mismatch target DNA (i.e. complementary DNA sequence with a single non-complementary nucleobase).

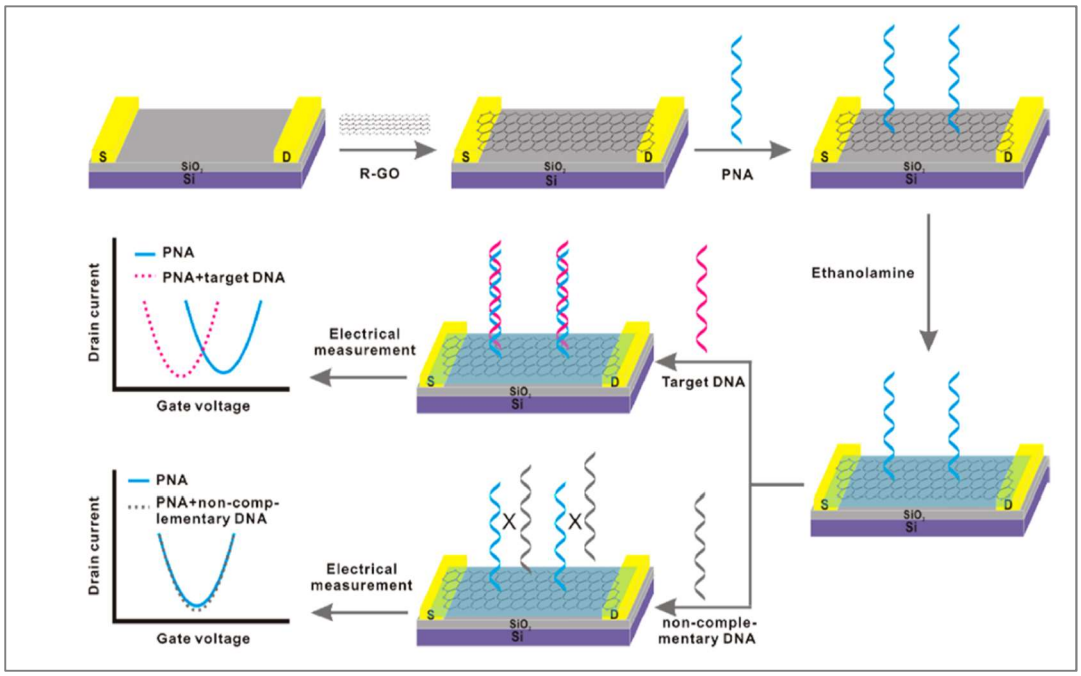

Figure 2.13. Scheme of sensor modification reported in [97] to develop the FET-based genosensor. Reprinted with permission from Cai et al. © 2014 American Chemical Society

In 2019, Campos et al. reported the fabrication of a genosensing FET in extended-gate configuration (EGFET), i.e. a configuration where the gate electrode is physically separated from the sensing membrane responsible for analyte recognition, with a single graphene layer connecting source and drain terminals. The graphene layer is derivatized in an analogous manner as reported by Cai et al., i.e. using a heterobifunctional linker (**Figure 2.14**). This system proved capable of reaching a limit of detection of 25 aM in DNA concentration with a good discrimination against single-nucleotide polymorphism [98].

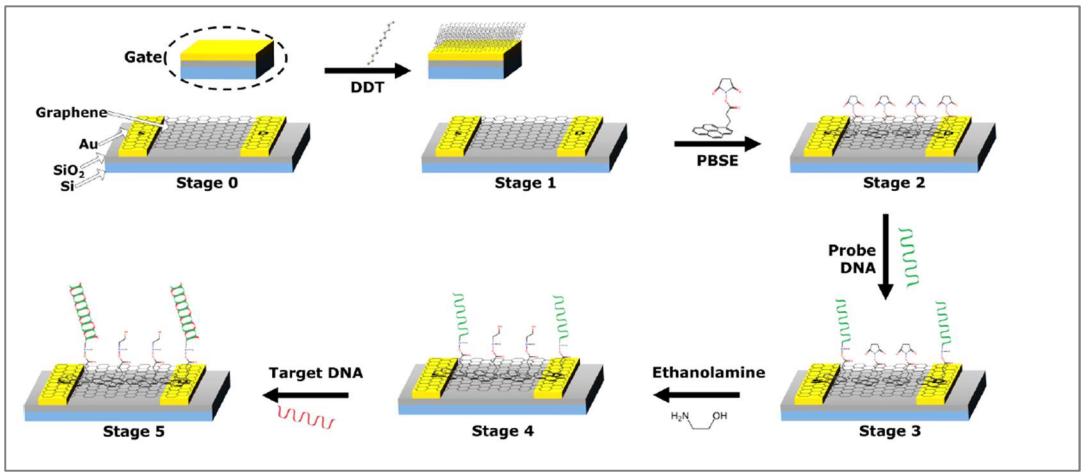

Figure 2.14. Functionalization scheme reported in [98]. 1-pyrenebutyric acid succinimidyl ester (PBSE) was attached to the graphene surface in order to covalently bind the PNA CP. Reprinted with permission from Campos et al. © 2019 American Chemical Society.

2.3.5. EIS

Electrical impedance spectroscopy (EIS), also known as Frequency Response Analysis (FRA), exploits the application of Alternating Current (AC) to an electrochemical cell in order to obtain information on the rate of the electrochemical reaction, the diffusion of species from bulk solution to the electrode surface, the charge distribution at the electrode/solution interface and the electric resistance of the solution. In an electrochemical cell, the electrical double layer that forms at the interface between the electrode and the solution behaves like a capacitor, whose opposition to the flow of AC is quantified by the electrical impedance. Therefore, the impedance is critically influenced by the modification that the sensor surface undergoes, making EIS a suitable and extensively exploited technique for biosensor fabrication [99]. Its main advantage is given by the fact that it does not require labelling of the analyte in order to generate a signal.

This method is particularly well suited for development of EIS-based genosensors. In fact, given that the hybridization process involves the formation of hydrogen bonds between nucleobases of the two complementary strands, as a consequence both water molecules and solvated ions are driven away from the surface where the hybridization has occurred, resulting in an observable decrease in the resistance of the solution [100]. Another frequently employed mechanism for the detection of the hybridization event is to employ a redox probe such as ferricyanide-ferrocyanide redox couple ($Fe(CN)_6^{3-/4-}$).

Given the negatively charged nature of DNA, when the surface is modified with ssDNA the electron-transfer resistance (R_{et}) of the redox couple is increased due to electrostatic repulsion. A further and more consistent increase is observed after the hybridization with complementary target oligonucleotide has occurred.

This basic technique has been furtherly developed by Bardea et al. in 1994 [101], where after the first hybridization between capture probe and target DNA, a second was conducted with another DNA strand labelled with biotin, leading to obtain a sandwich complex and another increase in the electron transfer resistance of the $Fe(CN)_6^{3-/4-}$. However, the biggest increase in R_{et} is obtained in the final step where the biotin interacts with an avidin molecule, which given its bulkiness, yields an increase in resistance of more than 2,5 times (**Figure 2.15**). Through this genosensing method a limit of detection of 3,5 pM was reported.

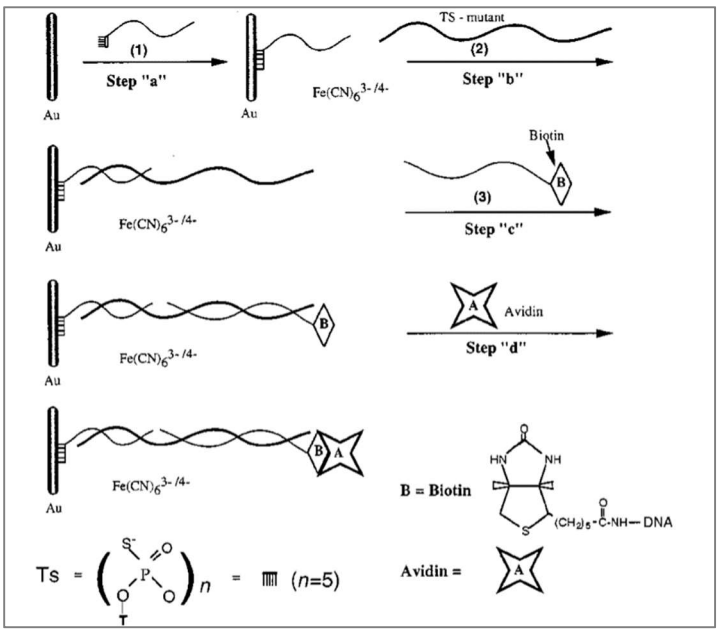

Figure 2.15. Scheme of surface functionalization carried out in [101]. The probe (1) self-assembles on the sensor surface thanks to Au-S interactions. Once the sandwich between probes (1), (2) and (3) is assembled the biotin interacts with avidin resulting in an increased bulkiness and reduced $Fe(CN)6^{3-/4-}$ accessibility to electrode surface. Reprinted with permission from Bardea et al. © 1999 Royal Society of Chemistry

In alternative to the above cited methods, it is possible to monitor the decrease in R_{et} as a consequence of the occurrence of the hybridization reaction. This was achieved by immobilization on the sensor surface of a molecular beacon, which was subsequently opened through hybridization with target analyte resulting

in an increased R_{et}. However, by addition of thionine, an intercalating positively charged molecule, its insertion on the DNA double strands rendered a cationic surface that attracted the $Fe(CN)_6^{3-/4-}$ probe, thus reducing R_{et} [102] (**Figure 2.16**).

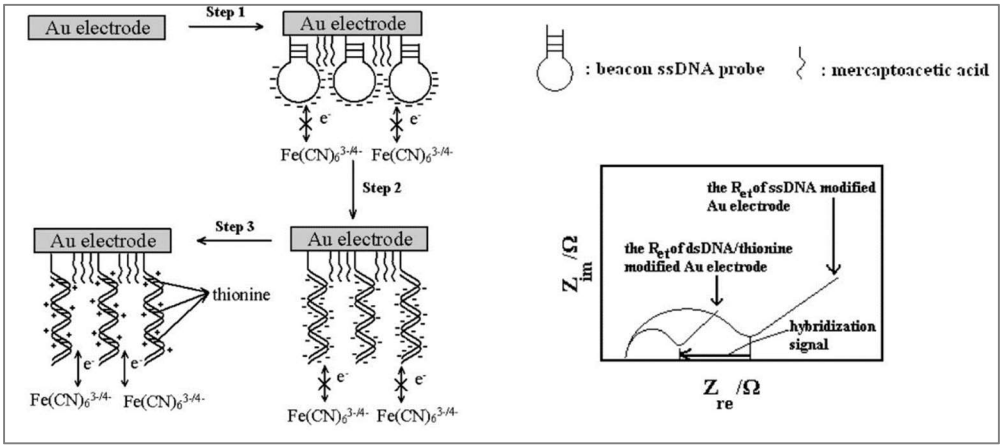

Figure 2.16. Genoassay scheme proposed in [102]. After the immobilization of the molecular beacon in step 1, the latter is opened by hybridization with complementary target in step 2. Finally, in step 3 thionine is inserted, resulting in positively charged hybrid that reduce R_{et}. Reprinted with permission from Xu et al. © 2006 WILEY-VCH Verlag.

In 2005 Liu et al. employed EIS in order to study the kinetics of hybridization between a PNA capture probe and a DNA target sequence [103]. The authors came to the conclusions that through EIS experiment it was possible to calculate the kinetics constant with an accuracy comparable to that of surface plasmon resonance-enhanced fluorescence spectroscopy. EIS has also been applied to determine the optimized amount of oligonucleotide probes immobilized on the sensor surface in order to maximize the hybridization events [104]. For this purpose, Keighley et al. immobilized on gold surface a mixture of thiolated oligonucleotide probe and a thiol spacer molecule, so that by changing the ratio of the two species it is possible to obtain a different probe coverage, assessed by chronocoulometry. It was found that no variation in the R_{et} generated by the $Fe(CN)_6^{3-/4-}$ couple is observable at probe densities lower than $2{,}5 \cdot 10^{-12}/cm^2$, while the maximum signal was obtained at a coverage of $5{,}4 \cdot 10^{-12}/cm^2$.

2.3.6. Voltammetry

Voltammetric techniques, that have been taken into consideration in paragraph 1.2, can be applied for genosensing purposes in a variety of configuration [105-

107]. The most direct applications to DNA detection consist in the oxidation of the nucleobases, typically guanine [108]. However, the slow kinetics of the electrochemical reaction of guanine yields modest peaks and, despite the possibility of overcoming this limitations by using a redox mediator such as tris(2,2′-bipyridyl) ruthenium(II) [109], at the relatively high potential necessary for the oxidation of guanine, noise currents arise. Furthermore, this method is applicable to quantify the presence of DNA, rather than detect a specific oligonucleotide sequence.
To resolve such limitations, it is possible to employ redox indicator molecules, which show different affinities towards ssDNA and dsDNA, and can interact through electrostatic means, groove binding and intercalation [110] (**Figure 2.17**).

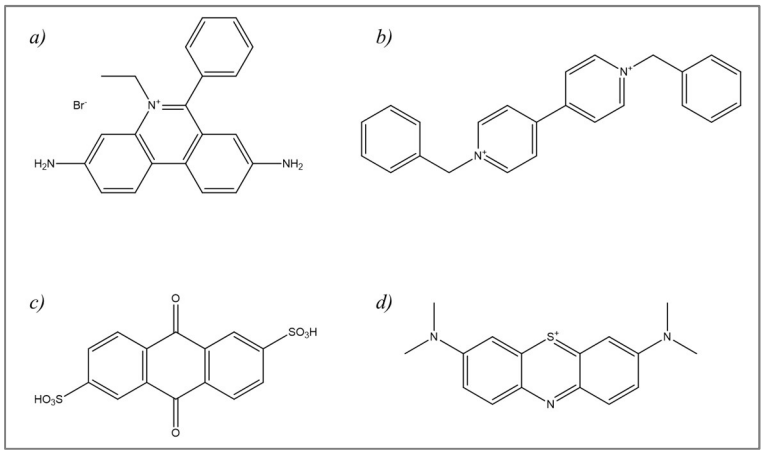

Figure 2.17. Structures of four molecules that can act as electrochemical label and possess intercalating properties. The molecules are a) Ethidium bromide, b) Benzyl viologen, c) Anthraquinone-2,6-disulfonic acid and d) Methylene blue.

As for the latter, a class of electroactive molecules are capable of interacting with dsDNA by insertion between two layers of paired nucleobases, driven by hydrophobic effect. In a recent work, Garcia-Melo et al. exploited doxorubicin as intercalating electroactive reagent, which allowed to reach a 43,92 pM limit of detection of a DNA sequence of the *Adenomatous polyposis coli* gene, considered responsible for the development of a series of cancers [111].
Redox molecules, such as ferrocene, can also be integrated in a secondary oligonucleotide probe (generally referred to as reporter probe or signalling probe) in order to form a three-probe sandwich with the target and capture probe, as reported by Ihara et al. [112] (**Figure 2.18**).

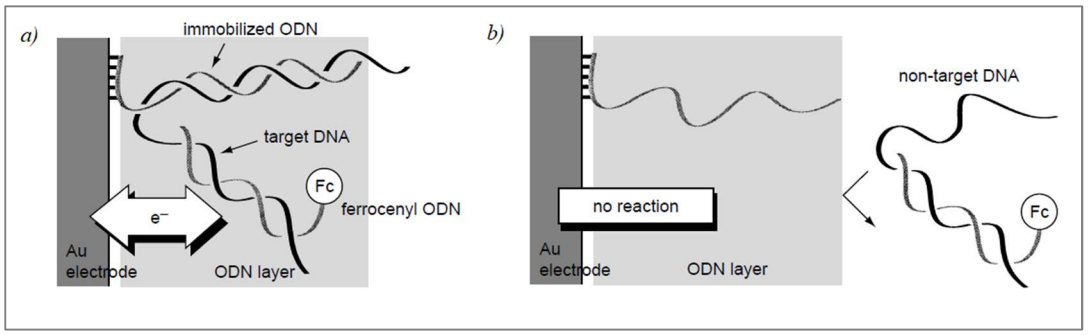

Figure 2.18. Sandwich complex proposed in [112], where an oligodeoxynucleotide (ODN) is immobilized on the Au sensing surface through self-assembly, while a ferrocene-tagged probe is hybridized to a DNA sequence. If a) the sequence is complimentary to the immobilized ODN then the sandwich is formed leading to the obtainment of an electrochemical signal, otherwise b) the DNA is not complementary and the sandwich complex does not assemble. Reproduced with permission from Ihara et al. © 1997 Royal Society of Chemistry.

From this basic configuration, over the years more elaborated detection methods have been developed [113]. In 2004, Immoos et al. proposed a genosensor where capture and ferrocene-labelled signalling probe are connected via a flexible poly-(ethylene glycol) bridge [114]. The hybridization of target DNA induces conformational changes that result in bringing the ferrocene tag close to the electrode surface, thus making the electron transfer reaction possible and turning on the electrochemical signal (**Figure 2.19a**). Another configuration has been proposed by Xiao et al. in 2006 [115], where the capture probe is completely hybridized with a methylene blue-labelled signalling probe, keeping the electroactive tag far from the electrode surface and preventing the electron transfer phenomena. Upon introduction of the complementary target DNA, a partial displacement of the signalling probe portion bearing the tag occurs, thus allowing for the tag to be in close proximity of the sensing surface and for the signal to be generated (**Figure 2.19b**).

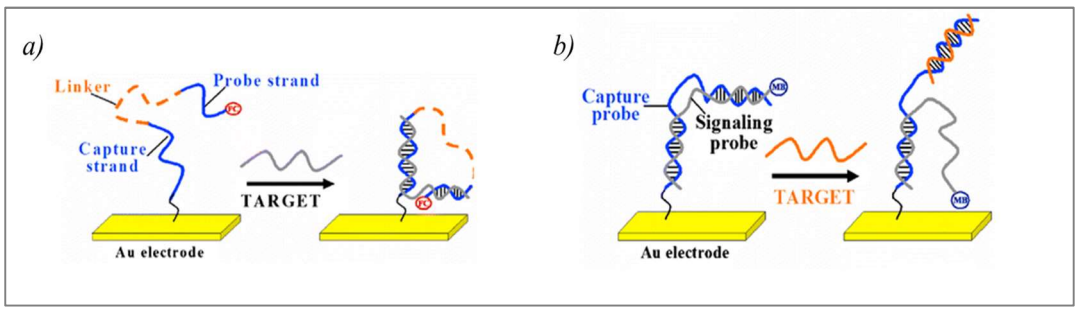

Figure 2.19. Different configurations for three-probe electrochemical genoassay. The configuration in a) reported in [114] employs a ferrocene tag for the development of the signal, while the configuration b) reported in [115] employs methylene blue. Reprinted with permission from Ricci et al. [109] © 2008 Springer-Verlag

An enhancement in sensitivity and signal intensity can be obtained by employing enzymatic reaction for the generation of the electroactive species. For this purpose, signalling probe is labelled with a species that can bind an enzyme or an enzymatic conjugate, e.g. biotin-labelled signalling probe that interacts with a streptavidin-enzyme conjugate. The most employed enzymes for genosensor fabrication are horseradish peroxidase, glucose oxidase and alkaline phosphatase (ALP). For example, in 2005, Giallo et al. developed a sandwich assay for the detection of *Salmonella* bacteria exploiting a biotin-tagged signalling probe [116]. After sandwich formation, a streptavidin-alkaline phosphatase conjugate was added and immobilized on the sandwich thanks to biotin-streptavidin interactions. Finally, the enzymatic substrate α-naphthyl was processed in order to obtain the electroactive α-naphthol, which generated the analytical signal. The proposed method was found capable of detecting amplified sequences of target DNA down to a concentration of 300 pM.

2.3.7. PCR

Polymerase Chain Reaction (PCR) represents one of the most revolutionary techniques uncovered during the last decades in the field of molecular biology [117,118]. Starting from a solution containing a low concentration of DNA molecules, its purpose is to exponentially replicate such molecules.
For the carry out of the PCR the basic reactants involved are a DNA that has to be amplified, primers that hybridize DNA in specific regions, deoxyribonucleotides, magnesium ions and a DNA polymerase enzyme. The process consists in repetition of cycles composed of a first denaturation of the dsDNA at 95 °C, followed by the hybridization of the primers to the ssDNA at 50-60 °C and finally the elongation of the primer strands carried out by the DNA polymerase enzyme at 68-72 °C. At the end of the process (cycles are repeated 25-50 times, usually in a thermal cycler) the concentration of DNA will be exponentially increased. This process can be applied also to RNA provided that, before the PCR process, the RNA is reverse-transcribed into its complementary DNA, in what is called Reverse Transcription Polymerase Chain Reaction (RT-PCR). However, PCR is not only exploited to amplify the DNA concentration of a sample but can be also employed to quantify its concentration using real-time PCR [119]. To this aim, a fluorescent species is introduced in the reaction medium, so that it would interact with the newly formed DNA amplicons yielding an optical signal. By using a thermal cycler equipped with a light source

capable of irradiating the sample at a specific wavelength, it is possible to introduce a fourth step in each PCR cycle, during which the fluorescence signal is registered at 80 °C in order to avoid the presence of primer dimers. Thus, by measuring on each cycle, it is possible to obtain a real-time monitoring of the amplification process.

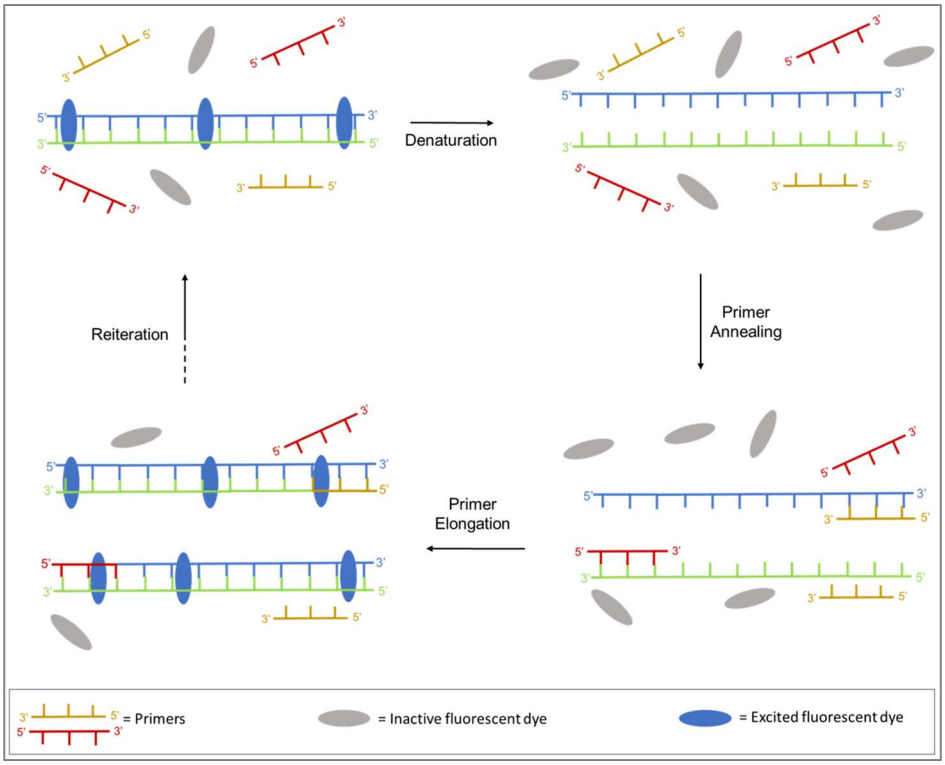

Figure 2.20. PCR mechanism employing fluorescent dyes.

The fluorescent signal can be obtained through two main methods. The first consists in using fluorescent molecules with intercalating abilities, which will yield a fluorescence signal after intercalation in dsDNA has occurred (**Figure 2.20**). However, this method lacks selectivity in the recognition process, and the main drawback is the risk of registering signals as a consequence of intercalation of the dyes in the primer dimers that may be present. As an alternative to fluorescent dyes, it is possible to employ fluorescent probe in order to obtain a specific recognition of the DNA products. One of the most common probes employed in real-time PCR is the TaqMan probe (**Figure 2.21**) [120,121], a generic probe containing a fluorescent tag at one end and a quencher at the other end, this way the ssDNA probe in solution has its fluorescence quenched. The mechanism for the detection is based on the 5' to

3'exonuclease activity of the polymerase enzyme used, i.e. the thermostable *Thermus aquaticus* (Taq). In fact, when the DNA-based probe is present in solution, it hybridizes to the DNA template along with the primer. During elongation of the primer, when the Taq reaches the probe, its exonuclease activity degrades the probe releasing the fluorescent molecule in solution which is no longer in spatial proximity of the quencher. As the amount of replicated DNA increases, the amount of fluorescent species in solution increases, allowing for a real time quantification of the PCR amplicons produced.

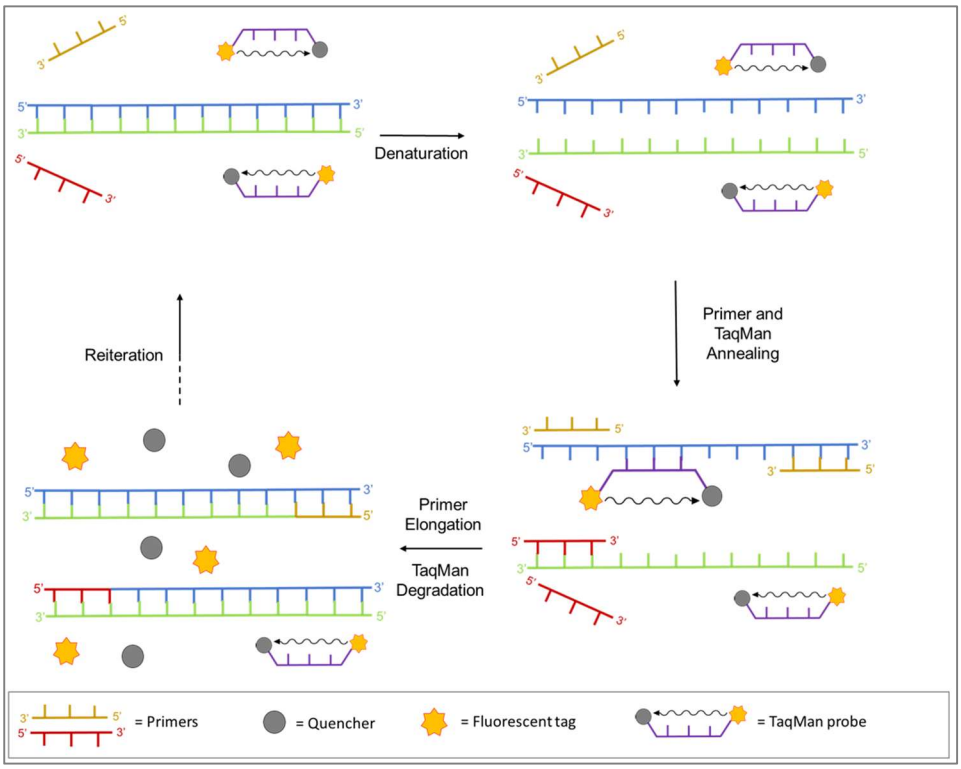

Figure 2.21. PCR mechanism employing TaqMan Probe.

However, it is not trivial to obtain the value of DNA/RNA concentration in the original sample, since after a few tens of cycles, the process reaches a plateau. Two main approaches are employed: the absolute quantification and the relative quantification. The former requires the construction of a calibration curve, through which it is possible to obtain the DNA concentration of unknown samples. The latter exploits some reference genes as internal standards, expressing the difference between gene expression, in terms of cDNA obtained from the mRNA, between unknown samples and genes of known expression.

The real time PCR is widely employed in a range of applications, spanning from food authenticity [122] to medical diagnostics [123]. For example, in 2018 Liu et al. reported a method based on real time quantitative PCR to detect *Aeromonas schubertii* bacteria infection in Snakeheads fish tissues [124]. For this purpose, a minor groove binder TaqMan probe was used to carry out real time PCR analysis, through which the authors were capable of detect a concentration as low as 18 copies/μL, which is reported as 100 times more sensitive than conventional PCR.

2.4. Genetically modified organisms

The World Health Organization (WHO) defined in 2014 Genetically Modified Organisms (GMOs) as "Organisms (i.e. plants, animals or microorganisms) in which the genetic material (DNA) has been altered in a way that does not occur naturally by mating and/or natural recombination" [125]. The aim of genetic modification is typically to introduce new traits such as a resistance to antibiotics or herbicides. This is achieved by introduction of a gene from a species into another through genetic engineering techniques (**Figure 2.22**). The first example of development of a GM species was performed in 1973 by Cohen et al. by transferring the resistance to the kanamycin antibiotic of a bacterium to other bacteria in vitro. [126] This study paved the way for the following studies that developed the first transgenic mouse in 1974 [127] and the first genetically modified crop in 1983 [128].

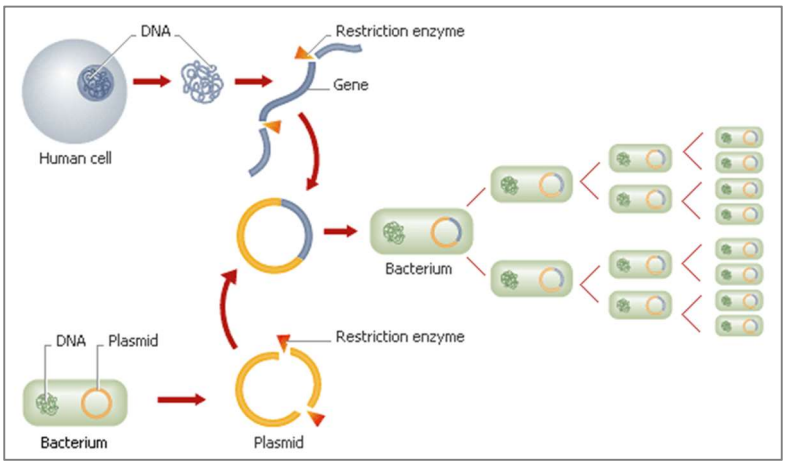

Figure 2.22. Schematic process for genetic engineering process.

The production of a genetically modified organisms starts with the isolation of the gene that has to be inserted in the organisms that will undergo genome editing. To this gene are subsequently added a promoter and terminator sequences, necessary for the expression of the gene, as well as a selectable marker, through which it will be possible to verify the occurrence of the genome modification. Then this new sequence has to be introduced in the organism's genome. For this purpose, different techniques are available such as microparticle bombardment [129], viral vectors [130] etc. However, the most efficient method for gene editing involves the use of the CRISPR-Cas9 technique [131] (**Figure 2.23**). Cas9 is an endonuclease capable of degrading both strands of DNA creating a double-stranded break (DSB). However, the location of this DSB is not random but it is in fact guided by a "guide RNA", whose engineering allows to target the organism genome in a specific sequence. Once the DSB has been produced, it can be repaired either by non-homologous joining which results in gene knockout or by insertion of a new endogenous DNA sequence. The latter is therefore used for introduction of the new gene.

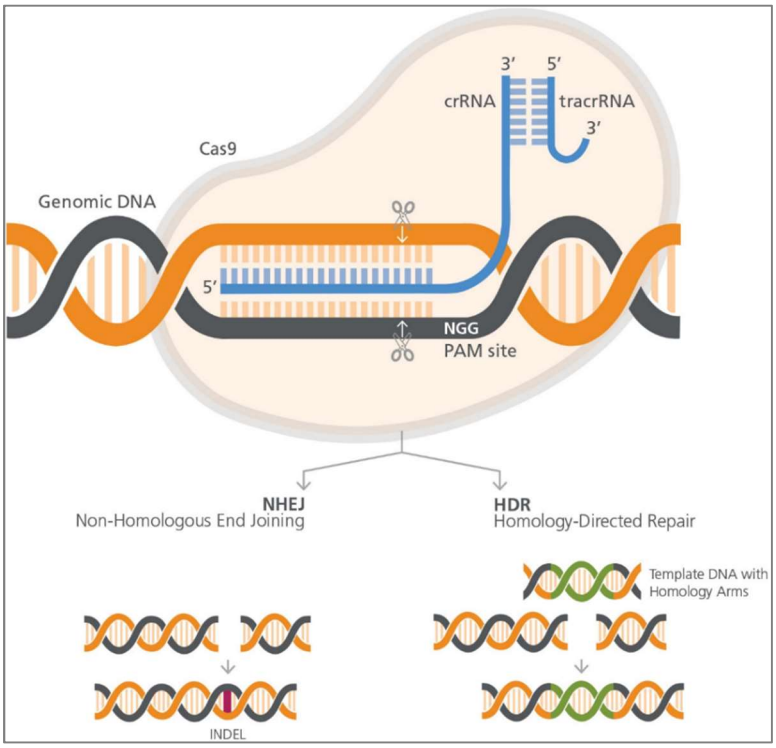

Figure 2.23. Schematic representation of the working mechanism of CRISPR-Cas9 technique. The double strand break is obtained by the targeting of guide RNA (blue) composed of CRISPR RNA (crRNA) and trans-acting CRISPR RNA (tracrRNA). The DSB can be then repaired inserting the new gene (green) or through insertion or deletion (INDEL). Reprinted with permission from StemCell™.[132] © StemCell™ technologies

Finally, in order to obtain the GMO, the cell that has undergone genome editing must be regenerated, which for plants is conducted through tissue culture, while in the case of animals the genome editing must be conducted on embryonic stem cells.

2.4.1. GMOs in food

The main field of application for GMOs is in the agronomic area. In fact, genetic engineering of crops is a powerful and promising tool to face current issues affecting cultivations. The most critical difficulty is given by the simultaneous increase of population, which requires an enhancement of crop yields in order to resolve undernourishment issues, and continuous decrease of arable land. For these reasons a possible solution is provided by genetic manipulation of crops in order to insert genes which would result in an increase of yields per cultivated acre, e.g. pests- and herbicide-resistance. However, the application of genome editing to food resources raises some questions of potential risks alongside its undoubtedly desirable benefits [133-135].
The main benefits, as stated previously, is given by the introduction of resistance to herbicides and pests, traits that would require decades to be obtained through conventional breeding, if possible at all (**Figure 2.24**).

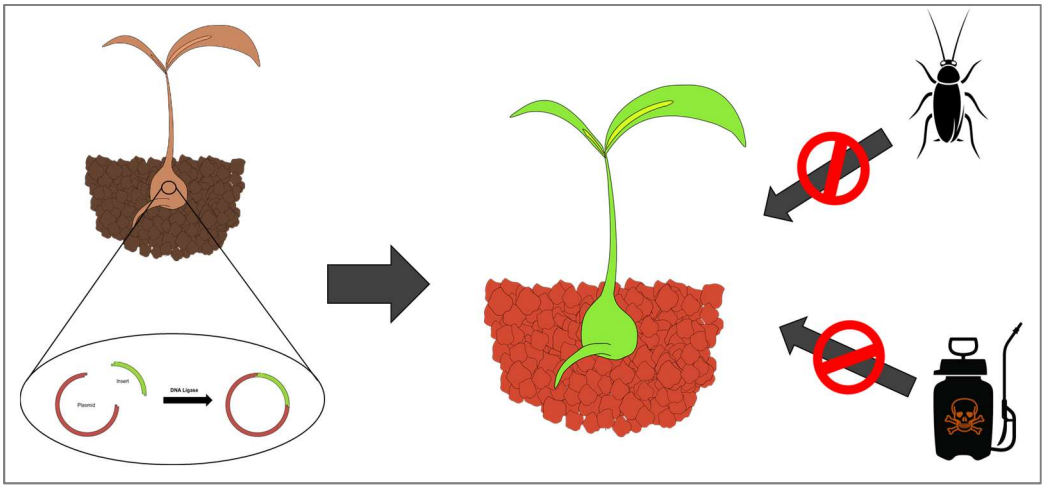

Figure 2.24. Conceptualization of genetic manipulation on crops to include desirable properties such as pest and pesticide resistance.

These resistances allow to enhance the yield of cultivation without a simultaneous increase in area of cultivated lands that would require higher demand of water, fertilizers, pesticides, herbicides, etc. Along with this, other

benefits can be achieved through the use of GM crops. By modification of the chemical composition of foods, achieved through the increase or decrease of specific protein expression, foods enriched in nutrients such as vitamins and probiotics can be obtained. An example can be found in the genetic manipulation of rice to obtain "Golden Rice", a variety enriched with β-carotene to help contrast vitamin A deficiency [136]. Genetic engineering can also provide foods with improved features for their commercialization, as in the case of "Flavr Savr" tomatoes, in which the expression of a protein has been suppressed, consistently slowing down the ripening of the fruit [137,138]. Finally, it has been demonstrated the possibility of GMOs to express viral or bacterial antigens, effectively working as oral vaccines [139].

Opposed to the reported advantages of employing GM crops, different concerns have been raised over their application, both for health and ecological matters. Health risks are taken into account primarily by allergenicity and toxicity [140]. An example is given by the "Starlink Maize" corn variety, where the GM product not approved for human consumption contaminated food products and was suspected to have caused allergic reactions, which resulted in a recall of hundreds of products [141]. However, bigger concerns are related to secondary effects which can be caused by the introduction of a new gene in the organism, that might be involved in the modification or the disruption of some metabolic pathway. The outcomes of these modifications are mostly unforeseeable and unpredictable, thus raising the biggest concerns.

As for the ecological issues, different risks can be pointed out. It must be taken into consideration that crops with resistance to pests will have a great impact on the food chain, by reducing the number of some pest species, thus facilitating the expansion of minor pests. Furthermore, as mentioned previously, during genetic engineering antibiotic resistance is often employed as selectable marker to prove the effectiveness of genetic manipulation. However, it is well-known that bacteria are capable of transfer genes between species, this poses the potential risk of transferring antibiotic resistance from GM food to the bacteria of the intestinal flora of the consumer (animal or human) and in the worst case this can happen towards possibly present pathogens.

Given the controversial topic of genetic modifications in food and feed, regulations have been put in order to guarantee the safety of consumers and monitor the possible side effects in which the ecosystems might incur. However, regulations on release and labelling of GM products can vary in each country. In Europe, GM products destined to food consumption are subjected to two

regulations. The first, regulation EC 1829/2003 [142], defines that GM plants intended for human consumption must undergo an authorization process during which European Food Safety Authority (EFSA) first gives a scientific evaluation on relevant aspects of the GM product, then a specific committee, taking into account EFSA report, votes on whether approve or reject the authorization for the new GM product. The second regulation, EC 1830/2003 [143], deals with the labelling of GM products requiring mandatory labelling for all food and feed containing a percentage of GM products greater than 0,9%.
Therefore, it is of critical importance detect and quantify GM products in a robust and sensitive manner. For this purpose, many methodologies have been proposed over the years that rely on different genosensing techniques [144-148], most of which are based on PCR, but also electrochemical biosensor, SPR, piezoelectric devices etc. proved fit for the purpose.

2.4.2. Roundup Ready Soy

Genetically modified soybeans are one of the most cultivated GM crops, along with maize, cotton and canola. In particular, it has been reported that, in 2017, GM soy accounted for roughly 80% of the total soybean worldwide production [149]. The first soybean genetically manipulated crop, namely *Roundup Ready* (RR) soy, was introduced by Monsanto company in 1996 [150] with the first seed variety named GTS-40-3-2 followed by the MON89788 second-generation seed [151]. The genetic manipulation of soybeans was carried out in order to confer the plant resistance to a widely employed herbicide, the glyphosate, which is commercialized by Monsanto with the name *Roundup*. The glyphosate is an herbicide whose role is to interfere with the synthesis of essential aromatic amino acids [152]. In particular, it acts as an inhibitor for the 5-enolpyruvyl-shikimate3-phosphate synthase (EPSPS) enzyme of the Shikimate pathway (**Figure 2.25**), through which Phenylalanine, Tyrosine and Tryptophan are synthesized.

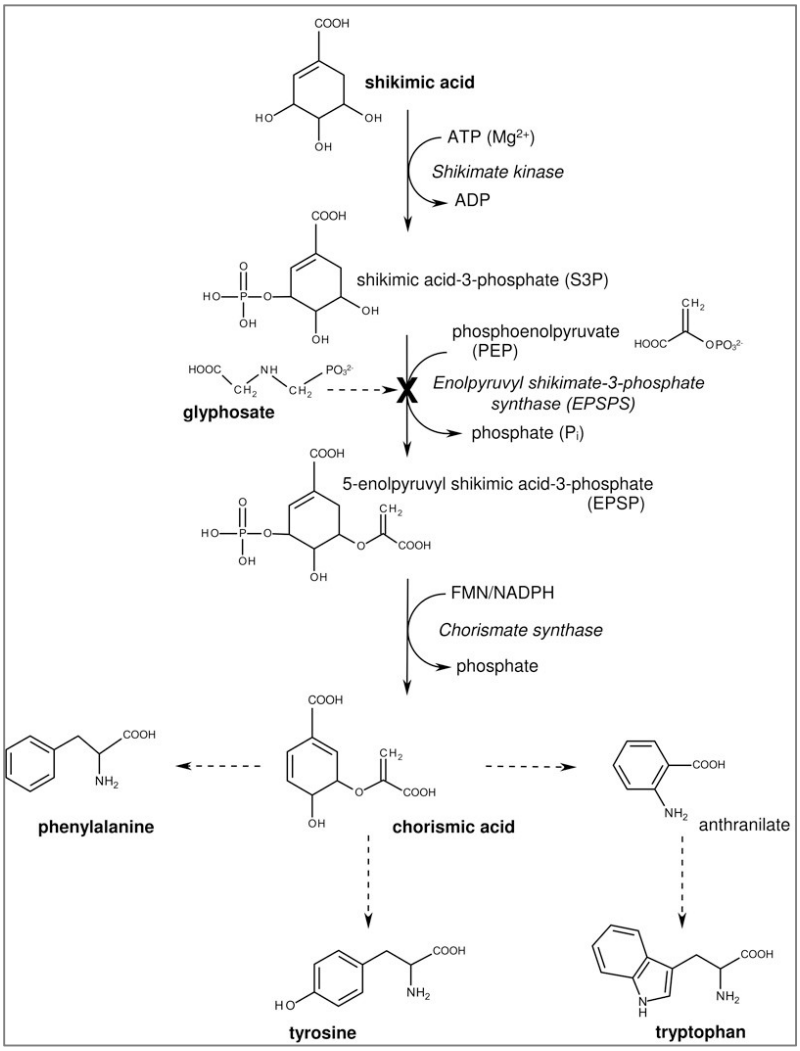

Figure 2.25. Shikimate pathway for the synthesis of essential amino acids in plants. If glyphosate is present, the pathway is interrupted at the EPSPS step. Reprinted with permission from Pollegioni et al. [153] © 2011 FEBS

This makes it capable of killing a broad spectrum of weeds, which, combined with its low-cost, granted the worldwide success of this herbicide [154]. However, its diffusion relies on the development of glyphosate-resistant crops. The genetic modification of RR crops consists in the introduction of a gene coding for an analogous EPSPS enzyme obtained from *Agrobacterium tumefaciens* strain CP4 which, remarkably, is not inhibited by the glyphosate (**Figure 2.26**) [155].

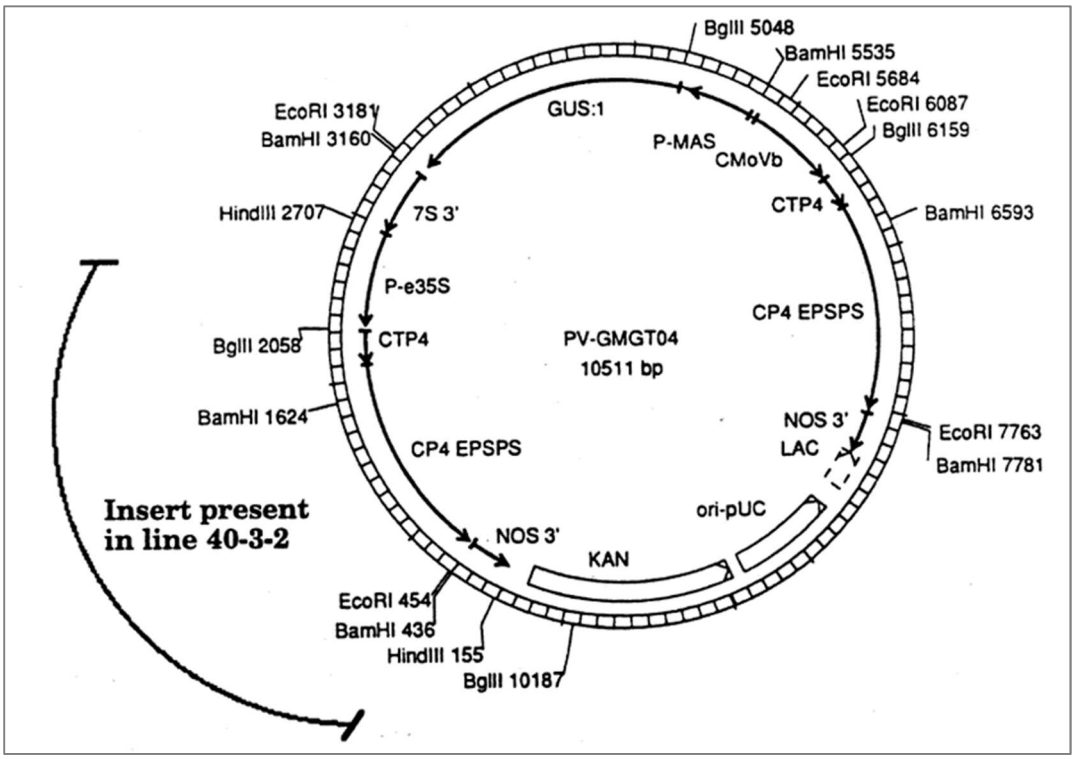

Figure 2.26. Plasmidic vector (PV-GMGT04) employed to obtain the GTS 40-3-2 variety of Roundup Ready soy.

Glyphosate toxicity remains to this day a controversial topic. In fact, even though different organisms such as EFSA concluded that it is unlikely that glyphosate poses a cancerogenic hazard [156], other agencies such as IARC concluded that it must be categorized as "probable human carcinogen" [157]. Taking into account such controversy, being able to efficiently detect and quantify the presence of RR genetic modifications in food plays a critical role in order to monitor the intake of materials treated with glyphosate, especially if its carcinogenicity will be reaffirmed in following studies.

2.5. Aim of the study

The purpose of the research conducted within this project is to develop a method capable of both detecting and quantifying the presence of GTS-40-3-2 variety of *Roundup Ready* Soy in food. With the aim of improving the hybridization efficiency, discrimination against mismatches in the recognized target sequence and exploit the integration of functional groups on the probes, PNA-based probes were employed for the development of the assay. A sandwich-type detection protocol was employed, based on the use of two PNA-based probes, i.e. the Capture Probe (CP) and Signalling Probe (SP). Both PNA sequences possess 20 nucleobases complementary to different portions of the chosen target, a 45-mer sequence of the DNA of RR soy, which, upon hybridization of both PNA probes, acts as a bridge between CP and SP, forming the sandwich complex. The CP molecule bears an amino function at the C-term, through which it can be covalently bound to different substrates. SP is modified with a biotin and thanks to its presence an amperometric signal can be generated. In fact, after the sandwich is assembled, an enzyme conjugate between streptavidin and alkaline phosphatase (ALP-Strp) is introduced, which will attach to the sandwich through biotin-streptavidin interactions. Finally, a non-electroactive substrate for ALP is exploited, namely hydroquinone diphosphate (HQDP), which upon enzymatic dephosphorylation yields the electroactive hydroquinone (HQ). Thus, the electrochemical signal generated from the HQ oxidation to quinone (Q) is correlated to the amount of ALP on the sensing system, which in turn is directly related to the amount of SP and therefore target DNA that led to the formation of the sandwich complex. This assay concept has been applied to different electrode substrates, namely Carbon (C), Carbon Nanotubes (CNTs) and reduced graphene oxide (rGO), in order to evaluate the best conditions for assay development. Furthermore, the reported sandwich system has also been implemented on magnetic microbeads (mMBs) in order to evaluate the improvements deriving from the different features of the magnetic substrates, with respect to the electrode surface.

2.6. Experimental

2.6.1. Reagents and solutions

Sodium chloride (NaCl), disodium hydrogen phosphate (Na_2HPO_4), ethylendiaminetetraacetic acid disodium salt dihydrate (Na_2EDTA), sodium bicarbonate ($NaHCO_3$), sodium dodecyl sulfate (SDS), Trizma® Base, magnesium chloride ($MgCl_2$), N-(3-dimethylaminopropyl)-N′-ethylcarbodiimide hydrochloride (EDC), N-hydroxysuccinimide (NHS), 4-morpholineethanesulfonic acid monohydrate (MES), Tween® 20, bovine serum albumin (BSA), Denhardt's solution 50x, 1-Pyrenebutyric acid (PBA), hydrochloric acid (HCl, 37%), sodium hydroxide (NaOH), streptavidin-alkaline phosphatase from *Streptomyces avidinii* (ALP-Strp), Dimethyl sulfoxide (DMSO), N,N-Dimethylformamide (DMF), methanol, Tetrahydrofuran (THF) were purchased from Sigma-Aldrich (Milan, Italy).

Dynabeads™ M-270 Carboxylic Acid were purchased from Thermo Fischer Scientific (Massachusetts, USA).

Hydroquinone diphosphate (HQDP) was purchased from Metrohm Italiana (Origgio, Varese, Italy).

The following synthetic DNA probes were purchased from biomers.net GmbH (Ulm, Germany):

- *Full-Match DNA* (FM DNA): 5′-ACT TGG GGT TTA TGG AAA TTG GAA TTG GGA TTA AGG GTT TGT ATC-3′
- *Mismatch DNA* (1-MM DNA): 5′-ACT TGG GGT TTA TGG AAA TTG GAA TTG GGA TTA AG**T** GTT TGT ATC-3′
- *Scramble DNA* (Scr DNA): 5′-ACT TGG GGT TTA TGG AAA TTG GAA TGG **TT**A **GA**A **TT**G **TG**T **GTA TG**C-3'

Soy flours from wild-type soy and *Roundup ready* genetically modified soy (RR soy) were purchased from European Commission, Joint Research Centre (JRC) (Geel, Belgium) as European Reference Material (ERM). Specifically, flours containing a different percentage of RR soy in wild type soy were employed, namely 0% (ERM-BF410ak), 1% (ERM-BF410dn), 10% (ERM-BF410gn).

The "ION Force DNA Extractor FAST" used for the extraction of the genomic DNA from the ERM samples was purchased from Generon (San Prospero, Modena, Italy).

Double-distilled and deionized water was used for buffer solutions preparation. Buffer solutions composition is reported below:

- *MES buffer*: 0.1 M MES (pH adjusted to 5 with NaOH).

- *MES beads buffer*: 25mM MES (pH adjusted to 5 with NaOH).
- *Tris Buffered Saline (TBS)*: 0.1 M Trizma® Base, 0.02 M $MgCl_2$ (pH adjusted to 7.4 with HCl).
- *Tris Buffered Saline-Tween (TBS-t)*: 0.1 M Trizma® Base, 0.02 M $MgCl_2$, 0.05% w/v Tween® 20 (pH adjusted to 7.4 with HCl).
- *Carbonate buffer (CB)*: 0.1M $NaHCO_3$, 0.1% w/v SDS (pH adjusted to 9 with NaOH).
- *Hybridization buffer (HB)*: 0.3 M NaCl, 0.02 M Na_2HPO_4, 0.1 mM EDTA (pH adjusted to 7.4 with HCl).
- *Blocking buffer (BB)*: 20 mg/mL BSA in TBS (pH 7.4).
- *Reading* buffer (RB): 0.1 M Trizma® base, 0.02 M MgCl2 (pH adjusted to 9.8 with HCl).

2.6.2. Apparatus

Thermoshaker "Thermal Shake Touch", pH meter "pHenomenal® 1000 L" connected to "pHenomenal® 221" refillable 3 in 1 glass pH electrode with temperature sensor and "Ultra-High Performance (UHP)" single-channel mechanical pipettes purchased from VWR Internation srl (Milan, Italy) and Sartorius CP225D analytical balance were used throughout the assay protocol.
A NanoDrop™ One Microvolume UV–Vis Spectrophotometer (Thermo Fisher Scientific, MA, USA) was employed for the quantification of the genomic DNA extracted from the ERM Soy flours.
MPW 260R refrigerated centrifuge was employed for the carry out of the genomic DNA extraction from ERM soy flours.
Magnetic support for Screen-Printed Electrodes (DRP-magnet) and Support for magnetic separation were purchased from Metrohm Italiana Srl (Origgio, Varese, Italy).
Disposable Screen-Printed electrodes, also purchased from Metrohm Italiana Srl, were used as platforms for the assembly of the genosensor, or in combination with magnetic microbeads as electrodic cell for the read-out step. Both Single Walled Carbon Nanotubes Screen-Printed Electrodes (SWCNT-SPEs) and Carbon (C-SPEs) were employed.
Interdigitated gold microelectrodes (ED-IDA1-Au) from were purchased from Micrux technologies (Oviedo, Spain).
The voltammetric readout was performed employing a PGSTAT-204 Potentiostat/Galvanostat purchased from Metrohm Italiana Srl (Origgio,

Varese, Italy), operated through NOVA 2.1.4 Advanced Electrochemical Software using a DropSens DRP-DSC plug for the connection of the SPEs to the potentiostat.
For the FET experiments, two custom-made flow-through single well cells containing two Micrux chips were connected through plastic tubing and were connected to KEYSIGHT U2722A USB Modular Source Measure Unit, for the acquisition of the output signal.

2.6.3. Genosensing assay on C-SPEs

2.6.3.1. *C-SPEs activation*

The Carbon electrode substrate was oxidized by performing a CV scan from -1 V to 1.7 V (10 scans, scan rate=100 mV/s; step potential= +0.00305 mV) while 50 µL of H_2SO_4 1 M was drop-casted on the electrode surface [7]. After the procedure, the electrode surface was thoroughly rinsed with water.

2.6.3.2. *CP immobilization*

A 50 µL drop of 0,2 M EDC and 0,05 M NHS in MES buffer was deposited for 1 hour for the activation of the carboxylic function on the electrode surface, after which the electrodes were rinsed with water. Subsequently, 50 µL of CP solution at the desired concentration in *CB* was drop-casted on the C-SPE for 2 hours. Finally, the electrode was washed with water.

2.6.3.3. Sandwich complex formation

In order to avoid nonspecific probes adsorption, 50 µL of a 500 nM solution of pyrene in DMSO was deposited on the surface for 1 hour, after which the surface was cleaned with DMSO followed by water. A solution containing both SP and synthetic target DNA at the desired concentration in *HB* was left under agitation at 1000 rpm for 3 hours at room temperature. The obtained solution was then transferred on the electrode for hybridization with the immobilized CP. After 2 hours, the electrode was rinsed with a solution of Tween® 0,05% w/v followed by water.

2.6.3.4. *Enzyme labelling and electrochemical readout*

A 1:100 diluted solution of ALP-Strp in *BB* was drop-casted on the electrode surface for 15 minutes, followed by thorough rinsing with *TBS-t* and *TBS*. Finally, 50 µL of 1 mg/mL HQDP in *RB* was deposited for 150 s in order to allow the carry out of the enzymatic reaction. Immediately after, the electrochemical readout was performed by acquiring a DPV scan, obtained imposing the following parameters:

- Start Potential: -0.5 V
- Stop Potential: +0.3 V
- Step Potential: +0.00495 V
- Modulation Amplitude: +0.04995 V
- Modulation Time: 0.102 s
- Interval Time: 0.4 s

2.6.4. *Genosensing assay on SWCNT-SPEs*

2.6.4.1. *CP immobilization*

A 50 µL drop of 0,2 M EDC and 0,05 M NHS in MES buffer was deposited for 1 hour for the activation of the carboxylic function on the CNTs, after which the electrodes were rinsed with water. Subsequently, 50 µL of CP solution at the desired concentration in *CB* was drop-casted on the SWCNT-SPE for 2 hours. Finally, the electrode was washed with water.

2.6.4.2. *Sandwich complex formation*

In order to avoid nonspecific probes adsorption, 50 µL of a 500 nM solution of pyrene in DMSO was deposited on the surface for 1 hour, after which the surface was cleaned with DMSO followed by water. A solution containing both SP and synthetic target DNA at the desired concentration in *HB* was left under agitation at 1000 rpm for 3 hours at room temperature. The obtained solution was then transferred on the electrode for hybridization with the immobilized CP. After 2 hours, the electrode was rinsed with a solution of Tween® 0,05% w/v followed by water.

2.6.4.3. *Enzyme labelling and electrochemical readout*

A 1:100 diluted solution of ALP-Strp in *BB* was drop-casted on the electrode surface for 15 minutes, followed by thorough rinsing with *TBS-t* and *TBS*. Finally, 50 µL of 1 mg/mL HQDP in *RB* was deposited for 150 s in order to allow the carry out of the enzymatic reaction. Immediately after, the electrochemical readout was performed by acquiring a DPV scan, obtained imposing the following parameters:

- Start Potential: -0.5 V
- Stop Potential: +0.3 V
- Step Potential: +0.00495 V
- Modulation Amplitude: +0.04995 V
- Modulation Time: 0.102 s
- Interval Time: 0.4 s

2.6.5. Genosensing assay on rGO chips

2.6.5.1. *rGO deposition*

The Micrux interdigitated gold chips were treated according to the procedure reported by Piccinini et al. [158] in order to deposit a layer of reduced graphene oxide on the glass surface between the gold electrodes, thus forming the channels of the FET.

2.6.5.2. *Pyrene Butyric Acid functionalization*

The chips functionalized with rGO were treated differently according to the solvent in which the PBA was dissolved to a final concentration of 1mM.
For PBA in methanol, the chips were immersed in a plastic tube containing the solution for 3 hours, after which they were rinsed with ethanol and water.
For PBA in DMF, the chips were immersed in a plastic tube containing the solution overnight. Subsequently they were rinsed with ethanol and water.
For PBA in DMSO, the chips were immersed in a plastic tube containing the solution overnight. Subsequently they were rinsed with ethanol and water.
For PBA in THF, the chips were covered with 20 µL of the solution and left until complete evaporation. This process was repeated for a total of 4 times, after which the chip surface was rinsed with THF.

2.6.5.3. *CP immobilization*

The chips were immersed in a solution of 0,2 M EDC and 0,05 M NHS in MES buffer for 30 minutes for the activation of the carboxylic function, after which they were rinsed with water. Subsequently, the chips were immersed in a solution of CP in *CB* at the desired concentration for 2 hours. Finally, they were rinsed with water.

2.6.5.4. *Sandwich complex formation*

In order to avoid nonspecific probes adsorption, the chips were immersed in a 500 nM solution of pyrene in DMSO for 1 hour, after which a washing step with DMSO followed by water was carried out. A solution containing SP, synthetic target DNA and Denhardt's solution at the desired concentration in *HB* was left under agitation at 1000 rpm for 3 hours at room temperature. The chips were then immersed in this solution for 2 hours. Finally, the chips were rinsed with a solution of Tween® 0,05% w/v followed by water.

2.6.5.5. *Enzyme labelling and electrochemical readout*

A 50 µL drop of 1:100 diluted solution of ALP-Strp in *BB* was deposited on the rGO chips surface for 15 minutes, followed by thorough rinsing with *TBS-t* and *TBS*.
The chips were then inserted in a single-well cell for the electrochemical readout (**Figure 2.27**).

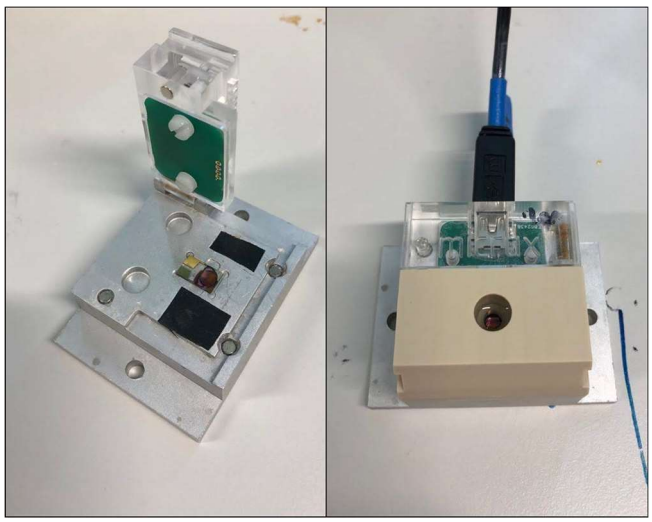

Figure 2.27. Single well cell for the carry out of the electrochemical measurements on Micrux chips.

The well was filled with 150 µL of 1 mg/mL HQDP in *RB*, in which a Pt counter electrode and an Ag/AgCl reference electrode were inserted. A waiting time of 150 s was observed in order to allow the enzymatic processing of the substrate. Immediately after, the electrochemical readout was carried out by acquiring a DPV scan, obtained imposing the following parameters:

- Start Potential: -0.5 V
- Stop Potential: +0.5 V
- Step Potential: +0.00495 V
- Modulation Amplitude: +0.04995 V
- Modulation Time: 0.102 s
- Interval Time: 0.4 s

2.6.5.6. *FET experiments*

The solution containing the target DNA at desired concentration was flowed through the two custom made cells (**Figure 2.28**) in which two functionalized Micrux chips were placed (Channel 1 and Channel 2), and the I_dV_g curves were monitored. An Ag/AgCl wire was inserted in the flow cell acting as gate electrode. The parameters imposed for the acquisition of the curves were:

- Voltage Drain-Source (Channel 1): 50 mV
- Voltage Drain-Source (Channel 2): 50 mV
- Start Potential: -300 mV
- Stop Potential: 500 mV
- Step Potential: +0.00495 V
- Scan Rate: 20 mV/s
- Step Size: 10 mV/s

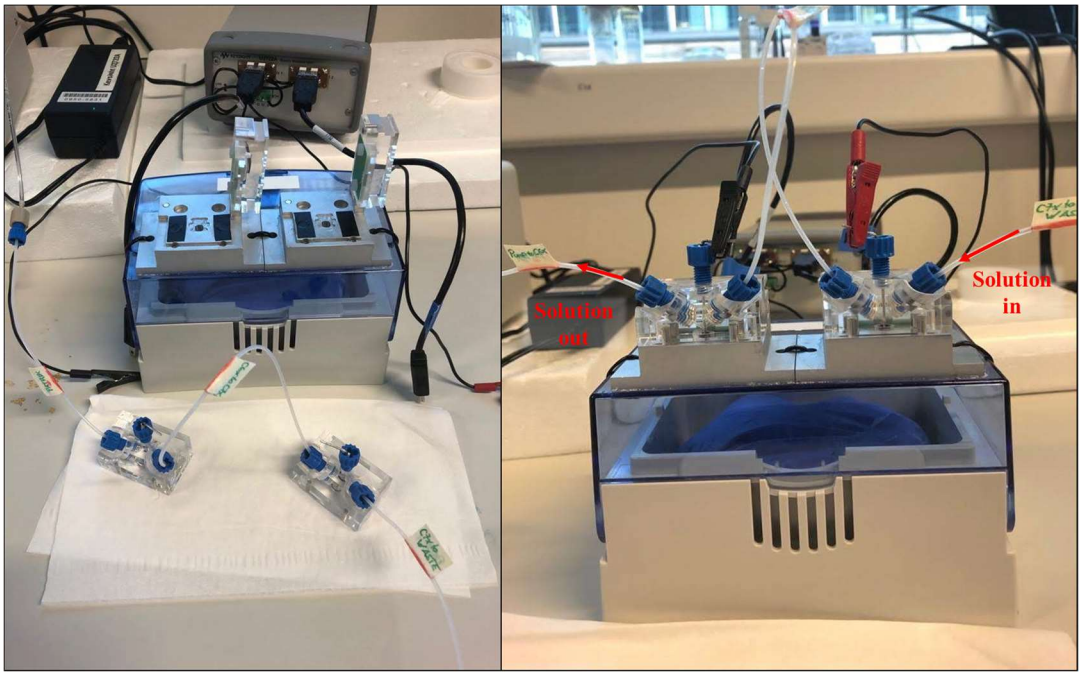

Figure 2.28. Open and closed flow-through cell where the Micrux chips are mounted and the solution containing target DNA is fluxed.

2.6.6. *Genosensing assay on carboxylic acid magnetic beads*

2.6.6.1. *CP immobilization on the beads surface*

The beads stock solution at concentration $2 \cdot 10^9$ beads/mL was diluted 1:25 in MES beads buffer. The beads were washed twice with MES beads buffer by suspension in the buffer, magnetic separation and elimination of the liquid. After washing, the beads were suspended in a solution of 25 mg/mL EDC and 25 mg/mL NHS for 30 minutes under agitation at 1500 rpm. Subsequently they were washed twice with MES beads buffer and suspended in a solution of 500 nM CP in *CB*. The reaction is left for 3 hours under agitation at 1500 rpm. Subsequently, the beads are washed twice with *CB*.

2.6.6.2. *Sandwich complex formation*

A solution containing SP, synthetic target DNA and Denhardt's solution at the desired concentration in *HB* was left under agitation at 1500 rpm for 3 hours at room temperature. The magnetic beads were then suspended in this solution for 2 hours under agitation at 1500rpm. Then, the beads were washed once with a solution of Tween® 0,05% w/v followed by a washing with *HB*.

2.6.6.3. *Enzyme labelling and electrochemical readout*

The beads were then suspended in a solution of ALP-Strp diluted 1:100 in *BB* for 15 minutes under agitation at 1500 rpm, after which they were washed once with *TBS-t* and twice with *TBS*. The beads were then suspended in a 1 mg/mL solution of HQDP in *RB* for 3 minutes, then 50 µL of the suspension were drop-casted on the surface of a SPE (C-SPE or SWCNT-SPE) which was mounted on the magnetic support for SPE in order to confine the magnetic particles on the electrode surface. The DPV scan were then acquired imposing the following parameters:

- Start Potential: -0.5 V
- Stop Potential: +0.2 V
- Step Potential: +0.00495 V
- Modulation Amplitude: +0.04995 V
- Modulation Time: 0.102 s
- Interval Time: 0.4 s

2.6.7. Genosensing assay using genomic DNA from real samples

For the testing on real samples, genomic DNA was extracted from European reference material soybean flours containing a different percentage of RR soy in wild type soy, namely 0% (ERM-BF410ap, ERM-BF410ak), 0,1% (ERM-BF410cp), 1% (ERM-BF410dp, ERM-BF410dn), 10% (ERM-BF410ep, ERM-BF410gn), >98% (ERM-BF410bp). The extraction was carried out using the "ION Force DNA Extractor FAST" kit following the procedure provided by the manufacturer. The DNA was employed without further amplification or purification, applying a dilution factor to obtain a signal in the linear range of the sensor response. The procedure for genomic DNA testing was the same as reported for the synthetic DNA with an additional step of heating at 95 °C for 30 minutes to melt the double strand of the DNA prior to addition of the SP.

2.6.8. Assessment of analytical performance

All the measurements carried out for the assessment of the best experimental conditions, as well as the signal values for construction of the calibration curve were replicated at least three times. Mean values and standard deviation are

shown in all figures. Method validation was performed by calculating linearity range, Limit of Detection (LOD) and Limit of Quantification (LOQ) according to “Eurachem Guidelines” [159].

2.7. Results and discussion

2.7.1. Genosensor working principle

A genosensor based on the formation of a three-probes "sandwich" complex has been developed for the detection of DNA target sequences. The complex is based on the hybridization of two different 20-mer PNA probes with a 45-mer sequence of target DNA that acts as a bridge between the two PNAs. The latter are the Capture Probe (CP), immobilized on the surface of either Screen-Printed Electrodes (SPEs) (**Scheme 2.1**), rGO-FET (**Scheme 2.2**) or magnetic beads (**Scheme 2.3**), and Signalling probe (SP), responsible for the detection of the occurrence of the hybridization event leading to the formation of the sandwich. In fact, the SP is tagged with biotin, that subsequently interacts with the streptavidin of an enzyme conjugate between the latter and Alkaline Phosphatase (ALP-Strp). The enzyme thus immobilized on the complex can then process a substrate in order to generate an electroactive species. For this study it was chosen to employ non-electroactive Hydroquinone Diphosphate (HQDP), which, upon enzymatic dephosphorylation, is converted in Hydroquinone (HQ) that is electrochemically detectable through its oxidation to Quinone (Q). Therefore, the signal given by the oxidation of HQ is related to the amount of ALP on the electrode surface, which in turn is proportional to the amount of sandwich complex formed. Since the concentration of DNA target is directly proportional to the amount of complex formed, by measuring the current generated by the oxidation of HQ it is possible to quantify the DNA concentration in the sample.

Transgenic *Roundup Ready* (RR) Soy has been chosen as a case of study for the development of the genosensor. In particular, the sequence was chosen on the basis of previous works conducted by the group of professor Roberto Corradini [160,161], with the aim of employing CP with enhanced length in order to obtain an increased stability of the hybrid with the DNA. In fact, during preliminary studies, it was observed that the use 15-mer CP would result in a signal much lower if compared to the 20-mer CP chosen for this study.

The same length was chosen also for the SP, whose hybridization with the target DNA is carried out in homogeneous phase prior to hybridization with the CP.

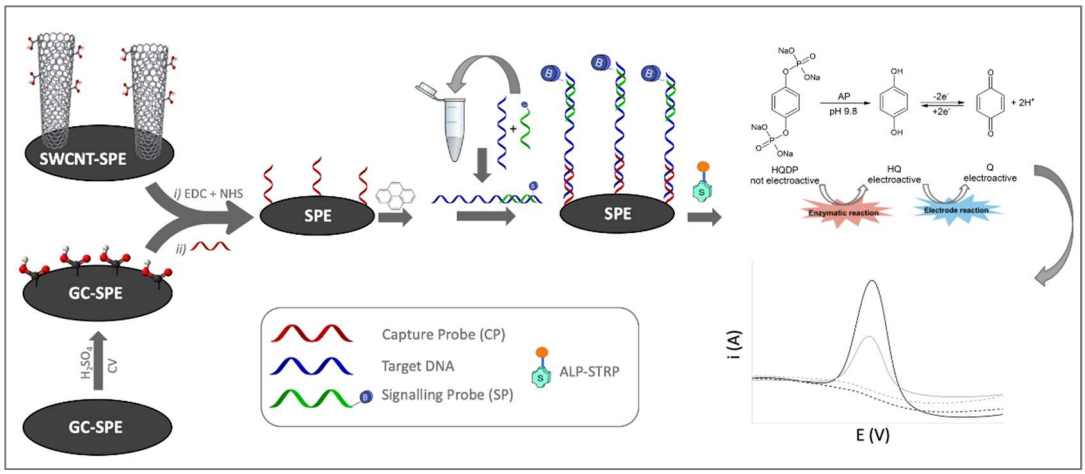

Scheme 2.1. Functionalization steps of the genosensor carried out on Screen-Printed Electrodes. For SWCNT-SPEs it is possible to directly activate the already present -COOH moieties, while on C-SPEs an oxidation of the surface exploiting CV must be carried out in order to generate -COOH functionalities.

2.7.2. CP immobilization

The CP is modified at its N-Term in order to include a primary amine, through which it can be covalently attached to the sensing substrates, exploiting their carboxylic functionalities for formation of amide bonds. This method was employed for the immobilization of the CP on the surface of the SPEs. Its immobilization was tested both on Carbon SPEs (C-SPEs) and Single-Walled Carbon NanoTubes SPEs (SWCNT-SPEs), which were chosen over Multi-Wall Carbon NanoTubes SPEs (MWCNT-SPEs) since the latter would result in an enhancement of the electrode substrate resistance. Moreover, employing such structures might result in the encapsulation of the CP between concentric nanotubes, thus reducing the possibility of hybridization with the analyte and precluding the interaction with the enzyme conjugate.

In order to immobilize the CP on the SPEs, carboxylic functionalities must be present and available on the sensor surface. In the case of C-SPEs these functionalities are not present natively, therefore they must be generated through a proper treatment. To this aim, it was chosen to oxidize the electrode substrate by drop-casting 0.1 M H_2SO_4 on the SPEs surface and performing 10 Cyclic Voltammetry scans, following the procedure reported by Zanardi et al. [7].

As for the SWCNT-SPEs, these electrodes are commercialized with the carbon electrode substrate modified with carboxyl-functionalized SWCNTs, therefore no additional treatment is required.

The carboxylic functions were then activated for the coupling reaction by means of EDC and NHS, yielding the dry-stable NHS-ester which will later react with the primary amine of the CP. To optimize the coupling reaction, the PNA was dissolved in Carbonate Buffer at pH 9 containing Sodium Dodecyl Sulphate, where the latter is added due to its effect of increasing the wettability of hydrophobic surface [162].

Preliminary tests have been conducted to determine the concentration of CP that leads to the highest loading on the sensor surface. For this purpose, a PNA probe analogous to the CP but bearing a biotin at the C-term (CP-Bio) was employed, through which it was possible to directly evaluate the amount of PNA probe bound to the surface. In fact, the biotin can directly interact with the ALP-Strp conjugate, avoiding the necessity of assembling the complete sandwich complex.

For the SWCNT-SPEs, four levels of CP-Bio concentrations were explored, namely 50 nM, 100 nM, 500 nM and 1000 nM (**Figure 2.29**). The signal increases with the concentration of CP-Bio until the 500 nM level, since no statistically significant difference (*p>0.05*) was observed between the latter and the 1 μM level.

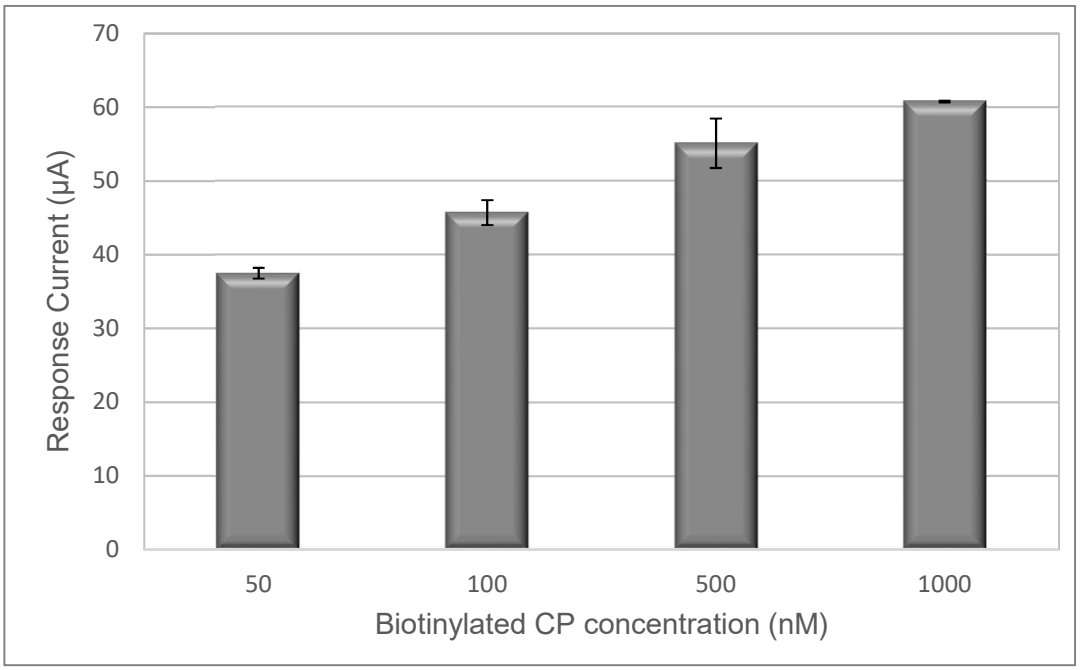

Figure 2.29. Response current observed increasing the concentration of CP-Bio on SWCNT-SPEs to evaluate the loading of PNA probes on the sensor surface.

As for the C-SPEs, the results of the analogous experiment showed no statistically significant difference (p>0.05) between the explored levels, with an overall lower current response (**Figure 2.30**).

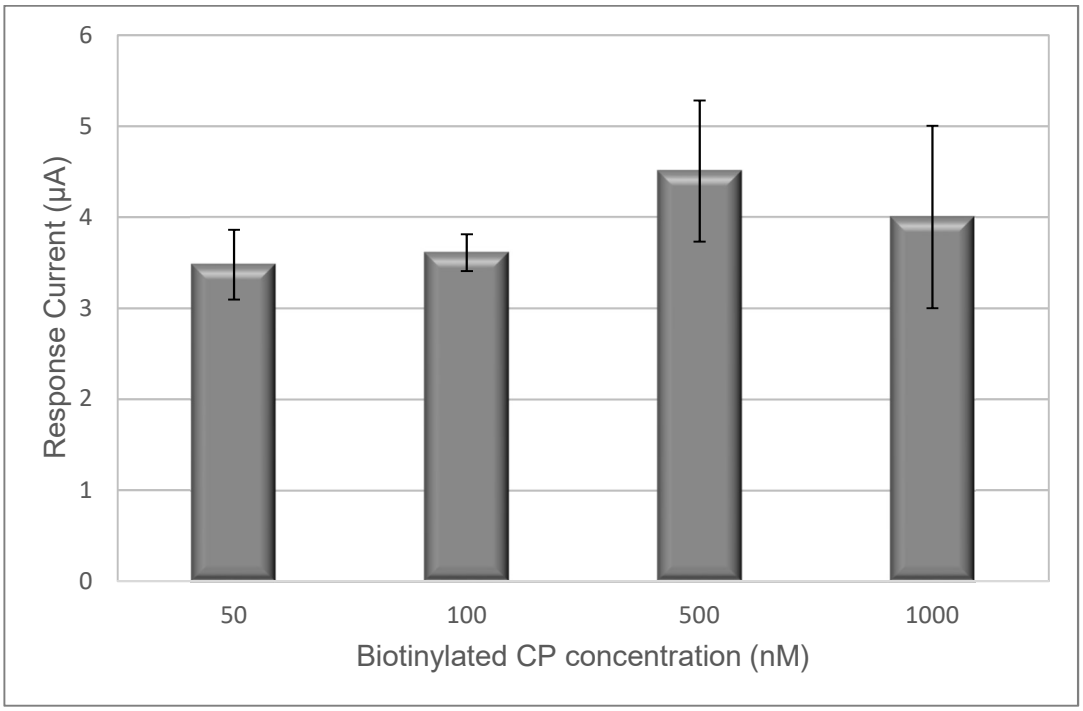

Figure 2.30. Response current observed increasing the concentration of CP-Bio on C-SPEs to evaluate the loading of PNA probes on the sensor surface.

Therefore, for C-SPEs a concentration of CP 50 nM is already sufficient to saturate the active carboxylic functions present on the surface.

As expected, the introduction of nanostructured substrates, yields a signal that is more intense compared to the output obtained on C-SPEs employing the same CP-Bio concentration. This observation can be rationalized on the basis of the synergic effects given by the inclusion of CNTs on the electrode substrate, which increase the amount of active surface, yielding both an increased electrode area and surface available for CP immobilization, and at the same time enhance the efficiency of the electron transfer phenomena [163-165].

Based on the above-mentioned results, it was decided to employ a concentration of CP of 500 nM for the functionalization of SWCNT-SPEs. Even though a 50 nM concentration of CP was sufficient to address the complete functionalization of C-SPEs, a 500 nM CP solution was also employed in order to reduce background signal (see paragraph 2.7.3).

2.7.3. Signal to Background ratio assessment

A common limitation involved in the employment of carbon-based electrode substrates for genosensor development is given by the occurrence of non-specific interactions between nucleobases and these electrode materials [166]. As a consequence of these interactions, the PNA- or DNA-based probe might non-specifically adsorb on the sensor surface. For a sandwich assay, such event would result either in a false negative if the species that non-specifically adsorbs on the surface is the target DNA or, conversely, in a false positive if the SP is present as a consequence of non-specific interactions instead of sandwich assembly. The former case can be avoided by conducting a hybridization between SP and target DNA in solution prior to incubation on the sensing surface. This way, all the DNA is hybridized to the SP avoiding its loss through non-specific interactions. As for SP adsorption, it is necessary to introduce a blocking step after the immobilization of the CP probe using a backfilling agent. In our case two strategies have been adopted to reduce the occurrence of such interactions between carbon-based electrode and SP nucleobases. The first is to use an excess of CP, which, beside covalently bind the activated carboxylic functions, would also non-specifically adsorb since such PNA probe is also subjected to the same kind of interactions. For this reason, on C-SPEs the CP was purposely employed in excess.

The second strategy employed is to introduce a blocking step following CP immobilization with a solution of 500 nM pyrene in DMSO. To evaluate the efficiency of this backfilling solution, the current signals in presence (signal) and absence (background) of target DNA were acquired without blocking and with pyrene solution (**Figure 2.31**). Upon increase of pyrene concentration to 5 μM no enhancement on the signal to background ratio (S/B) was obtained.

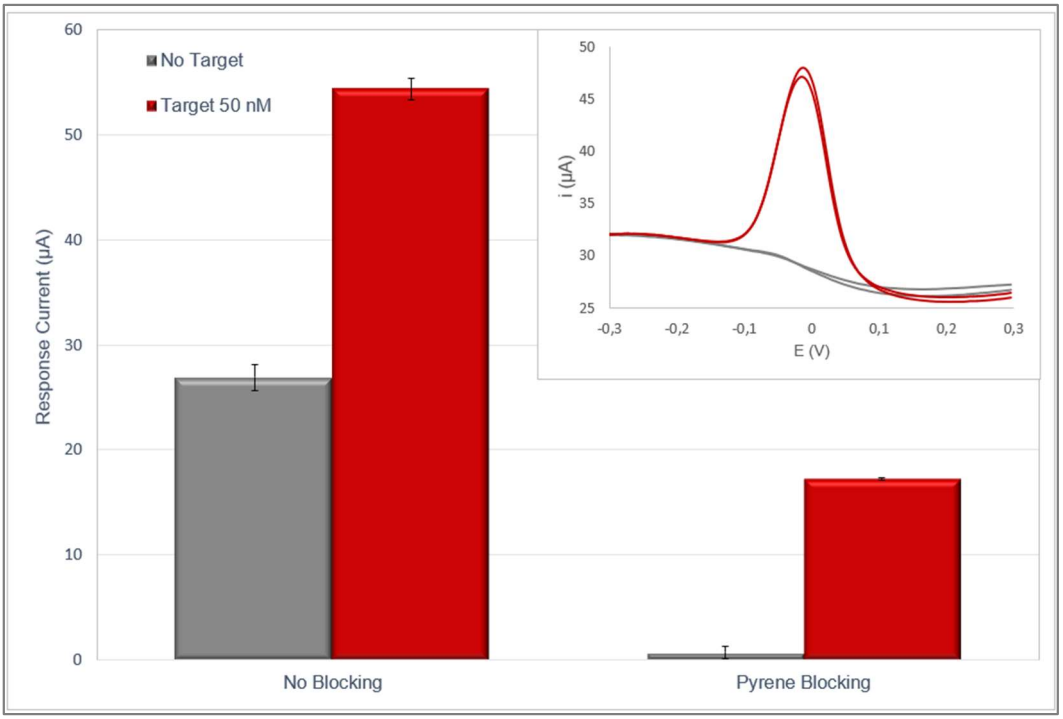

Figure 2.31. Comparison of the response current obtained with and without pyrene blocking in presence (signal, red) and absence (background, grey) of 50 nM target DNA. Inset: voltammograms acquired in presence (red) and absence (grey) of target DNA with pyrene blocking.

Since non-specific interactions between carbon-based substrates and nucleobases primarily arise from the establishment of π-π interactions, the effect of pyrene is to prevent non-specific adsorption by formation of the same kind of interactions. Furthermore, the DMSO creates a passivating layer which, in addition to the effect of pyrene, results in a drastic reduction of the background signal. As shown in **Figure 2.31**, even the positive signal is subject to a consistent decrease in intensity given by the removal of the non-specific component, which was present also in the positive signal. However, even though the absolute intensity of the positive signal is decreased by the employment of the pyrene in DMSO solution, the overall S/B ratio is enhanced. The effect of the SP concentration towards the efficiency of the backfilling solution on SWCNT-SPEs was also tested. The S/B ratio was obtained comparing the results obtained with three different levels of SP concentration, namely 10 nM, 20 nM and 50 nM in absence and in presence of equimolar target DNA (**Figure 2.32**). The best conditions were found for a SP concentration of 20 nM, yielding a S/B ratio of approximately 27.

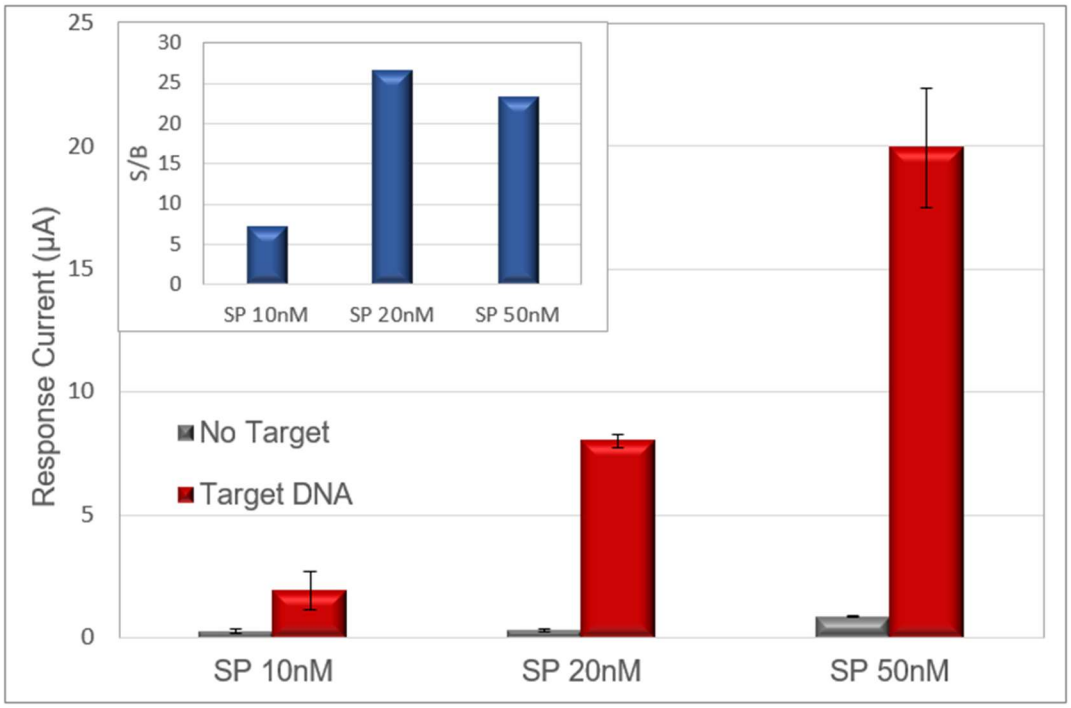

Figure 2.32. Representation of the output signals at different SP concentration in presence (red) and absence (grey) of Target DNA. The line represents the trend of the S/B ratio.

As evidenced in **Figure 2.32**, this backfilling strategy depends on the amount of SP used for the assembly of the sandwich complex. In particular, when its concentration is increased over a threshold value the efficiency of the blocking decreases yielding lower S/B ratios. Therefore, despite the outstanding ability of pyrene in DMSO solution to reduce the non-specific interactions between nucleobases and carbon-base electrode substrates, the dependency on the concentration of SP employed for the assay can constitute a limit in terms of linear response range achievable with this method.

Even though a more intense positive signal was achieved employing a SP concentration of 50 nM, taking into account the slightly lower S/B ratio and consistently higher data dispersion registered, it was chosen to set the concentration of SP at 20 nM for following experiments on SWCNT-SPEs.

As for C-SPEs, it was decided to set the SP concentration to 50 nM, in order to obtain a S/B of approximately 23 (**Figure 2.33**), comparable with the S/B obtained on SWCNT-SPE with 20nM SP. It is possible to observe a slightly lower intensity of signals on C-SPEs if compared to SWCNT-SPEs, in fact the presence of nanostructured electrode substrate allows to achieve higher signals in

presence of the same amount of electroactive species, due to the improvement of the electron transfer phenomena, enhanced by CNTs.

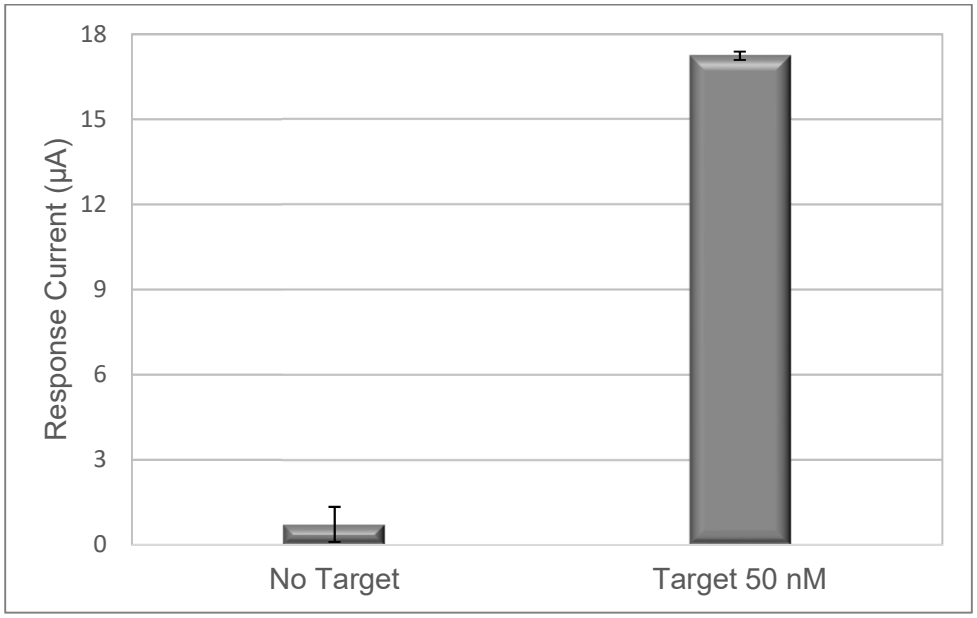

Figure 2.33. Response Current obtained on C-SPE employing SP at a concentration of 50 nM in presence and absence of target DNA at a concentration equimolar to SP.

2.7.4. Calibration curve on SWCNT-SPEs

After the selection of the best conditions for sandwich assembly in terms of CP and SP concentration, different concentration levels of 45-mer synthetic target DNA were explored on SWCNT-SPEs in order to assess the analytical performance of the genosensor. The target DNA concentration levels explored were 0.25 pM, 0.5 pM, 0.75 pM, 1 nM, 1.25 nM, 1.5 nM, 1.75 nM, 2.5 nM and 5 nM (**Figure 2.34**).

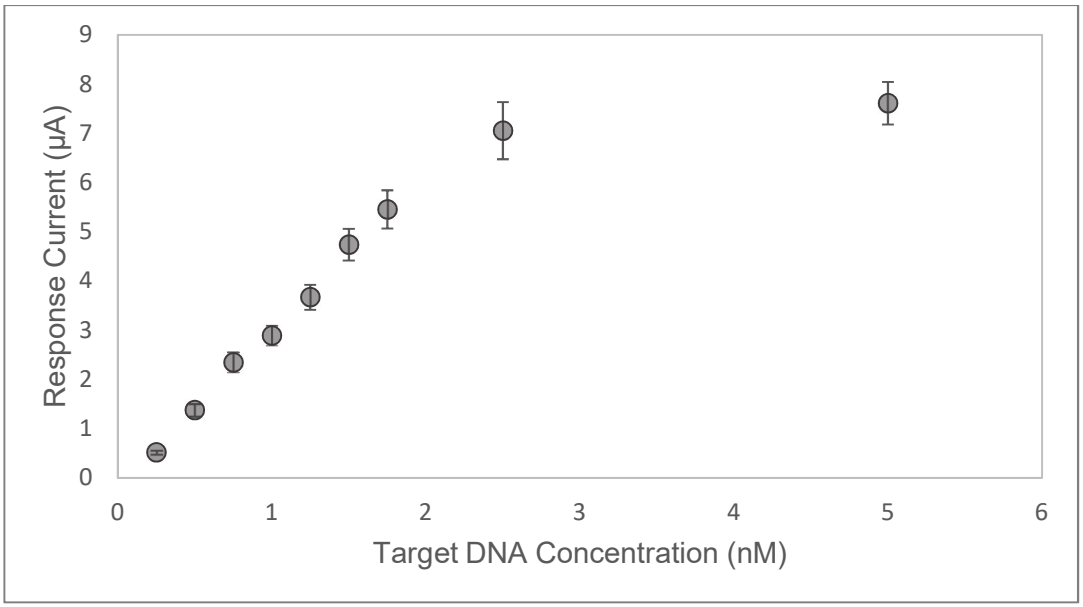

Figure 2.34. Calibration curve of the genosensor system obtained using synthetic DNA.

The saturation of the signal is reached at 5 nM, while the linear dynamic range spans from 0.25 pM to 2.5 nM (**Figure 2.35**). Through interpolation of this linear range it is possible to assess a limit of detection (LOD) of 64 pM and a limit of quantitation (LOQ) of 215 pM.

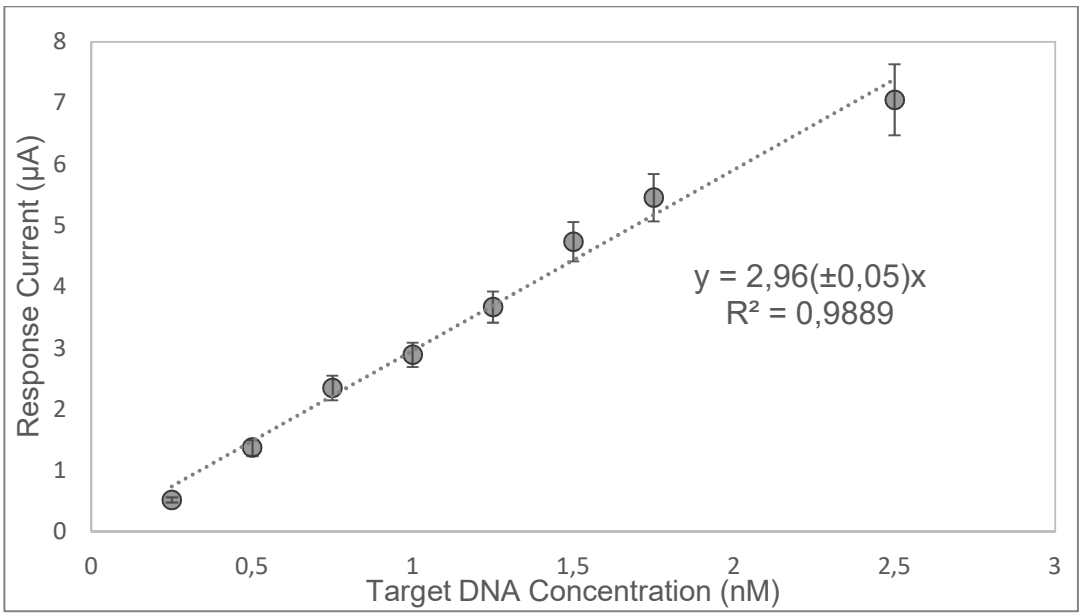

Figure 2.35. Linear dynamic range of the calibration curve fitted through linear interpolation. Mean and standard deviation (n>4) for each concentration level are reported.

2.7.5. Selectivity of the genosensor

An important parameter for a genosensor is given by its ability to discriminate between complementary target sequence and sequences containing mutations, i.e. mismatch sequences. The latter may contain a different nucleobase or the same nucleobase with a mutation in its structure that might result in the incurrence of a specific pathology or a different response mechanism towards drugs or pathogens. It is worth pointing out that for the purpose of detecting genetically modified organisms, the selectivity of the genosensor plays a minor role, since the aim of the assay is to detect the presence an entire sequence rather than discriminate between two that differ by a nucleobase. Nevertheless, the selectivity of the method was tested by comparing the responses obtained with the full-match (FM) target DNA with two other synthetic DNA sequences, namely the single mismatch (1-MM) containing a non-complementary nucleobase and the Scrambled (SCR) sequence with the same nucleobase composition but in a randomized order. The non-complementary nucleobases have been introduced in the 20-mer portion of the target DNA complementary to the CP. In fact, as the hybridization with the latter occurs in heterogeneous phase, the presence of a mismatch has a greater impact over the association of the probes with respect to the hybridization between target DNA and SP, which occurs in solution.

The results showed a reduction of the signal between the FM and 1-MM DNA of approximately 28%, while for SCR DNA the reduction was as high as 98% (**Figure 2.36**).

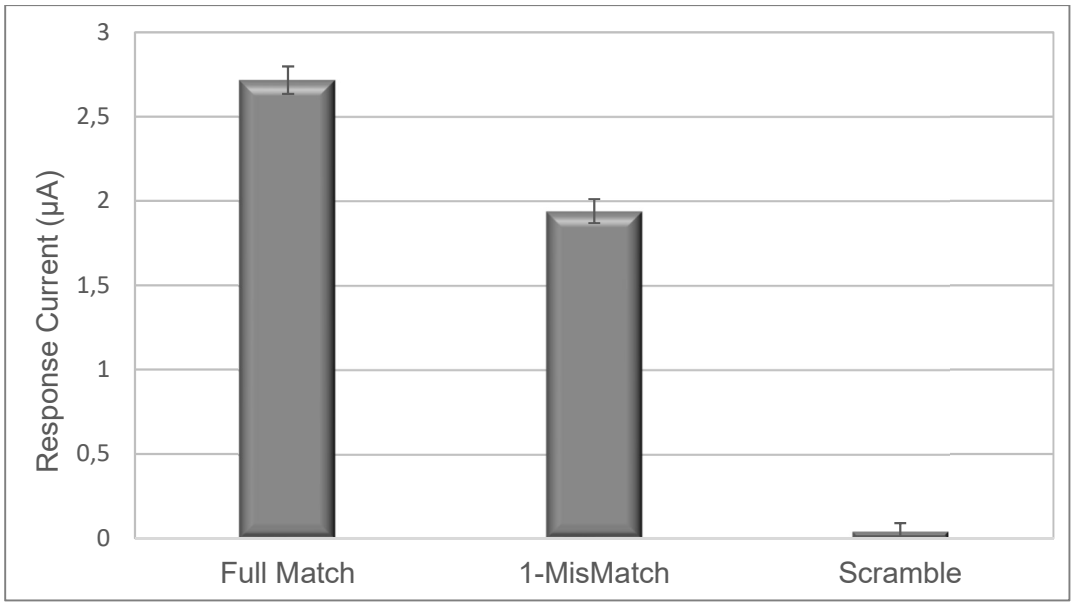

Figure 2.36. Response current obtained using the FM, 1-MM and SCR DNA

Such reduction of the signal in presence of a single non-complementary nucleobase represents a promising result, especially taking into account that the sequence over which the mismatches have been introduced has a 20-mer length while typically sequence used for selectivity purpose possess a reduced length [167,168].

2.7.6. Validation in real sample

The results reported above have been obtained employing a synthetic 45-mer DNA whose sequence reproduced a portion of the *Roundup Ready* soy DNA. For the validation of the method it was chosen to test the genosensor using extracts of genomic DNA from soy flours. In particular, the flours employed were European Reference Material (ERM) with a certified percentage amount of RR soy in wild-type (*wt*) soy. Taking into account the European regulation EC 1830/2003, which sets an upper limit of 0.9% of GM products contained in food and feed over which the product must be labelled as "genetically modified", the percentages of RR soy chosen were 10 % and 1% which were compared with *wt* soy.

Genomic DNA was extracted from the ERM soy flours using a commercial extraction kit. Subsequently to extraction, the amount of DNA extracted was assessed through spectrophotometric assay, considering that a 50 ng/µL concentration of DNA has an optical density of 1 at 260 nm [169]. The extraction

from 400 mg of ERM flour produced genomic DNA solutions with a concentration of approximately 60 ng/μL, with variations depending on the extraction efficiency. These solutions were then diluted in order to reach a DNA concentration for both concentration levels included in the linear range of the genosensing assay. However, taking into account that the extracts contain strands of genomic DNA of different lengths and the difficulty involved in determining the weight of such strands, it is not possible to precisely express the concentration of the solutions as molarity.

For the application of the analysis to genomic DNA a new step is required with respect to synthetic DNA. In fact, the extracted DNA will be present in solution paired with its complementary strand in a double helix, which must be opened in order to have the target sequence of the DNA available for hybridization with the SP and CP. This has been achieved by introducing a new step prior to hybridization of the DNA with the SP, where the DNA is heated at 95 °C for 30 minutes, during which the two natural complementary strands are unpaired. Immediately after this step the SP is added while the solution is slowly cooling down to room temperature.

It is worth mentioning that the SP cannot be mixed with DNA prior to the heating at 95 °C since it was observed that the SP cannot withstand such temperature for a prolonged time, which leads to the degradation of the molecule and the loss of the biotin tag. This results in the generation of a low background signal approximately three times more intense compared with the background observed at room temperature (**Figure 2.37**). However, because of the SP degradation, only a background signal is observed even when the complementary DNA is present in solution.

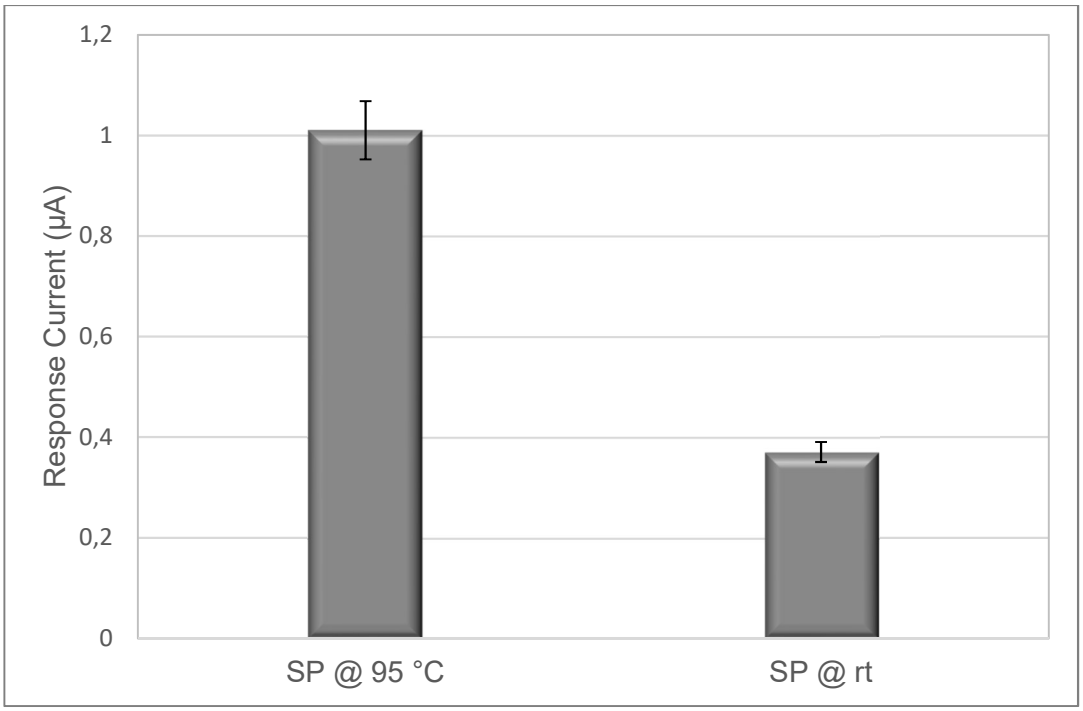

Figure 2.37. Comparison of response current obtained for blanks (in absence of DNA) with signalling probe incubated at 95 °C for 30 minutes (SP @ 95 °C) and SP at room temperature (SP @ rt).

For the carry out of the assay with genomic extracts, it was chosen to dilute the extracts to an equal final concentration of 0.36 ng/µL. Under these conditions it was possible to observe a good trend between the increasing concentration levels from blank (*wt*) to 10% *RR* (**Figure 2.38a**), with strongly significant difference (p<0.001) allowing to discriminate between *wt* flour and samples containing 1% genetically modified materials, very close to the threshold value established by EC regulation (0.9 %) (**Figure 2.38b**). Through the use of the developed assay it was possible to obtain the outstanding result of directly detect the presence of the target sequence without the need of DNA amplification. In fact, many genosensing methods require the amplification of a target sequence through means such as PCR, which even though it simplifies the assay recognition event, it also translates into a higher cost for the analysis and a greatly increased time for the carry out of the method, which negatively affect the efficiency of the method.

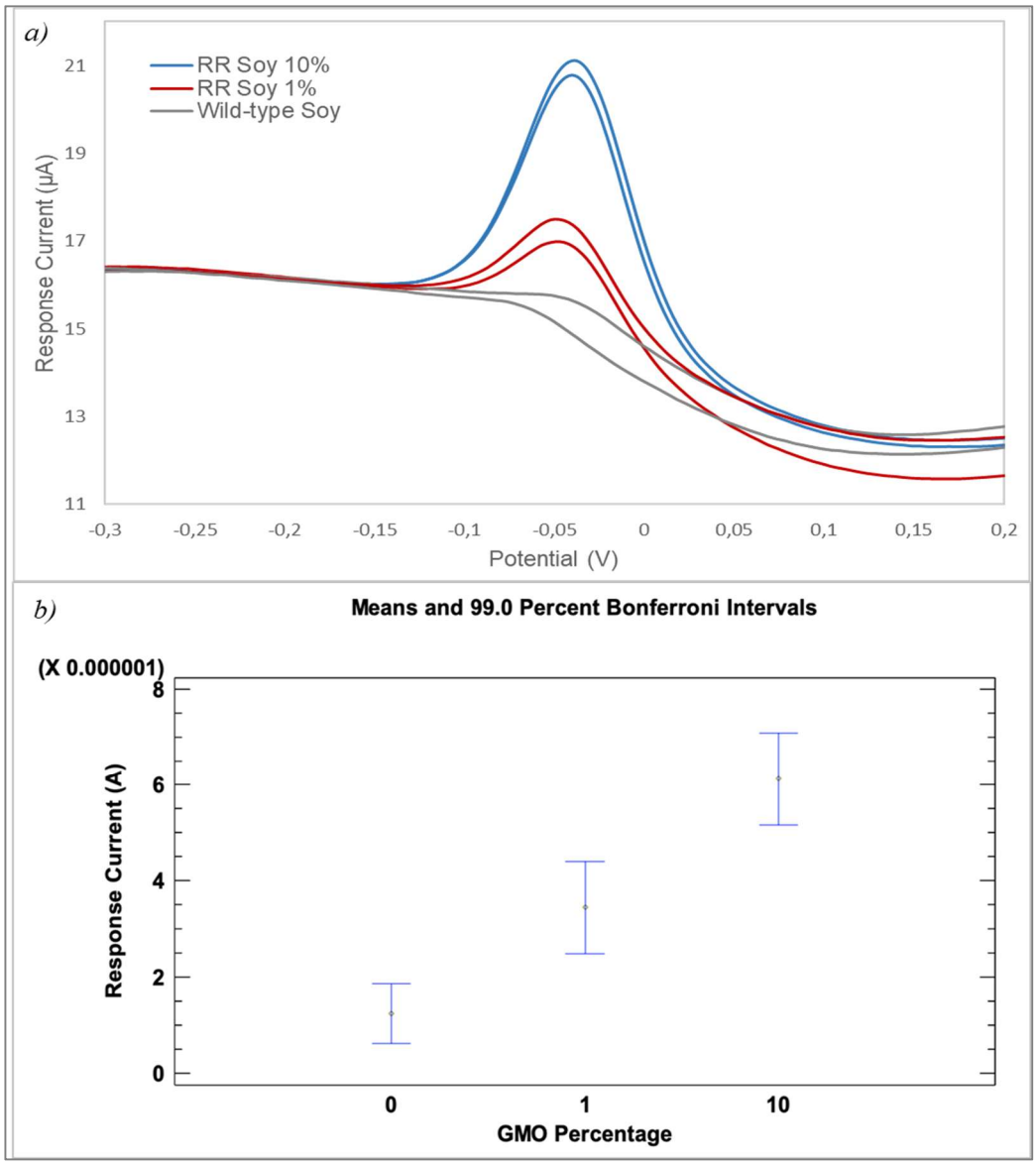

Figure 2.38. a) DPV voltammograms obtained from genomic DNA extracted from ERM flours containing wild-type soy (grey), 1% RR soy (red) and 10% RR soy (blue). b) ANOVA plot from the three levels of RR soy in genomic extracts.

It is worth pointing out that even though the case of study chosen for the development of the current genosensor was the detection of GM soy, genosening assays have a great versatility given by the possibility of modifying the target DNA recognized by simply changing the sequence of the probes. For this reason, the proposed method can be applied to a wide range of purposes.

2.7.7. *Calibration curve on C-SPEs*

An analogous assessment of the analytical performance of the assay was carried out on C-SPEs, employing the best conditions of CP and SP concentrations for this electrode substrate found during previous experiments. The results were then compared with those obtained exploiting the nanostructured electrode substrate to evaluate the benefit of CNT transduction.
The levels explored on C-SPEs were 1.5 nM, 2.5 nM, 5 nM, 7.5 nM and 10 nM, over which the genosensor yields a linear response (**Figure 2.39**). Through interpolation over this range it was possible to assess a LOD of 430 pM and a LOQ of 1.43 nM.

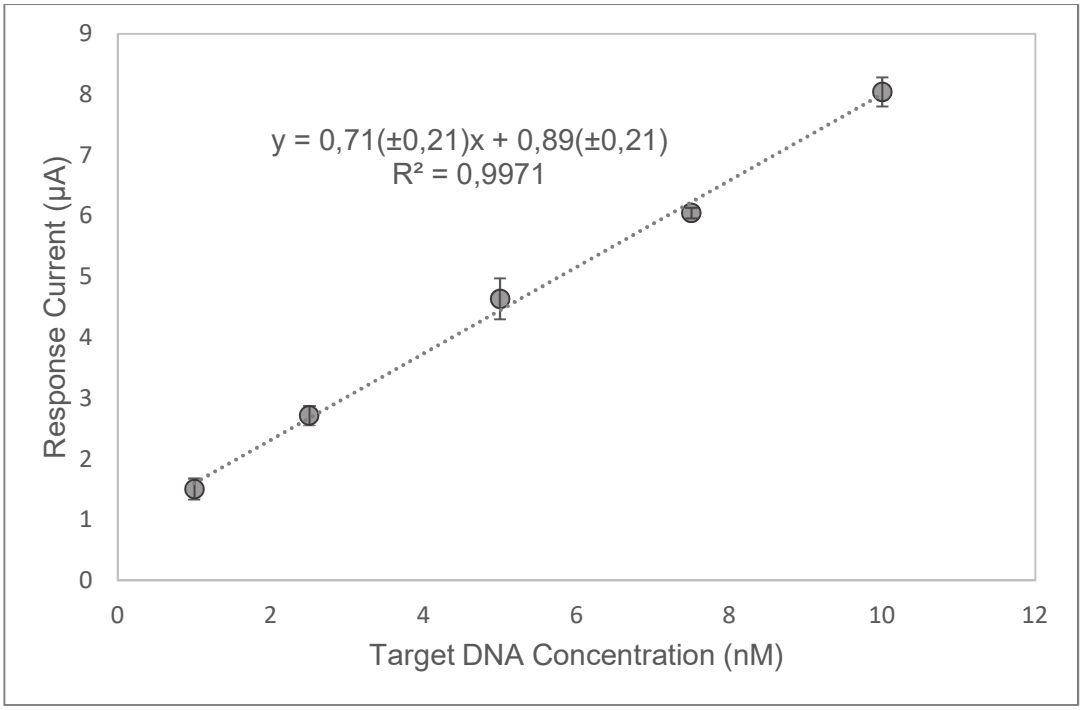

Figure 2.39. Linear dynamic range of response obtained on C-SPEs fitted through linear interpolation. Mean and standard deviation (n>4) for each concentration level are reported.

By comparison with the results obtained on SWCNT, it is possible to determine that the implementation of CNTs as electrode substrate allows to achieve a four-fold enhancement in sensitivity (**Figure 2.40**).

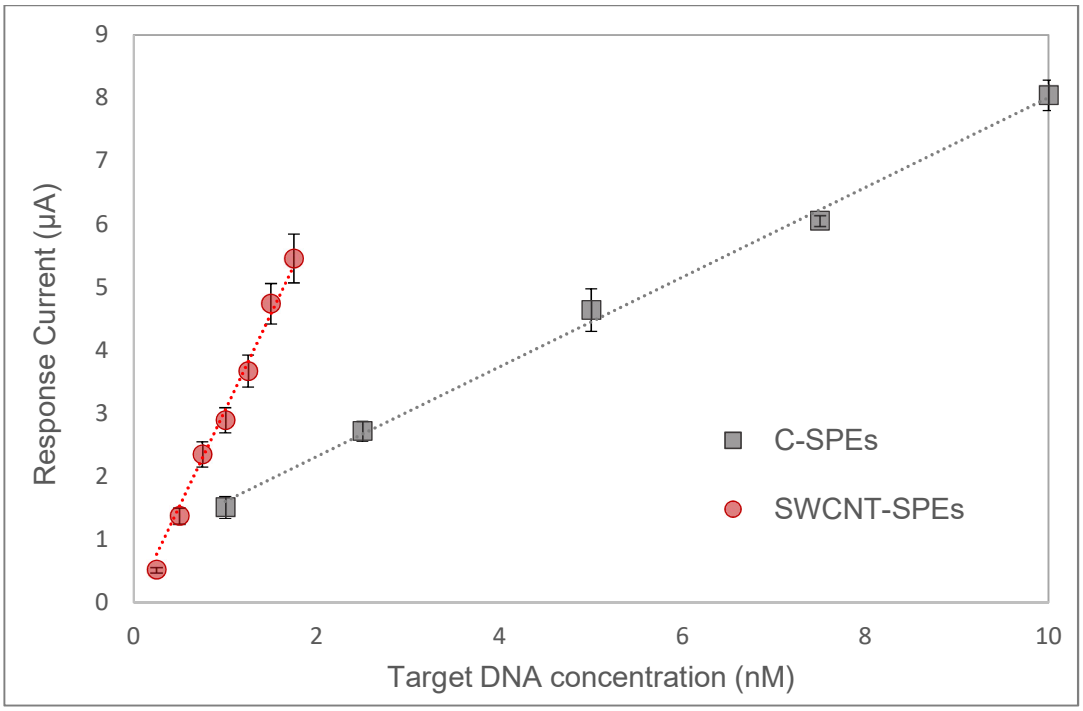

Figure 2.40. Comparison of the linear dynamic range of response on C-SPEs (grey) and SWCNT-SPEs (red)

In order to evaluate the increase in electroactive surface ascribable to nanostructured substrate, voltammetric measurements at different scan rates were carried out and interpolated by means of Randles-Sevcik equation [170,171]. CV scans were performed on C-SPEs and SWCNT-SPEs using 5mM $K_4Fe(CN)_6$ as redox probe and the electrode active surface was calculated from the slope obtained plotting the anodic (forward) peak current height versus the square root of the scan rate. An active area equal to 11.7 mm^2 was assessed, while the same parameter for SWCNT-SPEs was estimated at 18.4 mm^2, thus resulting in an enhancement of 1.57-fold. However, by comparing the slope of the calibration curves obtained on the two electrode substrates an enhancement of approximately 4.17 times was observed. This can be explained taking into account that carbon nanotubes signal enhancement effect is not limited to the increase in electrode surface but also to a higher efficiency in the electron transfer phenomena.

Therefore, on the basis of the application for which the genosensor must be employed and the sensitivity required, it is possible to choose on which electrode substrate the immobilization is carried out. In particular, the employment of C-SPEs translates in a reduction of the cost of the analysis,

however the enhancement in sensitivity granted by the carbon nanotubes outbalances the cost difference.

2.7.8. Transposition of the sandwich assay on rGO-FET

The following work has been carried out at the Austrian Institute of Technology in Tulln (Austria), where I was hosted by professor Wolfgang Knoll.
The aim of this work has been to assemble the developed genosensing assay on reduced-graphene oxide (rGO) which was deposited between interdigitated gold electrode for the development of a FET-based genosensor. Such system would generate a signal as a consequence of the hybridization of the target DNA without the aid of an enzyme for the generation of an electroactive species. In fact, the presence of charged species (i.e. DNA, which is a polyanionic molecule) between source and drain electrode would influence the current flowing between the two, which in turn depends on the voltage applied between gate and source electrode.
However, in order to verify the efficiency of the immobilization on the rGO chips and directly compare it with the data obtained on SPEs, the assay was maintained equal to the one carried out on SPEs, i.e. generating the electroactive species through enzymatic means and performing a DPV readout, which was possible by short-circuiting the source and drain contacts, thus using the interdigitated gold electrodes as working electrode.
For immobilization of the amino-functionalized CP it is necessary that the sensing surface presents carboxyl groups available for coupling reaction. Differently from SWCNT-SPEs, where such functions were natively present, on rGO-FET no carboxylic function is present after the reduction of the graphene on the surface, therefore a new strategy must be devised. To this aim it was chosen to employ a heterobifunctional molecule containing a pyrene moiety at one end, capable of attaching to rGO through the establishment of π- π stacking interactions, and a carboxyl group at the other end, which results exposed to solvent and can be exploited as anchoring point for the CP. The molecule exploited for rGO functionalization was pyrenebutyric acid (PBA) and, after its immobilization the assay is carried on as for SPEs (**Scheme 2.2**).

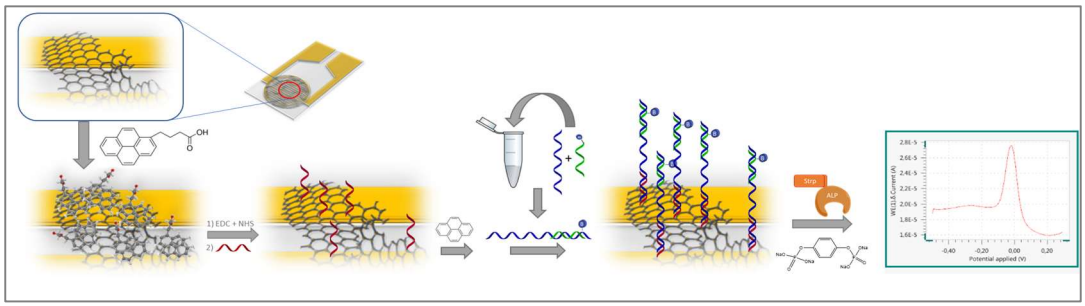

Scheme 2.2 Functionalization steps of the reduced-graphene oxide deposited as a bridge between interdigitated gold electrodes to form the FET sensor.

2.7.9. *PBA immobilization*

A crucial aspect for an efficient interaction between PBA and rGO is given by the solvent in which the PBA is diluted. Different solvents have been tested, namely methanol (MeOH), tetrahydrofuran (THF), dimethylsulphoxide (DMSO) and dimethylformamide (DMF) in which PBA was dissolved in order to reach a final concentration of 1 mM.

For the deposition from MeOH, the rGO chips were immersed for two hours in the PBA solution and the DPV signals obtained in presence (positive) and absence (background) of target DNA were compared (**Figure 2.41**). Even though the background signal is completely absent, the positive signal is approximately 65 times lower than the analogous signal recorded on SWCNT-SPEs. However, the most critical aspect was evidenced when the positive signal was compared with the signal obtained in presence of SP and target DNA on a rGO chip that has not undergone CP immobilization (blank CP) and with a chip on which a CP non-complementary to target DNA was immobilized (nc-CP blank) (**Figure 2.41**). In fact, in this case it is possible to observe that the positive and the nc-CP blank signals have the same intensity, while the blank CP is more intense. These results suggests that the immobilization of the CP was not successful, in fact both complementary and non-complementary CP reduce the signal as a consequence of their non-specific adsorption to the sensing surface (see paragraph 2.7.3), while, when no CP was incubated, the surface was left "clean" and more available towards establishing non-specific interactions with the DNA-SP hybrid.

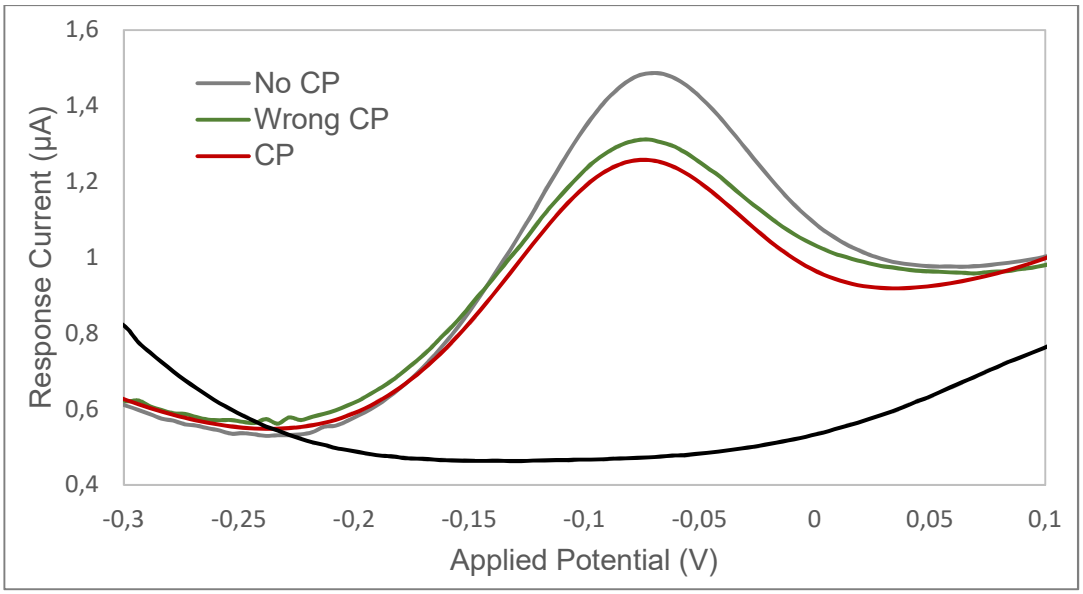

Figure 2.41. DPV signals acquired on rGO-modified Micrux chips where PBA was deposited from MeOH solution. The signal deriving from the complete sandwich assembly (red) was compared with those obtained in absence of Target DNA (black), in absence of CP (grey) and with a non-complementary PNA CP (green).

For rGO functionalization with PBA in DMF it was decided to extend the incubation time of the solution to overnight, in order to obtain the highest degree of functionalization possible. However, the comparison between the positive and blank CP (where no CP was deposited on the surface) led to equal results as for MeOH, i.e. blank CP is more intense than positive test (**Figure 2.42**).

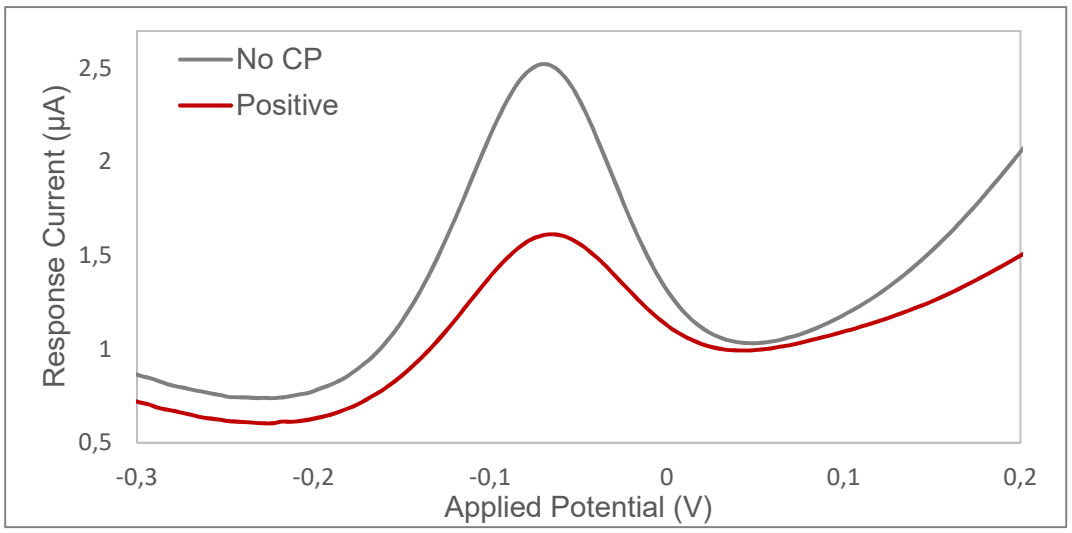

Figure 2.42. DPV signals acquired in presence (red) and absence (grey) of CP on rGO-modified Micrux chips where PBA was deposited from DMF solution

For further testing of CP immobilization on rGO it was chosen to employ the biotinylated PNA capture probe, thus avoiding the necessity of assembling the whole sandwich complex in order to generate the electroactive species leading to a simplification of the protocol and a reduction of the variables involved in each experiment.
For testing DMSO as solvent, the interaction of PBA solution with rGO chips was conducted overnight and the efficiency was evaluated by comparing the results obtained on sensors where the EDC/NHS activation was performed (positive) with those obtained in absence of activation (activation blank). In this case a modest S/B ratio of approximately 3.5 was obtained (**Figure 2.15**).
For the use of THF as a solvent, given its high volatility, an overnight immersion of chips in the solution was not performed. Instead, 10 µL of the PBA solution were drop-casted on the surface of the chips and left until complete evaporation, the process was then repeated for a total of four times. As for DMSO, blank activation and positive signals were compared to test the functionalization efficiency, registering a S/B ratio of approximately 5 (**Figure 2.43**).

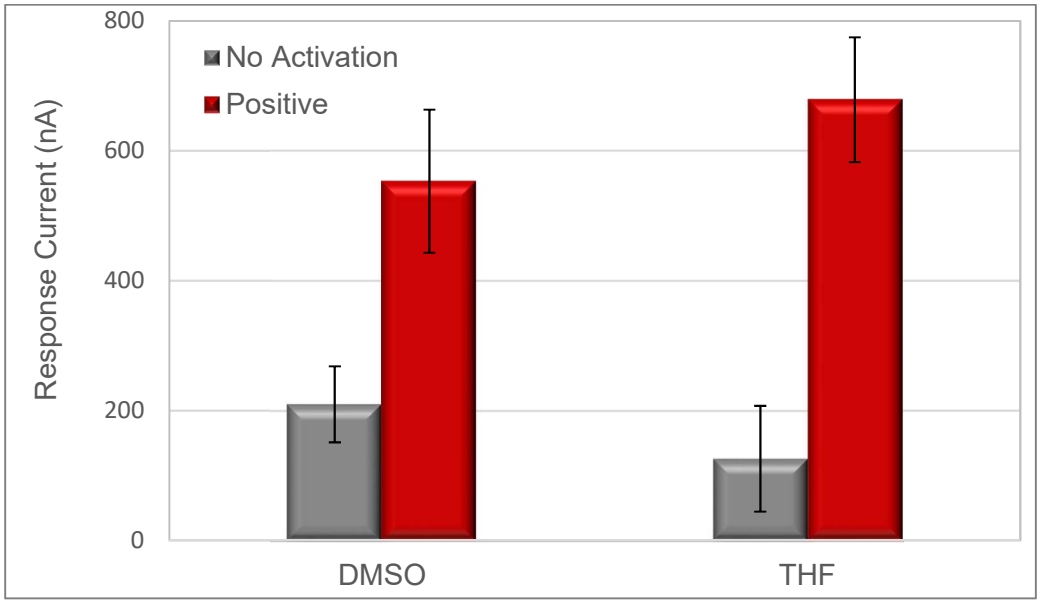

Figure 2.43. Comparison of the signals obtained on rGO-modified Micrux chips where PBA was deposited from DMSO or THF solution. The signals were obtained with EDC/NHS activation (red) and in absence of activation(grey).

On the basis of these results it was decided to employ THF as PBA solvent and test the assembly of the complete sandwich complex in presence and absence

of CP. It was observed that a higher background signal is generated, leading to a reduction of S/B ratio to 1.5 (**Figure 2.44**).

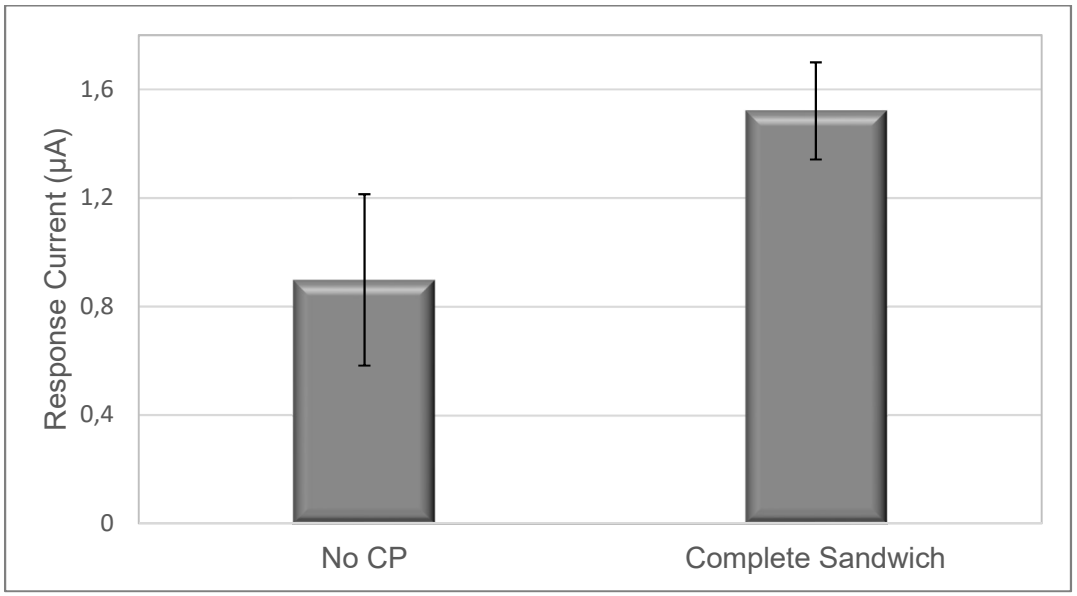

Figure 2.44. Signals obtained in absence and presence of CP on rGO-modified Micrux chips where PBA was deposited from THF solution.

This result excludes the possibility of applying the system as it is for FET analysis without reaching an enhancement of the S/B ratio first.

2.7.10. Blocking with Denhardt's solution

In order to achieve a better S/B ratio, the non-specific interactions between rGO and the DNA-SP hybrid must be reduced employing a new blocking strategy. In fact, this non-specific adsorption represents a critical limitation for the FET sensor since the signal is generated simply by the presence of DNA on the sensing surface. As a consequence, the adsorption of DNA would generate a false positive signal which does not depend on a specific recognition with CP probes, thus losing all of the sensor selectivity.

To reduce the background signal, beside the pyrene in DMSO solution, which has been used in all experiments after CP immobilization, the Denhardt's solution was introduced in the Hybridization Buffer (HB). The solution, in its commercialized form at concentration 50x, contains 1% Ficoll, 1% polyvinylpyrrolidone and 1% BSA and it is commonly used in assays involving the hybridization between oligonucleotide probes [172-174]. Its role is not limited to a blocking effect against the establishment of non-specific

interactions, but it also facilitates the interaction between complementary probes.

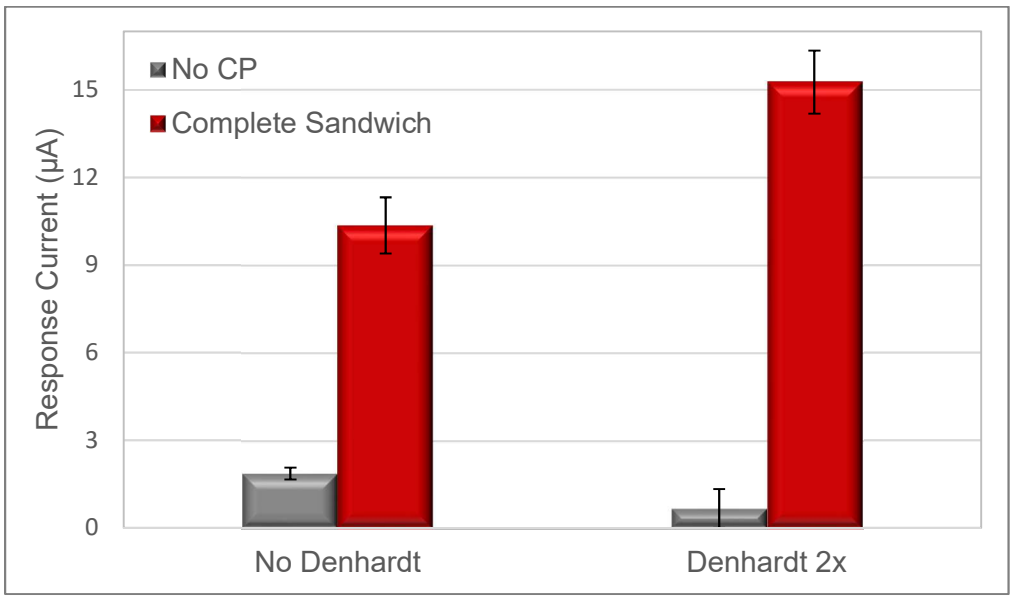

Figure 2.45. Effect of Denhardt's solution at concentration 2x registered on SWCNT-SPEs in presence (red) and absence (grey) of target DNA

As a preliminary test, the effect of Denhardt's solution at concentration 2x included in the HB was studied by carrying out the assay on SWCNT-SPEs (**Figure 2.45**). As expected, the new strategy had a double effect of reducing the non-specific adsorption of the DNA-SP hybrid, as shown by the reduction in the signal observed in absence of CP, while it simultaneously enhances the hybridization efficiency increasing the positive signal.

An analogous test was carried out on rGO-functionalized chips. In particular, to evaluate the effect of Denhardt's solution on S/B ratio, two different concentrations of the blocking solution were employed, namely 2x and 4x on chips were the sandwich assay was assembled exploiting PBA in THF solution for the generation of carboxylic functions. Once again, the results obtained in presence (positive) and absence (blank CP) of Capture Probe were compared to evaluate the S/B ratio (**Figure 2.46**).

It was observed that a modest improvement was obtained using Denhardt 2x, leading to a S/B ratio of approximately 2.5. However, an even bigger enhancement of the ration was obtained increasing the Denhardt's solution concentration to 4x, which allowed to achieve a S/B of 7.5. Also in this case the

improvement is a consequence of the simultaneous decrease in non-specific signal and increase in positive signal.

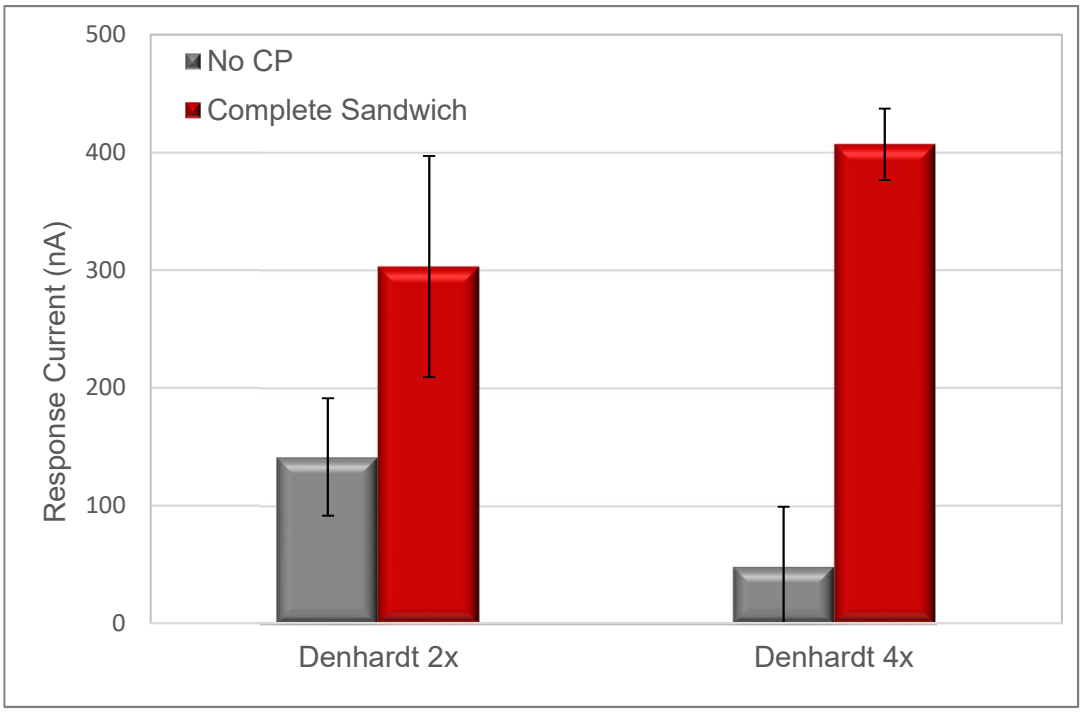

Figure 2.46. Effect of Denhardt's solution 2x and 4x on rGO-functionalized chips in presence (red) and absence (grey) of target DNA

Even though it was possible to improve the S/B ratio employing a proper solvent for PBA to achieve an efficient immobilization and the blocking strategies given by pyrene in DMSO and Denhardt's solution, a critical limit of the system is given by the absolute signal intensity of the positive tests. In fact, comparing the complete sandwich assembled on SWCNT-SPEs and rGO-functionalized chips in presence of Denhardt's solution it was observed that on the latter the signal was roughly 40 times less intense than the one recorded on the SPEs.

2.7.11. FET tests

The best conditions found in terms of PBA solvent and Denhardt's solution concentration were employed to perform the FET measurements. The experiments were carried out by using two connected flow chambers containing a Micrux chip functionalized with CP in one chamber and a non-modified rGO-chip in the second. The I_dV_g curves were acquired before and after

a solution containing the target DNA at 100 nM concentration was fluxed in the two chambers for two hours, however no shift in the two curves was observed (**Figure 2.47**).

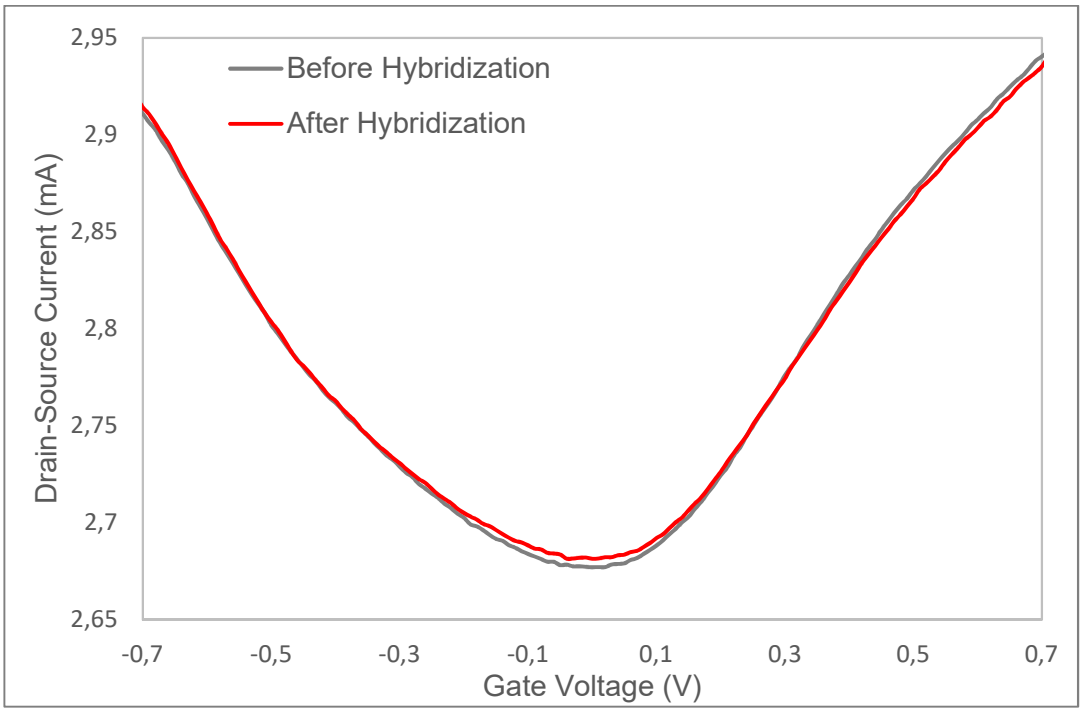

Figure 2.47. I_dV_g curves registered before (grey) and after (red) the target DNA solution was fluxed in the chamber containing rGO-modified chips functionalized with CP

Therefore, the system in this configuration possesses a sensitivity that is too low to detect the hybridization occurring on the surface. Furthermore, even reading in DPV, with the benefit connected to the enzymatic generation and amplification of the signal, the intensity was much lower than the one observed on SWCNT-SPEs. These findings suggest that the functionalization of rGO with PBA to generate anchoring points for PNA CP covalent immobilization had a modest efficiency, which is not sufficient to observe a signal given by target DNA hybridization during FET measurements. Furthermore, the low efficiency of this strategy also translates in a high data dispersion (10 % < RSD < 30 %) that was observed throughout all of the performed experiments, leading to a poor robustness of the method. As a consequence, new strategies for the immobilization of the PNA probes will be tested in future projects.

2.7.12. Sandwich genoassay on magnetic micro-beads

The genosensor developed by immobilization of the CP on SWCNT-SPEs proved to be fit for the detection of GM DNA in nonamplified genomic extracts of soy flours. However, some limitations are involved in the genosensing method, mainly given by the carbon-based electrode substrate. In fact, the presence of the latter requires the use of a backfilling agent, i.e. pyrene in DMSO solution, to avoid the establishment of nonspecific interactions between nucleobase-containing probes and electrode substrate. However, the employment of the blocking solution results in a consistent drop of the positive output signal as well as an upper limit on the SP concentration that can be employed in order to maintain the efficiency of the backfilling treatment (see paragraph 2.7.3), which in turn limits the dynamic range of response achievable through the genosensor analysis.

To overcome these limits, it was decided to transfer the sandwich protocol on magnetic micro-beads (mMB). In fact, the surface of mMB does not expose any carbon-based material, therefore no nonspecific interaction with nucleobase is expected to occur and backfilling strategies are no longer required. Furthermore, the modification of magnetic beads occurs in suspension, therefore by assembling the sandwich complex on the surface of magnetic beads, it is possible to carry out the incubation of the probes by suspending the beads in the reaction solution and under agitation. This way, a more effective interaction between probes on the surface and in the solution is achieved, increasing the hybridization efficiency. Finally, the magnetic properties of the beads allow for easy separation and cleaning steps, making the functionalization protocol easier and faster.

The size of the beads employed is in the micro scale (2.8 μm) and the surface is modified in order to expose carboxylic functions, which grant both a hydrophilic character, necessary to obtain an efficient interaction between probes on the surface and probes present in the aqueous phase, and anchoring points where the amino-terminated Capture Probe can be covalently immobilized through coupling reaction.

The general scheme for the assay development on magnetic mMB (**Scheme 2.3**) resembles the one performed on SWCNT-SPEs, since in both cases carboxyl groups are present on the surface. Therefore, a direct activation of the functionalities can be performed through EDC and NHS, followed by immobilization of the 20-mer PNA CP. Subsequently the sandwich is assembled

by hybridization of the CP with the target DNA-SP complex, which was previously formed by hybridization of the 20-mer PNA Signalling Probe to a portion of the 45-mer DNA different from the one recognized by the CP. Following the sandwich formation, the alkaline phosphatase-streptavidin conjugate is introduced, resulting in the immobilization of the enzyme through interaction between the biotin tag of the SP and streptavidin. Finally, the enzyme substrate Hydroquinone diphosphate is added and processed by the ALP to form the electroactive hydroquinone whose oxidation peak is registered in DPV. All of these steps are performed on mMB aqueous suspensions while for the final readout in DPV it is necessary to dispose of a three-electrode cell. In our case we employed SPEs assembled on a magnetic support that allows for mMB confinement on the WE of the SPE. Both C-SPEs and SWCNT-SPEs were tested to perform the final readout of the genoassay.

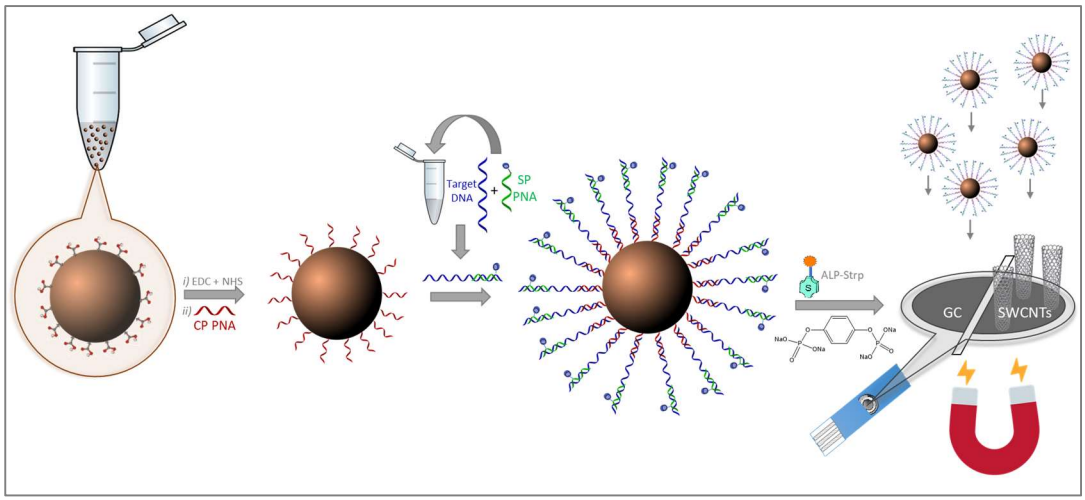

Scheme 2.3. Experimental protocol of the genoassay implemented on mMBs

2.7.13. CP loading on mMB

In order to determine the concentration of CP necessary to address all the activated carboxyl groups, different concentrations of biotinylated Capture Probe (CP-Bio) were immobilized on the surface of the magnetic beads. Given that these PNA probes expose a biotin, they can directly interact with ALP-Strp conjugate and subsequently generate the electroactive species responsible of the generation of the DPV signal, which in this case was measured by isolating the beads on the surface of C-SPEs.

The CP-bio concentration levels explored were 50 nM, 250 nM, 500 nM, 1 μM and 2 μM (**Figure 2.48**).

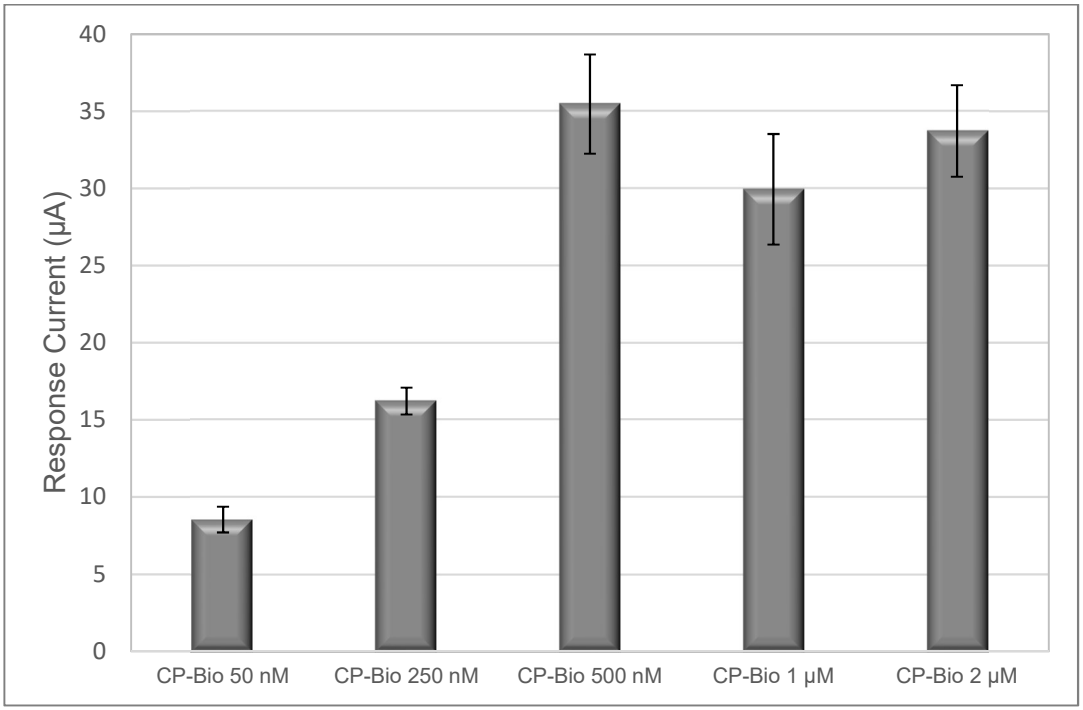

Figure 2.48. Responses obtained employing different concentrations of biotinylated capture probe immobilized on the surface of activated magnetic micro-beads.

The results evidenced that the signal increases up to a CP-Bio concentration of 500 nM, where the signal saturates, since no statistically significant difference is observed between 500 nM, 1 μM and 2 μM (p>0.05) while data dispersion increases at concentration higher than 500 nM. For this reason, it was chosen to employ CP at 500 nM concentration to obtain the highest probe surface coverage possible.

2.7.14. Assessment of background signal

To evaluate the presence of non-specific interactions between the PNA probes and the mMBs, the signal in absence of target DNA has been compared to the positive signal, generated by the assembly of the whole sandwich. Once again, the effect of SP concentration was taken into account comparing the positive and background signal at SP concentration levels 20 nM, 50 nM and 500 nM (**Figure 2.49**)

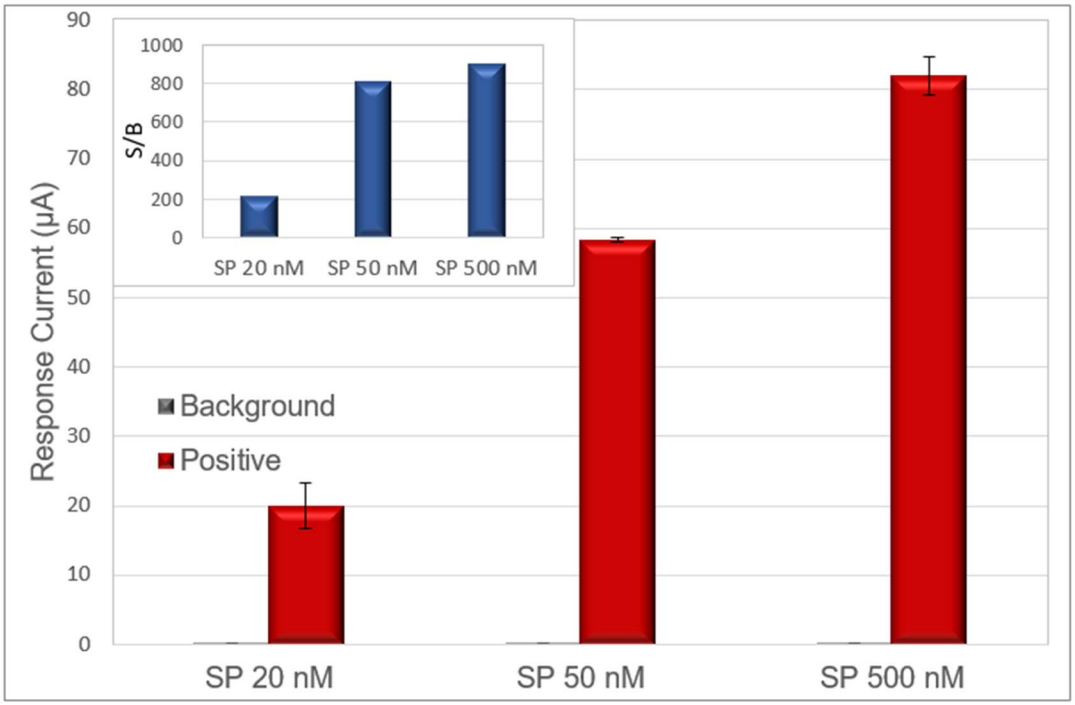

Figure 2.49. Comparison of the signals obtained in presence (positive, red) and absence (negative, grey) of target DNA equimolar to SP, at different SP concentration. The blue line represents the S/B ratio.

A very low neglectable background signal, not correlated to SP concentration was observed. Therefore, differently from what was observed on SWCNT-SPEs, no limit upper limit on this parameter has to be set, allowing to increase SP concentration as well as the target DNA concentration limit, resulting in a wider dynamic range of response.

It was then chosen to set the concentration of SP at 500 nM, at which the ratio observed between the blank (without DNA) and the positive obtained employing 1 nM target DNA was approximately 52 (**Figure 2.50**).

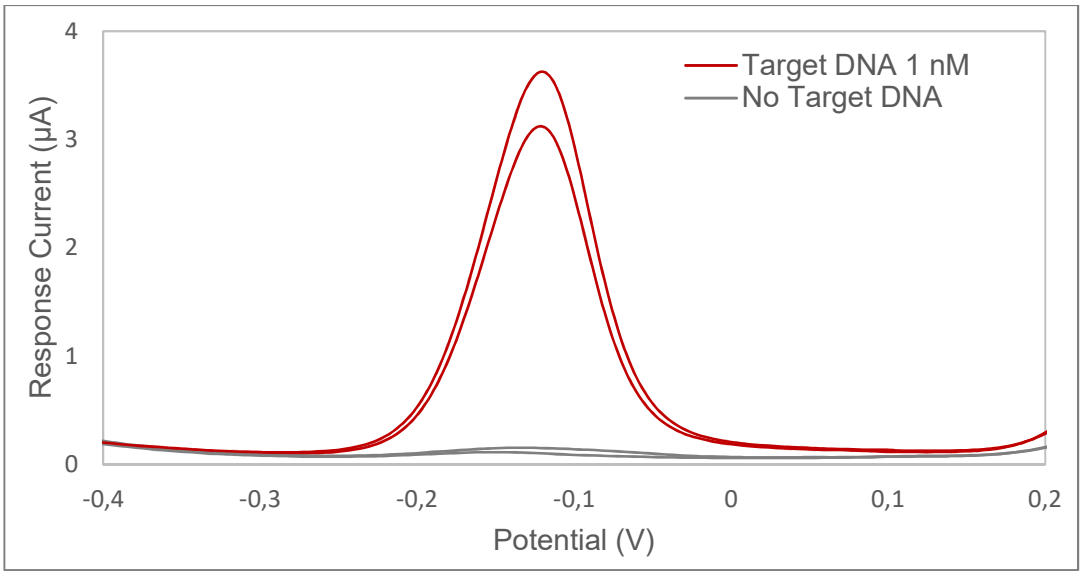

Figure 2.50. DPV voltammograms obtained in absence (background, grey) and presence (positive, red) of 1 nM Target DNA, with 500 nM SP on mMB

For further improvement on the hybridization efficiency the introduction of Denhardt's solution in the hybridization buffer (see paragraph 2.7.10) was tested. In particular the introduction of Denhardt's solution at concentration 4x was compared to the results obtained in absence of blocking solution (**Figure 2.51**).

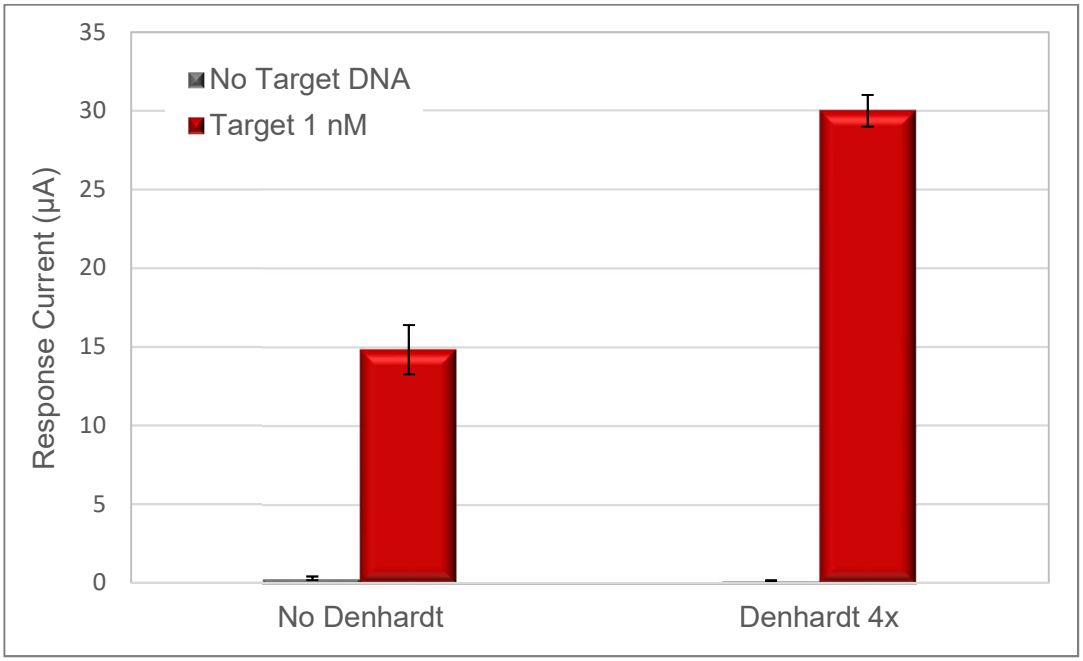

Figure 2.51. Effect of Denhardt's solution 4x on the positive (red) and background (grey) signal on mMB.

The effect on the background signal is minor since its intensity in absence of Denhardt's solution is already very low, nevertheless Denhardt's solution still decreases its intensity. As for the positive signals, the effect of the blocking solution is to increase the signal to approximately twice the intensity of the one registered in absence of Denhardt's. As a consequence, the S/B ratio increases from 52 to approximately 210.
As expected, the employment of mMB as substrate for probe immobilization grants the outstanding advantage of avoiding the presence of non-specific interactions between PNA or DNA strands and the immobilization surface. Therefore, no blocking step (e.g. pyrene in DMSO solution) must be performed, even though it was chosen to employ Denhardt's solution at concentration 4x to benefit from the increased hybridization efficiency involved with its presence in the HB.

2.7.15. Calibration curves

Using synthetic 45-mer target DNA, calibration curves have been built by evaluating the response obtained for different concentration levels of DNA. Since the readout step requires the use of SPEs, the results achievable using C-SPEs and SWCNT-SPEs have been compared.
As for the use of C-SPEs as readout platform, the concentration levels of Target DNA explored were 100 pM, 250 pM, 500 pM, 750 pM, 1 nM, 2 nM, 3 nM, 4 nM, 5 nM and 8 nM (**Figure 2.52**). The linear response range was found between 100 pM and 4 nM, over which the curve was linearly interpolated and allowed to assess a LOD of 8.2 pM and a LOQ of 27 pM.

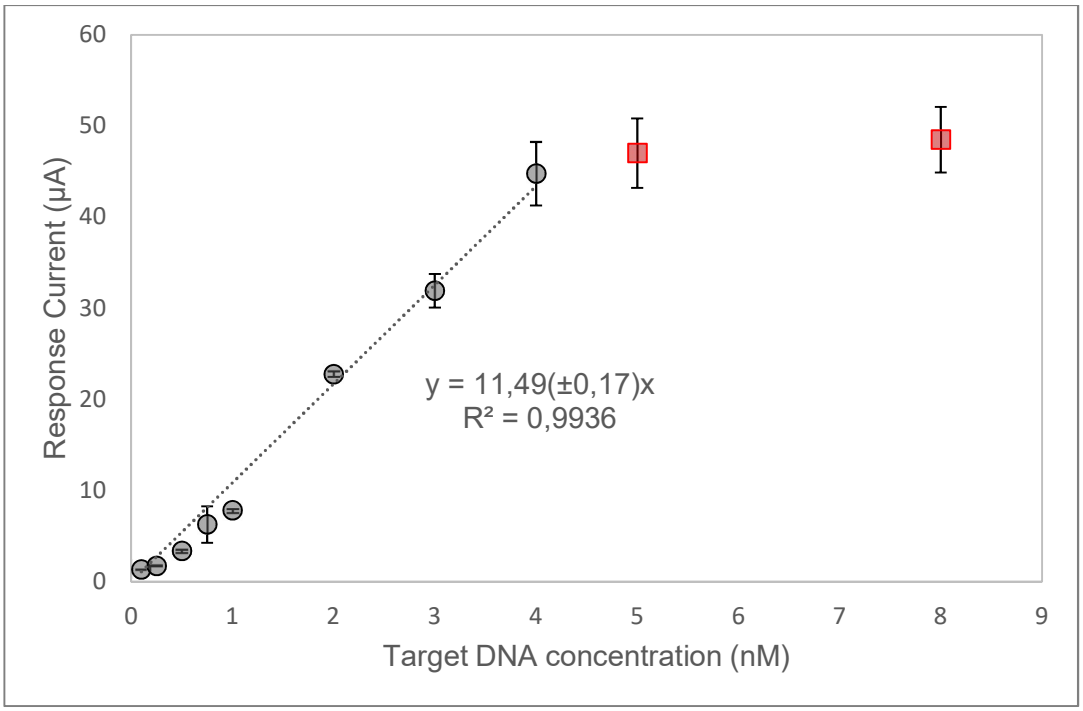

Figure 2.52. Calibration curve obtained employing mMB as immobilization substrate and C-SPEs for the electrochemical readout. Only points lying in the linear range (grey) were interpolated. Mean and standard deviation (n>4) for each concentration level are reported.

An analogous calibration curve was constructed employing SWCNT-SPEs for the DPV acquisition, in order to evaluate the improvement in analytical performance achievable employing nanostructured electrode substrate in combination with magnetic micro-beads as platform for sandwich assembly.
The target DNA concentration levels explored were 25 pM, 100 pM, 250 pM, 500 pM, 750 pM, 1 nM, 2 nM, 3 nM, 4 nM and 5 nM (**Figure 2.53**). The linearity was observed in the range between 25 pM and 3 nM, where the LOD and LOQ were assessed at 415 fM and 1.38 pM, respectively.
As expected, the exploitation of mMB as substrate for the carry out of the sandwich genoassay allowed to improve the LOD and LOQ, which translates in the ability of the method to detect and quantify lower DNA concentrations with respect to the method developed on SPEs. Furthermore, the linearity range over which the target DNA can be quantified was widened, involving more than two orders of magnitude when using SWCNT-SPEs for electrochemical readout.

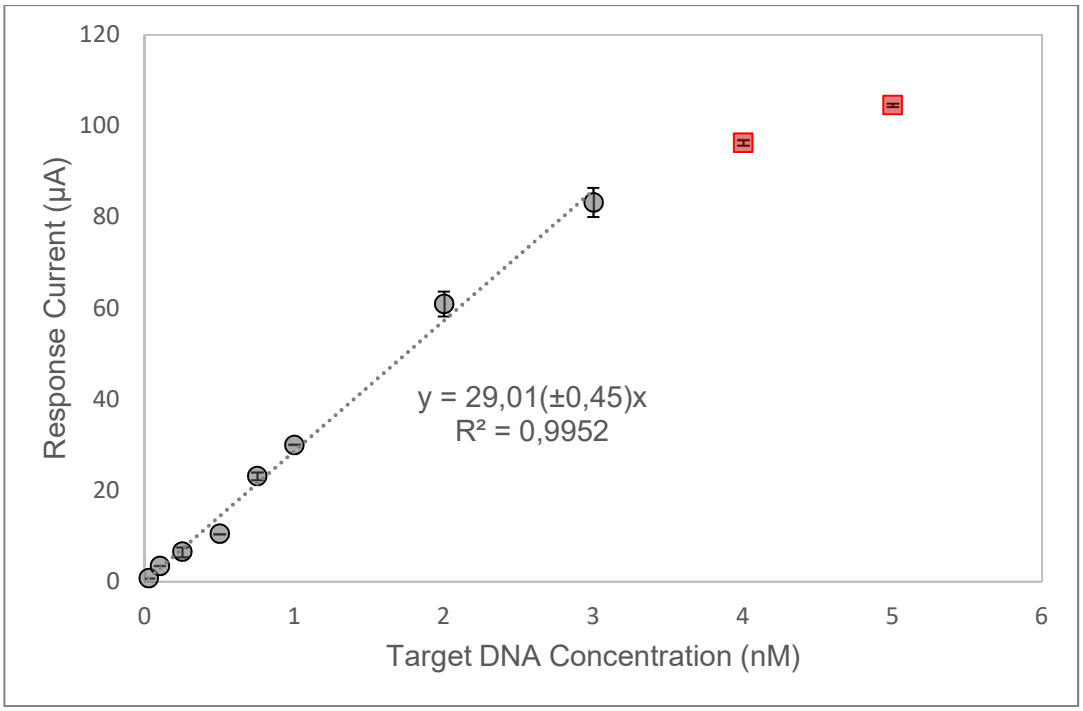

Figure 2.53. Calibration curve obtained employing mMB as immobilization substrate and SWCNT-SPEs for the electrochemical readout. Only points lying in the linear range (grey) were interpolated. Mean and standard deviation (n>4) for each concentration level are reported.

By taking into account the results obtained for the sandwich genoassay developed (**Figure 2.54**), it is possible to observe the increase in sensitivity given by the exploitation of nanostructured material for DPV signal acquisition as well as the enhancement given by mMB as immobilization substrate for the assembly of the three-probe sandwich complex. In particular, the sensitivity, in terms of slope of the linear interpolation line, has an approximate 40-fold increase between the method carried out with the immobilization of the probes on C-SPEs and the method exploiting mMB for immobilization and SWCNT-SPEs for electrochemical readout.

It is also worth pointing out that an increase in sensitivity of nearly 4 times can be achieved using mMB and C-SPEs compared to the method developed on SWCNT-SPEs, which allows to reduce the cost of the analyses since the method is based on the employment of cheaper screen-printed electrodes, while better analytical performances are obtained.

Furthermore, since only the last step, where the electrochemical readout is performed, involves the use of SPEs, it is possible to reuse an electrode, after thorough washing with water, up to four times without repercussions on the

analytical signal. This translates in a consistent reduction of the cost for each analysis.

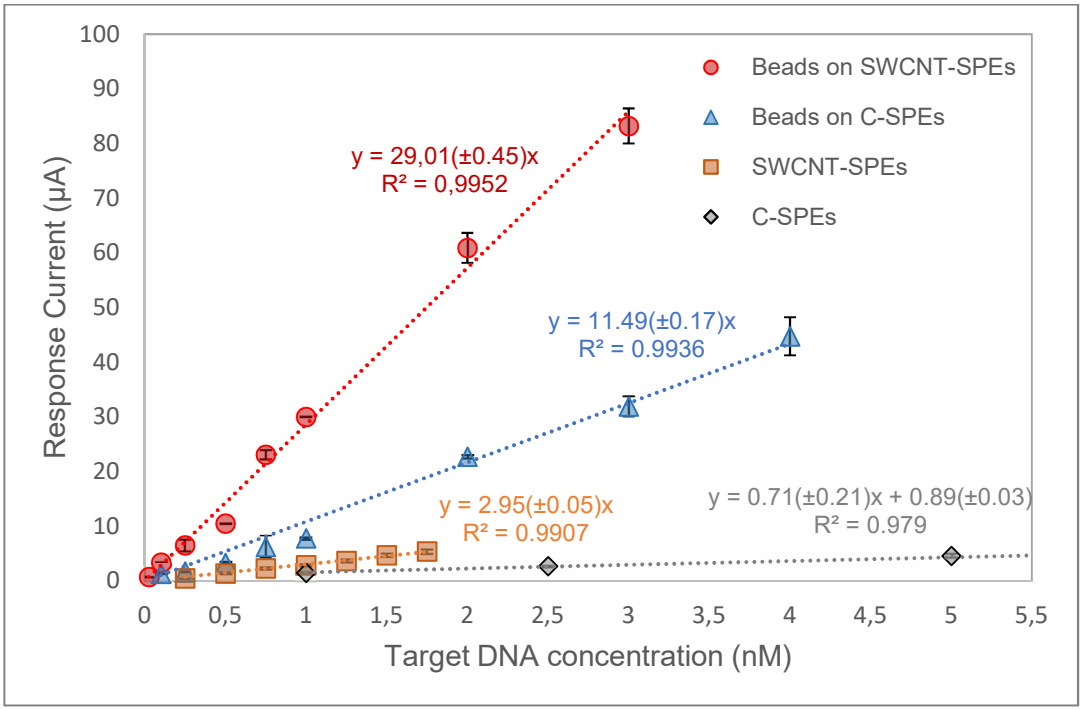

Figure 2.54. Comparison of the linear responses obtained employing the sandwich assay on different immobilization substrates. The calibration lines reported have been obtained using as immobilization platforms C-SPEs (grey diamonds), SWCNT-SPEs (yellow squares) and mMB with C-SPEs (blue triangles) and SWCNT-SPEs (red circles) for performing DPV acquisition.

2.7.16. Selectivity towards noncomplementary target

As performed for the genoassay developed on SPEs, also for the method exploiting mMB the variation of response in presence of noncomplementary synthetic DNA strands was tested. The DNA employed were the same used in the previous case (see paragraph 2.7.5), namely containing a single noncomplementary nucleobase (1-MM) and with completely randomized sequence (SCR). The noncomplementary nucleobases have been introduced in the portion of 45-mer DNA sequence complementary to the PNA CP.

The signal in absence of CP (blank CP) was also monitored for the hybrid between SP and DNA, however, as expected, no response signal was observed.

By comparing the signals recorded with different target sequences (**Figure 2.55**), it is possible to observe that employing the Scramble sequence (SCR) the signal is reduced by more than 99%. However, in the case of 1-MM sequence,

the reduction in output signal is only 13% compared to the signal registered with the FM target. This result is a consequence of the improved hybridization efficiency granted by the use of mMB that allow for the hybridization to occur under agitation in solution. As a result, the hybridization is promoted, yielding a more intense signal, however the presence of a single noncomplementary nucleobase has less impact in the formation of the sandwich with respect to the assemble of the complex in static conditions on SWCNT-SPEs.

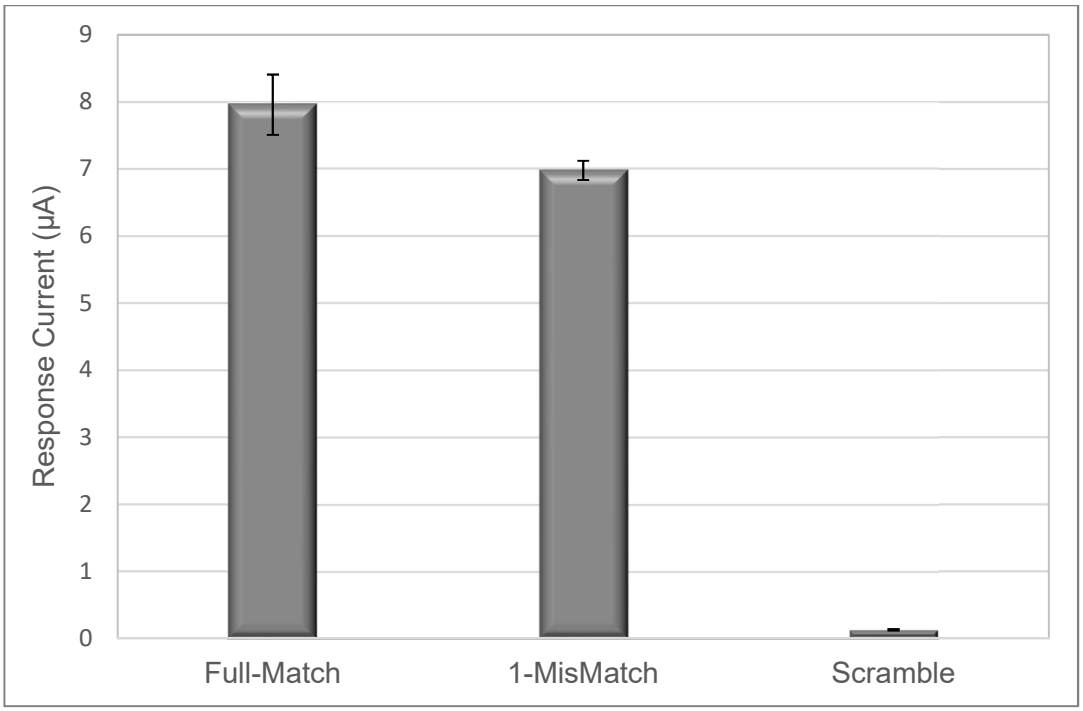

Figure 2.55. Response currents obtained employing complementary (FM), single-mismatch (1-MM) and noncomplementary (SCR) target DNA.

However, it is worth noting that to obtain high selectivity is beyond the purpose of this work, since the assay is aimed at detecting the presence of a whole sequence rather than highlight the mutation of a nucleobase, which is of critical importance for different clinical application.

2.7.17. Validation in real sample

After the analytical performance of the assay have been assessed, the ability of the method to detect *Roundup Ready* Soy genomic DNA extracted from flour has been tested. To this aim it was chosen to employ SWCNT-SPEs for

electrochemical readout since it allows to achieve the best analytical performance.
The extraction of genomic DNA was carried out from European Reference Material soy flours containing different percentages of *RR* soy in wild-type soy, following the same protocol as reported in paragraph 2.7.6. The concentration levels explored were 1 % and 10 % which were compared with wild-type soy. Through extraction with commercial kit it was possible to obtain a concentration of genomic DNA solutions of approximately 30 ng/μL which were then diluted to a final concentration, equal for all levels of 1 ng/μL, in order to obtain current responses within linear range. By using the extracted DNA for the carry out of the sandwich assay, it was possible to observe a statistically significant difference between all the levels explored (**Figure 2.56**).
Comparing these results with those obtained assembling the sandwich complex on SWCNT-SPEs, it is possible to observe that the signal relative to the 10 % RR soy concentration level is approximately four times more intense. This can be explained taking into account that the use of mMB leads to obtain a wider linear range, over which the RR soy can be quantified. Being that on SWCNT-SPEs this range was narrower, the 10 % concentration level was already above the saturation of the analytical signal.
Therefore, it was possible to validate on real sample the developed sandwich genoassay also on magnetic micro-beads, performing detection on nonamplified genomic DNA extracts, with the possibility of monitoring the presence of GM product over a wider range of concentration levels.

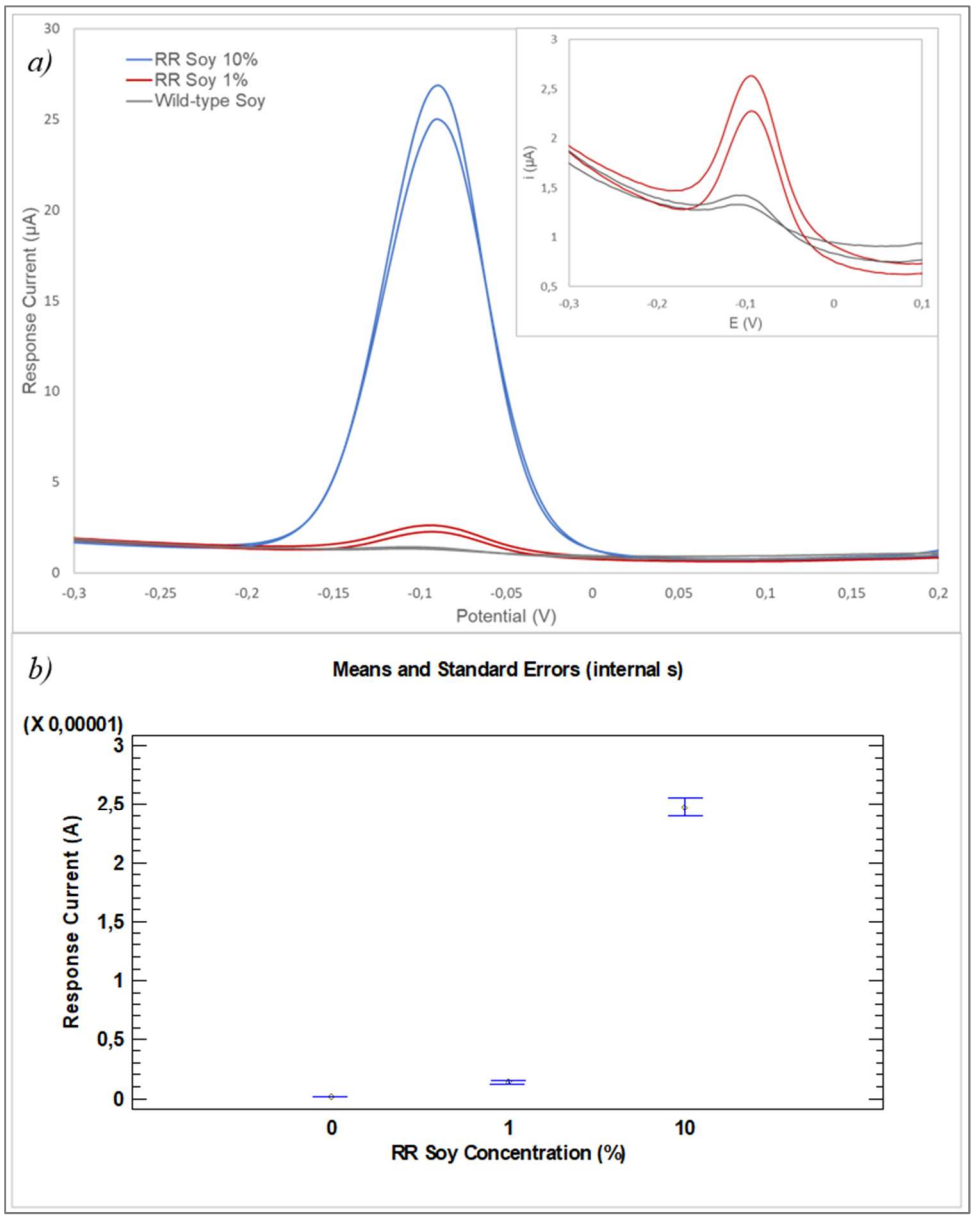

Figure 2.56. a) DPV voltammograms obtained using different RR soy concentration, namely 10% (blue), 1% (red) and wild-type (grey). b) ANOVA plot of current responses from analysis of genomic DNA extracts from ERM soy flour samples.

2.8. Future perspectives

For future development, the structure of the sandwich genoassay developed and validated for GM soy DNA, will be maintained and directed towards the detection of new targets of clinical interest. In particular, the G12-D mutation of the K-Ras gene will be targeted modifying the sequence of both Capture Probe and Signalling Probe. This mutation is involved in a series of different carcinomas and can be used for early diagnosis purposes.
Since the detection of mutation is the aim of the study, the CP length will be shortened in order to obtain a better selectivity in presence of Single Nucleotide Polymorphism. However, the effect of using a 14-mer CP will have to be evaluated with respect to the absolute intensity of the achievable signal.

This project led to the publication of the following papers:

- **Fortunati, S., Rozzi, A., Curti, F., Giannetto, M., Corradini, R., & Careri, M. (2019). Single-Walled Carbon Nanotubes as Enhancing Substrates for PNA-Based Amperometric Genosensors. *Sensors*, 19(3), 588.**

- **Fortunati, S., Rozzi, A., Curti, F., Giannetto, M., Corradini, R., & Careri, M. (2019). Novel amperometric genosensor based on peptide nucleic acid (PNA) probes immobilized on carbon nanotubes-screen printed electrodes for the determination of trace levels of non-amplified DNA in genetically modified (GM) soy. *Biosensors and Bioelectronics*, 129, 7-14.**

- **Fortunati, S., Rozzi, A., Giannetto, M., Corradini, R., & Careri, M. PNA-functionalized magnetic microbeads as substrates for enzyme-labelled amperometric genoassay for DNA sensing, *Manuscript in preparation*.**

[50] Zamecnik, P. C., & Stephenson, M. L. (1978). Inhibition of Rous sarcoma virus replication and cell transformation by a specific oligodeoxynucleotide. *Proceedings of the National Academy of Sciences*, 75(1), 280-284.

[51] Gleave, M. E., & Monia, B. P. (2005). Antisense therapy for cancer. *Nature Reviews Cancer*, 5(6), 468.

[52] Kurreck, J. (2003). Antisense technologies: improvement through novel chemical modifications. *European Journal of Biochemistry*, 270(8), 1628-1644.

[53] Sharma, V. K., Sharma, R. K., & Singh, S. K. (2014). Antisense oligonucleotides: modifications and clinical trials. *MedChemComm*, 5(10), 1454-1471.

[54] Altmann, K. H., Dean, N. M., Fabbro, D., Freier, S. M., Geiger, T., Hanera, R., Hiisken, D. A., Martina, P., Monia, B. P. B., Miiller, M., & Natt, F. (1996). Second generation of antisense oligonucleotides: from nuclease resistance to biological efficacy in animals. *CHIMIA International Journal for Chemistry*, 50(4), 168-176.

[55] Altmann, K. H., Fabbro, D., Dean, N. M., Geiger, T., Monia, B. P., Müllert, M., & Nicklin, P. (1996). Second-generation antisense oligonucleotides: structure—activity relationships and the design of improved signal-transduction inhibitors. *Biochemical Society Transactions*, 24 (3), 630–637.

[56] Shibahara, S., Mukai, S., Nishihara, T., Inoue, H., Ohtsuka, E., & Morisawa, H. (1987). Site-directed cleavage of RNA. *Nucleic acids research*, 15(11), 4403-4415.

[57] Braasch, D. A., & Corey, D. R. (2001). Locked nucleic acid (LNA): fine-tuning the recognition of DNA and RNA. *Chemistry & biology*, 8(1), 1-7.

[58] Amantana A, Iversen PL. (2005) Phamacokinetics and biodistribution of phosphorodiamidate morpholino antisense oligomers. *Curr. Opin. Pharmacol.*, 5, 550–5.

[59] Chan, J. H., Lim, S., & Wong, W. F. (2006). Antisense oligonucleotides: from design to therapeutic application. *Clinical and experimental pharmacology and physiology*, 33(5-6), 533-540.

[60] Koshkin, A.A., Singh, S.K., Nielsen, P., Rajwanshi, V.K., Kumar, R., Meldgaard, M., Olsen, C.E. & Wengel, J. (1998) LNA (locked nucleic acids): synthesis of the adenine, cytosine, guanine, 5-methylcytosine, thymine and uracil bicyclonucleoside monomers, oligomerisation, and unprecendented nucleic acid recognition. *Tetrahedron* 54, 3607–3630.

[61] Obika, S., Nanbu, D., Hari, Y., Andoh, J. I., Morio, K. I., Doi, T., & Imanishi, T. (1998). Stability and structural features of the duplexes containing nucleoside analogues with a fixed N-type conformation, 2′-O, 4′-C-methyleneribonucleosides. *Tetrahedron letters*, 39(30), 5401-5404.

[62] Petersen M, Wengel J. (2003) LNA: A versatile tool for therapeutics and genomics. *Trends Biotechnol*., 21, 74–81.

[63] Nielsen, P.E., Egholm, R.H., Berg, R.H. & Buchardt, O. (1991) Sequence-selective recognition of DNA by strand displacement with a thymine-substituted polyamide. *Science* 254, 1497–1500.

[64] Nielsen, P. E. (2004). PNA technology. *Molecular biotechnology*, 26(3), 233-248.

[65] Betts, L., Josey, J. A., Veal, J. M., & Jordan, S. R. (1995). A nucleic acid triple helix formed by a peptide nucleic acid-DNA complex. *Science*, 270(5243), 1838-1841.

[66] Nielsen, P.E. (1999) Antisense properties of peptide nucleic acid. *Methods Enzymol.* 313, 156–164.

[67] Braasch, D.A. & Corey, D.R. (2002) Novel antisense and peptide nucleic acid strategies for controlling gene expression. *Biochemistry* 41, 4503–4509.

[68] Hannon, M. J. (2007). Supramolecular DNA recognition. *Chemical Society Reviews*, 36(2), 280-295.

[69] Christensen, L., Fitzpatrick, R., Gildea, B., Petersen, K. H., Hansen, H. F., Koch, T., Egholm, M., Buchardt, O., Nielsen, P. E., Coull, J. & Berg, R. H. (1995). Solid-phase synthesis of peptide nucleic acids. *Journal of peptide*

science: an official publication of the European Peptide Society, 1(3), 175-183.

[70] Manicardi, A., Rozzi, A., Korom, S., Corradini, R. (2017) Building on the peptide nucleic acid (PNA) scaffold:A biomolecular engineering approach. *Supramol. Chem*., 29, 784–795.

[71] Upadhyayula, V. K. (2012) Functionalized gold nanoparticle supported sensory mechanisms applied in detection of chemical and biological threat agents: a review. *Analytica Chimica Acta*, 715, 1-18.

[72] Li, H., & Rothberg, L. (2004). Colorimetric detection of DNA sequences based on electrostatic interactions with unmodified gold nanoparticles. *Proceedings of the National Academy of Sciences*, 101(39), 14036-14039.

[73] Wang, Y., Zhan, L., & Huang, C. Z. (2010). One-pot preparation of dextran-capped gold nanoparticles at room temperature and colorimetric detection of dihydralazine sulfate in uric samples. *Analytical Methods*, 2(12), 1982-1988.

[74] Baetsen-Young, A. M., Vasher, M., Matta, L. L., Colgan, P., Alocilja, E. C., & Day, B. (2018). Direct colorimetric detection of unamplified pathogen DNA by dextrin-capped gold nanoparticles. *Biosensors and Bioelectronics*, 101, 29-36.

[75] Deen, J., Vranken, C., Leen, V., Neely, R. K., Janssen, K. P. F., & Hofkens, J. (2017). Methyltransferase-Directed Labeling of Biomolecules and its Applications. *Angewandte Chemie International Edition*, 56(19), 5182–5200.

[76] Deen, J., Wang, S., Van Snick, S., Leen, V., Janssen, K., Hofkens, J., & Neely, R. K. (2018). A general strategy for direct, enzyme-catalyzed conjugation of functional compounds to DNA. *Nucleic acids research*, 46(11), e64-e64.

[77] Persil, O., & Hud, N. V. (2007). Harnessing DNA intercalation. *Trends in biotechnology*, 25(10), 433-436.

[78] Bresloff, J. L., & Crothers, D. M. (1981). Equilibrium studies of ethidium-polynucleotide interactions. *Biochemistry*, 20(12), 3547-3553.

[79] Wu, F.-Y., Xie, F.-Y., Wu, Y.-M., & Hong, J.-I. (2007). Interaction of a New Fluorescent Probe with DNA and its Use in Determination of DNA. *Journal of Fluorescence*, 18(1), 175–181.

[80] Ahn, S., Kulis, D. M., Erdner, D. L., Anderson, D. M., & Walt, D. R. (2006). Fiber-optic microarray for simultaneous detection of multiple harmful algal bloom species. *Appl. Environ. Microbiol*., 72(9), 5742-5749.

[81] Tyagi, S., & Kramer, F. R. (1996). Molecular beacons: probes that fluoresce upon hybridization. *Nature biotechnology*, 14(3), 303.

[82] Huang, C., Stakenborg, T., Cheng, Y., Colle, F., Steylaerts, T., Jans, K., Van Dorpe, P., & Lagae, L. (2011). Label-free genosensor based on immobilized DNA hairpins on gold surface. *Biosensors and Bioelectronics*, 26(7), 3121-3126.

[83] Homola, J. (2008) Surface plasmon resonance sensors for detection of chemical and biological species. *Chem. Rev*., 108, 462–493.

[84] Viitala, T., Granqvist, N., Hallila, S., Raviña, M., & Yliperttula, M. (2013). Elucidating the signal responses of multi-parametric surface plasmon resonance living cell sensing: a comparison between optical modeling and drug–MDCKII cell interaction measurements*. PloS one*, 8(8)

[85] Kambhampati, D., Nielsen, P. E., & Knoll, W. (2001). Investigating the kinetics of DNA–DNA and PNA–DNA interactions using surface plasmon resonance-enhanced fluorescence spectroscopy. *Biosensors and Bioelectronics*, 16(9-12), 1109-1118.

[86] Liebermann, T., & Knoll, W. (2000). Surface-plasmon field-enhanced fluorescence spectroscopy. *Colloids and Surfaces A: Physicochemical and Engineering Aspects*, 171(1-3), 115-130.

[87] Wang, R., Tombelli, S., Minunni, M., Spiriti, M. M., & Mascini, M. (2004). Immobilisation of DNA probes for the development of SPR-based sensing. *Biosensors and Bioelectronics*, 20(5), 967-974.

[88] Mariotti, E., Minunni, M., & Mascini, M. (2002). Surface plasmon resonance biosensor for genetically modified organisms detection. *Analytica chimica acta*, 453(2), 165-172.

[89] Xu, F., Pellino, A. M., & Knoll, W. (2008). Electrostatic repulsion and steric hindrance effects of surface probe density on deoxyribonucleic acid (DNA)/peptide nucleic acid (PNA) hybridization. *Thin Solid Films*, 516(23), 8634-8639.

[90] Syedmoradi, L., Ahmadi, A., Norton, M. L., & Omidfar, K. (2019). A review on nanomaterial-based field effect transistor technology for biomarker detection. *Microchimica Acta*, 186(11), 739.

[91] Kotlowski, C., Aspermair, P., Khan, H. U., Reiner-Rozman, C., Breu, J., Szunerits, S., Kim, J.J., Bao, Z., Kleber, C., Pelosi, P. & Knoll, W. (2018). Electronic biosensing with flexible organic transistor devices. *Flexible and Printed Electronics*, 3(3), 034003.

[92] Wadhera, T., Kakkar, D., Wadhwa, G., & Raj, B. (2019). Recent Advances and Progress in Development of the Field Effect Transistor Biosensor: A Review. *Journal of Electronic Materials*, 48(12), 7635-7646.

[93] Veigas, B., Fortunato, E., & Baptista, P.V. (2015). Field Effect Sensors for Nucleic Acid Detection: Recent Advances and Future Perspectives. *Sensors* 15, 10380–10398.

[94] Xuan, C. T., Thuy, N. T., Luyen, T. T., Huyen, T. T., & Tuan, M. A. (2017). Carbon nanotube field-effect transistor for DNA sensing. *Journal of Electronic Materials*, 46(6), 3507-3511.

[95] He, Q., Wu, S., Yin, Z., & Zhang, H. (2012). Graphene-based electronic sensors. *Chemical Science*, 3(6), 1764-1772.

[96] Reddy, D., Register, L. F., Carpenter, G. D., & Banerjee, S. K. (2011). Graphene field-effect transistors. *Journal of Physics D: Applied Physics*, 44(31), 313001.

[97] Cai, B., Wang, S., Huang, L., Ning, Y., Zhang, Z., & Zhang, G. J. (2014). Ultrasensitive label-free detection of PNA–DNA hybridization by reduced graphene oxide field-effect transistor biosensor. *ACS nano*, 8(3), 2632-2638.

[98] Campos, R., Borme, J., Guerreiro, J. R., Machado, G., Cerqueira, M. F. G., Petrovykh, D. Y., & Alpuim, P. (2019). Attomolar label-free detection of

DNA hybridization with electrolyte-gated graphene field-effect transistors. *ACS sensors*. 4(2), 286-293.

[99] Lisdat, F., & Schäfer, D. (2008). The use of electrochemical impedance spectroscopy for biosensing. *Analytical and Bioanalytical Chemistry*, 391(5), 1555–1567.

[100] Hang, T. C., & Guiseppi-Elie, A. (2004). Frequency dependent and surface characterization of DNA immobilization and hybridization. *Biosensors and Bioelectronics*, 19(11), 1537–1548.

[101] Bardea, A., Patolsky, F., Dagan, A., & Willner, I. (1999). Sensing and amplification of oligonucleotide-DNA interactions by means of impedance spectroscopy: a route to a Tay–Sachs sensor. *Chemical Communications*, (1), 21–22.

[102] Xu, Y., Yang, L., Ye, X., He, P., & Fang, Y. (2006). Impedance-Based DNA Biosensor Employing Molecular Beacon DNA as Probe and Thionine as Charge Neutralizer. *Electroanalysis*, 18(9), 873–881.

[103] Liu, J., Tian, S., Nielsen, P. E., & Knoll, W. (2005). In situ hybridization of PNA/DNA studied label-free by electrochemical impedance spectroscopy. *Chemical Communications*, (23), 2969.

[104] Keighley, S. D., Li, P., Estrela, P., & Migliorato, P. (2008). Optimization of DNA immobilization on gold electrodes for label-free detection by electrochemical impedance spectroscopy. *Biosensors and Bioelectronics*, 23(8), 1291–1297.

[105] Drummond, T. G., Hill, M. G., & Barton, J. K. (2003). Electrochemical DNA sensors. *Nature Biotechnology*, 21(10), 1192–1199.

[106] de-los-Santos-Álvarez, P., Lobo-Castanon, M. J., Miranda-Ordieres, A. J., & Tuñón-Blanco, P. (2004). Current strategies for electrochemical detection of DNA with solid electrodes. *Analytical and bioanalytical chemistry*, 378(1), 104-118.

[107] Ricci, F., & Plaxco, K. W. (2008). E-DNA sensors for convenient, label-free electrochemical detection of hybridization. *Microchimica Acta*, 163(3-4), 149-155.

[108] Wang, J., Cai, X., Jonsson, C., & Balakrishnan, M. (1996). Adsorptive stripping potentiometry of DNA at electrochemically pretreated carbon paste electrodes. *Electroanalysis*, 8(1), 20–24.

[109] Popovich, N. D., Eckhardt, A. E., Mikulecky, J. C., Napier, M. E., & Thomas, R. S. (2002). Electrochemical sensor for detection of unmodified nucleic acids. *Talanta*, 56(5), 821-828.

[110] E. Ferapontova, E. (2011). Electrochemical Indicators for DNA Electroanalysis. *Current Analytical Chemistry*, 7(1), 51–62.

[111] Garcia-Melo, L. F., Álvarez-González, I., Madrigal-Bujaidar, E., Madrigal-Santillán, E. O., Morales-González, J. A., Pineda Cruces, R. N., Campoy Ramírez, J. A., Matsumura, D. P., Aguilar-Santamaría, M. D. L. A., & Batina, N. (2019). Construction of an electrochemical genosensor based on screen-printed gold electrodes (SPGE) for detection of a mutation in the adenomatous polyposis coli gene. *Journal of Electroanalytical Chemistry*., 840, 93-100.

[112] Ihara, T., Nakayama, M., Murata, M., Nakano, K., & Maeda, M. (1997). Gene sensor using ferrocenyl oligonucleotide. *Chemical Communications*, (17), 1609–1610.

[113] Miranda-Castro, R., de-los-Santos-Álvarez, N., Lobo-Castañón, M. J., Miranda-Ordieres, A. J., & Tuñón-Blanco, P. (2009). Structured nucleic acid probes for electrochemical devices. *Electroanalysis: An International Journal Devoted to Fundamental and Practical Aspects of Electroanalysis*, 21(19), 2077-2090.

[114] Immoos, C. E., Lee, S. J., & Grinstaff, M. W. (2004). DNA-PEG-DNA Triblock Macromolecules for Reagentless DNA Detection. *Journal of the American Chemical Society*, 126(35), 10814–10815.

[115] Xiao, Y., Lubin, A. A., Baker, B. R., Plaxco, K. W., & Heeger, A. J. (2006). Single-step electronic detection of femtomolar DNA by target-induced strand displacement in an electrode-bound duplex. *Proceedings of the National Academy of Sciences*, 103(45), 16677–16680.

[116] Giallo, M. L. D., Ariksoysal, D. O., Marrazza, G., Mascini, M., & Ozsoz, M. (2005). Disposable Electrochemical Enzyme-Amplified Genosensor for Salmonella Bacteria Detection. *Analytical Letters*, 38(15), 2509–2523.

[117] Mullis, K. B., & Faloona, F. A. (1989). Specific synthesis of DNA in vitro via a polymerase-catalyzed chain reaction. In *Recombinant DNA Methodology* (pp. 189-204). Academic Press.

[118] Saiki, R. K., Gelfand, D. H., Stoffel, S., Scharf, S. J., Higuchi, R., Horn, G. T., Mullis, K.B. & Erlich, H. A. (1988). Primer-directed enzymatic amplification of DNA with a thermostable DNA polymerase. *Science*, 239(4839), 487-491.

[119] Higuchi, R., Dollinger, G., Walsh, P. S., & Griffith, R. (1992). Simultaneous amplification and detection of specific DNA sequences. *Bio/technology*, 10(4), 413.

[120] Holland, P. M., Abramson, R. D., Watson, R., & Gelfand, D. H. (1991). Detection of specific polymerase chain reaction product by utilizing the 5'----3'exonuclease activity of Thermus aquaticus DNA polymerase. *Proceedings of the National Academy of Sciences*, 88(16), 7276-7280.

[121] Heid, C. A., Stevens, J., Livak, K. J., & Williams, P. M. (1996). *Real time quantitative PCR. Genome Research*, 6(10), 986–994.

[122] Miraglia, M., Berdal, K. G., Brera, C., Corbisier, P., Holst-Jensen, A., Kok, E. J., Marvin, H.J.P., Schimmel, H., Rentsch, J., van Rie, J.P.P.F., & Zagon, J. (2004). Detection and traceability of genetically modified organisms in the food production chain. *Food and Chemical Toxicology*, 42(7), 1157–1180.

[123] Heim, A., Ebnet, C., Harste, G., & Pring-Åkerblom, P. (2003). Rapid and quantitative detection of human adenovirus DNA by real-time PCR. *Journal of medical virology*, 70(2), 228-239.

[124] Liu, C., Guo, Y. M., Cao, J. Z., Zhang, D.-F., Chang, O.-Q., Li, K., Wang, F., Shi, C.B., Jiang, L., Wang, Q., Lin, L. (2018). Detection and quantification of Aeromonas schubertii in Channa maculata by TaqMan MGB probe fluorescence real-time quantitative PCR. *Journal of Fish Diseases*. 42(1), 109-117

[125] World Health Organization, 2014, https://www.who.int/foodsafety/areas_work/food-technology/faq-genetically-modified-food/en/

[126] Cohen, S. N., Chang, A. C., Boyer, H. W., & Helling, R. B. (1973). Construction of biologically functional bacterial plasmids in vitro. *Proceedings of the National Academy of Sciences*, 70(11), 3240-3244.

[127] Jaenisch, R. and Mintz, B. (1974) Simian virus 40 DNA sequences in DNA of healthy adult mice derived from preimplantation blastocysts injected with viral DNA. *Proc. Natl. Acad*. 71(4), 1250–54

[128] Fraley, R. T., Rogers, S. G., Horsch, R. B., Sanders, P. R., Flick, J. S., Adams, S. P., Bittner, M. L., Brand, L. A., Fink, C. L., Fry, J. S. , Goldberg, S. B., Hoffmann, N. L., Woo, S. C., & Galluppi, G. R. (1983). Expression of bacterial genes in plant cells. *Proceedings of the National Academy of Sciences*, 80(15), 4803-4807.

[129] M.A. Schmidt, P.R. LaFayette, B.A. Artelt, W.A. Parrott, A comparison of strategies for transformation with multiple genes via microprojectile mediated bombardment, *In Vitro Cell Dev. Biol. Plant* 44 (3) (2008) 162–168.

[130] Valvekens, D., Van Montagu, M., & Van Lijsebettens, M. (1988). Agrobacterium tumefaciens-mediated transformation of Arabidopsis thaliana root explants by using kanamycin selection. *Proceedings of the National Academy of Sciences*, 85(15), 5536-5540.

[131] Cong, L., Ran, F. A., Cox, D., Lin, S., Barretto, R., Habib, N., Hsu, P. D., Wu, X., Jiang, W., Marraffini, L. A., & Zhang, F. (2013). Multiplex genome engineering using CRISPR/Cas systems. *Science*, 339(6121), 819-823.

[132] https://www.stemcell.com/genome-editing-of-human-primary-t-cells-using-the-arcitect-crispr-cas9-system.html

[133] Zhang, C., Wohlhueter, R., & Zhang, H. (2016). Genetically modified foods: A critical review of their promise and problems. *Food Science and Human Wellness*, 5(3), 116-123.

[134] Bawa, A. S., & Anilakumar, K. R. (2013). Genetically modified foods: safety, risks and public concerns—a review. *Journal of food science and technology*, 50(6), 1035-1046.

[135] Kramkowska, M., Grzelak, T., & Czyzewska, K. (2013). Benefits and risks associated with genetically modified food products. *Annals of Agricultural and Environmental Medicine*, 20(3).

[136] Ye, X., Al-Babili, S., Klöti, A., Zhang, J., Lucca, P., Beyer, P., & Potrykus, I. (2000). Engineering the provitamin A (β-carotene) biosynthetic pathway into (carotenoid-free) rice endosperm. *Science*, 287(5451), 303-305.

[137] Sheehy, R. E., Kramer, M., & Hiatt, W. R. (1988). Reduction of polygalacturonase activity in tomato fruit by antisense RNA. *Proceedings of the National Academy of Sciences*, 85(23), 8805-8809.

[138] Kramer, M. G., & Redenbaugh, K. (1994). Commercialization of a tomato with an antisense polygalacturonase gene: The FLAVR SAVR™ tomato story. *Euphytica*, 79(3), 293-297.

[139] Sakakibara, K. Y.-, & Saito, K. (2006). Review: genetically modified plants for the promotion of human health. *Biotechnology Letters*, 28(24), 1983–1991.

[140] van Putten, M. C., Frewer, L. J., Gilissen, L. J., Gremmen, B., Peijnenburg, A. A., & Wichers, H. J. (2006). Novel foods and food allergies: a review of the issues. *Trends in food science & technology*, 17(6), 289-299.

[141] Herman, E. M., & Burks, A. W. (2011). The impact of plant biotechnology on food allergy. *Current opinion in biotechnology*, 22(2), 224-230.

[142] Regulation, E. C. (2003). No. 1829/2003 of the European Parliament and of the Council of 22nd September 2003 on genetically modified food and feed. Off J Eur Union Lt, 268, 1-23.

[143] Regulation, C. (2003). No 1830/2003 of the European Parliament and of the Council of 22 September 2003 concerning the traceability and labelling of genetically modified organisms and the traceability of food and feed products produced from genetically modified organisms and amending Directive 2001/18/EC. Official Journal, 50, 268.

[144] Miraglia, M., Berdal, K. G., Brera, C., Corbisier, P., Holst-Jensen, A., Kok, E. J., Marvin, H.J.P., Schimmel, H., Rentsch, J., van Rie, J.P.P.F., & Zagon, J. (2004). Detection and traceability of genetically modified organisms in the food production chain. *Food and Chemical Toxicology*, 42(7), 1157–1180.

[145] Anklam, E., Gadani, F., Heinze, P., Pijnenburg, H., & Van Den Eede, G. (2002). Analytical methods for detection and determination of genetically modified organisms in agricultural crops and plant-derived food products. *European Food Research and Technology*, 214(1), 3-26.

[146] Marmiroli, N., Maestri, E., Gulli, M., Malcevschi, A., Peano, C., Bordoni, R., & De Bellis, G. (2008). Methods for detection of GMOs in food and feed. *Analytical and bioanalytical chemistry*, 392(3), 369.

[147] Martín-Fernández, B., Manzanares-Palenzuela, C. L., Sánchez-Paniagua López, M., de-los-Santos-Álvarez, N., & López-Ruiz, B. (2017). Electrochemical genosensors in food safety assessment. *Critical reviews in food science and nutrition*, 57(13), 2758-2774.

[148] Manzanares-Palenzuela, C. L., Martín-Fernández, B., López, M. S. P., & López-Ruiz, B. (2015). Electrochemical genosensors as innovative tools for detection of genetically modified organisms. *TrAC Trends in Analytical Chemistry*, 66, 19-31.

[149] Briefs, I. S. A. A. A. (2017). Global status of commercialized biotech/GM crops in 2017: biotech crop adoption surges as economic benefits accumulate in 22 years.

[150] Dill, G. M. (2005). Glyphosate-resistant crops: history, status and future. Pest Management Science: formerly Pesticide *Science*, 61(3), 219-224.

[151] Lundry, D. R., Ridley, W. P., Meyer, J. J., Riordan, S. G., Nemeth, M. A., Trujillo, W. A., Breeze, M. L., & Sorbet, R. (2008). Composition of grain, forage, and processed fractions from second-generation glyphosate-tolerant soybean, MON 89788, is equivalent to that of conventional soybean (Glycine max L.). *Journal of agricultural and food chemistry*, 56(12), 4611-4622.

[152] Franz, J. E., Mao, M. K., & Sikorski, J. A. (1997). Glyphosate: a unique global herbicide. *American Chemical Society*.

[153] Pollegioni, L., Schonbrunn, E., & Siehl, D. (2011). Molecular basis of glyphosate resistance–different approaches through protein engineering. *The FEBS journal*, 278(16), 2753-2766.

[154] Duke, S. O., & Powles, S. B. (2008). Glyphosate: a once-in-a-century herbicide. Pest Management Science: formerly Pesticide *Science* 64(4), 319-325.

[155] Funke, T., Han, H., Healy-Fried, M. L., Fischer, M., & Schönbrunn, E. (2006). Molecular basis for the herbicide resistance of Roundup Ready crops. *Proceedings of the National Academy of Sciences*, 103(35), 13010-13015.

[156] European Food Safety Authority (EFSA). (2015). Conclusion on the peer review of the pesticide risk assessment of the active substance glyphosate. EFSA Journal, 13(11), 4302.

[157] International Agency for Research on Cancer. (2015). Some organophosphate insecticides and herbicides: diazinon, glyphosate, malathion, parathion, and tetrachlorvinphos. Monographs on the evaluation of carcinogenic risks to humans, 112.

[158] Piccinini, E., Bliem, C., Reiner-Rozman, C., Battaglini, F., Azzaroni, O., & Knoll, W. (2017). Enzyme-polyelectrolyte multilayer assemblies on reduced graphene oxide field-effect transistors for biosensing applications*. Biosensors and Bioelectronics*, 92, 661-667

[159] Eurachem Guide, The Fitness for Purpose of Analytical Methods – A Laboratory Guide to Method Validation and Related Topics, Available from, second ed., (2014) http://www.eurachem.org.

[160] D'Agata, R., Corradini, R., Ferretti, C., Zanoli, L., Gatti, M., Marchelli, R., Spoto, G., 2010. *Biosens. Bioelectron*. 25, 2095–2100

[161] Bertucci, A., Manicardi, A., Candiani, A., Giannetti, S., Cucinotta, A., Spoto, G., Konstantaki, M., Pissadakis, S., Selleri, S., Corradini, R., 2015. *Biosens. Bioelectron*.63, 248–254.

[162] Rossi, S., Scaravelli, E., Germini, A., Corradini, R., Fogher, C., & Marchelli, R. (2006). A PNA-array platform for the detection of hidden allergens in foodstuffs. *European Food Research and Technology*, 223(1), 1-6.

[163] Nugent, J. M., Santhanam, K. S. V., Rubio, A., & Ajayan, P. M. (2001). Fast electron transfer kinetics on multiwalled carbon nanotube microbundle electrodes. *Nano letters*, 1(2), 87-91.

[164] Pumera, M., Llopis, X., Merkoçi, A., & Alegret, S. (2006). Microchip capillary electrophoresis with a single-wall carbon nanotube/gold electrochemical detector for determination of aminophenols and neurotransmitters. *Microchimica Acta*, 152(3-4), 261-265.

[165] Crevillén, A. G., Ávila, M., Pumera, M., González, M. C., & Escarpa, A. (2007). Food analysis on microfluidic devices using ultrasensitive carbon nanotubes detectors. *Analytical chemistry*, 79(19), 7408-7415.

[166] Varghese, N., Mogera, U., Govindaraj, A., Das, A., Maiti, P.K., Sood, A.K., Rao, C.N.R., 2009. Binding of DNA nucleobases and nucleosides with graphene. *ChemPhysChem* 10 (1), 206–210.

[167] Hamidi-Asl, E., Raoof, J. B., Hejazi, M. S., Sharifi, S., Golabi, S. M., Palchetti, I., & Mascini, M. (2015). A genosensor for point mutation detection of P53 gene PCR product using magnetic particles. *Electroanalysis*, 27(6), 1378-1386.

[168] D'Agata, R., Breveglieri, G., Zanoli, L. M., Borgatti, M., Spoto, G., & Gambari, R. (2011). Direct detection of point mutations in nonamplified human genomic DNA. *Analytical chemistry*, 83(22), 8711-8717.

[169] Barbas III, C.F., Burton, D.R., Scott, J.K., Silverman, G.J., 2001. Quantitation of DNA and RNA. In: Barbas IIIC.F., Burton, D.R., Scott, J.K., Silverman, G.J. (Eds.), Phage Display, A Laboratory Manual. Cold Spring Harbor Laboratory Press, Cold Spring Harbor, NY.

[170] García-Miranda Ferrari, A., Foster, C., Kelly, P., Brownson, D., & Banks, C. (2018). Determination of the electrochemical area of screen-printed electrochemical sensing platforms. *Biosensors*, 8(2), 53.

[171] Bard, A. J., Faulkner, L. R., Leddy, J., & Zoski, C. G. (1980). Electrochemical methods: fundamentals and applications (Vol. 2). New York: wiley.

[172] Berney, H., West, J., Haefele, E., Alderman, J., Lane, W., & Collins, J. K. (2000). A DNA diagnostic biosensor: development, characterisation and performance. *Sensors and Actuators B: Chemical*, 68(1-3), 100-108.

[173] Saeed, A. A., Sánchez, J. L. A., O'Sullivan, C. K., & Abbas, M. N. (2017). DNA biosensors based on gold nanoparticles-modified graphene oxide for the

detection of breast cancer biomarkers for early diagnosis. *Bioelectrochemistry*, 118, 91-99.

[174] Spain, E., Keyes, T. E., & Forster, R. J. (2013). DNA sensor based on vapour polymerised pedot films functionalised with gold nanoparticles. *Biosensors and Bioelectronics*, 41, 65-70.

3. IoT-based portable device for diagnosis of Celiac Disease

3.1. Antigens and antibodies

Affinity recognition is based on the specific binding between a receptor and a ligand as a consequence of the establishment of noncovalent interactions that lead to a highly stable complex. Among affinity-based sensors, immunosensors are the most common. They exploit the highly specific interactions between antibodies and antigens as recognition mechanisms.

The element recognized by the antibody is the antigen, whose composition can vary between proteins, polysaccharides, small molecules such as mycotoxins and pesticides, etc. In fact, antigens are defined not on the basis of their structure, but as species capable of triggering an immune response aimed at its removal by the organisms onto which they are inserted, through the production of antibodies. The latter, in fact, recognizes a specific portion of the antigen, called epitope, in which given chemical functional groups are present, allowing for a specific recognition based on chemical and spatial requirements. Given that the antigen-antibody interactions are of noncovalent nature, the formation of the complex is reversible, even though it is usually characterized by a high affinity constant ranging between 10^5 and 10^{12} M^{-1}.

Antibodies [175] are a class of proteins belonging to the immunoglobulin (Ig) family, that organisms produce as part of an immunological response mechanism to the introduction of exogenous species aimed at the elimination of foreign elements. There are five categories of immunoglobulin, namely IgG (γ), IgA (α), IgM (μ), IgD (δ) e IgE (ε), among which IgG are the most abundant in serum. Antibodies possess a characteristic structure composed of two pairs of identical protein chains, a pair of light chains and a pair of heavy chains, connected by sulphur bonds and noncovalent interactions that yield a quaternary structure with a characteristic "Y" shape (**Figure 3.1**). This structure can be divided into two portions, a F_c (fragment, crystallizable) and F_{ab} (fragment, antigen-binding) portion. The former composes the domain at the basis of the "Y", consisting of heavy chains constant within an Ig isotype and organism, whose role is to bind F_c receptor as part of the organism immunological response. Therefore, based on the class of Ig that recognizes a certain antigen, a specific immune response mechanism is generated. The F_{ab} region composes the two arms of the "Y" which are responsible for antigen recognition. These two arms that compose the domain can be identical or different in order to recognize different epitopes. Each arm consists of both

heavy and light chains that form a variable portion, containing the so-called complementarity determining regions (CDRs) through which the interactions with the target antigen are established.

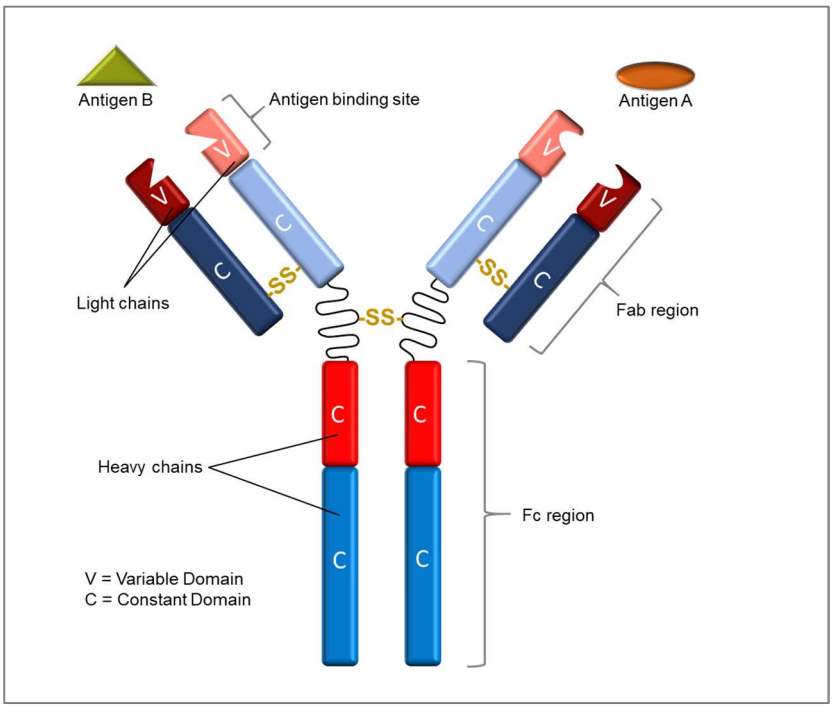

Figure 3.1. Schematic structure of a generic antibody.

It is possible to obtain antibodies both by inoculation of an animal organism with antigens or by cell culture. However, in the first case polyclonal antibodies are obtained, consisting in a mixture of antibodies capable of recognizing a different epitope of the antigen, while in the second case monoclonal antibodies are obtained that recognize a single epitope, thus improving the specificity of the process.

3.2. Immunoassays

The highly efficient and specific interaction occurring between an antigen's epitope and the F_{ab} domain of an immunoglobulin can be exploited as recognition mechanism for sensor fabrication. This is the case of immunosensors [176,177], which are capable of detecting both antigens and antibodies, depending on what species is used as receptor. Such sensing

systems can employ different transduction mechanism, which can be envisioned in two main categories, i.e. labelled and unlabelled detection.
The latter consist in monitoring changes in the output signal as a consequence of the recognition event. Some examples are given by monitoring the immobilization of the antigen/antibody by means of SPR [178], EIS [179] or through the use of quartz-crystal microbalance (QCM) sensors [180]. However, when using label-free detection, the possible occurrence of nonspecific interactions represents a critical limitation which greatly influences the selectivity of the method. In fact, the output change given by nonspecific adsorption cannot be distinguished from the signal generated by the specific recognition event. For this reason, efficient blocking strategies have to be considered in order to prevent the occurrence of such nonspecific interactions.
Detection of immunochemical reactions by means of labelled biomolecules can be achieved by means of conjugation with luminescent compounds [181,182] or, more frequently, with enzymes, as it is the case for the Enzyme-Linked Immunosorbent Assay (ELISA) [183,184].
ELISA tests are developed on multi-well plates where antigen or antibody receptors are covalently bound on each polycarbonate well. After the recognition event with the target molecule has occurred, an enzyme-labelled antibody is used to develop the output signal. Among the most commonly employed enzymes for ELISA tests are Horse Radish Peroxidase (HRP), Alkaline Phosphatase (ALP), glucose oxidase and luciferase. Usually the enzyme activity leads to a product that changes an optical property of the solution which is monitored in order to generate the output signal. The latter will result proportional to the amount of labelled enzyme, which in turn is correlated to the concentration of the immobilized analyte.
ELISA tests can be carried out following different assay formats, namely competitive and non-competitive, both of which are furtherly divided in direct and indirect detection methods (**Figure 3.2**).

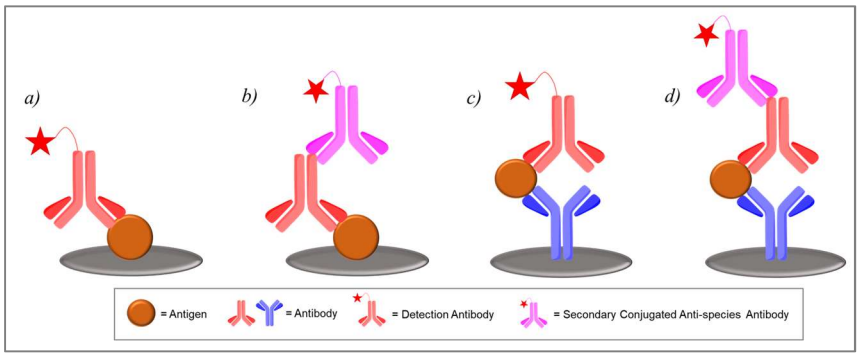

Figure 3.2. Schematic representation of a) competitive ELISA with direct detection, b) competitive ELISA with indirect detection, c) sandwich ELISA with direct detection and d) sandwich ELISA with indirect detection

3.2.1. Competitive and non-competitive ELISA

The format of the ELISA test is determined by the species that is covalently immobilized on the well surface.

For competitive ELISA the species immobilized is either an antigen or an hapten, which is a small molecule with structural and chemical properties analogous to a specific antigen thus allowing the hapten to be recognized by an antibody. Through this format it is possible to determine the presence of a specific antibody in solution (**Figure 3.3a**). In fact, when a sample, containing the target analyte, is incubated in the well, the antibody will recognize the antigen immobilized on the well surface. In this configuration the detection step is usually carried out in an indirect manner, i.e. employing a secondary detection antibody conjugated to an enzyme capable of selectively recognize and bind the F_c portion of the target antibody. However, the competitive format can also be used for detection of an antigen, exploiting an immunocompetition mechanism (**Figure 3.3b**). In particular, the assay mechanism consists in carrying out a competition for antibody interaction between the immobilized antigen and the target antigen in solution, whose concentration is to be assessed. The antibody will preferentially interact with the free antigen in solution, therefore, when no free target will be available, the antibody will interact with the immobilized antigen. Higher concentration of target will result in lower output signal and vice versa. In this case the detection can be carried out both in indirect and direct way. The latter involves the use of a labelled antibody, whose presence can be directly evaluated.

Non-competitive or sandwich format (**Figure 3.4**) is suitable only for the detection of target antigens. It consists in a first recognition between the

receptor and the target, followed by incubation of a second antibody, which recognizes an epitope of the antigen not involved in receptor binding. The second antibody can be labelled to carry out a direct detection, conversely a secondary enzyme-conjugated antibody is employed for indirect detection purposes.

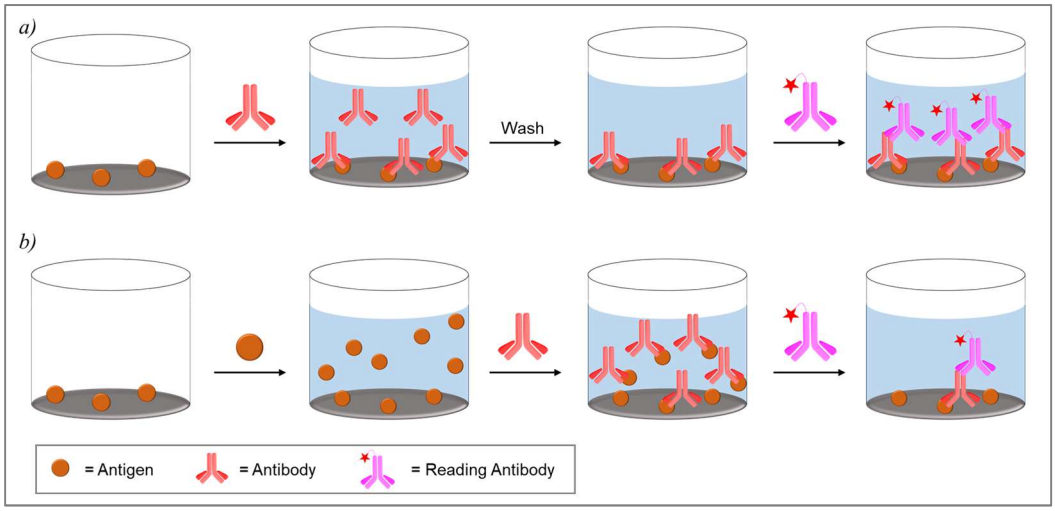

Figure 3.3. Schematic functionalization process during competitive ELISA format. In a) the presence of a specific antibody in solution is assessed, while in b) the concentration of antigen in solution is determined through an immunocompetition with the antigen immobilized on the well surface.

Even though the direct detection allows for the development of easier assay protocol, some issues are connected to its use. In fact, this method requires that the antibody complementary to a specific antigen is conjugated with an enzyme, a condition that cannot be always met since for some enzymes this conjugation might pose stability issues or difficulties in the conjugation process. Even worse, the introduction of an enzyme might alter the properties of the antibody to the extent that its ability to recognize the antigen is compromised. To overcome these limitations an indirect protocol is preferable, since for this approach enzyme-labelled antibodies are easier to obtain given that their requirement involves the complementarity to only the F_c domain, constant within the immunoglobulin isotype of an organism. However, it has to be taken into account that using an indirect approach require an extra step during the carry out of the assay.

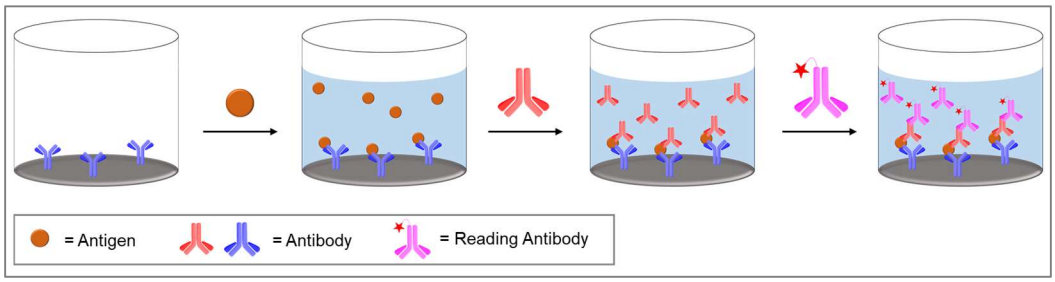

Figure 3.4. Schematic representation of the non-competitive or sandwich ELISA immunoassay for determination of antigen concentration.

3.2.2. *Electrochemical immunosensors*

Usually ELISA protocols conclude with the formation of an enzymatic product whose emission wavelength is in the UV-vis range. However, the same classes of enzymes, mentioned in paragraph 3.2, can be exploited in order to obtain electrochemically active products. This allows to transpose the ELISA systems on three-electrode cell in order to detect antigens or antibodies by means of electrochemical transduction [185]. In particular, immobilization of antigen/antibody on electrode substrate allows for a direct adaptation of ELISA protocol to electrochemical sensing, that can be performed through the techniques reported in chapter 1. Furthermore, adapting the enzymatic reaction to develop an electroactive product bears an intrinsic advantage connected to the high enzymes processivity, that allows the transformation of a high amount of non-electroactive substrate into electroactive product. Over the last years, electrochemical immunosensors proved to be a powerful analytical tool for a wide range of application, spanning from food safety to diagnostic purposes [186-189].

3.3. *Celiac Disease*

Celiac disease (CD) [190,191] is an autoimmune disorder generating inflammatory responses after the ingestion of gluten. The damage generated by the disease primarily affects the small intestine, resulting in issues such as abdominal pain, malabsorption of nutrients, increased risk of developing adenocarcinoma or lymphoma, etc. The incidence of this pathology attests at roughly 1% of the population, however the figure is increasing each year. No cure has been developed to this day, however following a strict gluten-free diet can avoid the manifestation of symptoms in the majority of patients afflicted by CD, even though in 7 to 30 % of patients the treatment proves ineffective [192].

Gluten is an ensemble of protein which can be found in different cereal grains such as wheat, barley, rye and oats. It possesses a composition rich in glutamine and proline which determines its insolubility in water. It is comprised of two proteins, i.e. prolamines and glutelins, the latter being responsible for the triggering of the autoimmune disorder (**Figure 3.5a**). These proteins are characterized by a partial resistance to digestion enzyme, that allows for large peptides to reach the intestinal mucosa and permeate through it generating an adaptive immune response by the organism. Subsequently, the prolamins are subjected to deamidation process operated by the tissue transglutaminase (tTG) enzyme (**Figure 3.5b**) which acts as the autoantigen for CD [193] and promotes their binding with the HLA DQ2 and DQ8 systems followed by recognition by the CD4+ T lymphocytes. The latter express a series of cytokines that trigger the cytotoxic effect that damages primarily the intestinal villous. Simultaneously to this adaptive immune response, an immune response is generated as a consequence of the presence of gliadin on the intestinal epithelium, resulting in intraepithelial lymphocytosis [194].

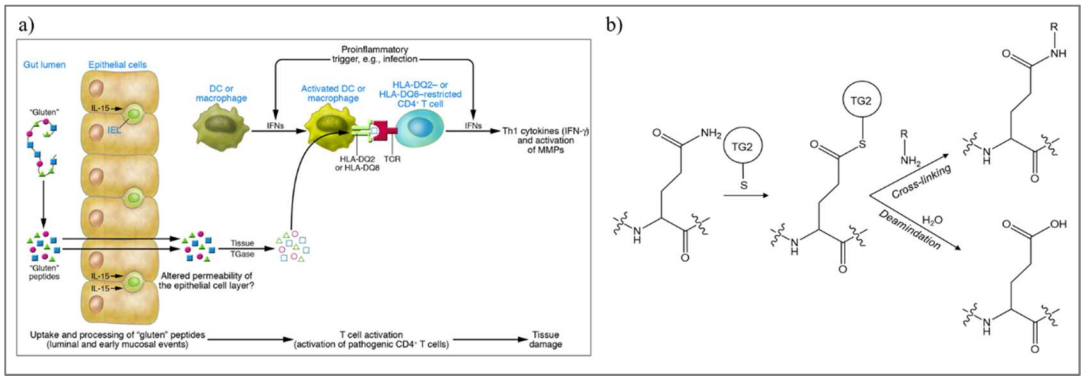

Figure 3.5. a) infographic on the pathogenesis of Celiac Disease [195] and b) deamidation and cross-linking reactions catalysed by tissue transglutaminase (TG2) enzyme activity.

For the diagnosis of CD, the duodenal biopsy is the recognized standard, through which histological analyses can be performed to evaluate the presence of damages of the intestine villous characteristic of the autoimmune disease. However, multiple biopsies are recommended and given the invasiveness of the procedure, the development of a reliable serological assessment would represent a precious alternative. In particular, during the pathogenesis of CD, different antibodies are involved that can be used as targets for the diagnostical purposes, namely antigliadin antibodies, anti-endomysial antibodies and anti-tTG antibodies. Among these, anti-tTG proved to be an excellent marker for

rapid and reliable diagnosis of CD. The best sensitivity is connected to the determination of antibodies in their IgA isotype, however CD often determines a selective deficiency in IgA antibodies. When this condition is verified, the determination of serological markers is performed on the analogous IgG antibodies.

Tissue transglutaminase can be found in two different configurations, namely open and closed (**Figure 3.6**). The latter is the configuration of the protein in normal physiological condition where the enzyme is not active. The open configuration is adopted by the enzyme as a response to traumas or tissue damages, and it allows tTG to carry out its activity of deamidation and cross-linking. This configuration is stabilized in presence of Ca^{2+} ions and the enzyme substrate, however by employment of an inhibitor compound instead of the substrate it is possible to stabilize the open conformation [196].

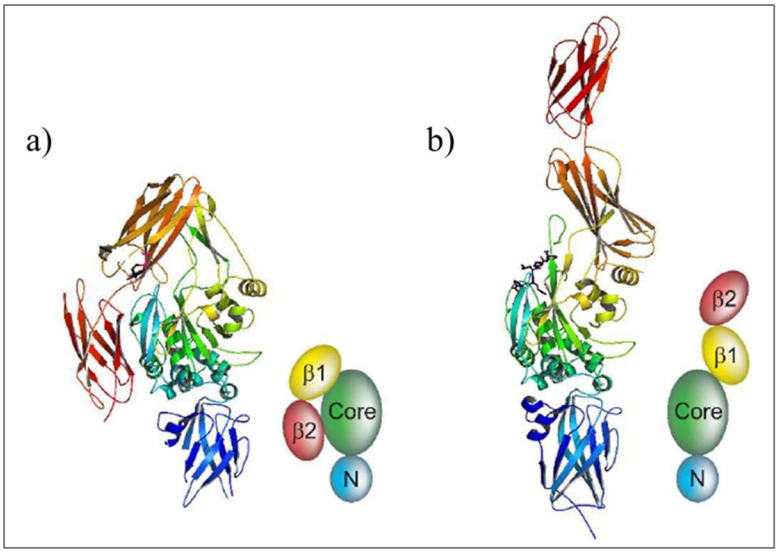

Figure 3.6. Comparison of tissue transglutaminase enzyme in its a) closed and b) open conformation.

Since the recognition between the enzyme and anti-tTG antibodies occurs when the latter are in open configuration, the immobilization of open-tTG as a receptor for immunoassays allows to achieve lower detection limit and to improve the diagnostic sensitivity of the method [197,198].

3.4. The Internet of Things

The last decades have seen an extraordinary technological development that bred a new class of devices, which, exploiting integrated internet connection,

are capable of performing “smart tasks” in addition to their classical function. An example can be found in smartwatches, smart thermostats, etc., which are capable of gathering information on the surrounding environment and share them through different data transmission protocols. This is the working principle at the basis of the Internet of Things (IoT) concept [199], which can be pictured as a network where the nodes are composed of smart objects that can transfer, through an internet gateway, the acquired data to a central storage unit, usually a cloud service, where they can be subsequently processed. This concept is particularly well suited for the development of wireless chemical sensors [200], which through IoT technologies can autonomously acquire and send data with the advantage of being capable of interfacing with other device in order to integrate information from different sources. The wireless connectivity and gathering of data in a remotely accessible location allows for on-site sampling as well as the collection of sensors output dislocated on different places which can be useful for environmental applications. Based on the above-mentioned reasons, wireless chemical sensors have created a great deal of interest in many different fields of application such as food and agriculture [201], environmental pollutant monitoring [202], fitness [203], homeland security [204] and healthcare [205]. For the latter, biomedical devices are integrated with connection protocols for the sharing of the analysis results. As a result, the efficiency of the biochemical sensing platform is conjugated to the possibility of real-time sharing with the physician or the hospital structures, through a cloud service, that allows for a high storage capability of the analyses data.

A common and widely used connection protocol such as Wi-Fi technology allows to exploit infrastructures that are very diffused in households and workplaces. The integration of such technology in an IoT sensing device grants it the feature of direct connection to the internet, without the need of a gateway as in the case of Bluetooth connection, where the data are transferred to a smart device, such as a smartphone, which in turn sends the data to a cloud exploiting its internet connectivity. However, the disadvantage in implementing Wi-Fi connectivity for data sharing consists in a relatively high power consumption, that lowers the battery life of the device. However, it is worth noting that for a sensing device this issue is consistently reduced by the fact that the device does not require a continuous connection and data transfer through Wi-Fi connection, which generates the highest power consumption, in fact the data are only transferred at the end of each analysis.

The development of smart sensing device for point-of-care technologies represents an important resource for disease monitoring, allowing for rapid response in case of sudden critical events or follow-up monitoring of patients.

3.5. Aim of the study

This project purpose was to develop a portable device with WiFi connection protocols for the diagnosis of celiac disease. In particular, a prototype of the measuring device has been built by the research group of Professor Ilaria De Munari of the department of Engineering and Architecture from the University of Parma. The device has been conceived as a portable instrument replacing the role of the benchtop potentiostat and capable of acquiring a DPV signal generated from the oxidation of hydroquinone (HQ) to quinone (Q). Once the signal is obtained, the results is sent via WiFi to a *cloud* service, capable of storing a great amount of raw data. After the signal height is evaluated, the diagnostically useful result can be sent via internet to the patient or the physician for real-time share of the data.

As case of study for the development of the system, the diagnosis of celiac disease (CD) was chosen. During previous works conducted by our research group, both amperometric and piezoelectric immunosensors were developed and validated [206,207] for the detection of antibodies anti-tissue transglutaminase (anti-tTG) in both isotype IgA and IgG, which are considered reliable marker of CD (**Scheme 3.1**).

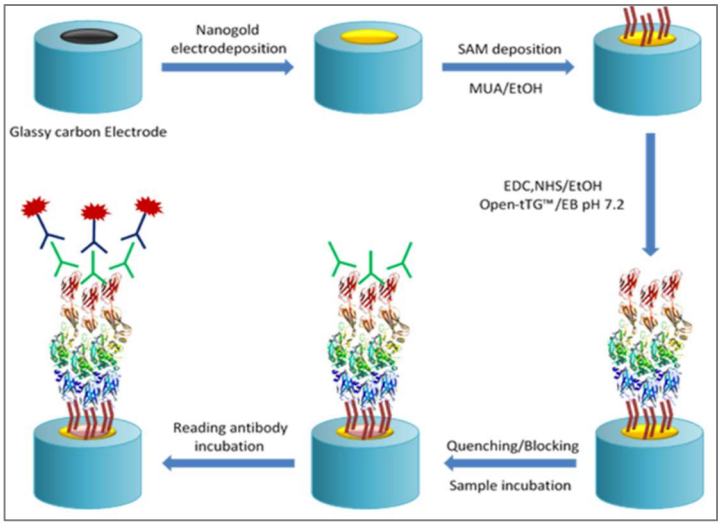

Scheme 3.1. Functionalization steps of the immunoassay developed on reusable glassy carbon electrode

The amperometric sensing device was based on the functionalization of glassy carbon electrode, which, after electrodeposition of gold to obtain gold nanoparticles on the electrode surface, was functionalized with the heterobifunctional mercaptoundecanoic acid (MUA) to form a self-assembled

monolayer (SAM). In particular, the MUA possesses a thiol function that interacts with the gold nanoparticles while the carboxyl group remains exposed to the solvent and, subsequently to activation with EDC and NHS, can covalently couple with the tTG enzyme antigen in its open conformation. After covalent attachment of tTG, the solution containing the anti-tTG was incubated, allowing for specific recognition between the antigen and the analyte antibody. In order to reveal the occurrence of this event, a secondary antibody conjugated to Horseradish Peroxidase (HRP) has been employed. The electrochemical measurement was carried out by addition of thionine, whose electrochemical conversion between oxidized (TH^+) and reduced (THH) form has been monitored through cyclic voltammetry measurements. The activity of HRP affects the redox activity of thionine as a consequence of the addition of the enzyme substrate H_2O_2, which oxidizes the HRP (HRP-ox), which in turn is capable of oxidizing the THH to TH^+. This has been observed in the CV scans as an increase in the cathodic current, referred to as Peroxidase Induced Current Shift (PICS), ascribable to the enzyme activity that produces a larger amount of oxidized species with respect to the one produced by the voltammetric process alone.

The aim of the work reported in this chapter was to optimize the response and improve the previous method [206] in terms of time consumption, portability, ease of carry out, etc. in order to exploit the assay as a case of study for the development of the IoT-WiFi device. To this aim, the reusable glassy carbon electrode was replaced with disposable Screen-printed Electrodes (SPEs) and the tTG enzyme was directly chemisorbed on gold nanoparticles, instead of use a SAM from MUA as linker. Furthermore, the secondary reading antibody enzymatic tag was changed from Horseradish Peroxidase to Alkaline Phosphatase (ALP). In fact, the latter generates the electrochemical signal as a consequence of its presence rather than a shift in signal as PICS and only requires a substrate which is converted in electroactive species, while HRP requires the redox probe (thionine) as well as the enzymatic substrate (H_2O_2).

3.6. Experimental

3.6.1. Reagents and solutions

Sodium chloride (NaCl), ethylendiaminetetraacetic acid disodium salt dihydrate (Na_2EDTA), DL-dithiothreitol (DTT), calcium dichloride hexahydrate ($CaCl_2 \cdot 6H_2O$), Trizma® Base, magnesium chloride ($MgCl_2$), Tween® 20, bovine serum albumin (BSA), human serum, Alkaline phosphatase-labelled rabbit anti-human immunoglobulins IgA (anti-H-IgA-AP) and IgG (anti-H-IgG-AP), hydrochloric acid (HCl, 37%), sodium hydroxide (NaOH), Potassium hexacyanoferrate(III) ($K_3Fe(CN)_6$), Potassium hexacyanoferrate(II) trihydrate ($K_4Fe(CN)_6 \cdot 3H_2O$) and potassium chloride (KCl) were purchased from Sigma-Aldrich (Milan, Italy).
Hydroquinone diphosphate (HQDP) was purchased from Metrohm Italiana (Origgio, Varese, Italy).
Human tissue transglutaminase in its open conformation (open tTG®) and ZediXclusive Open tTG®-Ab (IgA), ZediXclusive Open tTG®-Ab (IgG) ELISA kits were purchased from Zedira GmbH (Darmstadt, Germany). The ELISA kits contain six anti-tTG antibodies solutions (0, 1, 3, 10, 30, 100 AU/mL) along with a positive and negative control solutions.
Buffer solutions composition is reported below:

- *Enzyme buffer (EB)*: 20 mM Trizma® Base, 1mM DTT, 150 mM NaCl, 10 mM $CaCl_2 \cdot 6H2O$ (pH adjusted to 7.2 with HCl).
- *Tris Buffered Saline (TBS)*: 0.1 M Trizma® Base, 0.02 M $MgCl_2$ (pH adjusted to 7.4 with HCl).
- *Tris Buffered Saline-Tween (TBS-t)*: 0.1 M Trizma® Base, 0.02 M $MgCl_20$, 0.05% w/v Tween® 20 (pH adjusted to 7.4 with HCl).
- *Reading* buffer (RB): 0.1 M Trizma® base, 0.02 M MgCl2 (pH adjusted to 9.8 with HCl).
- *Sample buffer (SB) and Wash buffer (WB)* were contained in the ELISA kits mentioned above.

3.6.2. Apparatus

pH meter “pHenomenal® 1000 L” connected to “pHenomenal® 221” refillable 3 in 1 glass pH electrode with temperature sensor and “Ultra-High Performance (UHP)” single-channel mechanical pipettes purchased from VWR Internation

srl (Milan, Italy) and Sartorius CP225D analytical balance were used throughout the immunoassay.
Disposable Gold nanoparticle-functionalized Screen-Printed electrodes (GNP-SPEs, DRP-110GNP) were purchased from Metrohm Italiana Srl (Origgio, Varese, Italy).
The voltammetric readout was performed employing a PGSTAT-204 Potentiostat/Galvanostat purchased from Metrohm Italiana Srl (Origgio, Varese, Italy), operated through NOVA 2.1.3 Advanced Electrochemical Software using a DropSens DRP-DSC plug for the connection of the SPEs to the potentiostat.

3.6.3. Immunosensor assay protocol

3.6.3.1. *Enzyme linking*

In order to obtain interactions between the gold nanoparticle and the enzyme, 25 µL of a solution of open-tTG properly diluted in *EB* were drop-casted on the GNP-SPE surface. After 3 hours the electrode was thoroughly rinsed with *EB.* To prevent nonspecific interactions between the electrode surface and other proteins, a 20 mg/mL solution of BSA in *EB* was incubated for 60 minutes on the SPE after which a washing step with *EB* was carried out.

3.6.3.2. *Antibody incubation*

The samples containing the anti-tTG antibodies (standards solutions contained in the ELISA kits or anti-tTG antibody standards diluted 1:100 in human serum) were drop-casted on the electrode surface for 60 minutes. Subsequently the SPE was washed first with *WB* and then *TBS*.

3.6.3.3. *Enzyme labelling and electrochemical readout*

A properly diluted solution of anti-H-IgA-AP or anti-H-IgG-AP in *SB* was drop-casted on the electrode for 1 hour, then the electrode surface was rinsed with *SB*.
Finally, 50 µL of a 1 mg/mL solution of HQDP in *RB* were deposited on the surface for 90 seconds and the DPV scans were acquired by imposing the following parameters:

- Start Potential: -0.5 V
- Stop Potential: +0.3 V

- Step Potential: +0.00495 V
- Modulation Amplitude: +0.04995 V
- Modulation Time: 0.102 s
- Interval Time: 0.4 s

3.6.4. Acquisition using ferro/ferricyanide as redox probe

A properly diluted solution of equimolar $K_3Fe(CN)_6$ and $K_4Fe(CN)_6$ in KCl 0.1 M was produced and 50 µL of it deposited on the surface of a C-SPE interfaced with either the PGSTAT-204 or the IoT-WiFi device. The DPV acquisitions were performed imposing the following parameters:

- Start Potential: -0.4 V
- Stop Potential: +0.4 V
- Step Potential: +0.00495 V
- Modulation Amplitude: +0.04995 V
- Modulation Time: 0.102 s
- Interval Time: 0.4 s

3.6.5. Assessment of analytical performance

At least three replicate measurements were carried out for all standards and samples. Intermediate precision was obtained performing at least three replicated measurements for each concentration levels on independently fabricated immunosensors. Method validation was performed by calculating limit of detection (LOD) and limit of quantification (LOQ) according to "Eurachem Guidelines" [159].

3.7. Results and Discussion

3.7.1. Immunoassay working principle

A new protocol for the carry out of the detection and quantitation of anti-tTG based on the use of SPEs was conceived (**Scheme 3.2**).

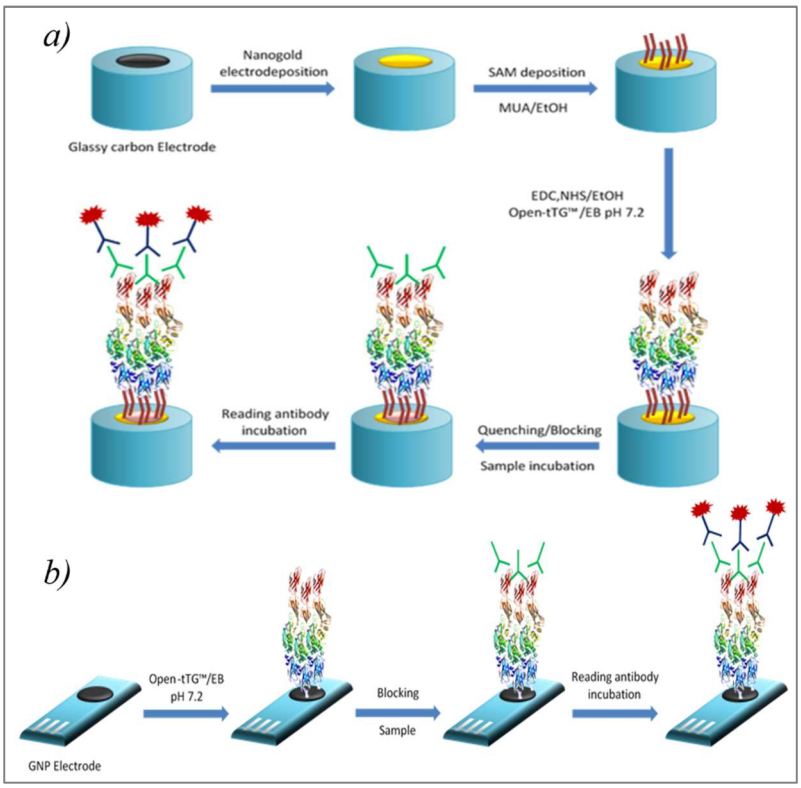

Scheme 3.2. Comparison of the immunoassay previously developed on reusable glassy carbon electrode [206] and the novel method based on disposable Screen-Printed Electrodes.

Different electrode substrates were tested, mainly carbon-based and gold-based. For the former, a first step of activation with EDC and NHS is required to covalently attach the tTG enzyme in its open conformation (open-tTG™), while, in the latter case, the enzyme can be directly bound to the gold substrate exploiting the cysteine residues of the enzyme, provided that the epitope involved in the binding is different from the one responsible for antibody recognition. After blocking step with BSA to avoid non-specific interactions between antibodies and sensor surface, the sample containing anti-tTG antibodies is incubated on the surface, followed by incubation of the secondary reading antibody, i.e. Alkaline phosphatase-labelled rabbit anti-human immunoglobulins IgA or IgG (anti-H-IgA-AP, anti-H-IgG-AP). Finally, a solution

of enzymatic substrate, i.e. Naphthyl Phosphate (NP) or Hydroquinone Diphosphate (HQDP), is added, in order to generate the electroactive species and its oxidation peak is acquired in DPV. The signal obtained will be directly proportional to the amount of ALP present on the surface, which in turn will depend on the amount of anti-tTG bound on the open-tTG™ covalently attached to the sensor surface.
For the development of the new protocol, different aspects have been taken into considerations, in order to identify the best working conditions:

- Electrode substrate of the SPEs, i.e. carbon (C), Single-Walled Carbon Nanotubes (SWCNT), gold (G), gold nanoparticles deposited on carbon substrate (GNP), single-walled carbon nanotubes-gold nanoparticles composite (CNT-GNP).
- Reading enzyme substrate, i.e. HQDP, NP.
- Concentration of open-tTG™ enzyme.
- Concentration of anti-H-ALP conjugate

To evaluate the best working conditions, the results obtained employing the positive and negative control solutions from the ZediXclusive Open tTG™-Ab ELISA kits as sample solutions were compared.

3.7.2. Comparison of SPEs electrode substrates

To achieve the best positive to negative ratio (P/N) different electrode substrates were evaluated for open-tTG™ immobilization, namely C-SPEs, SWCNT-SPEs, G-SPEs, GNP-SPEs and CNT-GNP-SPEs. However, the immobilization of the enzyme on the surface requires different treatments based on the nature of the substrate. In particular, for C- and SWCNT-SPEs the immobilization must be carried out through coupling interactions between carboxylic functions and amino residues present on the enzyme. On SWCNT-SPEs the activation with EDC and NHS of the natively present carboxyl groups can be carried out directly, while for C-SPEs a first step of oxidation in CV depositing H_2SO_4 must be preventively carried out (see paragraph 2.7.2). Conversely, on G- and GNP-SPEs the immobilization of open-tTG™ can be carried out without any prior treatment, by drop-casting of a solution of the enzyme on the sensor surface. In fact, in this case Au-S interactions are established between the electrode substrate and the thiol-containing residues. Finally, for CNT-GNP-SPEs, an activation of the carboxyl group by means of EDC and NHS is carried out in order to immobilize the enzyme on both the

nanotubes and the metal nanoparticles, thus achieving the highest degree of functionalization.
For the evaluation of the P/N, the concentrations of both antigen and secondary antibody were set at constant value, corresponding to a dilution factor of 1:500 and 1:1000 respectively, while the enzymatic substrate used was NP.
Comparing the results obtained employing different electrode substrate (**Figure 3.7**) it was observed that even though the highest intensity for positive signal is achieved on SWCNT-SPEs, the best P/N ratio of 2.2 is reached on GNP-SPEs. Furthermore, data dispersion is also reduced on the latter if compared to immobilization on carbon nanotubes.

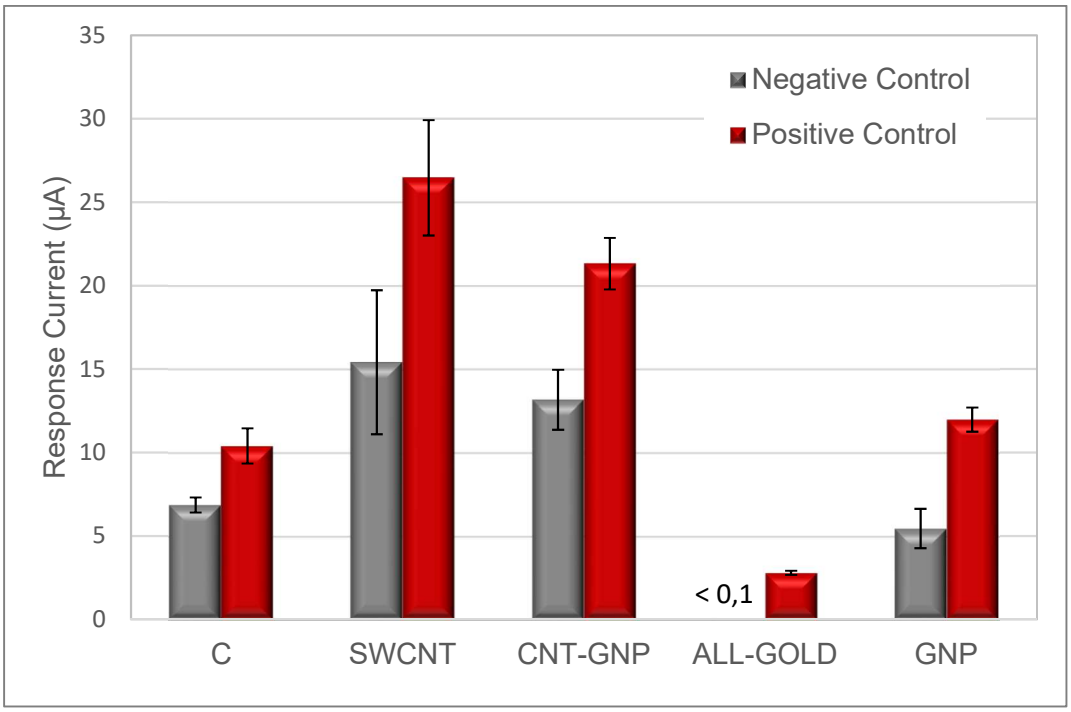

Figure 3.7. Comparison of the current responses obtained by incubation of positive (red) and negative (grey) control solutions on SPEs with different electrode substrate onto which the antigen was immobilized.

The employment of GNP-SPEs as platforms for the development of the immunoassay translates in an easier and faster protocol, since the immobilization on the antigen is carried out by simple drop-casting of a properly diluted open-tTG™ solution.
It is worth noticing that for both immobilization strategies (i.e. coupling reaction and Au-S interactions), the epitope of the antigen involved in surface attachment is different from the one responsible for antibody recognition,

otherwise no difference would be observed between positive and negative signals.

3.7.3. Enzymatic substrate

After identifying the electrode substrate capable of giving the best results in terms of P/N ratio, the latter was also measured to assess which enzyme substrate is more suitable for assay development. In particular, two substrates have been taken into account, namely Naphthyl Phosphate and Hydroquinone Diphosphate. By employing both at the same concentration, i.e. 1 mg/mL, using the same incubation time of 90 s over which the enzymatic processing is carried out and setting the dilution factors of both open-tTG™ and anti-H-ALP conjugate to 1:1000, the signal obtained by incubation of positive and negative controls were compared (**Figure 3.8a**). The P/N ratios were comparable, measuring 2.5 when using NP and 2.63 when using HQDP, even though with NP the absolute intensity of signals resulted higher. Nevertheless, HQDP was chosen as enzymatic substrate given that data dispersion resulted lower with respect to NP and the DPV peaks obtained were sharper when using HQDP (**Figure 3.8b**).

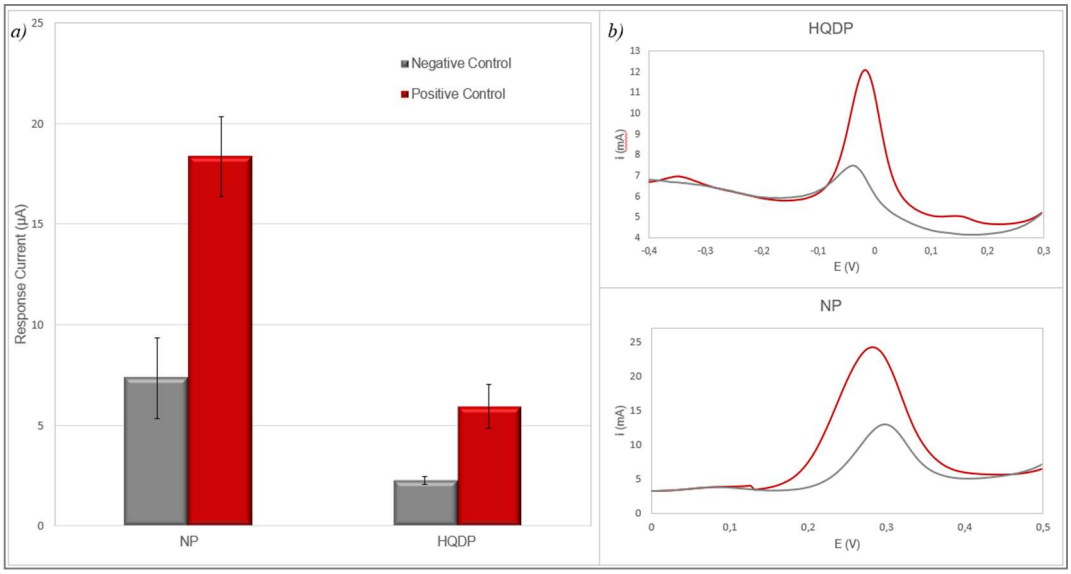

Figure 3.8. a) response current obtained using as enzymatic substrate NP and HQDP. b) DPV voltammograms obtained using NP and HQDP as enzymatic substrate.

3.7.4. *Optimization of P/N response*

To optimize the conditions leading to the best analytical performance towards the detection and quantitation of anti-tTG antibodies of both isotypes (i.e. IgA and IgG), it was chosen to apply a full-factorial experimental design with two factors and three levels. The P/N ratio was optimized taking into account the variations of the two factors i.e. both open-tTG™ and anti-H-ALP conjugate concentrations, over three levels of concentration each, which varied on the base of the antibody isotypes (**Table 3.1**).

		Determination of IgA anti-tTG	**Determination of IgG anti-tTG**
	Level	*Dilution factor*	*Dilution factor*
open-tTg™	-1	1:1000	1:500
	0	1:500	1:250
	+1	1:250	1:100
anti-H-ALP	-1	1:2000	1:1000
	0	1:1000	1:500
	+1	1:500	1:250

Table 3.1 Factors and levels employed for the experimental design aimed at optimization of both open-tTG and anti-H-ALP conjugate concentrations

The study was conducted for both IgA and IgG isotypes of antibodies, by applying the same experimental matrix (**Table 3.2**).

Experiment	**open-tTg™**	**anti-H-ALP**
1	-1	-1
2	-1	0
3	-1	+1
4	0	-1
5	0	0
6	0	+1
7	+1	-1
8	+1	0
9	+1	+1

Table 3.2 Experimental matrix for the full-factorial design

3.7.5. *Optimization of IgA antibodies response*

The results obtained for the detection of IgA anti-tTG antibodies were analysed by means of two-way ANalysis Of VAriance (ANOVA) with interactions.

Through this analysis the significance of factor A (open-tTG™), factor B (anti-H-IgA-ALP) and their interactions AB resulted significant ($p<0.01$).
Subsequently, through Bonferroni post-hoc analysis, the difference between each level of factor A and B was investigated. It was observed that for the open-tTG™ each level significantly differs ($p<0.05$) from the others (**Figure 3.9a**), while for the anti-H-IgA-ALP no difference was found between level -1 and 0, however all the other differences are significant (**Figure 3.9b**).

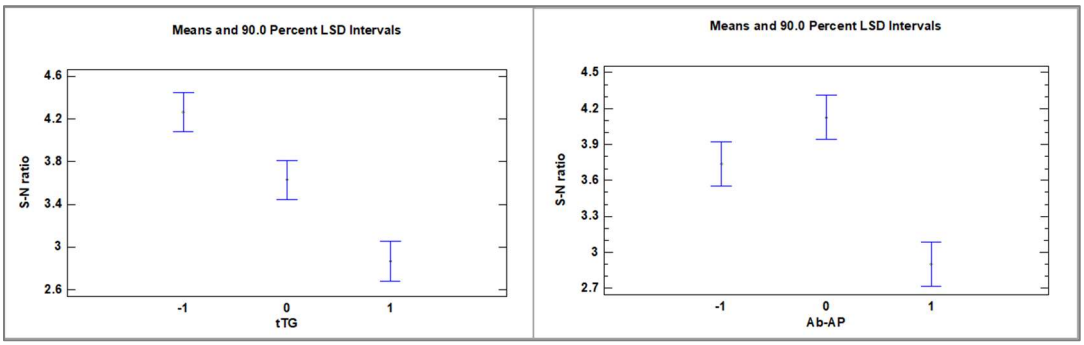

Figure 3.9. a) ANOVA plot for factor A (open-tTG™) on IgA antibodies and b) Bonferroni test for factor B (anti-H-IgA-ALP) on IgA antibodies

Furthermore, it was possible to build interaction plot on which the P/N ratio is reported as a function of one of the two factors, keeping the other factor constant (**Figure 3.10**).

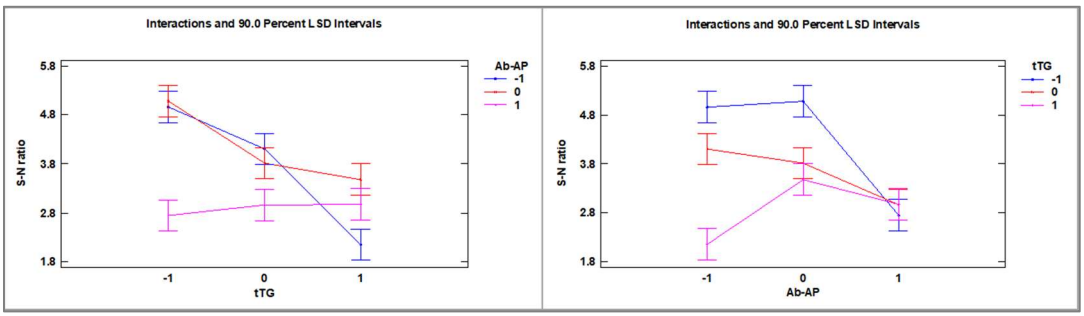

Figure 3.10. Interaction plots obtained keeping a) the anti-H-IgA-ALP and b) open-tTG™ concentrations constant.

The highest P/N ratio have been identified for the experiment where the factor A and factor B were employed at level -1 and 0, translating in a dilution factor of 1:1000 for both open-tTG™ and anti-H-IgA-ALP.

3.7.6. Optimization of IgG antibodies response

Each test of the experimental matrix was repeated for the detection of IgG anti-tTG antibodies and the results were analysed through two-way ANOVA with interactions also in this case. The same order of factors was also maintained, with open-tTG™ labelled as factor A and anti-H-IgG-ALP labelled as factor B.
As for IgA, also in the case of IgG the two factors and their interaction AB resulted statistically significant (p<0.01).
Through Bonferroni post-hoc analysis it was possible to determine that for open-tTG™ the only two levels that differ significantly are the -1 and +1 (**Figure 3.11a**), while for anti-H-IgG-ALP each level results significantly different from the others (**Figure 3.11b**).

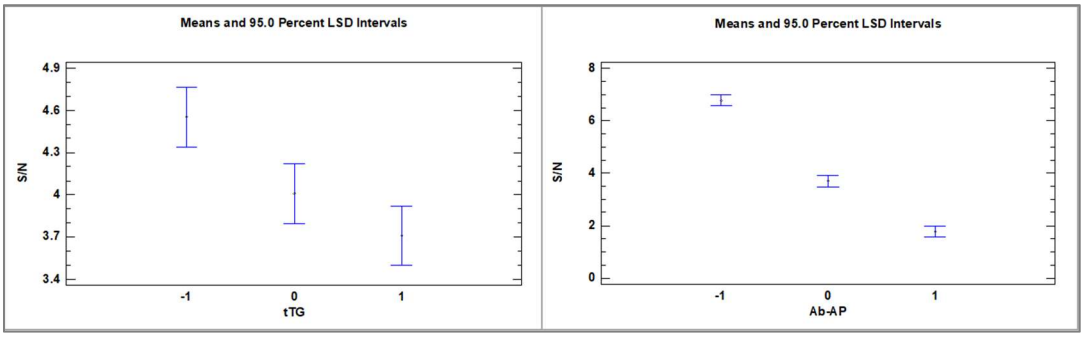

Figure 3.11. a) ANOVA plot for factor A (open-tTG) on IgG antibodies and b) Bonferroni test for factor B (anti-H-IgG-ALP) on IgG antibodies

Also in this case it was possible to evaluate the effect that the two factors have on the P/N ratio through interaction plots (**Figure 3.12**).

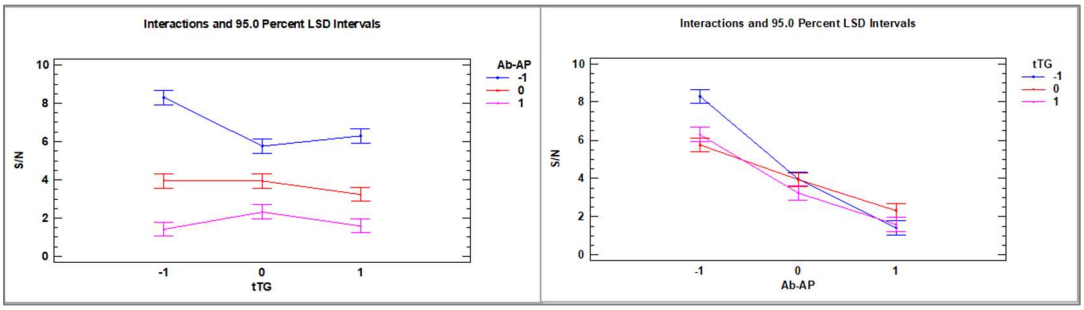

Figure 3.12. Interaction plots obtained keeping a) the anti-H-IgG-ALP and b) open-tTG concentrations constant.

Through the implementation of the factorial design, it was possible to identify the optimized conditions for IgG anti-tTG detection in terms of concentration

of both open-tTG™ and anti-H-IgG-ALP, corresponding to 1:500 (level -1 for factor A) and 1:1000 (level -1 for factor B), respectively.

3.7.7. Calibration curves

Using the optimized conditions identified using the 3^2 full-factorial design, a calibration curve for each isotype of analyte antibody has been built. To this aim, the standard solutions at known anti-tTG concentrations were spiked with human serum diluted 1:100, in order to simulate the real matrix, and the immunoassay measurement was performed. The concentration levels investigated were 3 AU/mL, 10 AU/mL, 20 AU/mL, 30 AU/mL and 100 AU/mL. For both IgA and IgG isotypes, the calibration curves obtained showed linear response in the range between 3 AU/mL and 30 AU/mL, were linear interpolation was performed.

In the case of IgG anti-tTG antibodies (**Figure 3.13**), the values for LOD and LOQ calculated were, respectively, 1.3 AU/mL and 2.3 AU/mL. The threshold value, over which further tests are required for the confirmation of the patology, is found at 3 AU/mL according to specifications from commercial ELISA kit, used as reference method for validation purpose, with negative control showing an anti-tTG concentration lower than 2.6 AU/mL while for the positive control it is higher than 3.5. Based on these considerations, the developed assay is capable of efficiently discriminate between positive and negative samples.

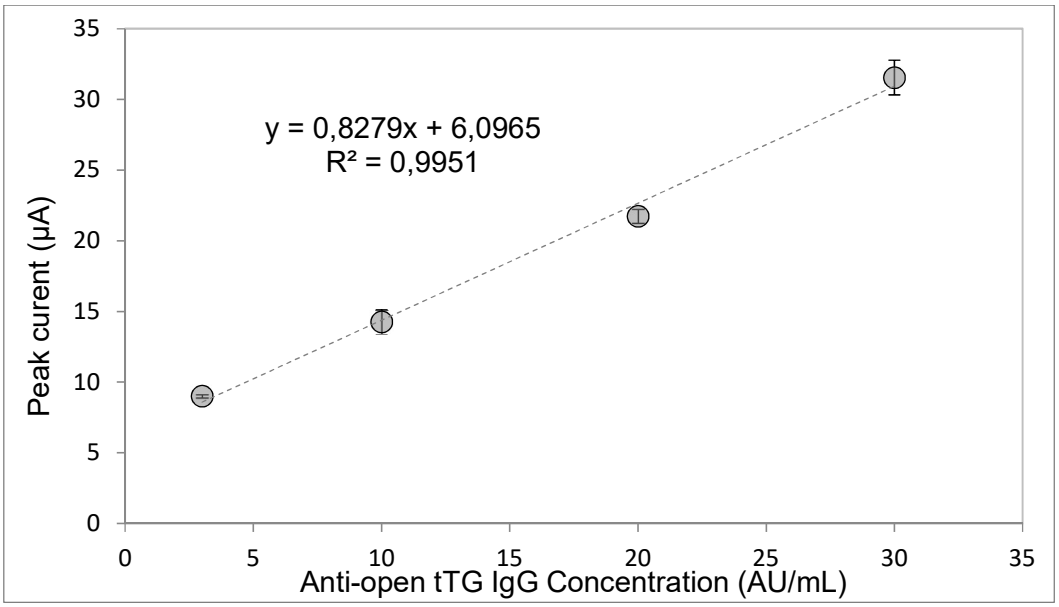

Figure 3.13. Calibration line for determination of IgG anti-tTG antibodies. Mean and standard deviation (n=3) for each concentration level are reported.

As for the calibration line obtained for IgA anti-tTG (**Figure 3.14**), the LOD and LOQ values calculated were, respectively 3.1 AU/mL and 6.9 AU/mL. Being the threshold value 3 AU/mL, the LOD of the method allows for a qualitative discrimination between positive and negative samples close to threshold value, allowing quantification of IgA anti-tTG for concentrations higher than LOQ.

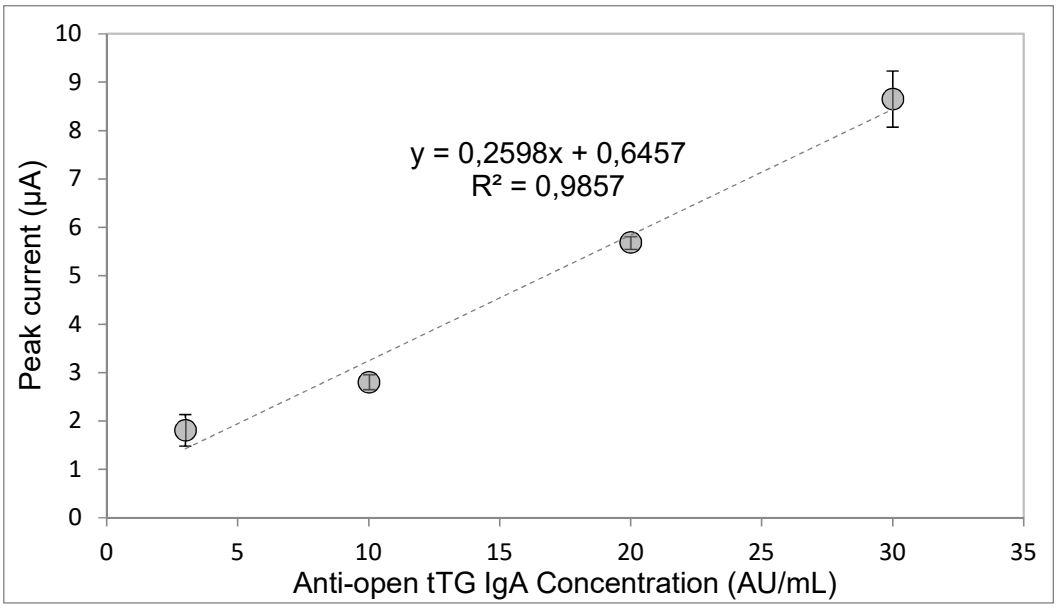

Figure 3.14. Calibration line for determination of IgA anti-tTG antibodies. Mean and standard deviation (n=3) for each concentration level are reported.

3.7.8. Interference studies

In order to assess the specificity of the immunological assay towards the anti-tTG antibody analyte, anti-deamidated gliadin (DGPx1-Ab) human IgG and IgA antibodies were tested as potential interferents. These antibodies were chosen since their expression often occurs in CD positive patient, especially in pre-diagnostic stage. The effect of the presence of anti-deamidated gliadin antibodies was tested in absence of anti-tTG to ensure that no non-specific signal was connected to the presence of the interferent, as well as in presence of anti-tTG to confirm that its presence does not affect the recognition with the analyte. DGPx1-Ab were spiked at different concentrations in the control solutions, namely 3 AU/mL, 18 AU/mL and 100 AU/mL. In all the cases tested, no significant difference (p>0.05) was observed between signal responses where the interferent was present and the signal recorded in absence of interferent. Therefore, the immunoassay proved to possess a good specificity towards the detection of anti-tTG antibodies.

3.7.9. Acquisition with the IoT-WiFi device

The research group of Professor I. De Munari assembled a prototype of portable device for the readout of the immunoassay capable of storing the analysis results on a cloud service for elaboration and visualization, from which it can be shared in real-time.

The prototype is composed of two development boards (**Figure 3.15**).

The first (**Figure 3.15a**) contains a System on Chip (CC3200) mounted on the board (LaunchPad XL board) which acts as motherboard of the device and carries out the tasks of data sampling, processing and transmission. This board is responsible for the connectivity of the device, containing, among others, the WiFi module and is employed for the realization of IoT devices. This board allows the device to securely transfer data to a cloud service via internet connection and is characterized by low power consumption.

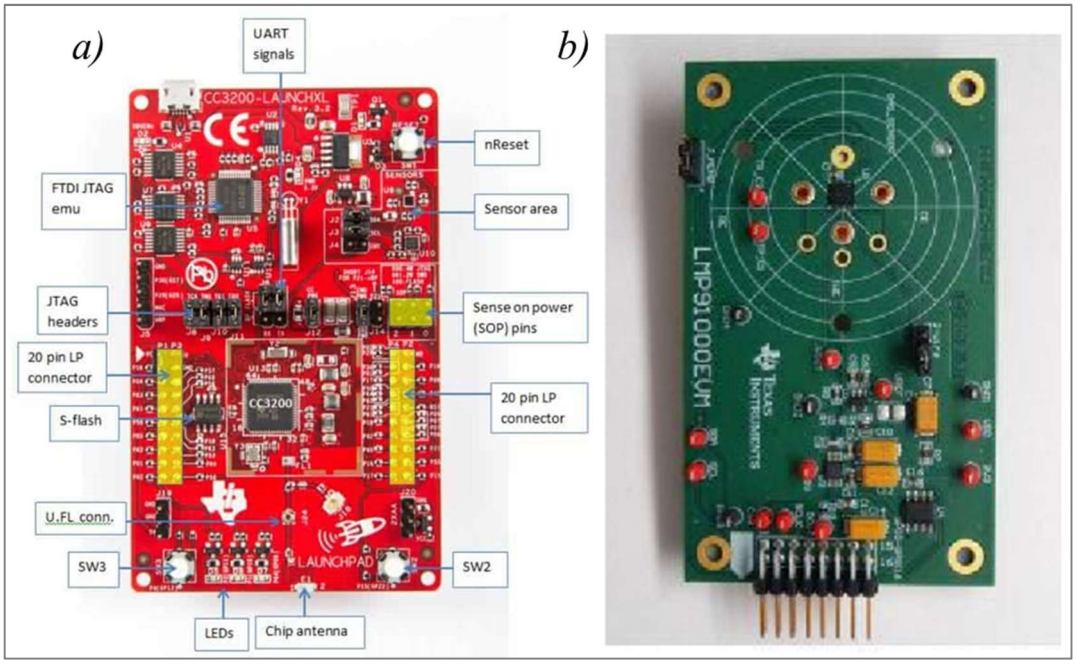

Figure 3.15. Development boards used for the assembly of the IoT WiFi device prototype. a) LaunchPad XL with CC3200 SoC and b) LMP91000 board.

The second development board (**Figure 3.15b**) contains the integrated potentiostat LMP91000, allowing the device to polarize the cell and perform the DPV measurements. The board was programmed in order to be capable of covering a voltage range useful for HQDP detection, i.e. from -0.6 V to 0.5 V, over which a DPV ramp was imposed. However, the compact dimensions of the prototype translate in a reduced computational capacity and a limited amount of points that can be acquired in a single DPV scan (**Figure 3.16**). In particular, in the selected voltage range, it was possible to acquire 17 points for each scan, while on a common benchtop potentiostat the number of acquired points is approximately 150. The board containing the LMP91000 contains a connector that allows the device to interface with SPEs, on which the electrochemical measurement is performed.

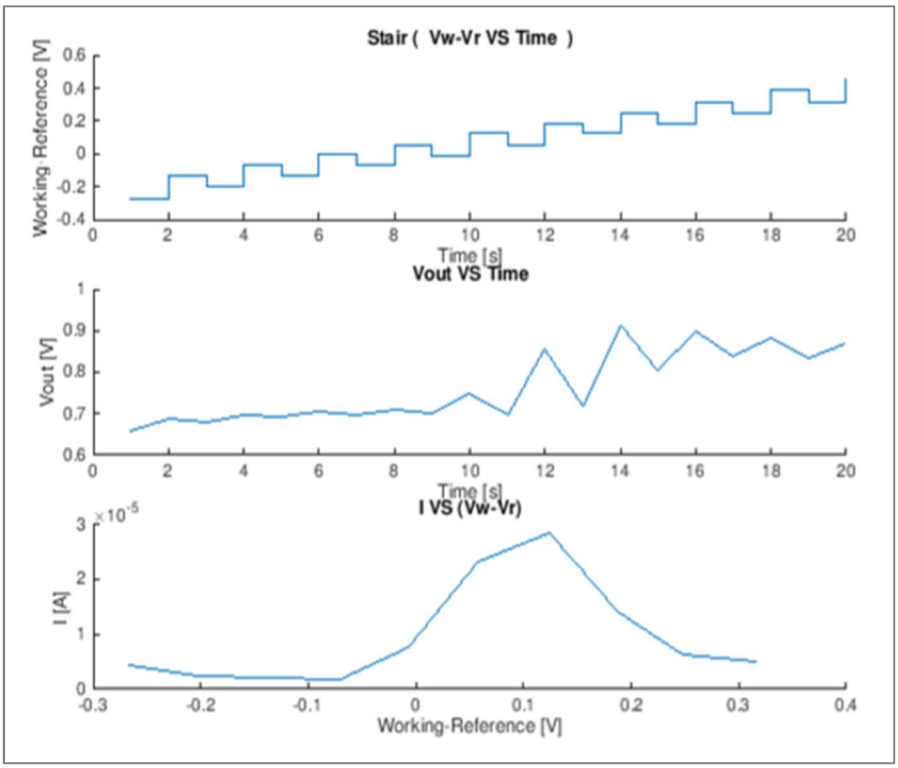

Figure 3.16. DPV scan performed by the IoT WiFi device developed

After the analysis is performed, the results were sent to Mathworks® ThingSpeak™ cloud platform, which supports MATLAB® data analysis resources. For development purposes, the raw data were sent to the cloud where the elaboration and visualization of the results is then carried out. Yet, the transmission of the complete acquisition implies a higher amount of data transferred compared to the sharing of the results, leading to a higher power consumption required by the WiFi connection. However, after the development of the device is carried out, the data elaboration can be performed on-board, allowing for the transmission of results only, obtaining a longer battery life.

This prototype has been used to test positive and negative control solutions for both anti-tTG isotypes. In particular the DPV acquisition performed with the IoT WiFi device were compared with those obtained using a benchtop potentiostat (**Figure 3.17**). As expected, a consistent decrease in P/N ratio is observed when using the portable device, as a consequence of the reduced amount of points acquired, connected to the compactness of the device.

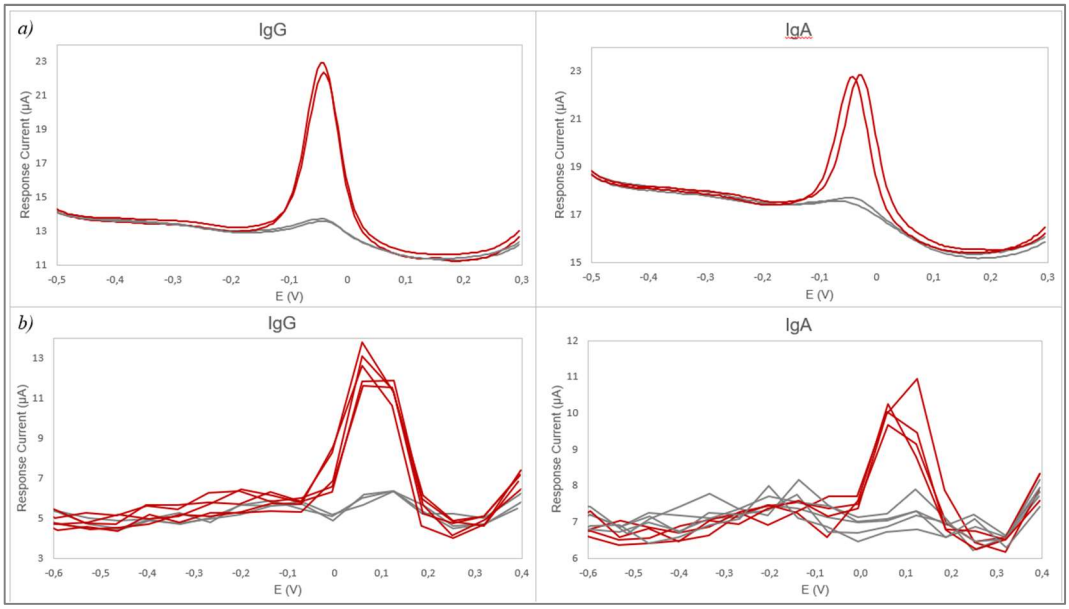

Figure 3.17. Comparison of the DPV voltammograms of positive (red) and negative (grey) control solutions obtained using a) the benchtop potentiostat with b) those obtained using the IoT WiFi device for both IgA and IgG isotypes of anti-tTG antibodies.

However, the reduction of the P/N ratio did not affect the discriminating capability of the device. In fact, for both IgA (**Figure 3.18a**) and IgG (**Figure 3.18b**) anti-tTG analysis, it was possible to discriminate between negative and positive with a high level of confidence (p<0.001).

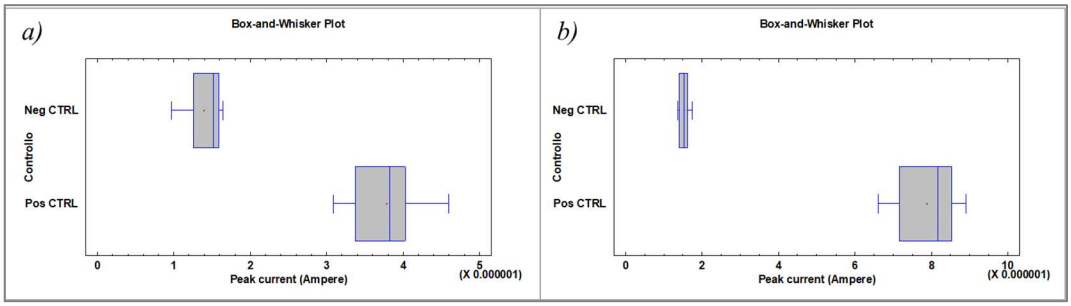

Figure 3.18. Box and Whiskers plots relative to anti-tTG a) IgA and b) IgG detection for positive and negative controls. n=3 for each control sample.

Therefore, taking into account the specificity towards analyte recognition and the ability to discriminate between positive and negative samples with high significance, the device proved to possess remarkable capability for the diagnosis of celiac disease. In fact, the quantitative assessment of anti-tTG markers is beyond the purpose of this device, whose intended role is to represent a portable and user-friendly screening tool for at-home self-diagnosis. In fact, the developed instrument does not require complicated

hardware, custom software applications or devices with specific operative systems in order to obtain the results, which is readily available and can be shared, exploiting cloud service resources, with a selected number of users, ranging from the patient to the clinician.
However, it is worth pointing out that Celiac Disease was taken into account as a case of study, while the device itself possesses a high versatility for different applications. In fact, it can be employed with any system that exploits HQDP for the generation of the electrochemical signal, e.g. the genosensing assay developed in chapter 2. For this reason, the device can represent a powerful tool for a variety of biomedical devices and point-of-care applications.

3.7.10. Improvement on device resolution

As reported in paragraph 3.7.9, the acquisitions carried out on the IoT-WiFi prototype were affected by a decrease in P/N ratio as a consequence of the limited amount of points acquired by the device, that reduce the resolution of the peaks. In order to overcome this limit, the prototype has been modified by replacing the LMP9100 with a custom-made analog front-end. To test this newly developed device, DPV acquisitions were carried out using ferri/ferrocyanide redox probe in aqueous solution containing 100 mM KCl as supporting electrolyte. In particular, different concentrations were tested on both the device and a benchtop potentiostat (Autolab PGSTAT-204) and the results were compared (**Figure 3.19**).

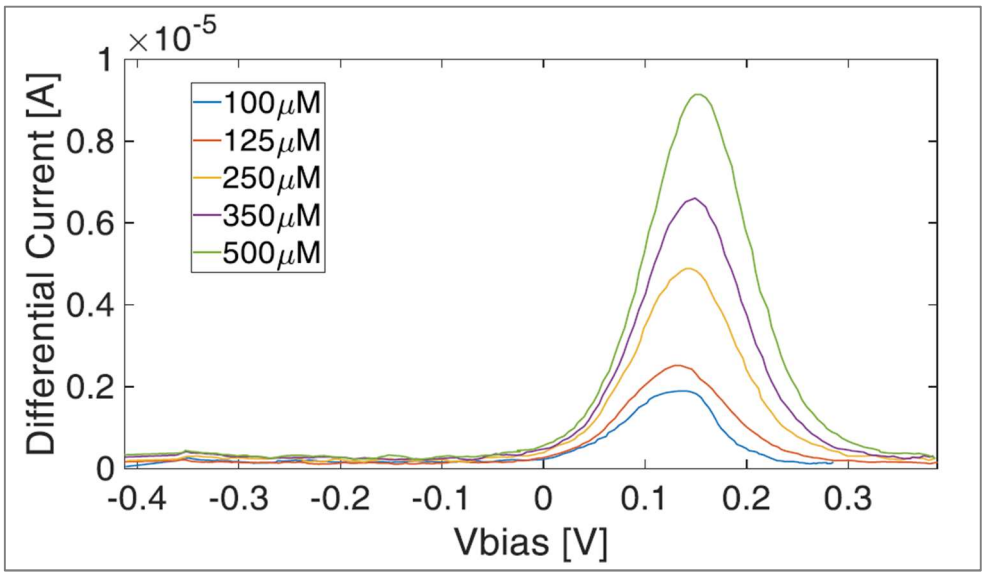

Figure 3.19. DPV voltammograms acquired on IoT-WiFi device at different ferri/ferrocyanide concentration.

In particular, five redox probe concentration were tested, namely 100 µM, 125 µM, 250 µM, 350 µM and 500 µM, where, for each concentration, 50% of ferricyanide and 50% of ferrocyanide were employed. By employing a step potential of 5 mV in the voltage range -0.4/+0.4 V, it was possible to achieve a total of 302 points acquired for each scan, which translates in 151 points in the DPV voltammogram (**Figure 3.19**). By testing the five concentration of redox probe reported above it was possible to generate calibration curves employing the benchtop potentiostat and the IoT-WiFi device (**Figure 3.20**). The current responses showed a good repeatability, displaying an RSD < 10% for all the levels explored. By comparing the two calibration lines it is possible to observe that the points acquired on the two platforms are nearly superimposable, yielding slopes values that are not significantly different (p>0.05), namely 1,87 $\cdot 10^{-8}$ for the portable device and 1,77 $\cdot 10^{-8}$ for the benchtop instrument.
It is also worth noting that in this new iteration of the device, standard batteries can be employed for power supply, with an estimated battery lifetime of 3.8 years taking into account five measurements per day. This greatly enhances the portability of the device, rendering it completely cable-free.

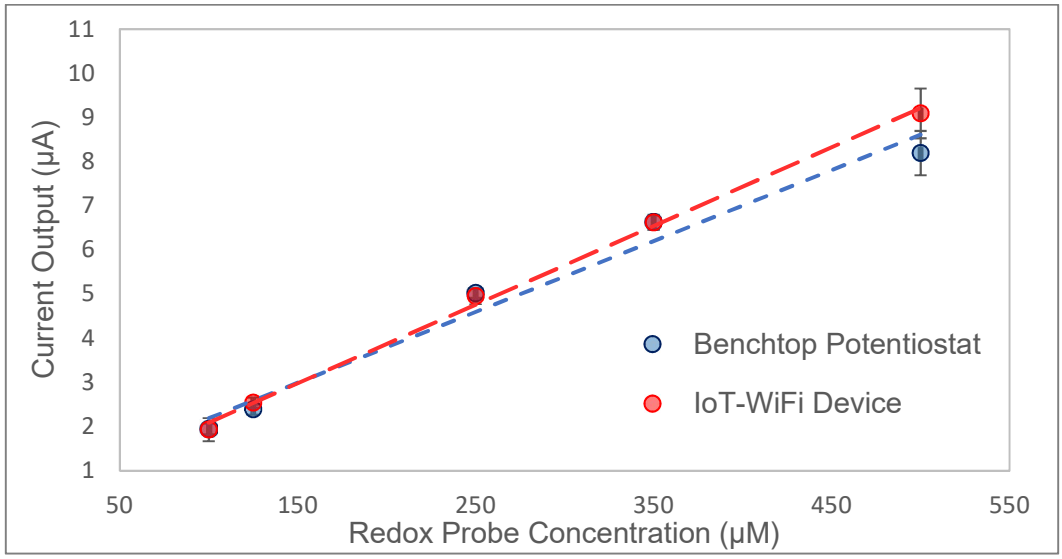

Figure 3.20. Comparison of the calibration curves obtained on the benchtop potentiostat (blue) and on the proposed device (red). Mean and standard deviation (n=3) for each concentration level are reported.

In conclusion, the improvements included in the new prototype of the IoT-WiFi device led to the obtainment of a low-cost portable potentiostat with enhanced resolution, comparable to benchtop instrumentation, which allows it to

perform precise qualitative and quantitative electrochemical analyses suitable for amperometric biosensors.

3.8. Future perspectives

In future studies, the developed IoT-WiFi device will be employed for the assessment of other relevant biomarker for clinical purposes. In fact, the most interesting application for this kind of device is point-of-care testing, given the possibility of real time sharing of the data between patient and hospital, physicians, etc. In this perspective, an ideal application for the device, rather than a one-time diagnosis, would be in connection to a disease which requires a routinely follow-up of a specific marker. In fact, in such cases, the patient is required to perform constant evaluation of the presence of specific biomarkers, while, by exploiting this new portable device, an at-home self-diagnosis could be achieved.

This project led to the publication of the following papers:

- **Giannetto, M., Bianchi, V., Gentili, S., Fortunati, S., De Munari, I., & Careri, M. (2018). An integrated IoT-Wi-Fi board for remote data acquisition and sharing from innovative immunosensors. Case of study: Diagnosis of celiac disease.** ***Sensors and Actuators B: Chemical*****, 273, 1395-1403.**

- **Bianchi, V., Boni, A., Fortunati, S., Giannetto, M., Careri, M., & De Munari, I. (2019). A Wi-Fi cloud-based portable potentiostat for electrochemical biosensors.** ***IEEE Transactions on Instrumentation and Measurement*****.**

3.9. References

[175] Liddel, E. (2013) Antibodies, in The Immunoassay Handbook: theory and applications of ligand binding, ELISA and related techniques (ed. D. Wild), Newnes, pp. 245-266.

[176] Luppa, P. B., Sokoll, L. J., & Chan, D. W. (2001). Immunosensors—principles and applications to clinical chemistry. *Clinica chimica acta*, 314(1-2), 1-26.

[177] Gopinath, S. C., Tang, T. H., Citartan, M., Chen, Y., & Lakshmipriya, T. (2014). Current aspects in immunosensors. *Biosensors and Bioelectronics*, 57, 292-302.

[178] Gobi, K. V., Iwasaka, H., & Miura, N. (2007). Self-assembled PEG monolayer based SPR immunosensor for label-free detection of insulin. *Biosensors and Bioelectronics*, 22(7), 1382-1389.

[179] Rahman, M. A., Shiddiky, M. J., Park, J. S., & Shim, Y. B. (2007). An impedimetric immunosensor for the label-free detection of bisphenol A. *Biosensors and Bioelectronics*, 22(11), 2464-2470.

[180] Su, X. L., & Li, Y. (2005). A QCM immunosensor for Salmonella detection with simultaneous measurements of resonant frequency and motional resistance. *Biosensors and Bioelectronics*, 21(6), 840-848.

[181] Cui, R., Pan, H. C., Zhu, J. J., & Chen, H. Y. (2007). Versatile immunosensor using CdTe quantum dots as electrochemical and fluorescent labels. *Analytical chemistry*, 79(22), 8494-8501.

[182] Kerman, K., Endo, T., Tsukamoto, M., Chikae, M., Takamura, Y., & Tamiya, E. (2007). Quantum dot-based immunosensor for the detection of prostate-specific antigen using fluorescence microscopy. *Talanta*, 71(4), 1494-1499.

[183] Lequin, R. M. (2005). Enzyme immunoassay (EIA)/enzyme-linked immunosorbent assay (ELISA). *Clinical chemistry*, 51(12), 2415-2418.

[184] Crowther, J. R. (1995). ELISA: theory and practice (Vol. 42). Springer Science & Business Media.

[185] Ricci, F., Adornetto, G., & Palleschi, G. (2012). A review of experimental aspects of electrochemical immunosensors. *Electrochimica Acta*, 84, 74-83.

[186] Felix, F. S., & Angnes, L. (2018). Electrochemical immunosensors – A powerful tool for analytical applications. *Biosensors and Bioelectronics*, 102, 470–478.

[187] Kokkinos, C., Economou, A., & Prodromidis, M. I. (2016). Electrochemical immunosensors: Critical survey of different architectures and transduction strategies. *TrAC Trends in Analytical Chemistry*, 79, 88–105.

[188] Giannetto, M., Bianchi, M. V., Mattarozzi, M., & Careri, M. (2017). Competitive amperometric immunosensor for determination of p53 protein in urine with carbon nanotubes/gold nanoparticles screen-printed electrodes: A potential rapid and noninvasive screening tool for early diagnosis of urinary tract carcinoma. *Analytica chimica acta*, 991, 133-141.

[189] Giannetto, M., Costantini, M., Mattarozzi, M., & Careri, M. (2017). Innovative gold-free carbon nanotube/chitosan-based competitive immunosensor for determination of HIV-related p24 capsid protein in serum. *RSC Advances*, 7(63), 39970-39976.

[190] Green, P. H., & Cellier, C. (2007). Celiac disease. *New england journal of medicine*, 357(17), 1731-1743.

[191] Lebwohl, B., Sanders, D. S., & Green, P. H. R. (2018). Coeliac disease. *The Lancet*, 391(10115), 70–81.

[192] O'mahony, S., Howdle, P. D., & Losowsky, M. S. (1996). management of patients with non-responsive coeliac disease. *Alimentary pharmacology & therapeutics*, 10(5), 671-680.

[193] Dieterich, W., Ehnis, T., Bauer, M., Donner, P., Volta, U., Riecken, E. O., & Schuppan, D. (1997). Identification of tissue transglutaminase as the autoantigen of celiac disease. *Nature medicine*, 3(7), 797.

[194] Abadie, V., Discepolo, V., & Jabri, B. (2012, July). Intraepithelial lymphocytes in celiac disease immunopathology. In Seminars in immunopathology (Vol. 34, No. 4, pp. 551-566). Springer-Verlag.

[195] Kagnoff, M. F. (2007). Celiac disease: pathogenesis of a model immunogenetic disease. *The Journal of clinical investigation*, 117(1), 41-49.

[196] https://zedira.com/data/newsletter/Zedira_presents_Open_tTG_at_Medica.pdf

[197] Lindfors, K., Koskinen, O., Kurppa, K., Laurila, K., Collin, P., Haimila, K., Partanen, J., Saavalainen, P., Maki, M., & Kaukinen, K. (2011). Serodiagnostic assays for celiac disease based on the open or closed conformation of the autoantigen, transglutaminase 2. *Journal of clinical immunology*, 31(3), 436-442.

[198] Giannetto, M., Mattarozzi, M., Umiltà, E., Manfredi, A., Quaglia, S., & Careri, M. (2014). An amperometric immunosensor for diagnosis of celiac disease based on covalent immobilization of open conformation tissue transglutaminase for determination of anti-tTG antibodies in human serum. *Biosensors and Bioelectronics*, 62, 325-330.

[199] Borgia, E. (2014). The Internet of Things vision: Key features, applications and open issues. *Computer Communications*, 54, 1-31.

[200] Kassal, P., Steinberg, M. D., & Steinberg, I. M. (2018). Wireless chemical sensors and biosensors: A review. *Sensors and Actuators B: Chemical*, 266, 228-245.

[201] Ruiz-Garcia, L., Lunadei, L., Barreiro, P., & Robla, I. (2009). A review of wireless sensor technologies and applications in agriculture and food industry: state of the art and current trends. S*ensors*, 9(6), 4728-4750.

[202] Tuna, G., Arkoc, O., & Gulez, K. (2013). Continuous monitoring of water quality using portable and low-cost approaches. *International Journal of Distributed Sensor Networks*, 9(6), 249598.

[203] Imani, S., Bandodkar, A. J., Mohan, A. V., Kumar, R., Yu, S., Wang, J., & Mercier, P. P. (2016). A wearable chemical–electrophysiological hybrid biosensing system for real-time health and fitness monitoring. *Nature communications*, 7, 11650.

[204] Potyrailo, R. A., Nagraj, N., Surman, C., Boudries, H., Lai, H., Slocik, J. M., Kelley-Loughnane, N., & Naik, R. R. (2012). Wireless sensors and sensor networks for homeland security applications. *TrAC Trends in Analytical Chemistry*, 40, 133-145.

[205] Darwish, A., & Hassanien, A. E. (2011). Wearable and implantable wireless sensor network solutions for healthcare monitoring. *Sensors*, 11(6), 5561-5595.

[206] Giannetto, M., Mattarozzi, M., Umiltà, E., Manfredi, A., Quaglia, S., & Careri, M. (2014). An amperometric immunosensor for diagnosis of celiac disease based on covalent immobilization of open conformation tissue transglutaminase for determination of anti-tTG antibodies in human serum. *Biosensors and Bioelectronics*, 62, 325-330.

[207] Manfredi, A., Mattarozzi, M., Giannetto, M., & Careri, M. (2014). Piezoelectric immunosensor based on antibody recognition of immobilized open-tissue transglutaminase: An innovative perspective on diagnostic devices for celiac disease. *Sensors and Actuators B: Chemical*, 201, 300-307.

4. QCM sensitive coating for environmental monitoring

4.1. Quartz crystal microbalances

Mass-sensitive transduction has been extensively employed for the development of a wide range of biosensing devices [208,209]. The working principle of such transduction is based on the generation of a signal as a consequence of interactions with analyte on the sensor surface, which yield a mass change. To this aim, the piezoelectric property of specific crystals, mainly quartz, is exploited [210]. In fact, these crystals are capable of generating an electrical polarization given by crystal lattice distortion as a result of mechanical stress. Furthermore, the process is reversible, being that through the application of a voltage to the crystal, a lattice distortion is obtained. In particular, upon application of an AC voltage to the crystal surfaces, the lattice undergoes periodic deformation, resulting in a vibration of the crystal characterized by a resonant frequency (f_0). Piezoelectric devices composed of two metal electrodes, usually gold, attached to the opposing surfaces of a quartz wafer (**Figure 4.1**), obtained through a specific cut (AT cut), are commonly referred to as Quartz Crystal Microbalances (QCM).

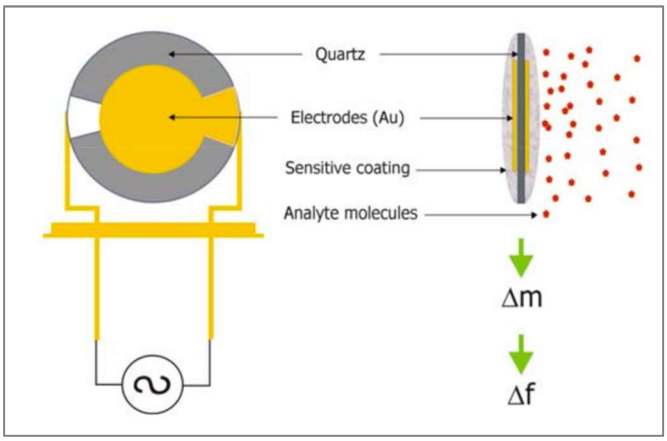

Figure 4.1. Schematic representation of a piezoelectric quartz crystal. Reprinted from Yuwono et al. [211]

The employment of QCM as a platform for sensors development allows to exploit a very straightforward transduction mechanism, since any recognition event occurring on the sensor surface results in a modification of the mass deposited on the crystal surface [5,212]. Therefore, usually no labelled species are required for the signal generation, however in some cases they are employed in order to obtain higher mass changes and increase the sensitivity of the system. Furthermore, the acoustic wave generated by the application of

the voltage, propagates through the bulk material and over a definite length beyond the crystal surface, thus allowing for probing the adjacent medium in order to obtain material-specific parameters.
When an AC is applied to a QCM, an acoustic wave is generated which propagates in a direction perpendicular to crystal surface with a wavelength dependent on the quartz thickness (t_q). The resonance frequency of the wave is correlated to its velocity (v) and t_q, however v can be expressed as a function of the propagating material parameters, specifically the Young modulus (E) and the density (ρ), which in turn depends on the materials area (A) and, most importantly, its mass (m). Taking into account these relations it is possible to obtain the Sauerbrey equation [213], which states the variations in frequency as a result of the variation of the mass deposited on the crystal.

$$\textbf{\textit{Equation 4.1}}\textbf{:}\ \Delta f_0 = -\frac{2}{\sqrt{E\cdot\rho}}\, f_0^2 \cdot \frac{\Delta M}{A}$$

Equation 4.1 establishes a linear relation between the variation in mass deposited and resonant frequency, i.e. a decrease in the latter is observed as a consequence of mass increases. However, the Sauerbrey equation is valid only in the assumption that the mass deposited or film generated is uniform with the bulk crystal acoustic properties, thus resulting in a system that can be envisaged as a thicker crystal. Such an assumption often fails, in particular when working with the QCM sensor in contact with a fluid, resulting in a dissipation of the acoustic wave given by viscoelastic coupling with the fluid or the layer deposited on the quartz surface. In such cases the Kanazawa-Gordon equations must be taken into consideration to assess both the reduction in resonant frequency related to fluid viscosity (ρ_L) and density (η_L) and the wave decay length (δ).

$$\textbf{\textit{Equation 4.2:}}\ \ \Delta f = -f_0^{3/2} \cdot \sqrt{\frac{\rho_L \eta_L}{\pi\, E\, \rho}}$$

$$\textbf{\textit{Equation 4.3:}}\ \ \delta = \sqrt{\frac{2\eta_L}{\omega\rho_L}}$$

Equation 4.2 establishes a linear correlation between the decrease in frequency and the product between density and viscosity of the fluid. **Equation 4.3** introduces the decay length parameter, which also depends on η_L and ρ_L,

however it is worth noticing that it is also dependent on the angular frequency ω, which in turn depends on the frequency of the quartz. As a consequence, the fundamental frequency of the quartz determines the maximum length at which the generated acoustic wave can probe the environment surrounding the sensor surface.
Therefore, when analysing the variation in frequency of a QCM sensor, both the Sauerbrey and Kanazawa-Gordon equations must be taken into account to evaluate the response resulting from mass changes and viscoelastic damping.

4.2. Conducting polymers

Through polymerization of specific monomeric species, it is possible to obtain highly conjugated structures that possess outstanding electrical, optical and mechanical properties. Among these so-called conducting polymers [214,215], polyacetylene, polyaniline, polypyrrole, poly(3,4-ethylene dioxythiophene) (PEDOT) and polythiophene are some of the most employed (**Figure 4.2**).

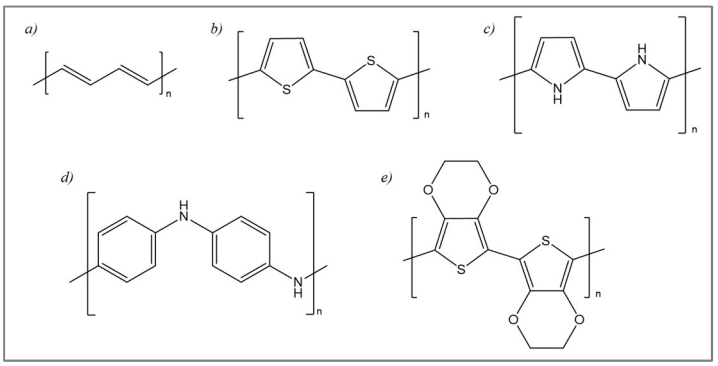

Figure 4.2. Structures of some of the most employed conducting polymers, namely a) polyacetylene, b) polythiophene, c) polyaniline, d) polypyrrole and e) PEDOT.

The main feature of these materials is given by their structure, in fact the highly conjugated polymer can be subjected to a doping mechanism that results in the generation of several charges. Usually conducting polymers have a structure that allows for two doping events, through which the polymer, starting from a non-conductive neutral form, is excited first to a conductive charged form (polaron) and subsequently to a second charged form (bipolaron) with increased conductivity (**Figure 4.3**).

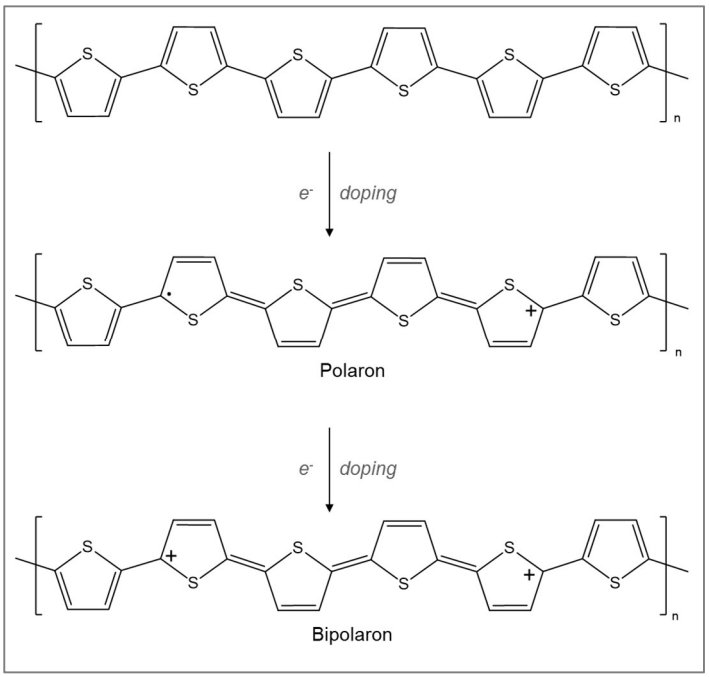

Figure 4.3. Schematic example of doping mechanism for polythiophene.

Alongside these electrical properties, the conjugated structure results in the ability of the polymer to interact with UV-Visible light, exhibiting fluorescence properties. Such properties are influenced by the amount of charges of the polymer, therefore neutral, polaron and bipolaron forms show different colours and optical properties.

The polymerization can occur via chemical or electrochemical routes. The electropolymerization however grants a higher degree of control over the reaction rate and morphology of the produced layer. Furthermore, for sensing application, it allows to obtain a conducting film already confined and deposited on the working electrode. Taking into account the case of thiophene (**Figure 4.4**), the polymerization starts with the oxidation of monomers to cation radicals, which will subsequently couple with other radicals or neutral monomers, yielding oligomers, with various degree of cross-linking. While the polymer length increases, the solubility of the polymer decreases up to a point where the polymer becomes insoluble in the electrolyte solution and deposits on the electrode surface.

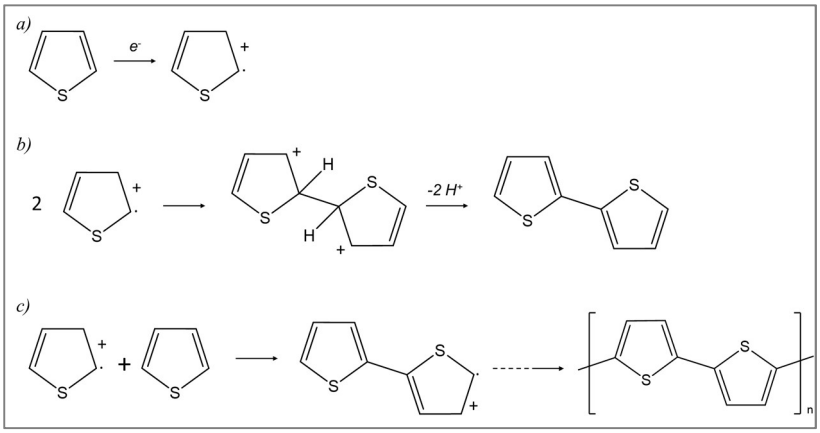

Figure 4.4. Reactions involved in the electropolymerization of thiophene. a) electron transfer reaction, b) radical cations coupling and c) radical cation propagation.

By employing Cyclic Voltammetry as electropolymerization technique, the alternation between anodic and cathodic reactions in each cycle allows for the oxidation of the polymer first to polaron followed by the bipolaron structure, followed by reduction from the latter to the neutral state. During the oxidation, the electrolytes present in the polymerization solution are included in the polymer to balance the positive charges generated and are subsequently expelled as the polymer returns to its neutral state, granting the final polymer a porosity which depends on the dimensions of the counterions and results in an enhancement of the polymer surface area and higher doping levels of the film as its thickness increases [216]. Typical electrolytes used for electropolymerization are lithium perchlorate or quaternary amine salts (e.g. tetrabutylammonium hexafluorophosphate). Furthermore, by using CV it is possible to obtain a polymer both in the doped or undoped form, depending on the voltage at which the polymerization is interrupted, while those obtained through potentiostatic methods can only be found in conductive state.

An instance of QCM-based sensor exploiting the electropolymerization of a sensitive coating is offered by the work of Ayankojo et al. which in 2018 reported the selective detection of Amoxicillin in water media through the employment of a QCM piezoelectric sensor coated with molecularly imprinted poly (phenylenediamine) [217]. The working principle is based on the selective recognition of the antibiotic molecule by the sensitive coating which is electropolymerized on the electrode surface in potentiostatic conditions. Monitoring the frequency shifts caused by the adsorption of the analyte on the molecularly imprinted polymer, the authors were able to obtain a LOD of

0.2 nM and a good selectivity for Amoxicillin over other antibiotics that can be present in wastewater such as Doxycycline and Sulfamethizole.
It is worth pointing out that bithiophene monomers can be derivatized in order to tune its electrochemical properties. For example, the introduction of electron donating groups on the monomers results in a reduction of the potential at which the oxidation occurs, since these groups stabilize the cation radicals generated [218]. This effect can also be achieved by exploiting electrolytes that possess catalytic effects towards the polymerization reaction, such as boron trifluoride diethyl etherate (BFEE) which being a Lewis acid, is capable of catalysing the deprotonation of thiophene leading to a reduction in the oxidation potential of the monomer [219].
Furthermore, the derivatization of the thiophene monomers is required for sensors fabrication in order to introduce receptor molecules on the polymer films [220-223]. This modification results in a variation of the film properties that must be thoroughly examined, since it can interfere with the reactivity of the monomer towards the electropolymerization process, change the solubility of the thiophene and modify the film chemical and physical properties. The introduction of new functionalities can be carried out by inserting a linker between the monomer and the receptor, which carries out a double function. In fact, it keeps the two portions at a correct distance in order to prevent steric hindrance that might hamper the polymerization reaction. Furthermore, based on the linker used, i.e. unsaturated or saturated chain, an electronic communication can be maintained between the polymer and the receptor. This aspect is important when dealing with sensor that detect ionic species as a consequence of their inclusion on the receptor molecules, which determines a variation in the optical or resistive properties of the film that can be measured only with a conjugated linker connecting the receptor and the polymer.
Among different classes of receptors that are used in combination with bithiophene for chemical sensing, crown ethers [224], calixarenes [225] and resorcinarenes can be found. The latter [226] are a class of cavitand composed of resorcinol rings connected by a methylene bridge usually bearing functional groups that define the *lower rim*, while the *upper rim* consists in the hydroxyl groups exposed by the resorcinol moieties.

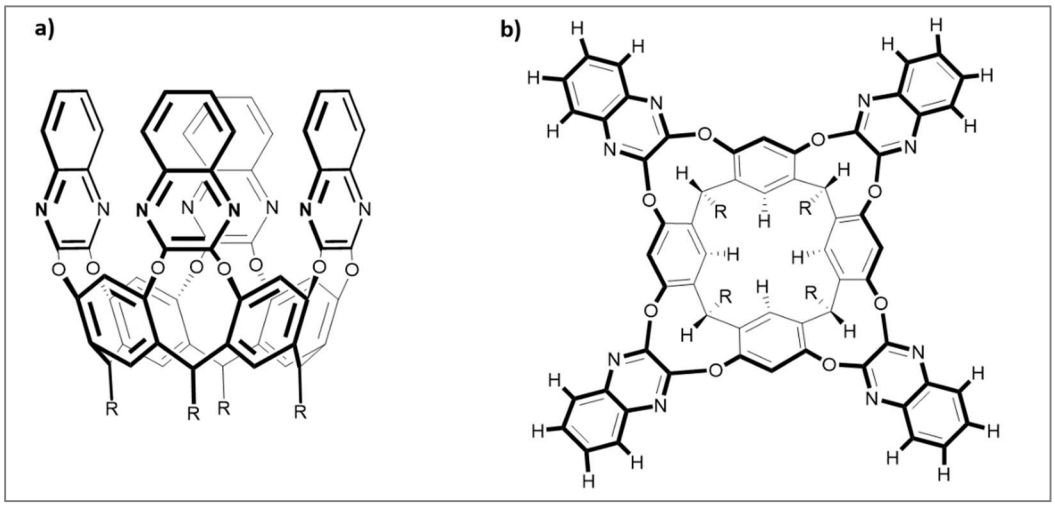

Figure 4.5. a) side-view and b) view from above of tetraquinoxaline resorcinarene cavitand.

By introducing quinoxaline moieties at the *upper rim* it is possible to obtain tetraquinoxaline cavitand (**Figure 4.5**) [227,228] capable of entrapping aromatic molecules in their cavity. In fact, they act as host molecules establishing well-known supramolecular interactions (i.e. π-π and CH-π) with hydrophobic aromatic guests. This property has been exploited in order to selectively trap organic molecules that represent pollutants in wastewaters [229]. The presence of such species, consisting in organic solvents, pesticides, aromatic chlorinated compounds etc. can occur in waters as a consequence of industrial activity, inadvertent oil spills, cultivations products, etc. [230] These compounds constitute a concern for human and environmental safety, therefore their *in situ* detection represents a topic of critical importance. While detection of aromatic molecules has been carried out in vapour phase [231], detection in water has been scarcely explored [232,233]. For such task, quinoxaline cavitand can be linked to bithiophene molecules and electropolymerized on piezoelectric quartz crystals, in order to obtain a polymeric coating exposing cavitands as receptors capable of selectively trapping organic molecules.

4.3. Aim of the study

The purpose of this study was to electropolymerize a resorcinarene cavitand on Piezoelectric Quartz Crystals (PQC) in order to evaluate its host properties towards a group of hydrocarbon molecules of environmental interest.
The monomer (4QxCav-BT), synthesized by the group of professor Enrico Dalcanale and Roberta Pinalli of the Department of Chemistry, Life Sciences and Environmental Sustainability of the University of Parma, was a tetraquinoxaline cavitand functionalized at the upper rim to introduce a bithiophene moiety, through which it was possible to carry out the electropolymerization (**Figure 4.6**). The latter was performed on PQC, in order to obtain a polymeric film containing the cavitand capable of establishing non-covalent interactions with a class of molecules. Therefore, a piezoelectric mass sensor based on Quartz Crystal Microbalance equipment (QCM) was developed in order to monitor the mass variations obtained after the inclusion of guest molecules on the host molecules embedded in the sensing layer.

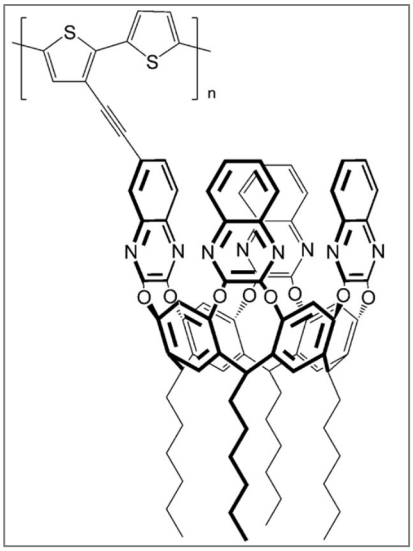

Figure 4.6. 4-QxCav-BT electropolymerizable monomer.

It was chosen to test the hosting ability of the 4QxCav polymer towards a class of representative aromatic and aliphatic hydrocarbons which are potentially present in wastewaters and represent environmental polluters. Even though different quinoxaline-based sensing layer have been previously conceived for the sensing based on their host properties, the recognition was carried out in vapour phase, while the purpose of the present work was to develop a sensor for the detection of pollutants capable of working in water flow. Therefore, after

the polymerization of the monomer on the PQC the analytical performance of the sensor was assessed in continuous flow of water in order to evaluate the efficiency of the method towards the detection of environmental pollutants.

4.4. Experimental

4.4.1. Reagents and solutions

Tetrabutylammonium hexafluorophosphate (TBAHFP), acetonitrile (CH_3CN), Dichloromethane (CH_2Cl_2), 2,2′-bithiophene, 1,2,4-trichlorobenzene, 1,2-dichlorobenzene, chlorobenzene, styrene, toluene, 4-nitrotoluene, aniline, trichloroethylene and tetrahydrofuran were purchased from Sigma-Aldrich (Milan, Italy).
The monomeric unit (4QxCav-BT) composed of the bithiophene unit connected to the tetraquinoxalinic cavitand, was synthesized as reported by Giannetto et al. [234]

4.4.2. Apparatus

"Ultra-High Performance (UHP)" single-channel mechanical pipettes purchased from VWR Internation srl (Milan, Italy) and Sartorius CP225D analytical balance were employed.
Piezoelectric Quartz Crystals (PQCs) (**Figure 4.7**) were purchased from Bioage srl (Lamezia Terme, Italy) with the following characteristics:

- AT-cut.
- 10 MHz frequency.
- Crystal diameter: 13,9 mm.
- Crystal thickness: 160 µm.
- Electrode material: gold.
- Electrodes diameter: 6,0 mm.

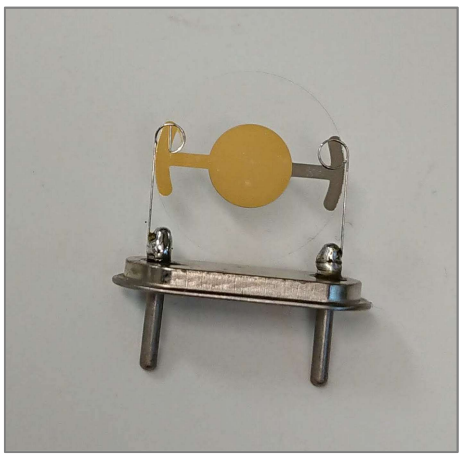

Figure 4.7. AT-cut 10 MHz Piezoelectric quartz crystal.

"Eureka" USB self-powered instrument for QCM/EQCM measurement was purchased from Bioage srl and used for both electropolymerization of the sensitive coatings and for the monitoring of the frequency shift as a consequence of the host-guest interactions. In fact, through the use of the Eureka 4.01 software it is possible to monitor the PQC resonance frequency as a function of time. The instrument is composed of a self-powered base (**Figure 4.8a**) that can be connected via USB to a computer and can be connected to a potentiostat in order to perform EQCM analyses. On this base a 5 mL Teflon cell can be mounted which was used for polymerization purposes (**Figure 4.8b**). For the monitoring of the host-guest interactions of the coatings a 100 µL flow-through chamber for liquids (**Figure 4.8c**) was mounted on the base.

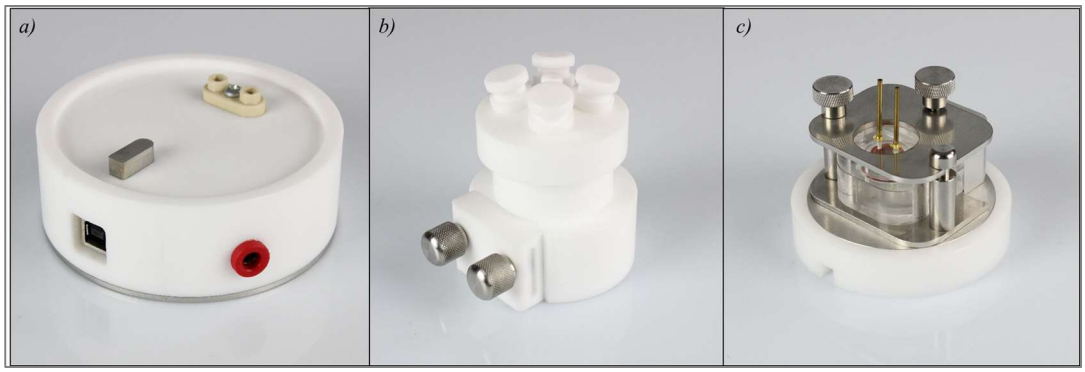

Figure 4.8. a) Self-powered base on which b) a 5 mL Teflon cell or c) a 100 µL flow-through chamber for liquids can be mounted.

An Autolab PGSTAT 20 potentiostat, purchased from Ecochemie (Utrecht, The Netherlands) and controlled by Ecochemie GPES 4.9 software, was interfaced with the Eureka instrument.
A "Watson-Marlow Sci-Q 323", purchased from Fischer Scientific (Massachusetts, USA) peristaltic pump was employed to obtain a continuous flow in the Eureka flow-through chamber.

4.4.3. Electropolymerization of the sensitive coatings

The electropolymerization of the monomer was conducted inserting the PQC in the 5 mL Teflon cell, filled with a solution composed of $5 \cdot 10^{-4}$ M 4QxCav-BT and 0,1 M TBAHFP dissolved in a 1:5 mixture of CH_3CN and CH_2Cl_2. The growth of the polymeric film was obtained in potentiodynamic conditions through the application of Cyclic Voltammetry scans and, employing the Eureka instrument, it was possible to monitor simultaneously the current flowing in the cell and the

frequency shift of the PQC. Using an EQCM configuration, the PQC gold electrode was employed as working electrode, an Ag/AgCl electrode as reference and a Pt rod as counter electrode. The scans were performed between -1 V and 1,3 V at a scan rate of 0,1 V/s for a number of scan sufficient to reach a frequency shift of -2,5 kHz, which corresponds to a deposition of $1 \cdot 10^{-5}$ g of polymeric film according to the Kanazawa-Gordon equation. After the frequency cut-off value was reached the potential was held at -1 V for 300 s in order to obtain a complete reduction of the polymer. Finally, the PQC coated with the 4QxCav-BT polymer was rinsed with CH_3CN. The same procedure was employed to electropolymerize the 2,2'-bithiophene, whose coating was exploited as reference for the host-guest interaction studies.

4.4.4. Host-Guest interaction studies

In order to evaluate the ability of inclusion of the sensitive coating towards analyte of environmental concern, the PQC coated with the polymeric film was inserted in the 100 μL flow-through chamber for liquids mounted on the base of the Eureka instrument. Exploiting the peristaltic pump, it was possible to establish a continuous flow of liquid between the chamber and a 5 mL flask filled with the solution of the chosen analyte in deionized water. The inclusion of the guest molecules in the cavitands was monitored by the reduction in the quartz resonating frequency, which was sampled every 2 s.

4.4.5. Assessment of analytical performance

The assessment of the analytical performance of the developed sensor was performed for the guest 1,2,4-trichlorobenzene, for which at least three replicated measurements were carried out for each concentration level and limit of detection (LOD) and limit of quantification (LOQ) were calculated according to "Eurachem Guidelines" [159].

4.5. Results and Discussion

4.5.1. Electropolymerization

In order to carry out the electrodeposition of the sensing layer, the electropolymerizable bitihiophene moiety of the 4QxCav-BT must be available for reaction. This condition was ensured performing X ray diffraction analysis on single crystal, through which the molecular structure of the compound obtained (**Figure 4.9**) confirmed that the ethynyl bridge maintains at a proper distance the bithiophene moiety from the cavity, avoiding inclusion.

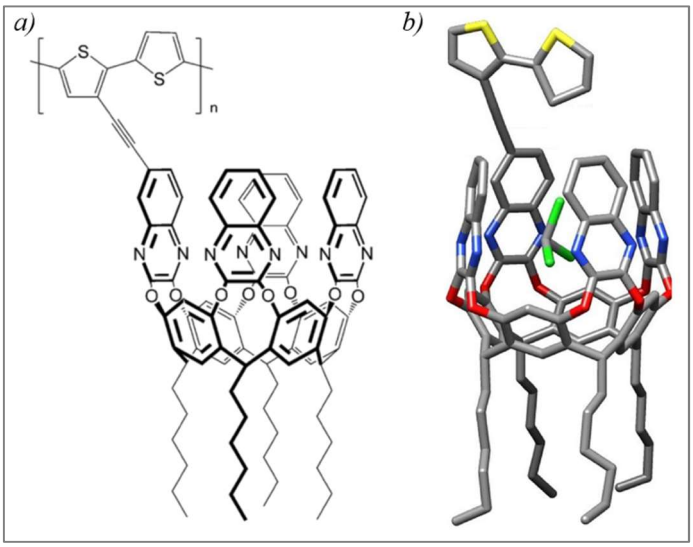

Figure 4.9. a) chemical structure and b) structure modelled from X-Ray diffraction analysis of 4QxCav-BT monomer.

The electrosynthetic approach chosen for the deposition of the sensing film was cyclic voltammetry, which allows a steady deposition over time, cycle after cycle, yielding homogeneous and reproducible coatings. A critical parameter is given by the solvent employed during the electropolymerization, which must solubilize the monomer, but allow to reach the critical solubility for the oligomers necessary for the deposition of the polymer coating on the electrode surface. It was observed that dichloromethane (DCM) solubilizes both the monomer and the oligomers, while acetonitrile (ACN) has poor solubility properties even towards the 4QxCav-BT monomer. Therefore, a mixture of DCM/ACN 1:5 v/v was successfully employed for the carry out of the electropolymerization.

The latter, was conducted under potentiodynamic conditions employing CV in Electrochemical QCM (EQCM) mode, i.e. monitoring simultaneously the frequencygram, where the deposition of the polymer translates in a loss of frequency, and the voltammogram, where an increase in both cathodic and anodic peaks is observed as a consequence of the growth of the electroactive polymer coating. It was observed that a polymer growth employing 500 µM 4QxCav-BT and tetrabutylammonium hexafluorophosphate (TBAHFP) yielded homogeneous and reproducible coatings (**Figure 4.10**).

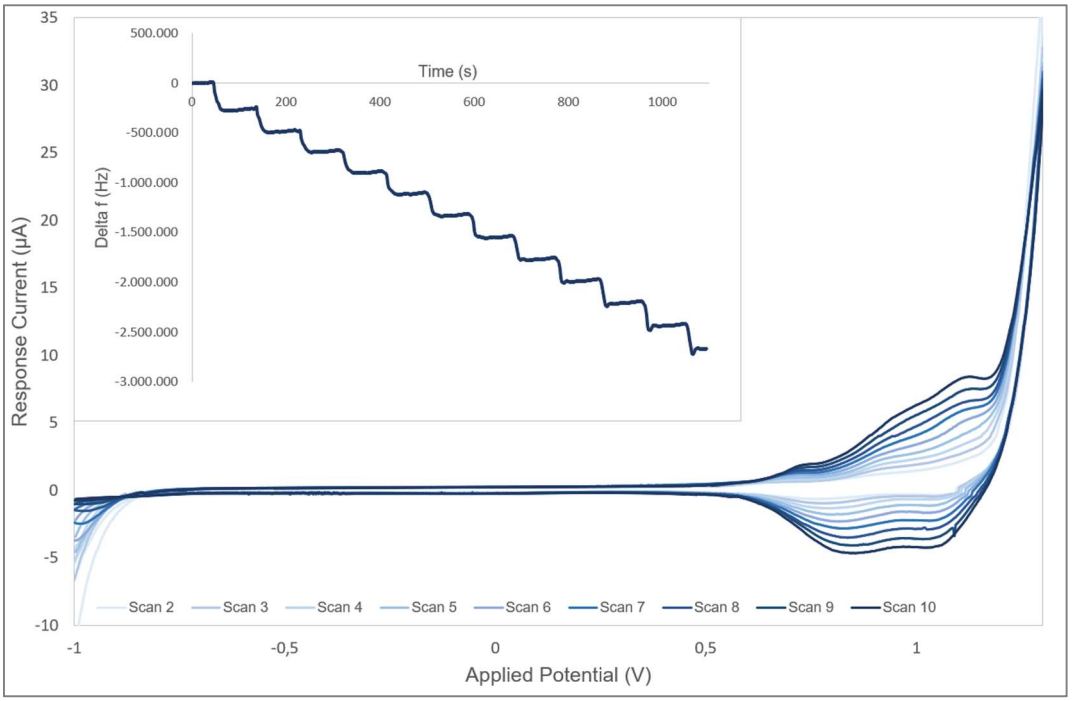

Figure 4.10. Voltammograms and frequencygram (inset) registered during 4QxCav-BT electropolymerization on PQC.

The regularity of the growth is documented by the constant frequency decrease (mass increase) observable in the frequencygram cycle after cycle, as well as the steady increment in current observed in the voltammogram. Taking into account the frequency variation undergone by the QCM and that 1 Hertz difference is obtained after the deposition of 3.59 ng of compound, the amount of polymer grown on the QCM surface was approximately 10 µg.

4.5.2. *Frequencymetric response*

The coating obtained was tested in relation to its ability to interact and include in the quinoxaline cavities aliphatic and aromatic water pollutants possessing different halogenation degrees. In particular, the host molecules taken in consideration (**Figure 4.11**) were representative of different classes, namely trichloroethylene, representative for halogenated hydrocarbons, styrene, toluene, 2-nitrotoluene and aniline for aromatic hydrocarbons and chlorobenzene, 1,2-dichlorobenzene and 1,2,4-trichlorobenzene for chlorinated aromatic hydrocarbons. Along with these, tetrahydrofuran (THF) was employed as control analyte given its hydrophilic nature, in order to monitor the influence of hydrophobicity of the guests on the sensor response.

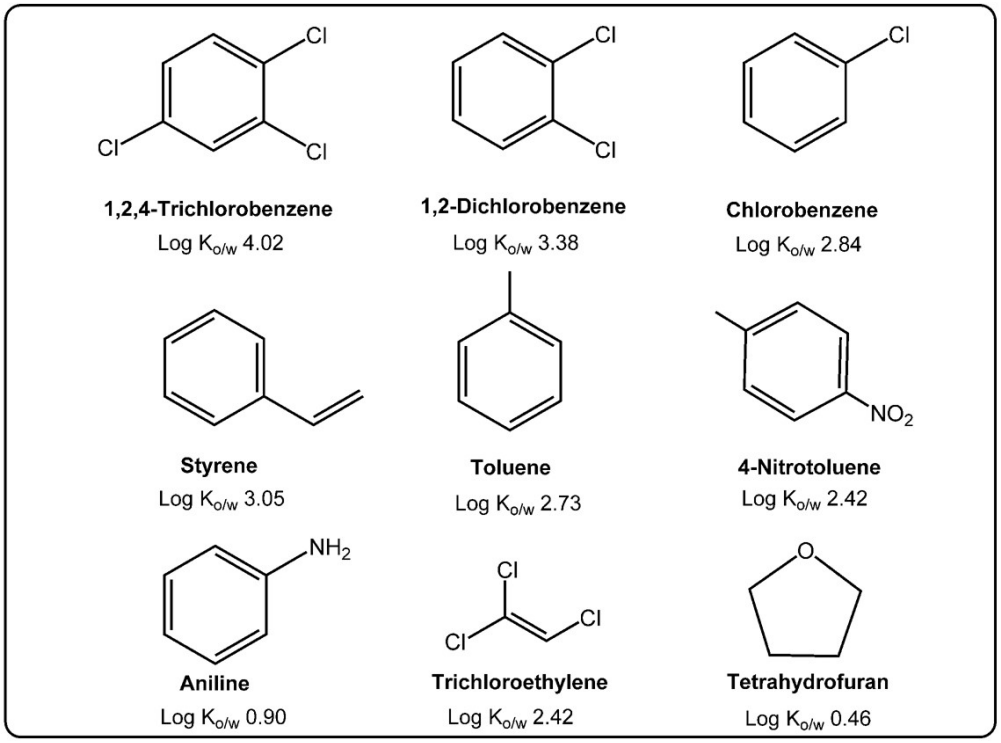

Figure 4.11. Representative compounds tested for inclusion in the sensitive coating. Below each compound the log $K_{o/w}$ is reported.

Furthermore, to assess the active role played by the cavitands on the frequency shifts, the results were compared with analogous experiments carried out on unfunctionalized poly-bithiophene (poly-BT) as reference "blank" polymer. The latter was obtained on PQC units following the same electropolymerization protocol employed for 4QxCav-BT, achieving a comparable amount of polymer

mass deposited on each quartz. To carry out the assessment of the sensor response towards guest analytes, the coated QCM units were mounted inside a flow cell in which, thanks to the implementation of a peristaltic pump in the system, a solution containing the guest molecules at different concentration was fluxed (**Figure 4.12**). This system allows to perform multiple consecutive injections of the analytes and monitor the response of the QCM in continuous water flow.

Figure 4.12. Apparatus employed for testing the sensitive coating host properties in continuous dynamic flow of water. Tests were carried out employing a flow rate of 0.45 mL/min.

As a preliminary study, the response of poly-4QxCav-BT was tested for single injections of analyte at 100 ppm concentration. The guest molecule employed in this phase were chlorobenzene, 1,2-dichlorobenzene and 1,2,4-trichlorobenzene (**Figure 4.13**).

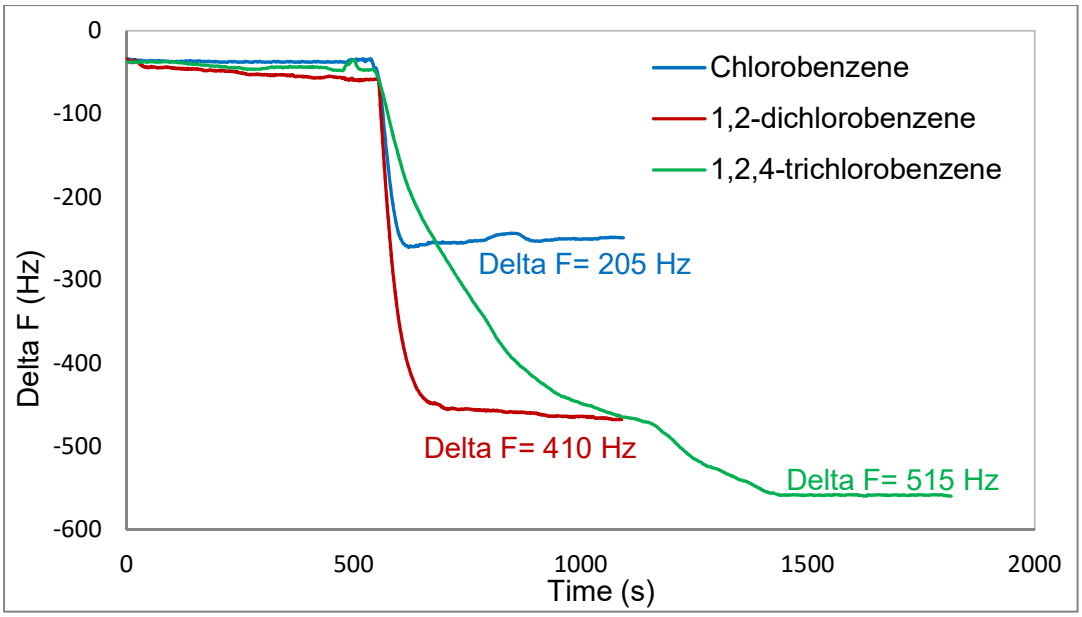

Figure 4.13. Sensograms reporting the frequency shifts generated by 100 ppm solutions of chlorobenzene (blue), 1,2-dichlorobenzene (red) and 1,2,4-trichlorobenzene (green)

The poly-4QxCav-BT showed a sharp frequency shift in relation to the addition of the guest molecules, with a trend that reflects the degree of chlorination of the analyte compound. The preference towards the inclusion of guest that possesses a higher degree of halogenation is also dependent on the increasingly higher log $K_{o/w}$ (**Figure 4.11**) which determines a higher hydrophobicity of the molecule and, therefore, an increased tendency to interact with the lipophile polymer coating.

4.5.3. Multipoint calibration of guest compounds

After the evaluation of the frequency shift generated by a single guest injection at high concentration, the dynamic response of the sensitive coating was tested by consecutive injection of analyte compound at fixed concentration. To this aim, the frequency shifts generated by five consecutive injection of 20 ppm chlorobenzene solution were acquired, reaching a final flowing concentration of analyte of 100 ppm (**Figure 4.14**). After each guest injection, a quick response by the poly-4QxCav-BT-coated QCM system was recorded, along with a high stability of the frequency signal, which was observed throughout the carry out of the experiment.

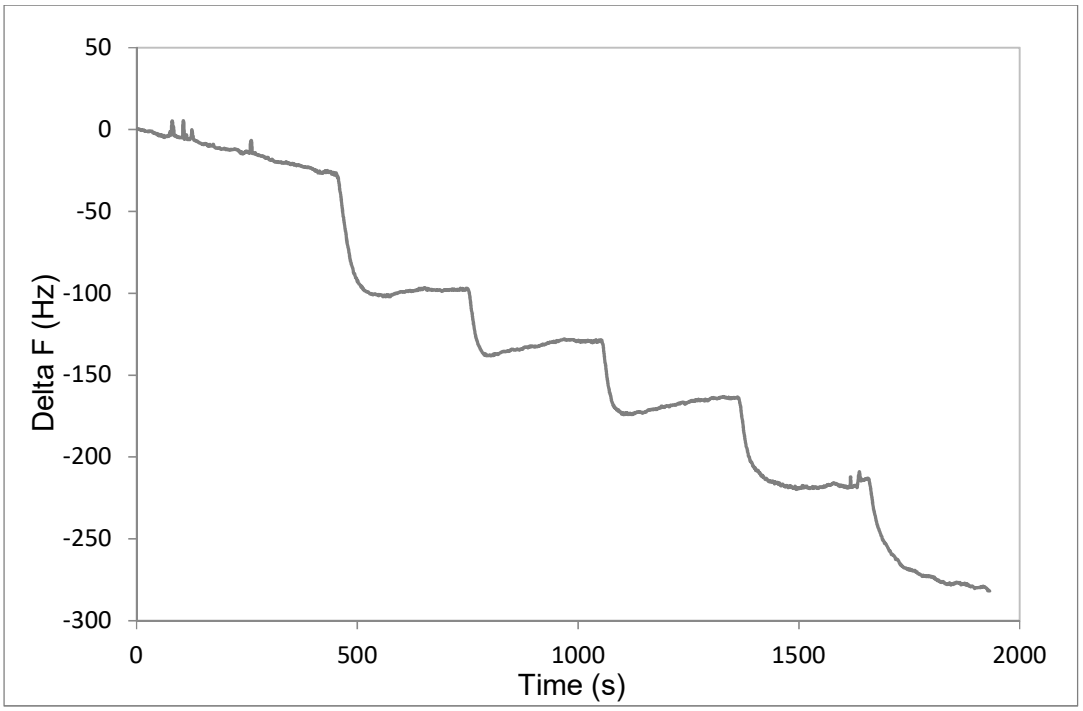

Figure 4.14. Sensogram acquired during consecutive injections of 20 ppm chlorobenzene on poly-4QxCav-BT-coated PQC.

The data obtained were employed to build a calibration line in the 20 – 100 ppm concentration range. The response to chlorobenzene was tested both on poly-4QxCav-BT and poly-BT and the results compared (**Figure 4.15**), confirming the affinity of the cavitand towards the selected guest.

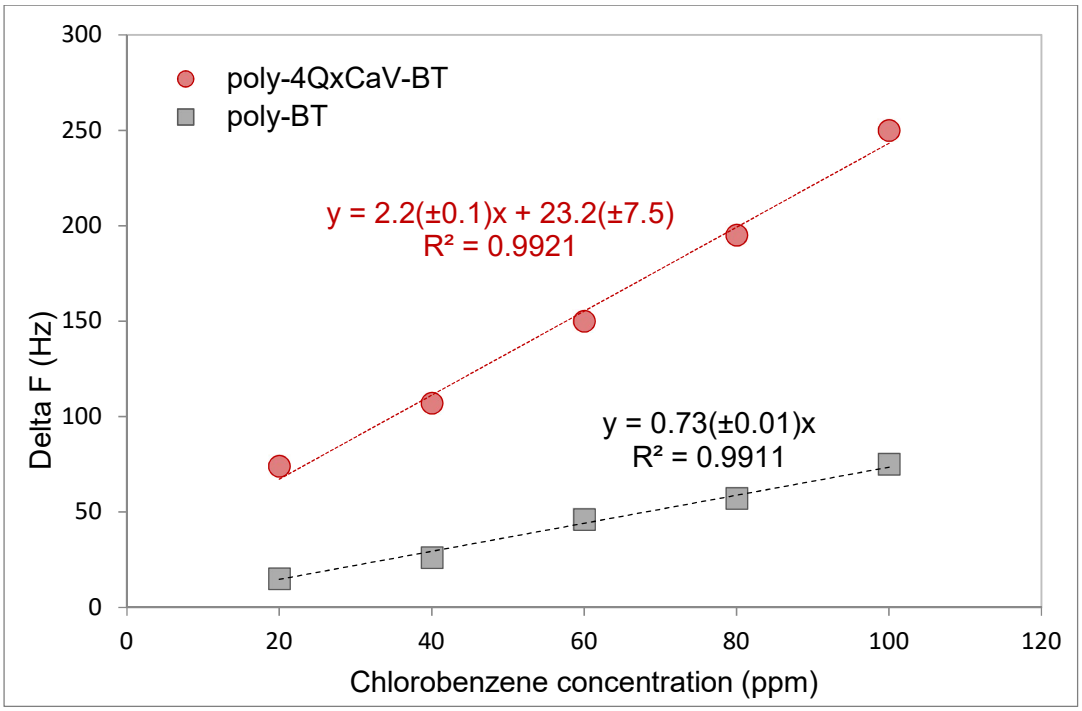

Figure 4.15. Comparison of the multipoint calibration lines obtained on poly-4QxCav-BT- (red) and poly-BT-coated PQCs (grey) using chlorobenzene as guest analyte.

After chlorobenzene, a multipoint calibration was carried out for the other guests as well, employing the same method of consecutive injections in continuous water flow covering a 20 – 100 ppm concentration range (**Figure 4.16**). However, since the response to 1,2,4-trichlorobenzene showed a remarkably higher sensitivity, the calibration of this guest was carried out in a lower concentration range, namely 1 – 25 ppm. The QCM response showed a sensitivity that increases with the degree of chlorination of the compound as well as with the degree of unsaturation, showing a higher response for aromatic compounds with respect to aliphatic. Even though such behaviour can be explained on the basis of the log $K_{o/w}$ of the guests, hydrophobicity is not the only factor to be considered. In fact, despite the lower log $K_{o/w}$ of 4-nitrotoluene compared to chlorobenzene, the sensitivity of the poly-4QxCav-BT towards these guests is comparable. This can be explained taking into account that for 4-nitrotoluene the presence of the electron-withdrawing group enhances the CH-π interactions of the aromatic hydrogens with the cavity walls.

As for THF, the low response of the sensitive coating to this guest does not produce a significant slope (p>0.05) in the multipoint calibration line, therefore the data cannot be fitted.

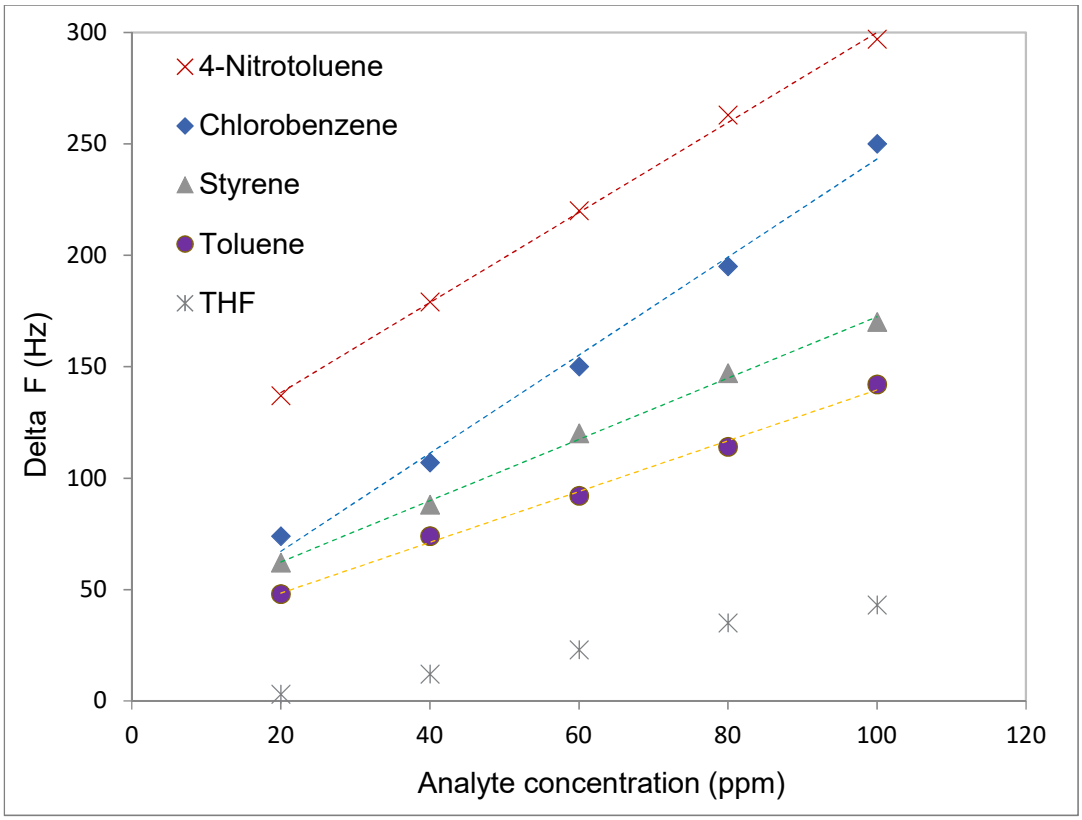

Figure 4.16. Calibration lines obtained through consecutive injections of guest compounds on QCM coated with poly-4QxCav-BT.

1,2,4-trichlorobenzene was employed as model guest for the assessment of the analytical performance of the sensor, on the basis of the high sensitivity observed.

By construction of the calibration line on the 1 – 25 ppm concentration range (**Figure 4.17**) it was possible to achieve a very good sensitivity given by the value of the slope of 2.15 Hz/ppm and an excellent intermediate precision, as proven by an RSD < 5% for each level explored. Furthermore, it was possible to reach remarkable LOD and LOQ of 0.17 ppm and 1.79 ppm, respectively.

Control experiments were performed on poly-4QxCav-BT-coated PQCs by consecutive injections of acetonitrile and ethyl acetate both in the 20-100 ppm concentration range. The former did not yield any observable frequency shift, while the latter resulted in a very poor sensitivity.

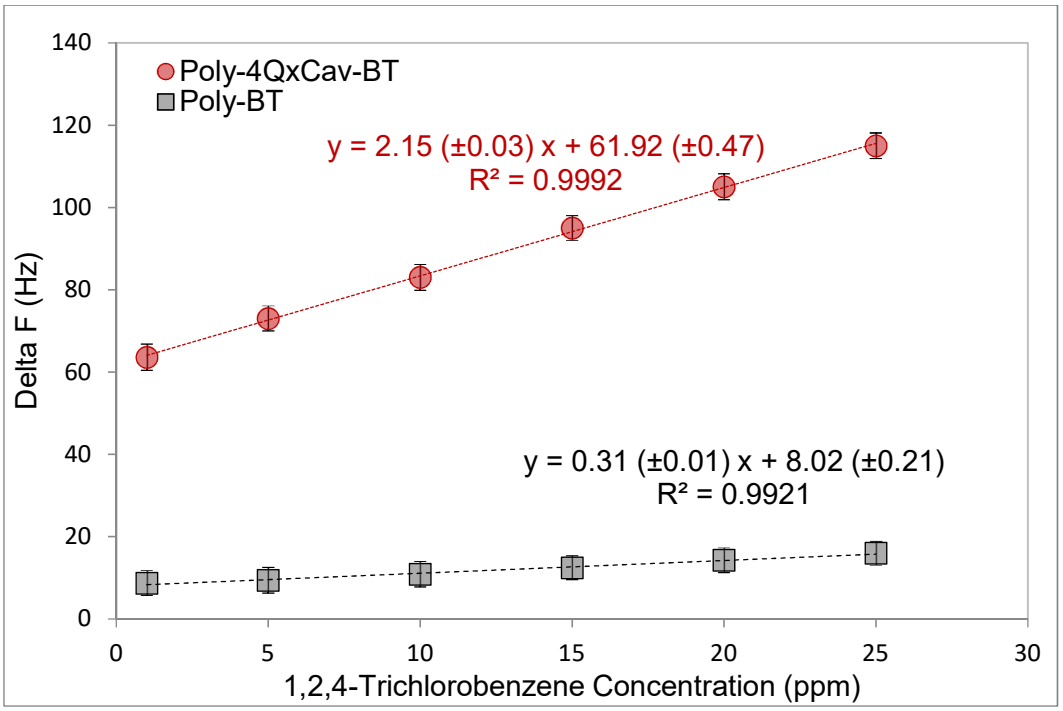

Figure 4.17. Calibration lines obtained through consecutive injections of 1,2,4-trichlorobenzene on QCM coated with poly-4QxCav-BT (blue) and poly-BT (red). Mean and standard deviation (n=3) for each concentration level are reported.

For each analyte compound, a calibration line was constructed also on poly-BT-coated PQCs. An overall sensitivity parameter was obtained dividing the slope of linear function measured on poly-4QxCav-BT and the one measured on poly-BT. By evaluating the ratio of the slopes for every compound (**Table 4.1**) it was possible to confirm that the highest sensitivity is registered for 1,2,4-trichloroethylene (6.9), followed by 4-nitrotoluene (3.5), chlorobenzene (3.0), trichloroethylene (2.8), aniline (2.8), styrene (1.8) and finally toluene (1.6), while THF did not generate a significant frequency shift on poly-4QxCav-BT. By comparison of the log $K_{o/w}$ of the compounds examined as guests with the sensitivity values obtained, it is possible to observe that the hydrophobicity alone is not the drive for cavity inclusion. In fact, a major role is played by the presence of electron-withdrawing groups, responsible for the enhancement of the non-covalent interactions between the host cavity and the guest compound. In conclusion, the developed QCM sensor is capable of detecting the presence of environmental water pollutants such as aromatic and aliphatic halogenated compounds with high sensitivity and reproducibility, with a LOD below the limit imposed by Italian regulations which is set at 0.19 ppm.

	Poly-4QxCav-BT slope (Hz/ppm)	*Poly-BT slope (Hz/ppm)*	**Poly-4QxCav-BT/ Poly-BT ratio**
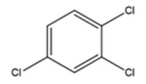	2.15	0.31	6.9
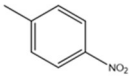	2.02	0.57	3.5
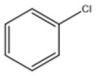	2.2	0.73	3
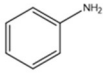	1.79	0.64	2.8
	1.66	0.59	2.8
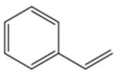	1.37	0.76	1.8
	1.14	0.7	1.6
	-	0.67	-

Table 4.1 Comparison of the slopes of the calibration lines obtained employing different guest compounds on either poly-4QxCav-BT or poly-BT as sensitive PQC coating.

Furthermore, it is worth noting that the proposed system is capable of working in continuous water flow, a feature that is seldom met and makes it suitable for the development of on-line sensing system.

4.6. Future perspectives

The monomer unit employed for this project is composed by the functionalization of the cavitand at the upper rim with a bithiophene electropolymerizable moiety, through which its electrodeposition on the surface of the PQC is possible. However, even though the functionalization at the upper rim can be achieved through less synthetic efforts, a new monomer with the bithiophene at the lower rim will be synthesized and tested. The new position for the electropolymerizable moiety should result in a better positioning of the cavity, which, being more exposed to the solvent, should result in an enhancement of the sensitivity of the system.
Furthermore, the introduction of phosphonate moieties at the upper rim of the cavitand should improve the establishment of interaction with guest molecules, allowing for the detection of a series of illegal recreational drugs, resulting in the development of a sensor for the application in the law enforcement field.

This project led to the publication of the following paper:

- **Giannetto, M., Pedrini, A., Fortunati, S., Brando, D., Milano, S., Massera, C., Tatti, R., Verucchi, R., Careri, M., Dalcanale, E., Pinalli, R. (2018), Sensing of halogenated aromatic hydrocarbons in water with a cavitand coated piezoelectric device. *Sensors and Actuators B: Chemical*, 276, 340-348.**

[208] Su, X. L., & Li, Y. (2005). A QCM immunosensor for Salmonella detection with simultaneous measurements of resonant frequency and motional resistance. *Biosensors and Bioelectronics*, 21(6), 840-848.

[209] Rasheed, P. A., & Sandhyarani, N. (2016). Quartz crystal microbalance genosensor for sequence specific detection of attomolar DNA targets. *Analytica chimica acta*, 905, 134-139.

[210] Ferreira, G. N., Da-Silva, A. C., & Tomé, B. (2009). Acoustic wave biosensors: physical models and biological applications of quartz crystal microbalance. *Trends in biotechnology*, 27(12), 689-697.

[211] Yuwono, A. S., & Lammers, P. S. (2004). Odor pollution in the environment and the detection instrumentation. *Agricultural Engineering International: CIGR Journal*.

[212] Marx, K. A. (2003). Quartz crystal microbalance: a useful tool for studying thin polymer films and complex biomolecular systems at the solution− surface interface. *Biomacromolecules*, 4(5), 1099-1120.

[213] Sauerbrey, G. Z. (1959). The use of quarts oscillators for weighing thin layers and for microweighing. *Z. Phys.*, 155, 206-222.

[214] Li, C., Bai, H., & Shi, G. (2009). Conducting polymer nanomaterials: electrosynthesis and applications. *Chemical Society Reviews*, 38(8), 2397-2409.

[215] Das, T. K., & Prusty, S. (2012). Review on conducting polymers and their applications. *Polymer-plastics technology and engineering*, 51(14), 1487-1500.

[216] Fu, M., Shi, G., Chen, F., & Hong, X. (2002). Doping level change of polythiophene film during its electrochemical growth process. *Physical Chemistry Chemical Physics*, 4(12), 2685-2690.

[217] Ayankojo, A. G., Reut, J., Boroznjak, R., Öpik, A., & Syritski, V. (2018). Molecularly imprinted poly (meta-phenylenediamine) based QCM sensor for detecting Amoxicillin. *Sensors and Actuators B: Chemical*, 258, 766-774.

[218] Shi, G., Xu, J., & Fu, M. (2002). Raman spectroscopic and electrochemical studies on the doping level changes of polythiophene films during their electrochemical growth processes. *The Journal of Physical Chemistry B*, 106(2), 288-292.

[219] Shi, G., Jin, S., Xue, G., & Li, C. (1995). A conducting polymer film stronger than aluminum. *Science*, 267(5200), 994-996.

[220] Ng, S. C., Zhou, X. C., Chen, Z. K., Miao, P., Chan, H. S. O., Li, S. F. Y., & Fu, P. (1998). Quartz crystal microbalance sensor deposited with Langmuir− Blodgett films of functionalized polythiophenes and application to heavy metal ions analysis. *Langmuir*, 14(7), 1748-1752.

[221] Si, P., Mortensen, J., Komolov, A., Denborg, J., & Møller, P. J. (2007). Polymer coated quartz crystal microbalance sensors for detection of volatile organic compounds in gas mixtures. *Analytica chimica acta*, 597(2), 223-230.

[222] Giannetto, M., Mastria, V., Mori, G., Arduini, A., & Secchi, A. (2006). New selective gas sensor based on piezoelectric quartz crystal modified by electropolymerization of a molecular receptor functionalised with 2, 2′-bithiophene. *Sensors and Actuators B: Chemical*, 115(1), 62-68.

[223] Mattarozzi, M., Giannetto, M., Secchi, A., & Bianchi, F. (2009). Novel coating for solid-phase microextraction: electropolymerization of a molecular receptor functionalized with 2, 2′-bithiophene for the determination of environmental pollutants at trace levels. *Journal of Chromatography A*, 1216(18), 3725-3730.

[224] Batista, R. M., Oliveira, E., Costa, S. P., Lodeiro, C., & Raposo, M. M. M. (2008). Synthesis and evaluation of bipendant-armed (oligo) thiophene crown ether derivatives as new chemical sensors. *Tetrahedron Letters*, 49(46), 6575-6578.

[225] Giannetto, M., Mori, G., Notti, A., Pappalardo, S., & Parisi, M. F. (2001). Calixarene–Poly (dithiophene)-Based Chemically Modified Electrodes. *Chemistry–A European Journal*, 7(15), 3354-3362.

[226] Timmerman, P., Verboom, W., & Reinhoudt, D. N. (1996). Resorcinarenes. *Tetrahedron*, 52(8), 2663-2704.

[227] Moran, J. R., Karbach, S., & Cram, D. J. (1982). Cavitands: synthetic molecular vessels. *Journal of the American Chemical Society*, 104(21), 5826–5828.

[228] Moran, J. R., Ericson, J. L., Dalcanale, E., Bryant, J. A., Knobler, C. B., & Cram, D. J. (1991). Vases and kites as cavitands. *Journal of the American Chemical Society*, 113(15), 5707-5714.

[229] Dalcanale, E., Costantini, G., & Soncini, P. (1992). Removal of organic pollutants from water via molecular inclusion within a cavitand. *Journal of inclusion phenomena and molecular recognition in chemistry*, 13(1), 87-92.

[230] Dalton, T., & Jin, D. (2010). Extent and frequency of vessel oil spills in US marine protected areas. *Marine pollution bulletin*, 60(11), 1939-1945.

[231] Dickert, F. L., Bäumler, U. P., & Stathopulos, H. (1997). Mass-sensitive solvent vapor detection with calix [4] resorcinarenes: tuning sensitivity and predicting sensor effects. *Analytical Chemistry*, 69(6), 1000-1005.

[232] Dalcanale, E., & Hartmann, J. (1995). Selective detection of organic compounds by means of cavitand-coated QCM transducers. *Sensors and Actuators B: Chemical*, 24(1-3), 39-42.

[233] Hartmann, J., Hauptmann, P., Levi, S., & Dalcanale, E. (1996). Chemical sensing with cavitands: influence of cavity shape and dimensions on the detection of solvent vapors. *Sensors and Actuators B: Chemical*, 35(1-3), 154-157.

[234] Marco Giannetto, Alessandro Pedrini, Simone Fortunati, Davide Brando, Sabrina Milano, Chiara Massera, Roberta Tatti, Roberto Verucchi, Maria Careri, Enrico Dalcanale, Roberta Pinalli (2018). Sensing of halogenated aromatic hydrocarbons in water with a cavitand coated piezoelectric device. *Sensors and Actuators B: Chemical*, 276, 340-348.